Molecular and cellular characterization of apical and basal progenitors in the primate developing cerebral cortex

Marion Betizeau

THÈSE

en vue de l'obtention du grade de

Docteur de l'Université de Lyon, délivré par l'École Normale Supérieure de Lyon

Discipline : Biologie

Laboratoire Institut cellule souche et cerveau. Inserm U846

École Doctorale Biologie Moléculaire Intégrative et Cellulaire

présentée et soutenue publiquement le 24 octobre 2013

par Madame Marion BETIZEAU

Molecular and cellular characterization of apical and basal progenitors in the primate developing cerebral cortex

---

Directeur de thèse : Dr. Colette DEHAY

Après l'avis de : Prof. Zoltan MOLNAR
Prof. David PRICE

Devant la commission d'examen formée de :

Dr. Laure BALLY-CUIF, Laboratoire Neurobiologie et Développement (Membre)
Dr. Colette DEHAY, Institut cellule souche et cerveau (Membre)
Prof. Germain GILLET, SFR Santé Lyon Est (Président)
Dr. Henry KENNEDY, Institut cellule souche et cerveau (Membre)
Prof. Zoltan MOLNAR, Université d'Oxford (Rapporteur)
Prof. David PRICE, Université d'Edimbourg (Rapporteur)

Publications, oral presentations from this work

Publications:

Betizeau. M, Cortay. V, Patti. D, Pfister. S, Gautier.E, Bellemin-Ménard. A, Afanassieff. M, Douglas. R, Kennedy. K, Dehay. C. Precursor diversity and complexity of lineage relationships in the outer subventricular zone (OSVZ) of the primate. Neuron, in press.

Pfister, S., **Betizeau, M**., Dehay, C., Douglas, R., Robust 3D cell segmentation by local region growing in convex volumes. *IEEE International Symposium on Biomedical Imaging*. 2013 (in press).

Betizeau, M., Dehay, C., Kennedy, H., 2012. Conformity and specificity of primate corticogenesis. *The New Visual Neurosciences*, MIT Press, Cambridge MA (in press)

Pilaz, L.-J., Patti, D., Marcy, G., Ollier, E., Pfister, S., Douglas, R.J., **Betizeau, M**., Gautier, E., Cortay, V., Doerflinger, N., Kennedy, H., Dehay, C., 2009. Forced G1-phase reduction alters mode of division, neuron number, and laminar phenotype in the cerebral cortex. *PNAS*,106, 21924–21929

Pfeiffer. M, **Betizeau. M**, Pfister. S, Dehay. C, Douglas. R. A new clustering tool for cell lineage data analysis, application to primate cortical development. Manuscript in preparation.

Oral presentation:

Betizeau. M, Cortay. V, Patti. D, Kennedy. K, Dehay. C, Characterization of monkey cortical progenitors. SECO meeting, Capo Caccia, Italy, April 27th 2012.

Betizeau. M, Cortay. V, Patti. D, Kennedy. K, Dehay. C, Database of biological parameters in the monkey. SECO meeting, Capo Caccia, Italy, April 28th 2011.

Posters:

Betizeau. M, Cortay. V, Patti. D, Bellemin-Ménard. A, Pfeiffer. M, Pfister. S, Douglas. R, Kennedy. H, Dehay. C. Unique dynamics of germinal zones and precursor diversity during primate corticogenesis. Congrès de la société des neurosciences françaises, Lyon, 22-24 May 2013.

Betizeau. M, Girard. R, Cortay. V, Pfeiffer. M, Pfister. S, Douglas. R, Kennedy. H, Dehay. C. Characterisation of primate neural stem cells during corticogenesis. SFN (Society for Neuroscience) meeting, New Orleans, USA, 13-17 October 2012.

Betizeau. M, Girard. R. V, Pfeiffer. M, Pfister. S, Douglas. R, Kennedy. H, Dehay. C. Specificities of primate embryonic cortical stem cells. 4th International congress on stem cells and tissue formation. Quantitative stem cell biology: from models to applications. Dresden, Germany, 18-20 July, 2012.

Betizeau, M., Cortay, V., Gautier, E., Patti, D., Doerflinger, N., Kennedy, H., Dehay, C., 2010. Characterization of the primate cortex specific germinal zone: the outer subventricular zone. Congrès ENP (Ecole Nationale de Paris) Stem Cells, Abbaye des Vaux de Cernay, France, 15-17 June 2010.

Betizeau, M., Cortay, V., Gautier, E., Patti, D., Doerflinger, N., Kennedy, H., Dehay, C., 2010. Characterization of the primate cortex specific germinal zone: the outer subventricular zone. 18ème congrès ISDN (International Society for Development Neuroscience), Estoril, Portugal, 6-9 June 2010.

Acknowledgments

I am heartily thankful to my PhD supervisor Dr. Colette Dehay for her guidance and support all along these 4 years through the complexity of the macaque cortical precursors. I thank also Dr. Henry Kennedy for all the relevant discussions about the results.

I would like to thank our collaborators from INI in Zürich: Rodney Douglas, Sabina Pfister, Michael Pfeiffer and Andreas Hauri; for providing excellent ideas, new tools to deepen analyses and giving me the taste for the modeling approach.

I am grateful to Prof. Zoltan Molnar and Prof. David Price for accepting to evaluate my thesis, and Dr. Laure Bally-Cuif and Prof. Germain Gillet to be part of my PhD jury.

I am indebted to all the members of the team, Véronique Cortay, Dorothée Patti, Angèle Bellemin-Ménard for the joyful atmosphere in the P2 until late at night as well as the excellent technical assistance, and for the solidarity in the 24/7 monkey experiments. I also thank Nathalie Doerflinger for flawless plasmidic constructions and Souhila Zaraoui for perfect brain sections; Ugo Borello, Delphine Delaunay, Florence Wianny and the Julies (Fousse and Waltispurger)for the passionate discussions; Louis-Jan Pilaz and Elodie Gautier for showing me the way into the PhD life and Ken Knoblauch for help with statistics in the art of R.

I am deeply grateful to all the present and past members of the lab who made my PhD a very nice time and who were always ready to wear some colorful clothes. Thank you to all the students who actively participated to the student clubs. I would like to thank in particular Maïlys Faraut, Charlie Wilson (with a special thank you for all the english corrections), Frédéric Stoll, Pierre Enel, Raymond Najjar, Petteri Teikari, Christine Coutanson and Loïc Magrou for the support and the nice moments late in the lab.

I would like to thank my family for supporting me all along these years: in particular my parents, and I will not forget to thank my sister Camille and my brother Paul.

And all my friends outside the lab for these nice moments and great distractions from work; the B&Bs: Loan Dao-Thi, Mehrnaz Shamalnasab, Julia Neusiedler, Armel Nicolas, Monika Kuciak-Stanishevska, and also Andreas Hauri, Masooma Rasheed, Etera Livine, Lama Souiedan.

Disclaimer

I hereby declare that the work in this thesis is that of the candidate alone, except where indicated in the text, and as described below.

The use of "we" in the thesis refers to the candidate, but also contains intellectual input from Dr. Colette Dehay (thesis supervisor) and Dr. Henry Kennedy (expert of the macaque monkey model, cortical connectivity and development).

Abstract

The primate brain and more specifically the cerebral cortex underwent major modifications during evolution that enabled the development of high cognitive functions. A massive enlargement of the primate cerebral cortex occurred during evolution with the specific expansion of the supra granular layer neurons and the apparition of new frontal areas. The primate cortex possesses not only quantitative differences compared to the rodent but also qualitative differences. This points to potential qualitative differences in primate cortical development, which are the focus of the present PhD thesis.

Pioneering studies in the macaque model revealed the existence of an extra proliferating zone: the outer subventricular zone (OSVZ) which becomes the main proliferative zone as early as mid neurogenesis and during the generation of the supra granular layer neurons. It has been speculated that this zone is responsible for the expansion of the primate supra granular layer neurons but the cellular and functional properties of OSVZ precursors remain still elusive. We used quantitative long-term time-lapse video-microscopy (TLV) and immunofluorescence *in* and *ex vivo* to perform a detailed and exhaustive description of OSVZ precursor types and proliferative abilities at different stages of macaque cortical development.

Our results highlight major differences between rodent and primate cortical precursors. TLV observations revealed a much higher proliferative potential of OSVZ precursors that can perform up to 6 successive divisions, as opposed to only one and rarely two in the rodent SVZ. By contrast with the progressive increase of cell cycle exit associated with a progressive lengthening of the cell cycle length observed in mouse cortical development, in the macaque monkey we report variable rates of proliferation linked to cell cycle duration in a stage-specific manner. Quantitative TLV recordings allowed the formation of a large and unique database of primate precursor properties and lineages. The study of this database unraveled an unexpectedly high diversity of OSVZ precursor

morphologies. Five types were identified based on their morphology. Contrary to the prevalent hypothesis, each precursor type is able to self-renew and to directly generate neurons. OSVZ precursors are involved in complex lineage trees that present surprising bidirectional lineage relationships. The lineage topology is different for the generation of infra- and supragranular layer neurons suggesting that specific lineages are involved in the formation of these different types of neurons. In a parallel approach, we developed and used an unbiased clustering tool to automatically classify primate cortical precursors taking equally into account all TLV measured parameters. This technique returned the same five precursor types as the morphological classification as well as the bidirectional lineage relationships, which validates our first biological categorization.

The results of this PhD thesis provide new insights into primate cortical development specificities that contribute to cortical expansion and to the development of higher cognitive abilities.

Résumé

Le cerveau primate et plus spécifiquement le cortex cérébral a subi des modifications majeures au cours de l'évolution qui ont permis le développement de fonctions cognitives supérieures. Un accroissement massif du cortex cérébral primate a eu lieu avec l'extension spécifique des couches supragranulaires et une expansion tangentielle qui a conduit à l'apparition de nouvelles aires frontales. Le cortex primate ne possède pas simplement des différences quantitatives comparé au rongeur mais aussi des différences qualitatives. Ceci suggère des différences à la fois quantitatives et qualitatives au niveau du développement du cortex primate, ces différences sont l'objet de la présente thèse de doctorat.

Des études pionnières dans le modèle du singe macaque ont révélé l'existence d'une zone proliférative corticale supplémentaire: la zone subventriculaire externe (OSVZ) qui devient la zone proliférative principale dès la moitié de la gestation et pendant la formation des neurones supragranulaires. Cette zone est supposée être impliquée dans l'expansion des couches supragranulaires chez le primate mais les propriétés cellulaires et fonctionnelles des précurseurs de l'OSVZ restent mal connues. Nous avons utilisé des techniques de microscopie en temps réel et d'immunofluorescence *in* et *ex vivo* afin de réaliser une description exhaustive des types de précurseurs de l'OSVZ ainsi que de leurs propriétés proliferatives à différent stades de développement du cortex cérébral chez le singe macaque.

Nos résultats mettent en évidence des différences majeures entre les précurseurs corticaux primates et rongeurs. Les observations en temps réel révèlent des capacités prolifératives bien plus importantes des précureurs primates de l'OSVZ par rapport aux précurseurs rongeurs de la zone subventriculaire (SVZ). Nous avons observé jusqu'à 6 divisions successives dans l'OSVZ comparé à une et rarement deux divisions dans la SVZ des rongeurs. Contrairement à l'allongement progressif du temps de cycle cellulaire associé à l'augmentation du taux de sortie du cycle cellulaire observés chez le rongeur, les précurseurs primates de l'OSVZ présentent des taux de prolifération variables, à différents

stades de développement, liés à la cinétique du cycle cellulaire. Les enregistrements en temps réel quantitatifs ont permis la génération d'une base de données de propriétés et lignages de précurseurs primates d'une grande ampleur. L'analyse de cette base de données a mis en évidence une diversité morphologique inattendue des précurseurs de l'OSVZ. 5 types ont été identifiés sur la base de leur morphologie. Contrairement à l'hypothèse dominante, chaque type de précurseur a la capacité de s'autorenouveler et de générer directement des neurones. Les précurseurs de l'OSVZ sont impliqués dans des arbres de lignage complexes qui comprennent d'étonnantes transitions bidirectionnelles. La topologie des lignages est différente pour la génération des neurones infra- et supragranulaires ce qui suggère que des lignages spécifiques sont responsables de la formation de différents types de neurones. Dans une approche parallèle, nous avons développé et utilisé une méthode de classification non supervisée pour classer les précurseurs corticaux primates en prenant en compte de manière équivalente tous les paramètres mesurés sur les enregistrements en temps réel. Cette technique a identifié les mêmes 5 types de précurseurs que la classification morphologique ainsi que les relations de lignage bidirectionnelles, ce qui valide notre première catégorisation biologique.

Les résultats de cette thèse apportent de nouveaux éléments dans la compréhension des spécificités du développement cortical primate qui contribuent à l'expansion corticale et au développement de capacités cognitives supérieures.

Contents

Chapter 1

Introduction

The cerebral cortex is the center of higher cognitive abilities in the brain. It integrates environmental sensory information relayed by the thalamus and enables the individual to make an appropriate decision in a given context. The cerebral cortex is often compared to a computational device in which the processors are neurons, the electrical circuits the neuronal fibers, and the electrical signal the action potential diffusing along the neuronal fibers. Despite the exponential increase of computer power, the human brain remains by far the best and unrivaled computational machine. Computers might appear better because they have a very low computing time, but the brain is much more efficient at learning, generalizing and has the ability of abstraction. The brain detects statistical regularities in the environment and generates behaviorally relevant patterns by self-organizing the connections and their weights.

Understanding how the brain is built and how it becomes an efficient computing device by self-constructing during development has enormous interests for both the neuropathological and the artificial intelligence fields, since this will help find ways of curing neurobiological diseases and enable the creation of improved neuro-inspired computers and robots.

The brain and in particular the cerebral cortex becomes larger in the primate lineages and achieves its highest complexity in humans with a higher number of neurons and a particular wiring that enables enhanced cognitive abilities. A direct link between the number of neurons and cognitive abilities has been suggested (Deaner et al., 2007). Adding neurons to the brain has thus been a fundamental aspect in the evolution of the mammalian brain. The addition of extra neurons is, however, subject to many constraints. The brain

is delimitated by the skull, so the volume in which it can expand is limited. Neurons are very energy consuming due to the need to maintain differential membrane potentials and to the vesicle trafficking at synapses. Therefore having more neurons necessitates a higher energy intake or an adapted energy repartition (Fonseca-Azevedo and Herculano-Houzel, 2012).

The primate brain has not expanded isotropically. There is a specific increase of the supra granular layer neurons (layers 2 and 3) (Marin-Padilla, 1992) specialized in connecting different areas of the cortex, thus promoting associative functions. In its tangential dimension compared to rodents, the primate cortex underwent a particular expansion of the frontal lobe where the prefrontal cortex is located. The prefrontal cortex is involved in the executive control of behavior including decision making, action planning, and problem solving. Besides containing more neurons, primate brains have integrated these extra neurons in a way that favors higher cognitive processing.
These observations raise a number of far reaching questions: how was such a large brain expansion possible in primates? Why did it not occur in other mammalian orders as well? Why do humans have the primate brain that contains the most neurons?

Large brains exist in different mammalian orders, in rodents, cetaceans, proboscidea (elephants), and primates. However, recent studies have revealed that all mammalian brains do not scale in the same way (Herculano-Houzel, 2011). Herculano-houzel et al. and found different scaling rules between rodents and primates which enable the addition of more neurons in an identical volume or mass in primates. This difference in scaling indicates that the differences in the construction of the brain in rodents and primates are not merely quantitative. Instead innovations have occurred in the primate lineage since its divergence from the rodents 100 millions years ago that have enabled the emergence of bigger brains with more neurons arranged in a more efficient way.

In this PhD thesis we focused on the question of how more supra granular layer neurons are produced during primate cortical development, using the maccaca fascicularis as a model. A pioneering study shed light on an extra cortical proliferative zone during neurogenesis in the macaque cortex: the outer subventricular zone (OSVZ) (Smart et al., 2002). This zone appears at mid-neurogenesis and becomes the major proliferative zone when supra granular layer neurons are produced. The direct link between OSVZ precursors and the generation of the supra granular layer neurons was later demonstrated (Lukaszewicz et al., 2005). Although the source of much conjecture, the nature and pro-

liferative abilities of the OSVZ precursors remain unclear, as does their lineage (Lui et al., 2011). In this thesis, we addressed the importance of OSVZ precursors in primate cortical expansion. We directly assessed the proliferative abilities of OSVZ precursors in a unique set up of long-term quantitative time-lapse video-microscopy analysis. We found a higher proliferative potential in OSVZ precursors compared to rodent precursors associated with a higher diversity of precursor morphology. In addition, unlike in rodents where cortical precursor proliferation potential linearly decreases as neurogenesis proceeds, our results show that the proliferative potential of OSVZ precursors is not linear but modulated during corticogenesis. OSVZ precursors resume high proliferation at the time of supra granular layer neuron production. Exhaustive and quantitative live-imaging observations enabled the identification of 5 different OSVZ precursor types involved in complex lineages. Each type is able to self-renew and to generate neurons. These results provide a new framework for understanding primate cortical expansion during evolution.

In the thesis introduction, we will first give some background about the organization of the adult cerebral cortex and how it evolved in the mammalian order. We will focus on the scaling rules that govern mammalian brain expansion. We will give some insights into the increased brain expansion in primates and especially in humans compared to other mammalian orders. Then we will review what is known about rodent cortical development before concentrating on the already known primate specificities of cortical development. In the results section we will describe the different precursor types found in the macaque OSVZ as well as their proliferative properties and cell cycle kinetics. We will also explain how a comprehensive database of information about primate precursor morphology, proliferation and lineage has been gathered. This unique dataset enabled a first classification of OSVZ precursors based on their morphology. In a second part of the results section we will document the clustering method that we used to classify primate cortical precursors in an unsupervised way using all measured parameters. Finally, we will discuss all these results in the context of mammalian brain evolution.

1.1 The primate cerebral cortex: organization and evolution

In this first section, we will provide some general reminders about how the cerebral cortex is organized and wired. We will start by describing the general organization of the cerebral cortex as well as its cellular composition. We will then focus on the radial and tangential organization of the cerebral cortex. Finally, we will address the question of brain evolution. We will concentrate ourselves on the primate and rodent lineages and how brains of these two orders can scale to generate larger brains. We will also review the qualitative differences that have been reported in terms of brain expansion and primate specific neuronal subtypes.

1.1.1 The cerebral cortex: general organization and composition

The cerebral cortex is the peripheral sheet of neuronal tissue that covers the brain. It comprises the hippocampus also known as the archicortex and the neocortex. From now on, we will focus on the neocortex later simply referred to as the cortex. The cortex is highly convoluted in humans and divided into 4 lobes: frontal, parietal temporal and occipital that are involved in distinct functions (Figure 1.1). The cortex is the center of higher cognitive function of the brain. It receives environmental sensory inputs via the thalamus and integrates information to produce the appropriate behavioral patterns. It is connected in an intricate network with subcortical structures but most connections of cortical neurons are with other regions of the cortex itself (Braitenberg and Schuz, 1991).

The cerebral cortex is composed of neurons and glial cells (Kandel et al., 2000). Neurons are the support of information flow and information processing in the brain. They extend potentially long axonal fibers that compose the wiring of the brain. The information is transmitted in the form of an action potential propagated along the axons and is encoded as the rate of spikes. Information is passed chemically from neurons to neurons at the synapse via neurotransmitters that cross the gap between the two neuronal membranes and activate receptors on the next neurons.

Neurons are of two main kinds: excitatory or inhibitory depending of which neurotransmitter they release at their synapses. Local recurrent and long range projecting cor-

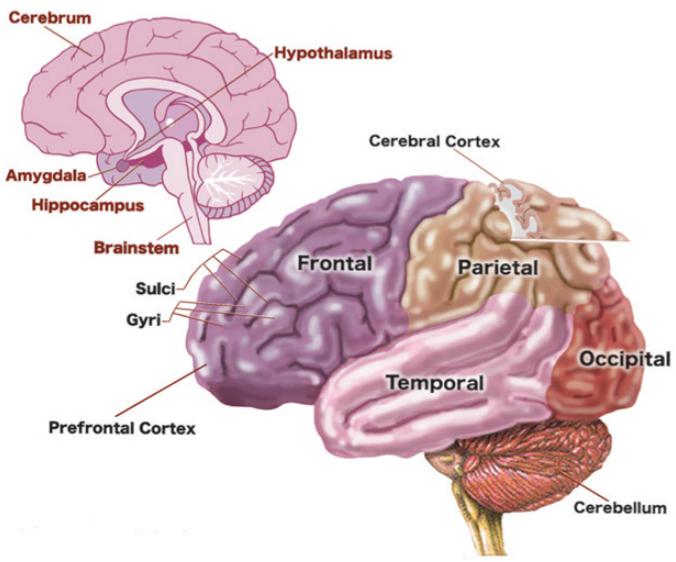

Figure 1.1. Organisation of the human brain (from www.urbanchildinstitute.org). The cortex is the superficial neuronal tissue of the brain divided in to 4 lobes. It is connected with other regions of the brain: the hippocampus, the cerebellum and the brainstem as well as with subcortical nuclei: the hippothalamus and the amygdala.

tical excitatory neurons include stellate and pyramidal glutamatergic neurons. Activity is finely tuned by locally projecting GABAergic neurons also called inhibitory interneurons, which serve to synchronize excitatory neurons thereby facilitating synaptic potentiation and the generation of potentiated cell ensembles (Bartos et al., 2007; Fishell and Rudy, 2011). Excitatory neurons are mainly projection or pyramidal neurons. They are characterized by a long apical dendrite reaching the exterior most part of the cortex and possess also several basal dendrites. They have a unique axon that projects to other cortical areas or brain regions (Figure 1.2). The second minor type of excitatory neurons are the stellate neurons that are considered interneurons because they project locally. They extend several dendrites around the soma and lack an apical dendrite. Unlike excitatory neurons inhibitory interneurons lack dendritic spines. Inhibitory interneurons constitute a heterogeneous population differing in their morphologies, connectivity, electrophysiological properties and the expression of the calcium binding proteins calbinding, somatostatin, calretinin and parvalbumin (Figure 1.2) (Ascoli et al., 2008). Cortical neurons are located almost exclusively in the gray matter.

In addition to neurons, the cortex contains the glial cells. Two types of glial cells are

found in the cortex astrocytes and oligodendrocytes. Astrocytes are the main energy supply for neurons and are closely associated with the vascular system. They have recently also been shown to modulate synaptic transmission (Panatier et al., 2011). Oligodendrocytes wrap axonal fibers with an insulating myeline sheet that enables a saltatory conduction of the action potential and thus a faster conduction. The myelinated sheet gives color to the white matter which contains axons of neurons projecting to other cortical areas or other brain regions.

1.1.2 Radial organization of the cerebral cortex

The cortical sheet is 2 to 4mm thick in the human brain with some local variations (Kandel et al., 2000). In mammals it is organized into six horizontal layers of neurons. Each layer contains distinct types of neurons based on their molecular identity, connectivity pattern and morphology (Figure 1.2).

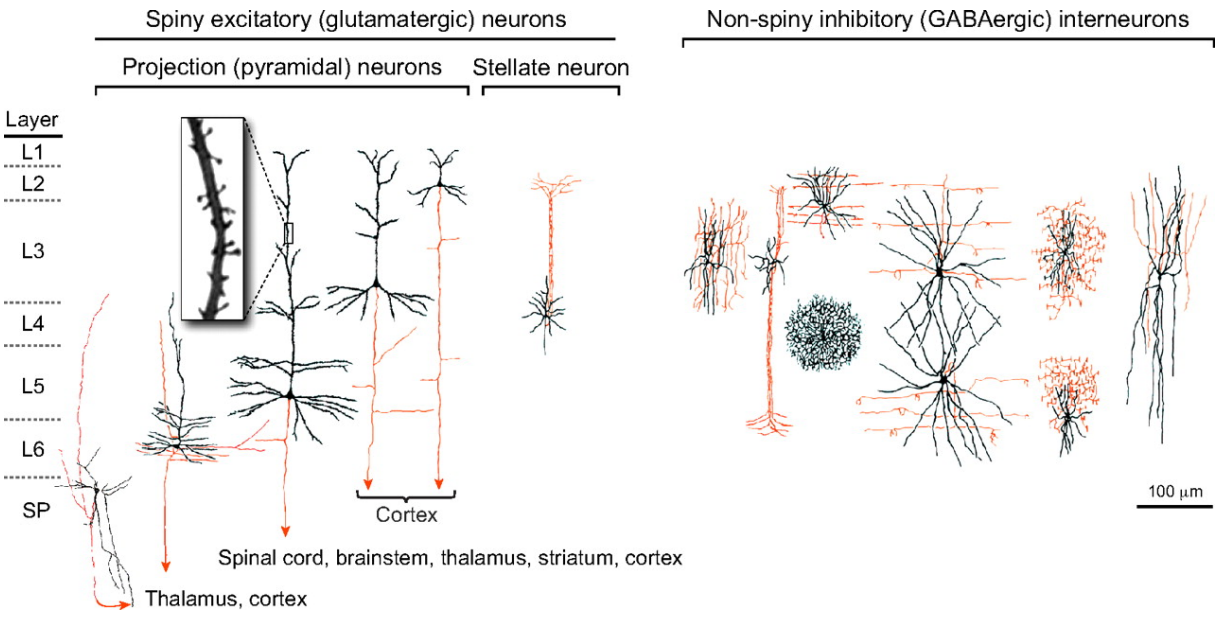

Figure 1.2. Laminar organization of the cortex. The characteristic morphologies of excitatory and inhibitory neurons in the different cortical layers are represented on the left and right panels respectively. Note the higher magnification of pyramidal neuron dendrites showing the spines. Dendritic arborisations are represented in black and axons in red. (Figure from (Kwan et al., 2012)).

Composition of the different cortical layers

Layer 1 has a low cell density. It contains scattered neurons a few Cajal-Retzius and spiny stellate cells but is mainly made of glial cells and apical dendrites of pyramidal neurons. Layers 2 and 3 are the supra granular layers. They contain chiefly pyramidal cells and stellate neurons. Layers 2 and 3 are the target of the inter hemispheric cortical efferents and are the principal source of cortico-cortical connections (Figure 1.2). Layer 4, also known as the granular layer is composed of pyramidal neurons and many stellate neurons especially in primary sensory areas. Layer 4 is the main target of thalamic input to the cortex. Layers 5 and 6 are the infra granular layers. Layer 5 contains large pyramidal neurons that project to subcortical regions including the basal ganglia, the brain stem and the spinal cord. Layer 6 is made of few large but mainly small pyramidal neurons. Layer 6 is involved in reciprocal connections with the thalamus (Molyneaux et al., 2007).

A columnar organization of the cortex

Does the laminar organization of the cortex correspond to a functional organization? Pioneer analyses of pyramidal neurons connections had pointed out that the dominant connectivity between neurons is vertical (Lorente de Nó, 1938). Evidence for a vertical functional organization of the cortex came from electrophysiological experiments in the cat somatosensory cortex. Mountcastle et al. found by performing single cell recording that vertically arranged neurons respond to a unique sensory input, thus have the same receptor field (Mountcastle, 1957). These experiments, together with Lorente De No's observations prompted Mountcastle to enunciate the principle of the cortical column as the functional unit of the cerebral cortex. This concept of cortical column had a tremendous impact on neuroscience research because it postulates that studying how the cerebral cortex functions can be reduced to understanding how one cortical column functions. A columnar organization was also found in the cat primary visual area which supported the Mountcastle model. Hubel and Wiesel found that neurons recorded along the same vertical line had the same receptive field orientation (Hubel and Wiesel, 1962). Although clear vertical stripes can be observed in the primary visual area with Nisl staining, they do not correspond to orientation columns, but support the fact that the cortex is organized in vertical units (Jones, 2000). A study by Rockel et al. even proposed that the cortical column contains approximately the same number of neurons in different cortical areas and

even different species (Rockel et al., 1980) and that it might be the same functional unit in all mammalian cortices. Pasko Rakic proposed a ontogenic origin of functional cortical column with his radial unit hypothesis that we will develop in section 1.3.7 (Rakic, 1988).

The different cortical columns are defined on various functional or anatomical characteristics and no consensus has been found so far to define the standard functional unit of the cortex, essentially demonstrating the discrepancy between anatomy and functional maps (Rakic, 2008). The sizes of the different functional and cytological columnar organizations differ. Researchers had to introduce the minicolumn unit that would directly derive from ontogenic columns and assemble together to form cortical columns. The physiological relevance of the minicolumns has yet to be demonstrated, mainly due to the poor spatial resolution of electrodes. Recent studies have undertaken the enormous labor of deciphering the fine grained neuronal composition and synaptic connections of a rat somatosensory column (Meyer et al., 2010; Wimmer et al., 2010). They further demonstrated that minicolumns are organised around thalamic axons terminations. But they failed to produce a standard columnar organization map and the functional relevance of such structure remains to be proven (Jones and Rakic, 2010).

Since Rockel et al findings, a substantial number of other studies investigated the potential basic uniformity of the cortex. This remains until now a matter of debate. Some authors found that columns of cortex possess various number of neurons in different cortical areas and species (Haug, 1987; Cheung et al., 2007; Herculano-Houzel et al., 2008; Polleux et al., 1997). However, a recent study aiming at reproducing exactly Rockel's experiments with the modern stereological methods was able to confirm the uniformity of the number of neurons under a square millimeter of cortex in different cortical areas (with the exception of the primate area 17), in mouse, rat, cat and rhesus macaque (Carlo and Stevens, 2013). They compared their results with 5 other studies using the same technique that yielded a number of neurons below a square millimeter of cortex in the same 4 species (Skoglund et al., 1996; DeFelipe et al., 2002; Schüz and Palm, 1989; Beaulieu and Colonnier, 1989; Hendry et al., 1987). The authors found that despite some outliers, the variations between studies can be explained by random counting errors and are thus compatible with a basic uniformity of the cortex. One of the main caveats of Rockel et al, and thus Carlo et al studies, is that they focus on a small number of areas in a few species. Another recent study undertook the tremendous work of counting the number of neurons in cortical columns in systematically sampled sites along the the

rostral-caudal, and medio-lateral axes of the cortex in several rodent and primate species. The chosen species have varying cortical sizes to account for species variations within taxa (Charvet et al., 2013). This study demonstrated a rostro-caudal gradient of the number of neurons in a cortical column, the more frontal columns containing less neurons than the more caudal ones. The gradient is not only due to the higher number of neurons in the primary visual area since when removing this area the gradient persists. The gradient seems to follow the neurogenesis gradient in the cortex. The difference is more pronounced in bigger brains, and in primates compared to rodents (variation factor of 1.64-2.13 in primates, and 1.15-1.54 in rodents). The gradient can be mainly attributed to variations in the supragranular layer neuron numbers. The results of Charvet et al., reconcile previous contradictory studies. The areas chosen by Rockel et al., were localized in the middle of the cortical surface which eliminates areas where the biggest variations from the mean number have been found.

Intra and inter species variations in the cortical columnar organization do not strengthens the importance of the functional role of the cortical column (reviewed in (Horton and Adams, 2005)). The existence of a canonical microcircuit composing the cortical column is still a matter of debate (Douglas and Martin, 2004; Nelson, 2002). The columnar organization of the cortex is well established but the cortical column as the functional unit of the cortex is now brought into question. Different cortical areas in different species might have different processing units.

1.1.3 Tangential organization of the cerebral cortex

The cortex is not a uniform sheet of cells. There are substantial variations in overall thickness of the cerebral wall ranging from 2 to 4 mm depending on the localization. Pioneer histological studies by Brodmann shed light on distinct relative sizes of the different cortical layers along the cortical sheet. He segmented the cortical sheet into discrete regions with the same laminar distribution or same cytoarchitecture that he named cortical areas (Brodmann, 1909), (Figure 1.3). It was later discovered that the anatomically defined cortical areas have a specific cognitive function. The relationship between cortical areas and cortical function was deduced from patients who lost a certain cognitive ability after a brain injury. The location of the brain injury was mapped and associated to this lost ability. For instance Broca discovered that a single cortical region was affected in patients

who lost speaking ability and that it was responsible for the language processing (Broca, 1861).

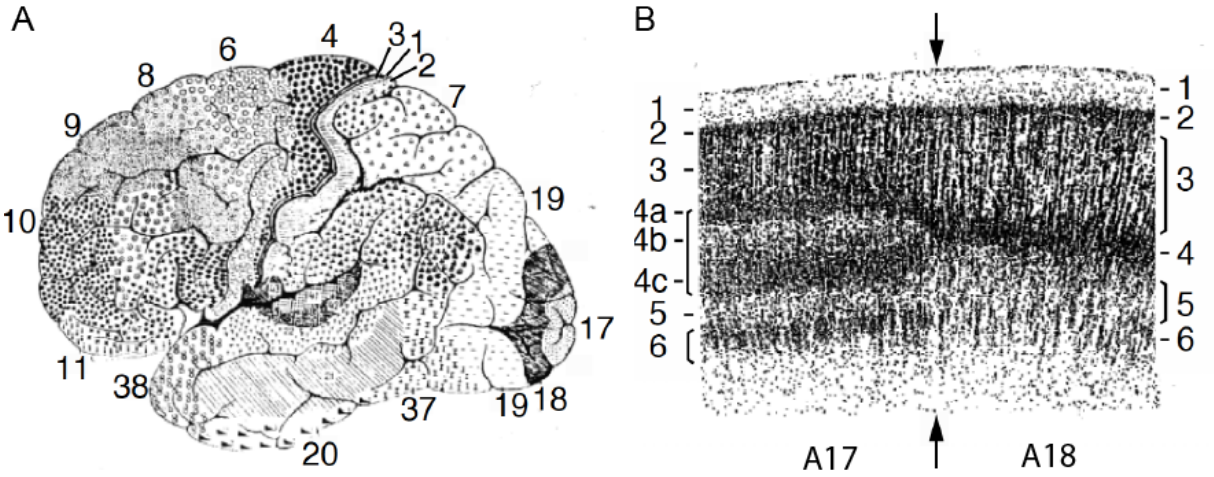

Figure 1.3. The segmentation of the cortex into cortical areas. **A.** Brodmann initial segmentation of the human brain. **B.** example of a sharp change of cytoarchitecture between the area 17 and area 18 primary and secondary visual areas respectively. Note the much thicker and complex layer 4 in area 17 compared to area 18. Adapted from (O'Leary and Nakagawa, 2002).

1.1.4 Evolution and specificities of the primate cerebral cortex

Evolution has produced a wide array of brain sizes and shapes (Figure 1.4). Brain mass varies by a factor of 100 000 in the mammalian order (Count, 1947) ranging from 0.060g for the insectivorous white-toothed pygmy shrew to 9.2kg for the sperm whale.

Do species with a larger brain have higher cognitive abilities? Many studies have tackled this issue using parameters relying on brain and body sizes but without establishing a clear relationship between their parameter and the actual intelligence degree of the different species. A recent study investigated the direct correlation between anatomical parameters and cognitive abilities in a meta-analysis of 24 primates (Deaner et al., 2007). They found that the best anatomical indicator of cognitive abilities was the absolute brain size and thus the number of neurons, independent of the body size. The authors claim that this rule applies to the primate order but elephants and cetaceans have much larger brains than humans but do not appear to have as high cognitive functions. There could

be several non mutually exclusive explanations. Brain size might not be directly correlated to neuron numbers in a similar fashion in different mammalian clades. That is, even though cetaceans brains can weigh 7 times more than humans they might not contain 7 times more neurons. Indeed some recent studies showed that there might be clade specific scaling rules in mammalian brains (Herculano-Houzel, 2011; Charvet et al., 2013). It is also possible that having a bigger brain and more neurons is a necessary but not sufficient attribute for a more intelligent brain. Computational machine efficiency depends on the number of its processors (neurons) and on the speed of the information flux between these processors, thus on the properties of the connections and on the arrangement of the whole structure that will determine the distances to travel. In the next paragraphs we will review the different pieces of evidence we have for how primate brains get bigger and the qualitative differences of the primate brain organization.

Are all brains made the same: a common scaling rule for cell number in all mammalian brains?

As seen in Figure 1.4 brain sizes are very heterogeneous in mammals. Do all brains result from a scaled up or a scaled down version of a same basic organization plan? In other words do brains of the same size contain the same number of neurons? Previous comparative neuroanatomical studies based on cellular densities and volumetric analyses argued for a common scaling rule for mammals (Haug, 1987; Stevens, 2001). In the brain, the cerebral cortex takes up a higher relative proportion and bigger brains are mainly constituted of cortex. In these studies, the calculation of cell densities has been carried out without taking into account the different clades and biased towards the cerebral cortex. The authors derived a general rule for a large group of mammals according to which bigger brains have more neurons, smaller neuronal densities and a higher glia to neuron ratio. They claimed that glial cells are the most numerous cell type of the brain outnumbering the neurons by up to 50 times (Kandel et al., 2000). However, these studies have been carried out in a restricted number of species and cell density measurements are subject to high discrepancies among studies, for example neuronal densities of the cerebral cortex varies up to 6-folds in different studies. Moreover, as brain tissue is heterogeneous in cell density, modern stereological techniques would necessitate segmenting the brain into hundreds of pieces of homogeneous cell density which would be a tedious and error-prone task.

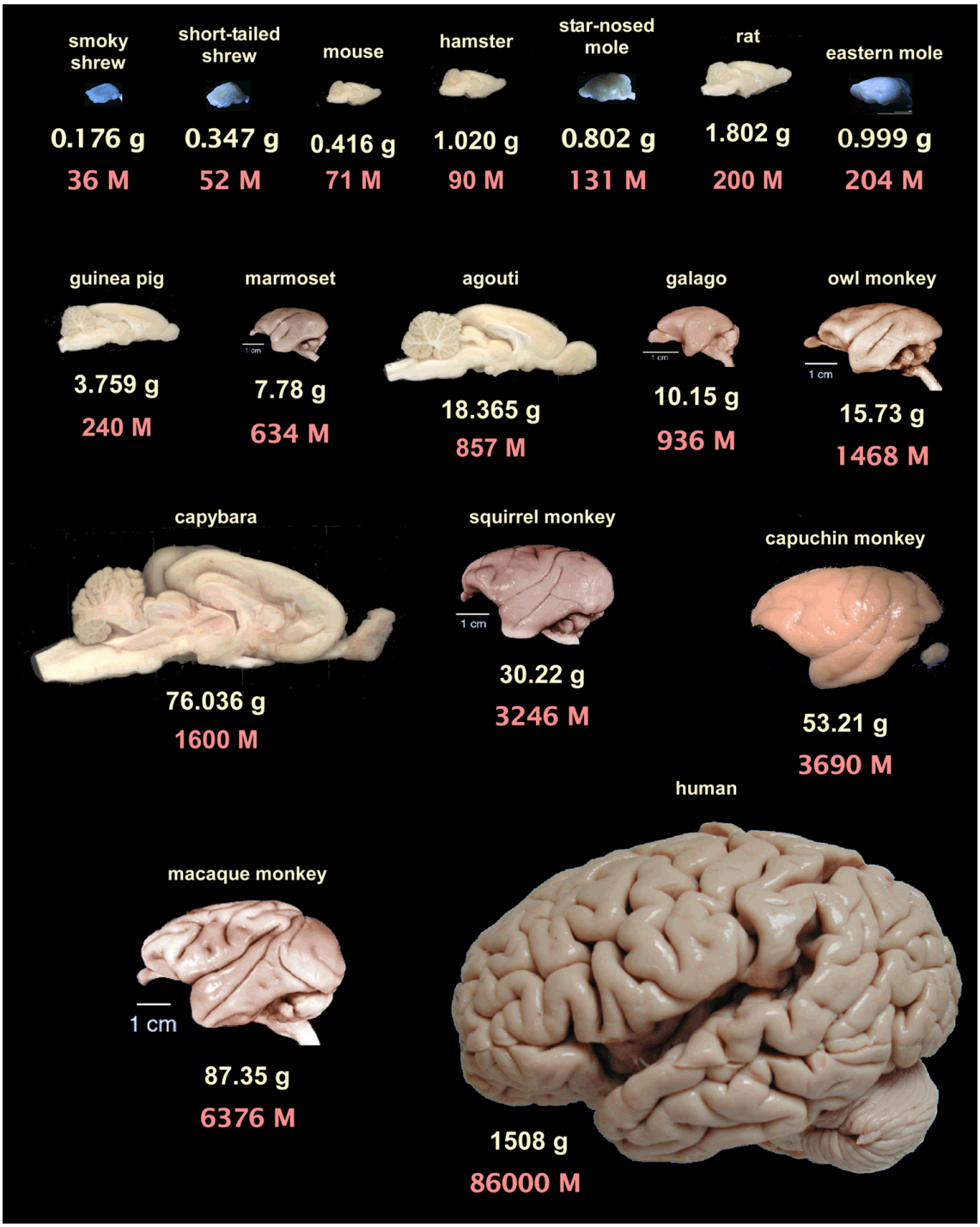

Figure 1.4. Diversity of brains and cortices among mammals (Figure from (Herculano-Houzel, 2009))

A new technique has been recently been developed which overcomes the caveats of the above mentioned protocols and enables the determination of absolute numbers of neuronal and non-neuronal populations in different brain regions (Herculano-Houzel and Lent, 2005). The isotropic fractionator is a nonstereological approach which relies on transforming the brain tissue into a homogeneous isotropic cell suspension. Such suspensions can then easily be stained with a neuronal marker and neuronal and non-neuronal cells can be automatically counted. Contrarily to stereological neuron counting on brain sections, the isotropic fractionator relies on dissecting unstained brain tissue where morphological landmarks are spare. This technique can thus only be applied to large pieces of tissue, and is not adapted to resolve inter cortical/ inter layer differences in neuron numbers, which can be a non negligible issue knowing the gradient of number of neurons in a cortical column along the rostro-caudal axis (Charvet et al., 2013). Moreover, several steps of the process need to be checked to fully validate the technique. The isotropic fractionator relies on generating a suspension of nuclei, but no definite proof of the retention of all nuclei has been given. In addition, the neuronal marker used NeuN is not an all-or-none staining, meaning that the discrimination between neuronal and non neuronal cells based solely on this marker might be error prone. More precise comparisons with stereological analyses need to be carried out in order to confirm the validity of this technique (Carlo and Stevens, 2013; Charvet et al., 2013). The following results need to be taken with care before they had been confirmed using other techniques taking into account possible local variation of neuron numbers.

The isotropic fractionator technique allowed the determination of brain cell numbers in various mammalian species and might lead to the revision of old dogmas. Over several years a dataset of 28 mammalian species belonging to 3 different clades has been gathered (Herculano-Houzel et al., 2006, 2007; Azevedo et al., 2009; Gabi et al., 2010; Sarko, 2009). This dataset enabled them for the first time to directly assess the cellular scaling rules at the gross structure level (cerebral cortex, cerebellum, rest of the brain) of different orders of mammals in a meta-analysis (Herculano-Houzel, 2011). The authors found different scaling rules for primates and rodents. For an equivalent body mass primates have a larger brain than rodents. The number of neurons scales also more rapidly with body mass for primates compared to rodents. Brain mass of rodents increases with the number of neurons raised to the power 1.5 whereas primate brain mass increases almost linearly. This clearly demonstrates that neuron numbers do not scale universally with brain mass

(Figure 1.5), this is also true for the cerebral cortex. The larger the brain, the bigger the difference of neurons between rodent and primate brains. This data invalidates brain size as a good indicator of neuron numbers. A rodent brain of 100g will contain 470 millions neurons, a primate brain of the same mass will contain 7.3 billions so more than 15 times more. Primate brains seem to be able to add neurons in a more economic way, less volume consuming than rodents.

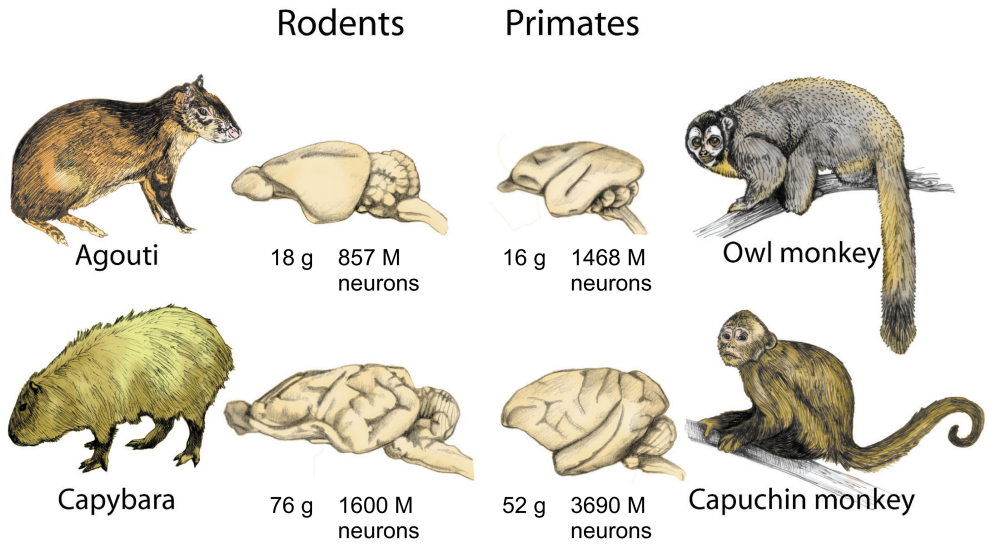

Figure 1.5. Number of neurons are not well predicted by brain size among mammalian orders. The Owl monkey whose brain mass is slightly smaller than the Agouti contains almost twice as many neurons.Along the same line, the Capucin monkey with a 52g brain possesses more than twice as many neurons as the Capybara whose brain weight 76g. Figure from (Herculano-Houzel, 2009).

The distribution of mass in the brain does not reflect the number of neurons of the structures. A relatively larger cerebral cortex does not contain a higher proportion of neurons in bigger brains. The cerebral cortex, although accounting for up to 80% of brain mass in humans, usually contains about 20% of the brain neurons and the cerebellum 70-80% (Azevedo et al., 2009). Interestingly the cerebellum and the cerebral cortex have also clade specific scaling rules with neuronal number in which the structure mass increases faster with neuron numbers in rodents (Herculano-Houzel, 2011). The two structures seem to gain neurons in a coordinated fashion at an average rate of 4.2 neurons in the cerebellum for one in the cerebral cortex. This result supports the hypothesis of an

integrated function of both structures and suggests that a common selective pressure might be at the origin of a concerted evolution (Balsters et al., 2010).

The neuronal density seems to be very heterogeneous among species and structures (Herculano-Houzel, 2011). The authors found the neuronal density to decrease as rodent brain size increases whereas contrarily to previous results primate neuronal density decreases only slightly when the brain size increases. Unlike neuron numbers, glial cell numbers have been reported to share common scaling rules in the different mammalian clades and even in the different structures. Glial cell number increases linearly with brain mass and their density is similar in the different brain structures. Brain size is actually a good indicator of glial cell number rather than neuron number. As glial cell density can be considered constant, the lower rodent neuronal density suggests a bigger neuronal size (soma and neuronal fibers) in rodents compared to primate as brain size increases.

Although the ratio glia/neuron had been shown to increase in bigger brains (Sherwood et al., 2006), using the isotropic fractionator the authors did not report this trend. They found that the ratio glial/neuron is heterogeneous among the different brain structures (in human, 0.99 on average but 3.76 in the cortex, 0.35 in the cerebellum and 11.35 in the rest of the brain; (Azevedo et al., 2009)). The ratio is found to increase only in the rodent brain as it increases in size. In primates the glia/neuron ratios remain constant in the different brain structures as brains scale up in size (Herculano-Houzel, 2011). Moreover, the glia/neuron ratio seems to be correlated to the average neuronal size. From this results Herculano-Houzel et al. proposed a mechanism to explain the relationship between neuron and glial cell numbers (Herculano-Houzel et al., 2006). Gliogenesis is known to be density-dependent (Zhang and Miller, 1996), glial progenitor proliferation stops at confluence probably by cell contact inhibition. As glial cell size does not scale with brain size, the glial/neuron ratio will depend only on the neuronal density, thus on neuronal size. It seems that glial cells properties are much more conserved among structures and clades than neuron cell properties indicating a stronger selection pressure and a fundamental role in the brain.

Compared to rodents, primates seems to have an advantage in making bigger brains, via a more economic way of adding neurons without greatly increasing the volume of the structure. This is mainly due to neuron size. Rodent neurons in bigger brains tend to have a larger average size whereas primate neuronal size does not increase with brain size. With this property, primate brains contain many more neurons in a brain of the same

size as rodents (Figure 1.5).

It has long been thought that the human brain was exceptional in the mammalian order by its composition and cognitive abilities (Deacon, 1997). However, Azevedo et al. found using the isotropic fractionator technique that the human brain is not an exception to the primate scaling rule (Azevedo et al., 2009). With its 86 billion neurons and 85 billion glial cells for 1.5kg, the human brain deviates only by 10% from the the primate scaling rule predictions. The relative size of the cerebral cortex is increased (82%) but it takes up only 19% of the brain's neurons. The human brain possesses two advantages compared to other mammalian brains. It is built according to the economical, space-saving primate scaling rules and it is the largest among those hence the one containing the most neurons. The number of neurons of the cetaceans and the elephant has not been assessed by the isotropic fractionator method. Based on previous estimates the false killer whale and the African elephant would have 11 billion neurons in the cerebral cortex, only slightly fewer than the 11.5 billions found in the human cerebral cortex using the same method (Roth and Dicke, 2005). They seem to obey rather the rodent than the primate scaling rules, showing a very low neuronal density. Even if these estimates of number of neurons are true, the difference between humans and elephants or whales is small, if any. The higher cognitive function achieved in the human brain might lie beyond the number of neurons.

An economic way of making larger brains in primates: more neurons, fewer wires, more folds

The primate scaling rules allow a brain of similar size to have more neurons than the rodents. Where do primates get the sparse space necessary for the extra neurons? As suggested above, knowing that glial cells scale uniformly between clades, one must suppose that the economy probably comes from the neuronal cell type and more precisely from the neuronal size (Herculano-Houzel, 2011). Neuronal size increases faster with brain size in rodents than in primates. Here neuronal size comprises the soma and all neuronal fibers. The average neuronal size depends on the diameter of the fibers, the connectivity index and the connectivity rules. The more long range connections there are the more the average neuronal size will be increased. Yet, in a bigger brain distances are increased and one might assume that the average axonal length would be increased too. In addition, connections between neurons are achieved by cortical fibers, and connection speed depends

on their conduction velocity as well as the distance between neurons (Roth and Dicke, 2005). Conduction velocity is mostly determined by the diameter of myelinated fibers, if distances increase the diameter of fibers should also increase to keep an acceptable speed of information flow. How do axonal length and diameter scale with brain size? Are the scaling rules different in rodent and primates?

A previous study had investigated how white matter scales with gray matter. They found a universal scaling rule between the volumes of the white and gray matter (Zhang and Sejnowski, 2000). However, as previously described brain size and volume are not directly indicative of neuron numbers especially across clades. Ventura-Antunes et al. investigated directly the scaling of the white matter with neuron number in 6 rodent and 10 primates species (Ventura-Antunes et al., 2013). They took advantage of the cell numbers previously determined by isotropic fractionator (Herculano-Houzel et al., 2006, 2008, 2010). On the other hand, they measured by histological analyses and surface or volume reconstructions the volume of the white and gray matter as well as their surface area - the surface of the white matter being the interface between white and gray matter. Although the volume of the white matter increases in rodents as predicted by an isometric volume expansion, in primates the white matter volume increases less than expected. They established that rodent white matter volume increases more rapidly with neuron number than in primates. The authors then investigated whether this increase in white matter volume was due to an increased total axonal length and/or an increased axonal diameter. Their data suggests that the total axonal length and the axonal caliber increase faster with neuron number in rodents than primates. Moreover, the cortical connectivity through the white matter decreases in primate species whereas it remains constant in rodents as neuron numbers increase (Kennedy et al., personal communication). As a result, a much larger proportion of neurons are connected throughout the white matter in rodents than primates. On the other hand, big brains are usually folded. The folding process enables the fitting of a larger surface in a given volume and consequently reduces distances between cortical areas. The folding process can potentially reduce axonal distances. The authors found that cortical folding increases more rapidly with gray matter volume and number of neurons in primates than rodents (Ventura-Antunes et al., 2013).
Those results support the fact that when neurons are added to a rodent brain, the neuronal density decreases, the cortical connectivity is unchanged, the average axonal caliber is increased, the white matter volume increases rapidly and cortical folding increases

slowly. On the contrary when neurons are added to a primate brain, the neuronal density remains constant, the cortical connectivity decreases, the average axonal caliber is unchanged, the white matter volume increases slowly and cortical folding increases rapidly. These differences lie in the scaling of the white matter and seem to be at the basis of the economical addition of neurons in the primate brain (Ventura-Antunes et al., 2013). This suggests that the way brains are wired is intricately linked to the ability to build a bigger and more efficient brain. The volume-saving scaling of the white matter has functional consequences. The propagation time is not too much increased and computational capacity can be estimated to scale more in primates than rodents as the number of cortical neurons increases across species.

Metabolism: a limiting factor of brain increase

How is brain size regulated? The brain is the third most energy-demanding organ of the body behind skeletal muscles and the liver (Aschoff, 1971). The brain consumes from 5% of the available energy in small mammals like mice, up to 13% in gorillas and 20% in humans although it composes less than 2% of the body mass. Increasing brain size implies a trade-off between energy cost and advantage of higher cognitive functions. There are two ways of increasing the amount of available energy: more intake or change in energy allocation.

In mammals, large brains are associated with big body size. However, humans have the largest brain and number of neurons although they do not have the largest body mass. Great apes can be up to three times bigger than humans but have three times fewer neurons than humans (Herculano-Houzel and Kaas, 2011). The authors postulate that having a large body and a large brain are mutually exclusive. They justify their claim by referring to differences in energy allocation. Indeed great apes dedicate more energy to their locomotion and so less is available for the brain. Fonseca-azevedo et al. proposed a model in which the type of diet and the limited feeding time are limiting factors for brain increase (Fonseca-Azevedo and Herculano-Houzel, 2012). They argue that the discovery of fire, which enabled the transition from a raw food diet to a cooked diet, was a necessary step in the human brain expansion. The higher caloric cooked diet reduced time spent feeding and allowed more free time where higher cognitive abilities could be developed.

Qualitative differences in primate cerebral cortices: specific growths, new types of neurons

The previously mentioned studies investigated the general scaling rules of the brain and the cerebral cortex without taking into account potential specific laminar or the tangential increases in primate cortices.

Beside a general tangential enlargement of the cortical sheet, tangential growth did not occur isotropically in primate brains. Although there is a common organization map of sensory cortical areas, some areas like MT (media temporal) in the visual system appeared during primate evolution. In addition, the contribution of the sensory related areas to the whole cerebral cortex decreases in higher primates (Krubitzer et al., 1998; Krubitzer, 2007). Primates also have a particularly developed prefrontal cortex involved in executive control of behavior (figure 1.6 A). However, contrary to the traditional view of a disproportionally large frontal cortex in humans, often considered to be the basis of our uniqueness, a recent study did not find a special expansion of the human prefrontal cortex compared to great apes (Semendeferi et al., 2002).

Compared to the other orders, the primate cortex is characterized by an overrepresented supragranular layer neuron compartment (layers 2 and 3, Figure 1.6B), where neurons are dedicated to the transfer of information between cortical areas (Marin-Padilla, 1992). A number of features of the supragranular layer neurons suggest that these layers play an important role in the evolution of the cortex. For instance they express high levels of genes associated with long-term potentiation and calcium signaling reflecting the considerable plasticity found in these layers (Figure 1.6, (Bernard et al., 2012)).

Primate brains and especially human brains also contain several types of neurons that have not been described or are rarely found in other species. The spindle cells, specialized deep-layer neurons, were first found unique to primates (von Economo and Koskinas, 1929; Allman and Hakeem, 2002) before being also identifies in the large brains of cetaceans and elephants (Butti et al., 2009; Hakeem et al., 2009). The human brain possesses high numbers of a subtype of interneurons: the double-bouquet cells, which reach their highest degree of development in primates (DeFelipe, 2011). The ratio of interneurons over the total number of cortical neurons is higher in primates. Interneurons account for 25 to 30% of all cortical neurons in primates and exhibit areal and laminar differences (Hendry et al., 1987) whereas they are thought to compose only 15 to 20% in rodents (Beaulieu, 1993).

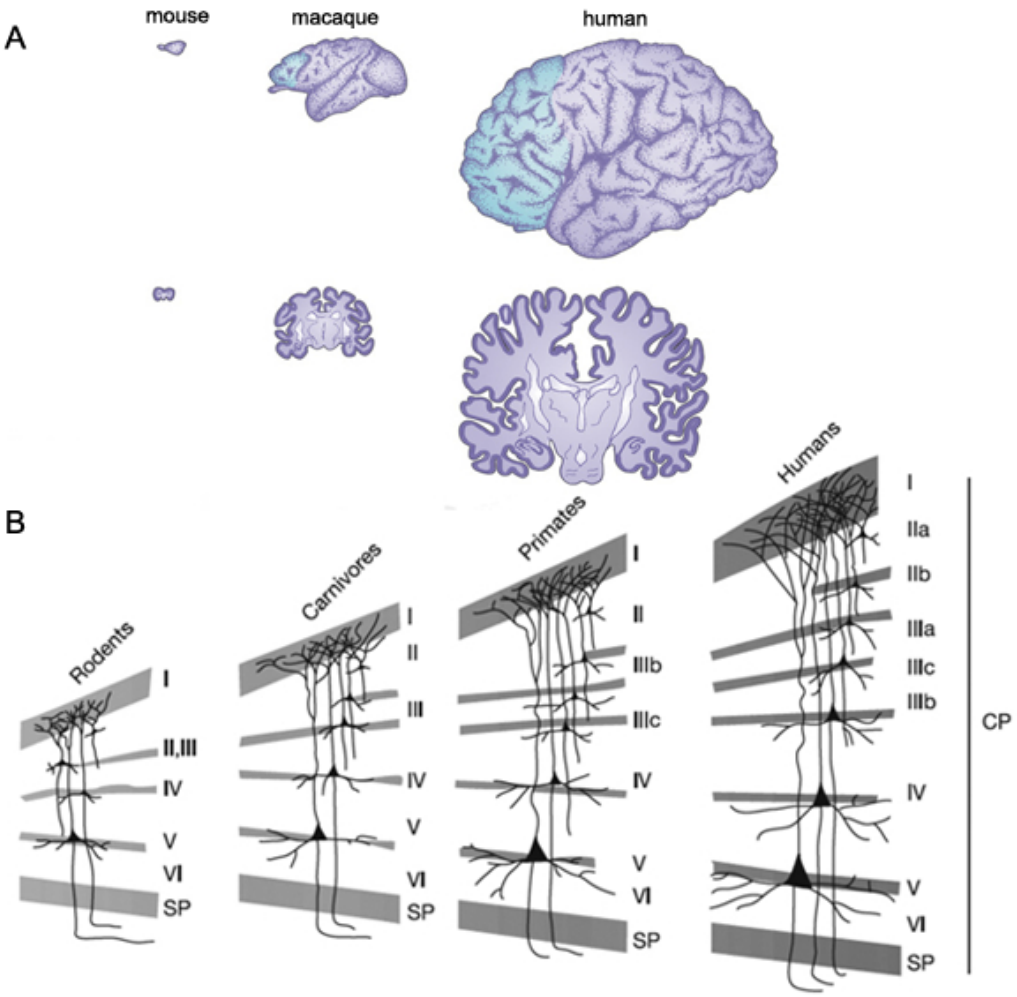

Figure 1.6. Tangential and radial expansion of the cortex with a specific enlargement of the frontal lobe and the supra granular layer neurons. Adapted from (Rakic, 2009) and (Hill and Walsh, 2005).

The blueprint of the primate brain allows a scaling of the number of neurons at a minimum volume and mass cost thanks to a limited connectivity achieved by a more local network with few long range connections and a limitation of axonal length by an appropriate folding of the cortical surface. As the distances between cortical areas are minimized, the diameter of the axonal fibers does not need to increase too much to keep a decent information flow speed. The primate brain can thus contain more neurons, more processing units

with a good information flow and thus allow higher cognitive abilities. The cost of the dramatic increase of neurons in the human lineage was probably compensated for by human energetic uptake adaptation.

These observations of different scaling rules across mammalian orders suggest differences of developmental processes. It means that there are not only quantitative differences during brain development but that there are also some qualitative differences that appeared after the divergence of the different orders. As proportionally fewer neurons connect through the white matter in primates, one can expect different overall networks in primates and rodents with a higher local connectivity. This might also mean that the connectivity rules that govern axonal growth and network building are different in primates and rodents. These qualitative differences allow the production of more neurons during development and thus imply differences in regulation of neuronal precursor pools. To better highlight primate specificities during cortical development, we will first review in the next section some relevant findings known from the rodent model. We will then focus in the last section of the introduction on some specificities that have already been identified in primate cortical development.

1.2 Corticogenesis: lessons from rodent models

The neocortex develops from the most rostral region of the nervous system called the proencephalon. The proencephalon can be further divided into the telencephalon and the diencephalon.The diencephalon gives rise to the retina and the thalamus, whereas the telencephalon generates the olfactory bulb (rostrally), the corpora striata (ventrally), the hippocampus (dorso-medially from the cortical hem) and the neocortex (dorso-laterally) (Price and Willshaw, 2000). Here, we will focus on the formation of the neocortex. The next section will review some principal findings about rodent corticogenesis, mainly from the mouse model.

1.2.1 Overview of mouse cortical development

From a uniform sheet of neural stem cells, the neuroepithelial cells, different cortical areas will emerge. Each area has a given surface, with a specific cytoarchitecture, that is with a specific number of neurons in the different layers. There is therefore a coordinated growth

both in surface and thickness that leads to the formation of the different cortical areas.

Corticogenesis can be divided in two phases. The first phase, from the closure of the neural tube at E8 to E11, corresponds to an amplification phase in which the pool of neuroepithelial precursors is expanded by symmetric proliferative divisions in the ventricular zone (VZ). The second phase is the neurogenic phase, from E11 to E18 in the mouse, where excitatory cortical neurons are produced. Neuroepithelial cells start to differentiate into radial glial cells (RGCs), which switch to an asymmetric mode of division. The first neurons produced by RGCs at E11.5 are the Cajal Retzius cells that form the prelate and secrete signal that will guide later neuron migration (Figure 1.7). At E12.5, VZ precursors start to produce a second type of precursors that divide basally and accumulate in the sub ventricular zone (SVZ). These two proliferative zones produce, in a coordinated manner, all the excitatory neurons of the cortex that migrate radially along the RGCs radial fibers to settle in the cortical plate (CP), which will become the 6-layer cortex (reviewed in (Dehay and Kennedy, 2007)). Interneurons are produced in the ventral telencephalon structures called ganglionic eminences and reach the cortex by tangential migration (Wonders and Anderson, 2006)(see section 1.3.3 for more details).

The cortical layers are produced in an inside-out fashion (Angevine and Sidman, 1961). Layer 6 neurons are produced first and settle in the deep layers of the cortex, later produced neurons migrate past the already generated neurons and settle on top (Section 1.2.3). The arrival of the first layer 6 neurons at E14 forms the beginning of the CP that splits the preplate into the marginal zone (MZ), later layer 1, and the sub plate (SP) (Boulder Committee, 1970), a transient structure in the mouse serving as scaffold and guide for cortico-thalamic connections. From E14 on, neurogenesis peaks and the proliferative zones become depleted. Gliogenesis starts at E18 and continues during the first postnatal month.

In the following sections, we will briefly review the concepts of cortical area specification (Section 1.2.2) and the inside out generation of the neuronal layers (Section 1.2.3). We will then focus on the cortical proliferative zones and describe the diversity of cortical precursors identified in mice, and their lineage relationships leading to the generation of cortical excitatory neurons (Section 1.2.4).

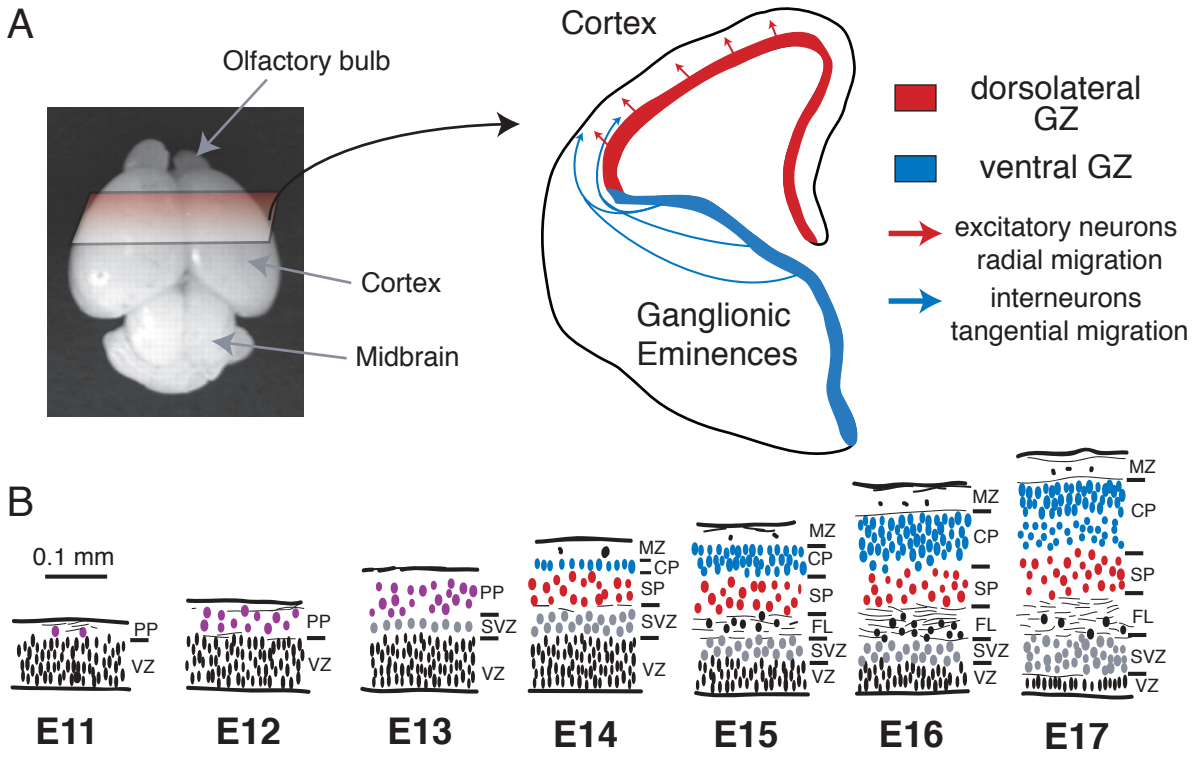

Figure 1.7. Overview of mouse corticogenesis. **A.** Picture of an embryonic mouse brain at E15 and schematic representation of a coronal section in the cortex showing the origin and migration routes of excitatory neurons and interneurons. **B.** Schematic representation of transects of the mouse cortex at different developmental stages spanning the period of cortical neurogenesis. VZ: ventricular zone, SVZ: sub ventricular zone, PP: prelate, IZ: intermediate zone, SP: subplate, CP: cortical plate, MZ: marginal zone, FL: fiber layer. Adapted from (Smart et al., 2002).

1.2.2 Specification of the cerebral cortex territories

The cortex is a highly complex structure formed by a multitude of cortical areas occupying a particular cortical surface and with a specific cytoarchitecture. This structure arises from a homogeneous sheet of neuroepithelial cells. Several theories have been put forward that explain the specification, and the formation (tangential expansion and specific cytoarchitecture) of cortical areas.

In the late 1980s, two influential and opposing theories were proposed: the *protomap* and the *protocortex*. The *protocortex* theory postulates that the neural plate remains a

homogeneous structure long during development. Regionalisation/arealisation occurs only when signals from subcortical structures reach the cortex (O'Leary, 1989). This hypothesis relies especially on the influence of thalamocortical axons (TCA) on cortical development. TCA display area-specificity during development and parallel CP differentiation. In the mouse, the role of TCA was uncovered by studies on the emergence of the barrel field in the somatosensory cortex (Van der Loos and Woolsey, 1973). Each vibrissae is isomorphically represented in the somato-sensory cortex. The formation of the barrel field is controlled by TCAs innervation of layer IV. The loss of a vibrissa results in the reorganization of the barrel field map (Woolsey and Wann, 1976). These pioneering experiments and other studies (Dehay et al., 1996, 1993) demonstrated the role of sensory peripheral inputs in shaping the cortex (Kennedy and Dehay, 1993).

However, early regional differences can be observed. The *protomap* theory states that regional differences appear early during development in response to patterning centers located at the edges and midline of the telencephalic vesicles (Figure 1.8, reviewed in (Borello and Pierani, 2010)). Patterning centers secrete morphogens in a graded and regional fashion that determine the cortical map formation by controlling the regional proliferation, differentiation, migration and apoptosis (Rakic, 1988; Sur and Rubenstein, 2005). Morphogen gradients generated by patterning center results in the differential expression of key transcription factors (Pax6, Emx2, Coup-TF1 and SP8). The combination of the expression level of these different transcription factor determines a positional information within the neuroepithelium that will orchestrate a particular growth and eventually lead to the formation of different cortical areas (Borello and Pierani, 2010).

The two hypotheses for cortical arealization were first considered mutually exclusive. However, recent data suggest that the *protomap* leads to the formation of a prespecified cortex that is refined by extra cortical input as predicted by the *protocortex* theory (Sur and Rubenstein, 2005; Dehay and Kennedy, 2007).

1.2.3 Inside-out generation of the cortical layers

The laminar structure of the cerebral cortex has been discovered by pioneer anatomists in the early 20th century but how this laminated structure is put together during development remained elusive until 1961. It was already known at that time that proliferation occurs close to the ventricular surface, away from the CP where neurons settle and then

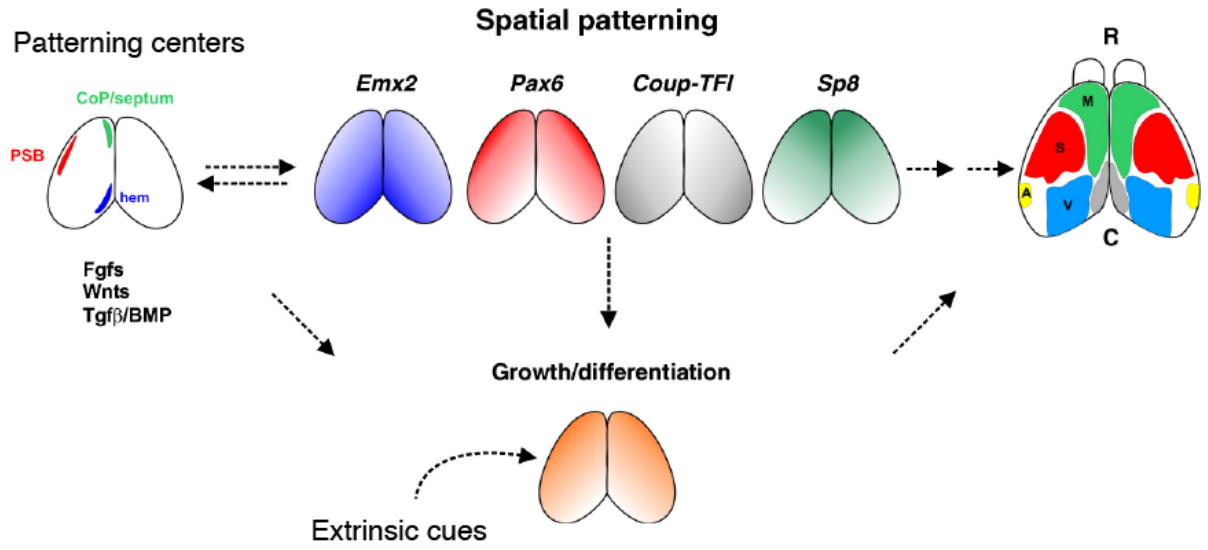

Figure 1.8. Mechanism for cortical realization: intrinsic and extrinsic influences. Patterning centers are established early during development and secrete morphogenes that regulate the graded expression of specific transcription factors (Emx2, Pax6, Coup-TF1 and SP8). These transcription factors establish an early regionalization of the cortex and control the proliferation and differentiation of cortical precursors. Extrinsic factors coming from the meninges and ingrowing vasculature and fibers play also a role in the arealization process. The direct relationships between these different steps remain elusive. Fgf8 is expressed at the rostral patterning center(CoP), Wnts and Tgfs/BMP by the hem. CoP: commissural plate, PSB: pallial-subpallial boundary, hem: cortical hem, R: rostral, C: caudal, M: frontal/motor area, S: somatosensory area, A: auditory area, V: visual cortex. Adapted from (Borello and Pierani, 2010).

form the 6-layered cortex. However, the timing of generation of the different layers and the question of neuronal migration were still open. Angevine and Sidman gave a first answer to the lamination process (Angevine and Sidman, 1961). They made use of the radioactive tritiated thymidine that is incorporated in S-phase of the cell cycle by cortical precursors and inherited by their progeny. Tritiated thymidine can be detected by autoradiography to trace back the origin of the different neuronal layers. The authors performed pulses of triatiated thymidine at different stages of mouse corticogenesis. They found that pulses performed at early neurogenesis label neurons in deep layers of the cortex and neurons labeled by pulses at later stages populate the more superficial layers. From those results Angevine and Sidman proposed the model of the inside out generation

of the cortical layers whereby the newly generated neurons migrate passed the already formed neuronal layers to settle at the top in the CP (figure 1.9). There is an exception to the inside out generation of the cortical layers, namely layer 1. The first neurons produced generate the preplate which is split by the arrival of layer 6 neurons into the subplate and the marginal zone that will become layer 1 and will always be the most superficial cortical layer (Valverde et al., 1995).

The mechanisms involved in the inside out lamination of the cortex were initially discovered by the study of a spontaneous mutant mouse: the reeler mutant (Falconer, 1951). These mice that have defects in motor functions are characterized by ataxia and reeling gate. Among others, they display malformations in the cortex with an inversion of the different layers and the border between layers are not as sharp as in wild type animals. Caviness et al. showed that the order of layer generation was not affected but that the layers were formed in an outside in fashion. The newly born neurons failed to bypass the previously generated neurons (Caviness and Sidman, 1973). The defective gene was identified in the 90s and called reelin (see for review (D'Arcangelo and Curran, 1998)). Reelin in a extracellular matrix glycoprotein secreted by the Cajal-Retzius cells in the marginal zone. Many contradicting theories exist concerning their role in lamination. It has been proposed to be a chemoattractant, or repellant for migrating neurons as well as a stop or detachment signal from radial glial fibers. More recent studies suggest that reelin influences non radial guided migration of neurons at the very end of their radial migration. Nadarajah et al. demonstrated by live-imaging that the last step of radial migration in the upper cortical plate was achieved by somal translocation (Nadarajah et al., 2001). Migrating neurons send their leading to the marginal zone and perform somal tranclocation. Franco et al. showed that this step is impaired in the reeler mutant suggesting that reelin stimulates detachment from radial glial fibers and glia independent somal translocation (Franco et al., 2011).

The inside out generation of cortical layer is not the most intuitive mechanism that one would have thought about for cortical lamination. In reptiles, which have a 3 layered cortex, the generation of the layers is outside in (Goffinet et al., 1986) Some other structures of the brain, like the dentate gyrus, display an outside in layer generation (D'Arcangelo and Curran, 1998). Why was this inside out layer generation selected in mammalian cortices? One hypothesis is that the upper layers, the supra granular layers involved in cortico-cortical connections and local circuits could have a direct access to

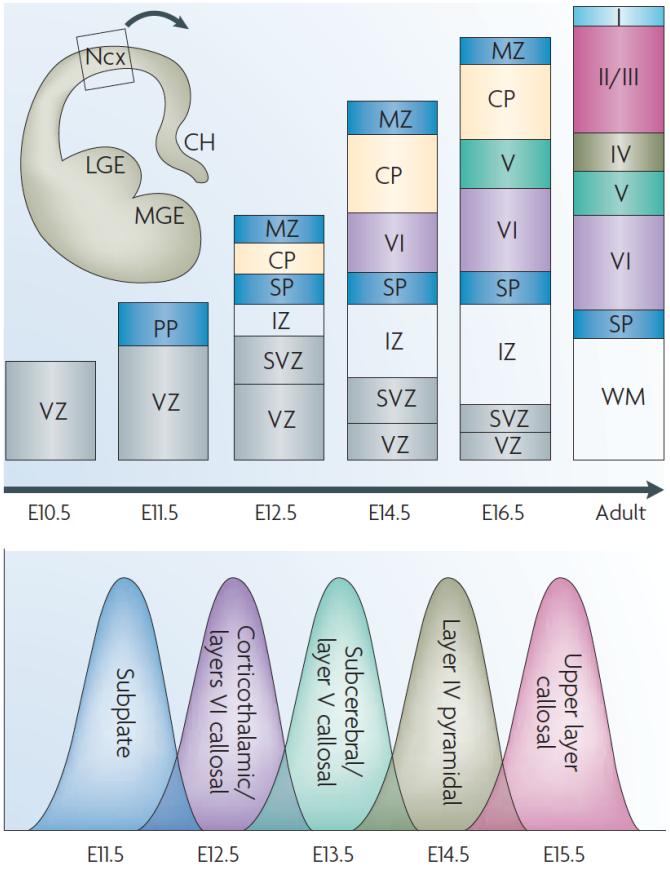

Figure 1.9. Temporal regulation of the birth date of the different cortical layers. Ncx: neocortex, CH: cortical hem, LGE: lateral ganglionic eminence, MGE: medial ganglionic eminence, VZ: ventricular zone, SVZ: sub ventricular zone, PP: prelate, IZ: intermediate zone, SP: sub plate, CP: cortical plate, MZ: marginal zone, WM: white matter. Figure from (Molyneaux et al., 2007).

layer 1 and axonal afferents (Aboitiz, 1999).

1.2.4 Origin of excitatory neurons

During rodent cortical development, neurons are produced conjointly by two proliferative zones: the ventricular zone (VZ) and the subventricular zone (SVZ). Each of these two zones contains specific types of precursors and generates specific neuronal types that reach the cortical plate by radial migration.

Ventricular zone: apical precursors

The VZ lines the lateral ventricles. VZ precursors are called apical precursors (AP) because they divide at the apical border of the ventricular surface. They comprise neuroepithelial cells, radial glial cells (RGCs), and short neural precursors (SNPs, Figure 1.10). APs first compose of a monolayer of neuroepithelial cells that expand tangentially in surface and in thickness to become a pseudo-epithelium (Williams and Price, 1995; McCarthy et al., 2001). From E12 to E14 neuroepithelial cells differentiate into RGCs that start to generate neurons by asymmetrical divisions (Götz and Huttner, 2005; Sahara and O'Leary, 2009). RGCs are elongated precursors with processes spanning the whole cortical thickness from the ventricular surface to the pial membrane important for radial migration of excitatory neurons. An extra AP type has recently been described: the SNPs. They are attached to the ventricular surface but have a short basal process that does not reach the pial surface (Gal et al., 2006).

All AP nuclei undergo a stereotyped movement of their nuclei in phase with the cell cycle called interkinetic nuclear migration (INM) (Sauer, 1935). Mitosis occurs at the ventricular surface, the nucleus migrates towards the basal side of the VZ during G1 phase, S phase is performed at the very basal side of the VZ and the nucleus moves back to the apical side of the VZ during G2 to divide at the ventricular surface. The RGCs were long considered as a mere scaffold guiding the radial migration of neurons toward the cortical plate but they were discovered as being neural stem cells by Magdalena Götz and Arnold Kriegstein groups (Malatesta et al., 2000; Noctor et al., 2001). RGCs and SNPs express specifically the transcription factor Pax6 that controls their mode of division (Götz et al., 1998; Warren et al., 1999; Quinn et al., 2007; Georgala et al., 2011). SNPs were initially shown to specifically drive Tα1 promotor activity (Gal et al., 2006) but a more recent study from the same group noted that RGCs can also drive Tα1 promotor activity. The authors redefined more precisely SNPs as APs driving Tα1 promotor activity but not Glast and Blbp promoters specific of RGCs (Tyler and Haydar, 2013).

Subventricular zone: basal progenitors

Mitoses in an abventricular location in the SVZ had been already noted by histologists in the late nineteenth century (Schaper 1897; His 1889). These precursors were however thought to contribute only to gliogenesis (Altman and Bayer, 1990). Time-lapse video

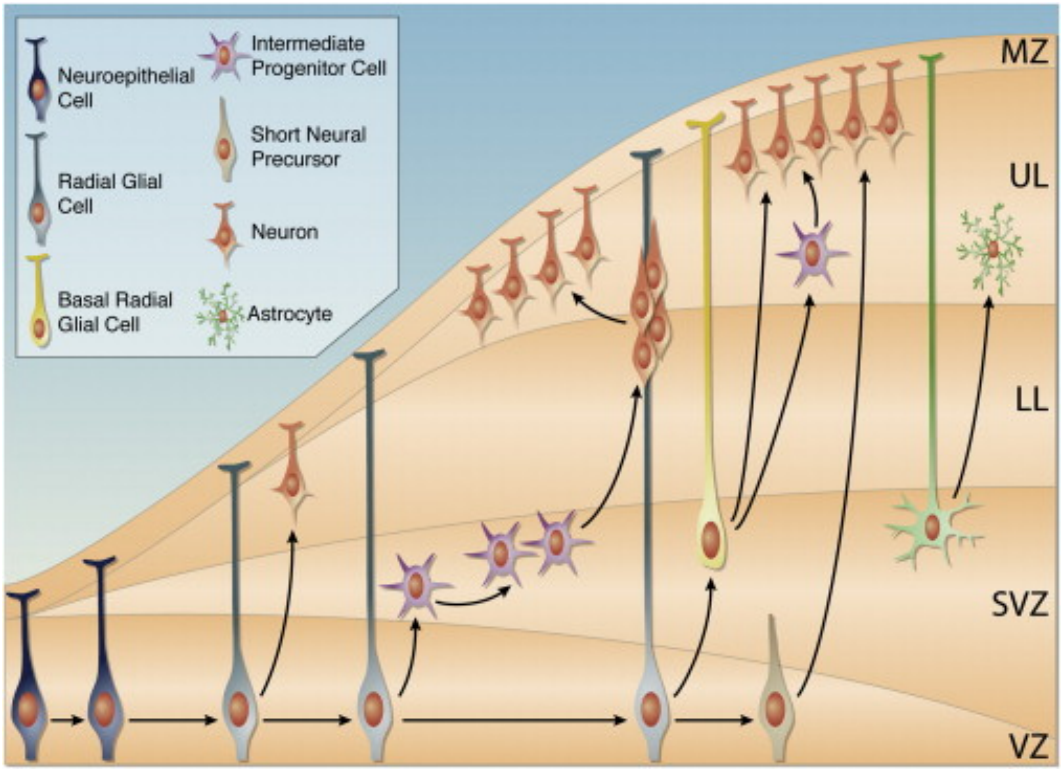

Figure 1.10. Different precursor types identified in the mouse cortical germinal zones. The x-axis represent time from E11 to E18. VZ: ventricular zone, SVZ: subventricular zone, LL: lower layer neurons, UL: upper layer neurons. Figure from (Franco and Müller, 2013).

microscopy (TLV) experiments enabled the direct assessment of SVZ precursors fate and gave the definite proof that they are highly neurogenic (Haubensak et al., 2004; Noctor et al., 2004; Miyata et al., 2004). SVZ multipolar precursors are generated by RGCs (Figure 1.10) and express the transcription factor Tbr2 (Englund et al., 2005). SVZ precursors have been called intermediate progenitors (IP) or basal progenitors (BP). In this thesis we will use the term BP to refer to all precursors dividing basally and reserve the term IP to the initially observed multipolar SVZ precursors.

Diversity of rodent cortical precursors

RGCs seemed to be a homogeneous population of neural stem cells characterized by their peculiar morphology and the expression of Pax6. Recent studies however point

to a significant heterogeneity of RGCs and have better characterized SNPs. RGCs are heterogeneous concerning their antigenic reactivity (Hartfuss et al., 2001). Pinto et al. found two subtypes of RGCs based on the GFP intensity driven by the hGFAP promotor which correspond to different lineages (Pinto et al., 2008). One subtype is specific to direct neurogenesis, the second subtypes generates basal progenitors and thus contributes to indirect neurogenesis. SNPs drive the expression of the Tα1 promotor but not of BLBP and Glast promoters, RGC specific transcription factors (Gal et al., 2006; Tyler and Haydar, 2013). Beside their morphological and molecular differences compared to RGCs, SNPs also display different cell cycle kinetics and lineages. They indeed have been shown to have a longer G1 phase and to mostly generate neurons directly at midneurogenesis whereas the majority of RGCs indirectly generate neurons via an IP step in the SVZ (Stancik et al., 2010). SNPs might thus be a subpopulation of the APs identified by Pinto et al. as responsible for direct neurogenesis, however the SNPs ability to drive the hGFAP promoter expression has not been assessed yet. The results by Stancik and colleagues need however to be reassessed because they studied all APs driving Tα1 promotor activity, and thus included a subset of RGCs.

Some recent studies have described a variety of BP in the mouse developing cortex. They never perform mitosis at the ventricular surface but can divide not only in the SVZ but also in the VZ and above the SVZ (Figure 1.11 provides a summary of the different mouse cortical precursors identified). IPs were the first type described in the SVZ with their characteristic multipolar morphology and specific expression of the transcription factor Tbr2 (Englund et al., 2005). Other studies by Hevner's group further showed a subtype of Tbr2+ IP that is radially oriented and can divide in the middle or the basal part of the VZ (and in some rare cases can even divide apically). They keep an apical anchor to the ventricular surface which potentially provides feedback signals on APs (Kowalczyk et al., 2009; Nelson et al., 2013). These precursors have been called IPvz and are different from SNPs by their molecular signature, they are Tbr2+ and not Pax6+, and have been shown to participate to different lineages (Tyler and Haydar, 2013; Nelson et al., 2013).

Another type of BPs: the basal Radial Glial-like cells (bRG) had first been described in human and ferret developing cortices (see section 1.3.5) (Fietz et al., 2010; Hansen et al., 2010; Reillo et al., 2011). bRGs have then also been found in rodents albeit at a much lower frequency (Shitamukai et al., 2011; Wang et al., 2011; Martinez-Cerdeno et al., 2012; Tyler and Haydar, 2013; Nelson et al., 2013). bRGs retain some epithelial features

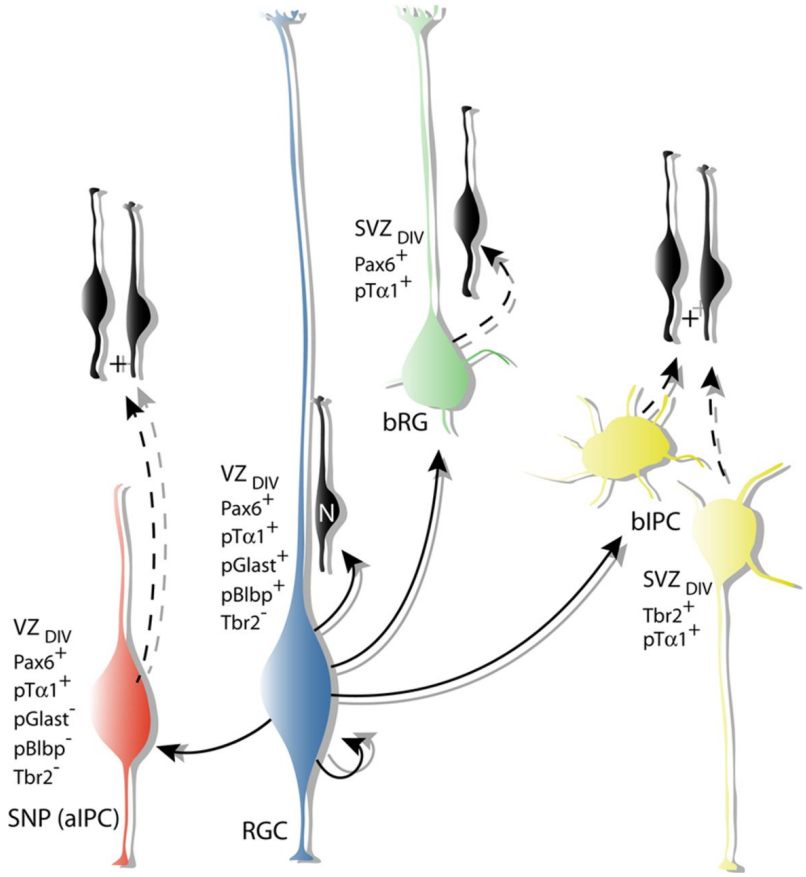

Figure 1.11. The different types of mouse cortical precursors and their lineage relationships at mid-corticogenesis. Figure from Tyler and Haydar, 2013.

characteristic of RGCs. They have a long basal process that reaches the pia membrane, but lack a substantial apical process. They express some RGCs specific markers (Pax6, Sox2, Nestin, GFAP) but not the apical polarity proteins (Par3, Prominin, aPKC and ZO-1) (Fietz et al., 2010; Hansen et al., 2010). bRGs undergo a basally directed movement at mitosis that enables them at each division to move more basally, potentially reducing the distance to migrate for post-mitotic neurons. They divide in the SVZ and also above in the disperse mitotic compartment (DMC) (Tabata et al., 2009; Smart, 1973).

A refinement of neuronal lineages

Fate map studies taking advantage of mouse line expressing the Cre-recombinase under the control of RGC specific promoters (Malatesta et al., 2003; Anthony et al., 2004)

found that all excitatory neurons derive from this cell type. However, with the profusion of recently identified precursor subtypes, one can imagine that the lineages from RGC to neurons can be complex and diverse.

TLV analyses have determined that RGCs can give rise to IP both in the SVZ and the VZ (Haubensak et al., 2004; Noctor et al., 2004; Miyata et al., 2004; Kowalczyk et al., 2009) and can also directly generate neurons (Miyata et al., 2001; Noctor et al., 2001). RGCs generate bRGs by delamination after an oblique or horizontal division (Shitamukai et al., 2011; Wang et al., 2011; Martinez-Cerdeno et al., 2012). IPs have been shown to mostly divide symmetrically generating two neurons (Haubensak et al., 2004; Noctor et al., 2004; Miyata et al., 2004) and to extremely rarely self-renew (Wu et al., 2005).

A recent elegant study using multiplex fate mapping revealed a variety of lineages leading to cortical neuron generation (Tyler and Haydar, 2013). This new fate mapping technique allowed the dissection of the different lineages of VZ and SVZ precursor subtypes and the establishment of their hierarchical relationships. The authors demonstrated that RGCs, beside directly generating neurons, have three pathways of amplification by indirect neurogenesis: via the IPsvz and IPvz cells Tbr2+, via the bRGs Pax6+ dividing basally and via the SNPs Pax6+ dividing apically (Figure 1.11). The quantitative importance and the type of neurons produced by the 4 neuronal parthways have not been assessed yet and might also vary depending on the developmental stage. The SNP origin and self-renewing abilities are still elusive. Whether SNPs can generate IP remains an open question.

A new bipolar progenitor type (SubApically Progenitor, SAP) has recently been identified in the ganglionic eminences (Pilz et al., 2013). SAPs divide in the middle of the VZ. They keep an apical anchor to the ventricular surface and a basal process of varying length. SAPs are extremely rare in the cortex and were shown to participate to precursor amplification in the ganglionic eminences. TLV analyses established that they arise by RGC divisions and give rise to bRGs, playing a role of intermediate between these two types. This GE specificity underlines the possibility of regional lineage particularities in different regions of the brain. Their role in cortical evolution has not be assessed yet even though bipolar progenitors have been detected in the ferret (Pilz et al., 2013).

Specific lineages for supra and infra granular layer neuron generation?

Numerous observations link production of infragranular layers to VZ precursors and SVZ precursors to production of supra granular neurons. Although SVZ precursors are thought to be derived from VZ precursors, there are clear differences in gene expression between the two precursor pools and these differences correlate with distinct neuronal progeny. For instance, Otx1 and Fez1 are both expressed in VZ precursors and are then subsequently up-regulated in subsets of deep-layer neurons and down-regulated in the SVZ (Arlotta et al., 2005; Chen et al., 2005; Frantz et al., 1994; Molyneaux et al., 2005). Recent studies in mice showed that several transcription factors (Cux2, Tbr2, Satb2, and Nex) (Britanova et al., 2005; Nieto et al., 2004; Zimmer et al., 2004; Wu et al., 2005), as well as the noncoding RNA Svet-1 (Teissier et al., 2011), are selectively expressed in both the SVZ and supra granular layer neurons. Moreover, upper layer defects have been noted in Cux2 (Cubelos et al., 2008) and Tbr2 (Sessa et al., 2008; Arnold et al., 2008) knock-out mice. The observation that a larger SVZ is correlated with increased upper-layers during evolution is another argument in favor of the lineage relationship between SVZ and supra granular layer neurons (Martinez-Cerdeno et al., 2006; Cheung et al., 2007; Pilaz et al., 2009).

However, evidence suggests that IPs contribute to all layers of the neocortex. Tbr2 positive mitoses are observed as early as E10.5 (Englund et al., 2005; Kowalczyk et al., 2009). Tbr2 conditional knock-out mice display defects of all cortical layer (Sessa et al., 2008; Arnold et al., 2008). Kowalczyk and colleagues using the *Tbr2::GFP* transgenic mouse line that GFP inherited from IPs could be seen in all cortical layers. Moreover, taking advantage of the *Tis21::GFP* knock-in mouse line (Iacopetti et al., 1999; Haubensak et al., 2004) reporter of neurogenic divisions, they also showed that the majority of neurogenic mitoses are Tbr2 positive (Kowalczyk et al., 2009).

Beside the possibility that IPs contribute neurons to all cortical layers, there is an alternative, rather speculative, explanation to the fact that Tbr2 KO mice have defects in all cortical layers and that the *Tbr2::GFP* transgenic mouse line shows GFP expression in neurons of all layers. Tbr2 could be involved in the delamination of all cells from the VZ epithelium, that is, expressed and required in delaminating IPs that will divide in the SVZ, but also in delaminating post-mitotic neurons generated by RGCs. Tbr2 (also known as Eomesodermine) was first identified in the early embryo as being crucial for the epithelio-mesodermic transition (Russ et al., 2000). In the Tbr2 mutant, mesodermic cells

fail to delaminate and to leave the epiblast epithelium. There is also evidence that all Tbr2 expressing cells might not be proliferative in the cerebral cortex (Puzzolo and Mallamaci, 2010; Pilaz et al., unpublished observations). Some Tbr2 positive cells were found in the opossum developing cortex in an abventricular location. However, these Tbr2 positive cells did not incorporate BrdU neither 1 hour, nor 12 hours after a pulse suggesting that there are young post-mitotic neurons (Puzzolo and Mallamaci, 2010). Tbr2 expression might be needed to allow the correct delamination of IPs and RGC produced neurons from the VZ. One can hypothesize that in the Tbr2 KO, the delamination of both neurons and IPs from the VZ is affected and result therefore into defects in all cortical layers. If neurons produced by RGCs transiently express Tbr2, GFP expression in the *Tbr2::GFP* transgenic mouse line will not be specific for IPs, GFP neurons in the cortical plate might thus derive directly from RGCs. Compensatory mechanisms for VZ delimitation cannot be excluded since in Pax6 KO mice, abventricular mitotic figures can still be observed despite the almost total absence of Tbr2 expression in these cells (Quinn et al., 2007).

These are still very indirect proofs in favor or against the relationship between SVZ and supra granular layer generation. More refined fate mapping studies enabling the delineation of the progeny of the different VZ and SVZ subtypes are still needed to resolve this issue.

Committed precursors in the developing cortex?

Although it is well established that all excitatory neurons derive from cortical RGCs, the lineages leading to the different neuronal types are still elusive. Are the lineages composed of multipotent progenitors that successively give rise to all types of neurons and then glia (Figure 1.12A.), or are there precursors intrinsically programmed to generate a given neuronal type (Figure 1.12B.)?

Pioneer transplantation studies in the ferret cortex have demonstrated that neural precursors become restricted in their ability to generate neuronal types as development proceeds (McConnell and Kaznowski, 1991). Early precursors grafted in a late developing cortex are able to change their initial fate (deep-layer neuron) to become the neuronal types generated in the host (upper-layer neuron). On the other hand, late precursors grafted in a younger host failed to change fate and gave rise to upper-layer neurons. This study demonstrated that although cortical precursors seem to be initially multipotent, their competence is progressively restricted. Environmental cues appear to be crucial in

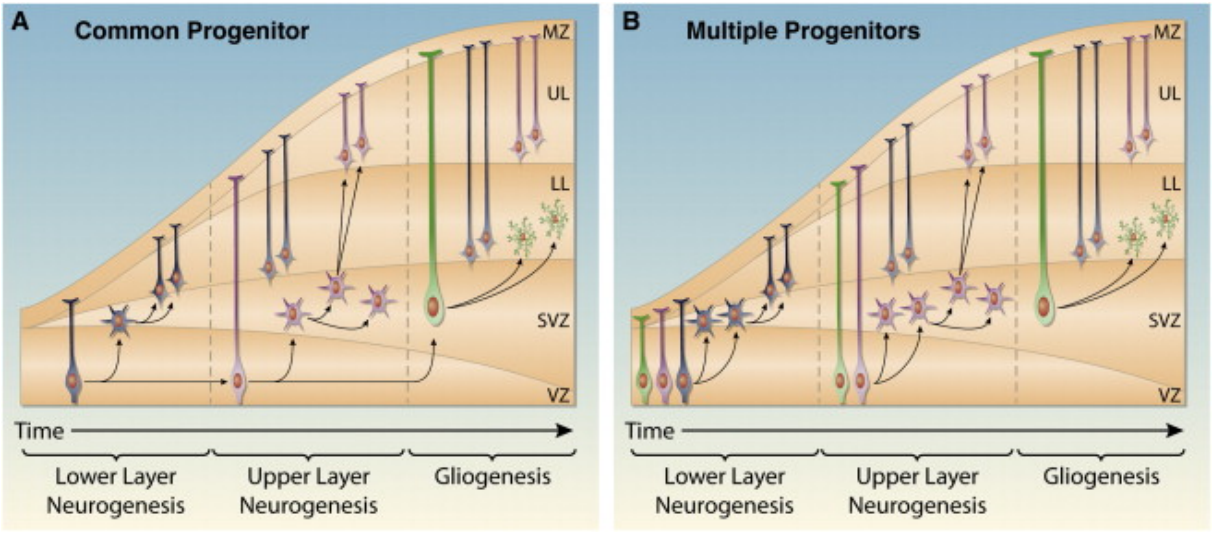

Figure 1.12. Hypotheses of lineages leading to the generation of cortical neurons. **A.** Hypothesis of a common multipotent precursor that sequentially generates all neuronal types. **B.** Hypothesis supposing the coexistence of multiple committed precursors in the VZ. Each precursor type will generate only lower layer neurons (LL), upper layer neurons (UL) or astrocytes. Figure from (Franco and Müller, 2013).

the fate determination of neural precursor progeny. Along the same line, *in vitro* TLV analyses showed that neural stem cells generate the different neuronal type in the right order and timing without environmental information (Shen et al., 2006). These experiments show that intrinsic genetic networks control the sequence of neuronal generation by multipotent precursors and that their birthdate determines the neuronal fate (Figure 1.12A.).

These studies have to be put in the context of the diversity of precursor types identified in the mouse germinal zones. Cortical neurons are produced by a mosaic or precursors (see section 1.2.4). A recent study calls for the reevaluation of the temporal restriction hypothesis. By specific fate mapping, Franco and colleagues identified a subset of RGCs expressing the transcription factor Cux2 that are committed early during development to the generation of only supra granular layer neurons (Franco et al., 2012). The authors support the vision that during early corticogenesis, precursors restricted to lower and upper neuron generation coexist in the VZ (Franco and Müller, 2013). Lower layer committed precursors start generating neurons via direct or indirect neurogenesis whereas upper layer fated precursors continue expanding during this period. The correlation between birth-

date and neuronal type would thus only be a consequence of fate-specification rather than a cause. The results are in favor of a multiple precursor model (Franco and Müller, 2013). However, although Franco and colleagues showed that there are some RGCs restricted to upper layer neuron generation, the absence of multipotent precursors able to generate all types of neurons as well as the existence of deep layer restricted precursors remain to be demonstrated.

1.3 Toward a better understanding of primate corticogenesis

The rodent model is an extremely valuable tool for the study of cortical development because genetic tools are powerful and easily available. However, the differences between rodent and primate adult cortex and especially the distinct scaling rules reported in section 1.1, call for a precise examination of primate cortical development. It is necessary to assess to what extent we can transpose results from rodents to primates. In the following section we will review some the work that was carried out in primate cortical development mainly in the macaque monkey and human. This will illustrate some of the identified similarities and differences between rodent and primate cortical development and set the context of the thesis work. A table of developmental stage correspondence in mice, macaque monkeys and humans is provided in table B.1.

1.3.1 The primate cortical lamination is also inside-out

After the discovery of the inside out lamination process in mouse by Angevine and Sidman (see section 1.2.3)(Angevine and Sidman, 1961), researchers wondered if it was a general mechanism for all mammals and thus also true for primates. Pasco Rakic found that this was indeed the case (Rakic, 1974). With a similar method as Angevine and Sidman he performed a single injection of tritiated thymidine at stages ranging from E45 to E140 in the rhesus macaque. The animals were sacrificed 2 to 5 months after birth to allow the newborn neurons to reach their final position in the CP and the localization of labelled neurons was assessed by autoradiography. He found that neurons are produced from E45 to E100 in area 17 of the macaque cortex (165 days of gestation in total) with a peak of neuronal production at E70. No neurons are produced in either in the last two months of gestation or the postnatal period. Neurons labeled by the E45 pulse were localized in the deeper part of layer 6 as well as in the white matter. Neurons labelled by later pulses always took a relatively more superficial position demonstrating that the lamination is also inside out in primates (for the precise layer birthdate see Figure 1.13). No additional neurons were produced during the last two months of gestation. Neurons are thus produced relatively earlier in macaque monkeys and also probably in humans compared to rodents where they continue to be produced until one day before birth. The

injection at E120 and E140 labelled only glial and endothelial cells suggesting that, like in rodents, gliogenesis occurs once neurogenesis is complete. A similar succession of layer formation was described in other cortical areas albeit with a slightly shifted timing (Rakic, 1974).

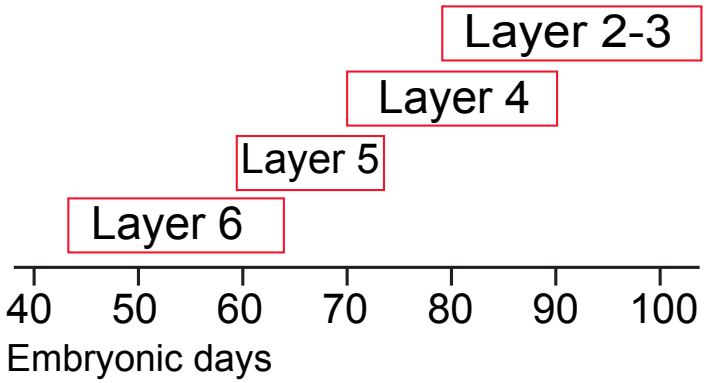

Layer	Start	End
6	43	63
5	60	72
4	70	90
2-3	80	102

Figure 1.13. Birthdate of the different neuronal layers of macaque area 17. The developmental stages are indicated in embryonic days. The macaque monkey pregnancy lasts 165 and neurogenesis takes place from E45 to E100. (Timings from Rakic, 1974)

1.3.2 A more complex early cortical development in primates

Although the general principle of inside out generation of cortical layers is conserved throughout the mammalian lineage, precise analysis of first steps of neurogenesis revealed primate specificities. These events might exist in rodents, but only the protracted primate period of corticogenesis enables the fine grained timing resolution necessary to detect them.

Bystron and colleagues described a new type of neuron, the predecessor neurons, which seems to be specific to humans since not yet been found in any other species (Bystron et al., 2006). They are the first neurons produced in the telencephalon. They arrive under the pial surface at around E30 before the cortical plate is formed. They have a bipolar morphology, express Beta3-tubulin and do not bear any axon. They presumably migrate from the ventral telencephalon by translocation in their long horizontal processes. They are different from Cajal-Retzius cells in that they do not express Reelin. Predecessor neurons are also negative for Dlx, an interneuron marker (Anderson et al., 2001). Some

predecessor neurons express however Tbr1, known in rodents to be specific for cortical glutamatergic neurons of cortical origin (Bulfone et al., 1995; Hevner et al., 2001). But the authors found it also expressed in human ventral forebrain neurons. So, Tbr1 does not seem to be specific for a cortical origin in humans. Predecessor cells form a dense network above the developing cortex and might play a role in guiding the migration of newly produced neurons.

The prelate covers the neuroepithelium before the generation of the cortical plate. It is split into the marginal zone and the subplate by the arrival of locally produced cortical neurons forming the cortical plate (Figure 1.15). The first steps of prelate formation as well as its composition are more complex in primates. Meyer and colleagues described in detail the prelate formation in humans (Meyer et al., 2000). The first Cajal Retzius cells appear at gestational week 5 (GW5) in the primordium plexiform layer and subsequently expand. Cajal Retzius cells are produced by the cortical hem and locally by the cortical VZ (Meyer, 2010). Calretinin and Calbinding interneurons then intermingle with Cajal Retzius cells in the prelate from GW 6.5 to 7. Layer 6 cortical neurons migrate from the underlying VZ and settle in the middle of the prelate below the Cajal Retzius cell layer at GW7.5. Cells expressing interneuron markers are presumably born in the ventral telencephalon and migrate tangentially to the preplate (Meyer et al., 2000).

1.3.3 Multiple origins of primate interneurons?

Primate and nonprimate interneurons differ in two major respects: their relative abundance compared to excitatory cells and their increased diversity in primates (DeFelipe, 2002; Gabbott and Bacon, 1996). Interneurons account for 25% to 30% of all cortical neurons in primates and exhibit areal and laminar differences (Hendry et al., 1987) whereas they are thought to comprise only 15% to 20% in rodents (Beaulieu, 1993). Interneurons constitute a heterogeneous population differing in their morphologies, connectivity, electrophysiological properties, and the expression of the calcium binding proteins calbindin, somatostatin, calretinin, and parvalbumin (Ascoli et al., 2008). Interneurons achieve their highest level of differentiation in primates (DeFelipe, 2002), and at least one type seems to be unique to this order: the double-bouquet cells (DeFelipe, 2011; Jones et al., 1988; Yanez et al., 2005). The increased number and diversity of primate interneurons is likely to arise through a more complex developmental process that is still not entirely

resolved. Glutamatergic neurons are generated exclusively by the cortical germinal zones in the dorsal forebrain and migrate radially to the overlying cortical plate. In contrast, interneurons in rodent and ferret originate subcortically from the ganglionic eminence (GE) in the ventral forebrain (Figure 1.14) (Anderson et al., 1997, 2002). They reach the cortical plate via two migration streams in the marginal and intermediate zones (Marin and Rubenstein, 2001; Métin et al., 2006; Tamamaki et al., 1997). Genetic fate mapping studies in mouse showed that parvalbumin positive cells are generated in the medial GE (MGE), somatostatin positive cells from the MGE and the caudal GE (CGE), and calretinin positive cells from the CGE (reviewed in (Wonders and Anderson, 2006)).

The ventral origin of some interneurons has been confirmed in primates (Jakovcevski et al., 2011; Letinic et al., 2002; Petanjek et al., 2008; Zecevic et al., 2011). However in primates an important fraction of cortical interneurons are produced locally in the cortical germinal zones of the dorsal forebrain. Rakic's group estimated that in human 65% of cortical interneurons originate from the cortex (Letinic et al., 2002) but this number has not been confirmed so far. Several studies actually suggest that the source of interneurons changes as corticogenesis proceeds in the primate. During the first half of corticogenesis, interneurons originate from the GE, and at midgestation interneuron precursors start to be detected in the primate cortical germinal zones during the generation of the supra granular layer neurons (Figure 1.14) (Jakovcevski et al., 2011; Zecevic et al., 2011).

Although these studies convincingly showed that many primate interneurons are produced in the cortical germinal zones, they did not determine their lineage. Cortical interneuron precursors may be generated by ventral precursors that undergo tangential migration and settle in the cortical SVZ, where they resume proliferation and generate interneurons. Such precursors have recently been described in late mouse corticogenesis (Wu et al., 2011). On the other hand, they could be generated by cortical precursors in the VZ or SVZ, as suggested in humans by in vitro genetic fate mapping (Yu and Zecevic, 2011) and *ex vivo* time-lapse experiments (Hansen et al., 2010). These two lineages are not mutually exclusive. The diversity of cortical interneuron precursors identified by the expression of various ventral markers is in favor of multiple lineages (Jakovcevski et al., 2011).

It is clear that the primate cortical germinal zones generate many more interneurons compared to nonprimates, where this process seems to be marginal. Only 5% of the interneurons are produced dorsally in the mouse, and they seem to be destined mainly

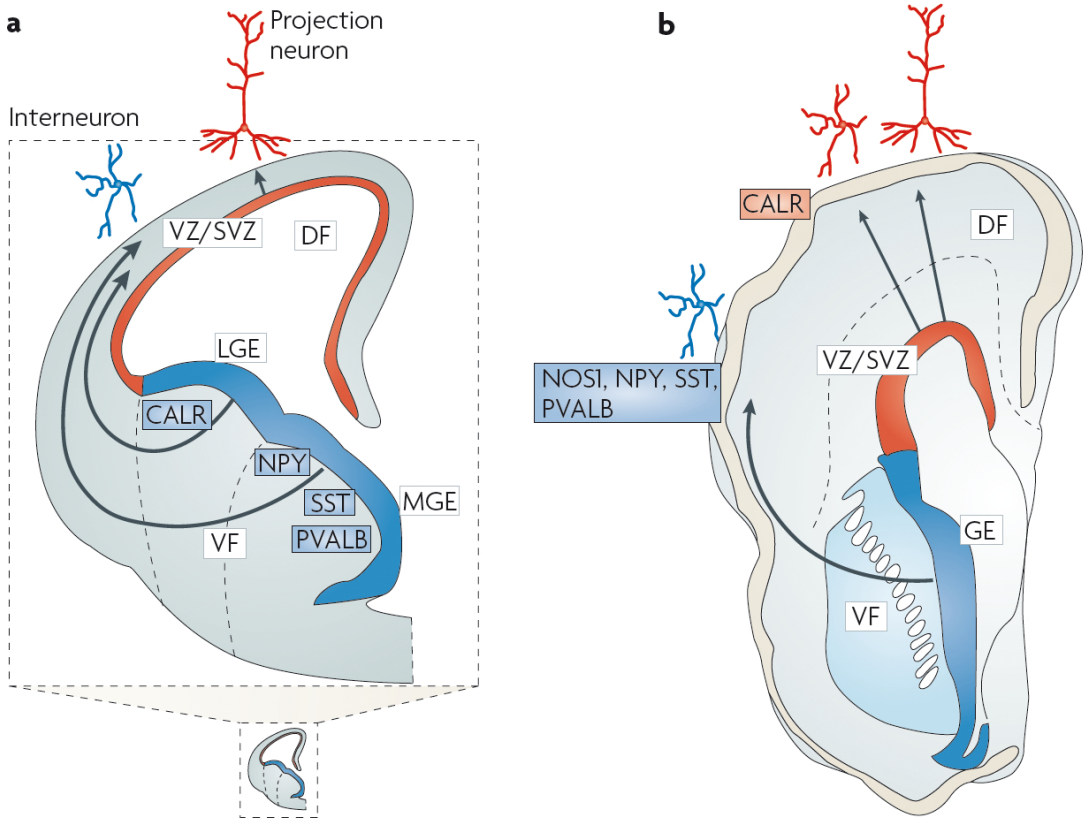

Figure 1.14. Origins of cortical neurons in rodents and primates. These schemes depict cross-sections of a hemisphere of a rodent (a) and a human (b) fetal brain. They are drawn to scale, but a zoom of the rodent section is displayed for better readability. Excitatory neurons in both rodents and primates are generated in the cortical ventricular zone/subventricular zone (VZ/SVZ) and migrate radially to settle in the cortical plate. In rodents the majority of cortical interneurons originate from the ganglionic eminence (GE), subdivided into a lateral and medial part (LGE and MGE, respectively), and migrate tangentially into the cortex. Some primate cortical interneurons originate also from the GE, especially at early stages, but a new source appears in the cortical VZ/SVZ at midgestation during the generation of the SGL. Different interneuron types are produced by the two sources in primates. Nitric oxide synthase 1 (NOS1), neuropeptide Y (NPY), somatostatin (SST), and parvalbumin (PVALB) positive interneurons originate from the GE, and calretinin (CALR) positive cells from the cortical VZ/SVZ. DF: dorsal forebrain; VF: ventral forebrain (from Rakic, 2009).

for the olfactory bulb (Kohwi et al., 2007), although one study reported a dorsal origin of some cortical interneurons produced postnatally (Inta et al., 2008). The higher diversity of interneuron sources in primates might be the path followed by evolution to provide a bigger cortex with more numerous and more diverse types of interneurons. The supra granular layers of the cortex are the most developed and complex layers of the primate brain. The timing of interneuron production in primates suggests that interneurons destined for the supra granular layers have mainly a cortical origin. It is also interesting to note that the primate-specific double-bouquet interneurons are mainly found in the supra granular layers (Defelipe et al., 1999; DeFelipe, 2011) and thus are likely to derive from cortical interneuron precursors.

1.3.4 An extra proliferative zone: the OSVZ

Work on the monkey cortical germinal zones showed that the primate has evolved a specialized and greatly expanded SVZ that is split into cytoarchitecturally distinct compartments: the inner SVZ (ISVZ) and the outer SVZ (OSVZ) (Smart et al., 2002). A number of studies have since confirmed in both human and non-human primates, that the cellular architecture and composition of the OSVZ differ strikingly from that of the rodent SVZ (Fietz et al., 2010; Hansen et al., 2010; Lukaszewicz et al., 2005; Zecevic et al., 2005). Further, in the human and macaque monkey cortex, the OSVZ reaches its maximum thickness during peak production of supra granular layer neuron (Fietz et al., 2010; Hansen et al., 2010; Smart et al., 2002).The link between the OSVZ and the supra granular layers has been formally established by birthdating experiments in the monkey (Lukaszewicz et al., 2005).

The discovery of the OSVZ in the primate has prompted numerous teams to reexamine the structure of the cortical germinal zones in a wide range of mammalian species. These studies have led to a revision of the classical compartmentalization of the germinal zones into VZ and SVZ and have uncovered a diversification of the germinal zones in carnivores (ferret, (Fietz et al., 2010; Reillo et al., 2011)) and larger brained mammals (agouti, marmoset, sheep (García-Moreno et al., 2011; Kelava et al., 2011; Reillo et al., 2011)). It is now considered that the SVZ of primates and of gyrencephalic mammals is subdivided into an inner SVZ and an outer SVZ while the SVZ of the laboratory rodent remains a thin and more homogeneous structure (Martinez-Cerdeno et al., 2012; Smart, 1973).

However, it is only in the primate order that the outer region of the SVZ takes on the full morphological features of a distinctive OSVZ. Recent data however show that some precursor cell types akin to those observed in the primate OSVZ are also found in the laboratory rodent SVZ, albeit at much lower frequencies (Martinez-Cerdeno et al., 2012; Shitamukai et al., 2011; Wang et al., 2011).

In the following section, we will describe the different primate proliferative zones, how the OSVZ has be identified and what is its progeny. We will also discuss the existence of an OSVZ in other large brained-mammals.

Identification of the OSVZ

Anatomical studies of the developing primate cortex started at the beginning of the 20th century with the work of His and Hochstetter (His, 1904; Hochstetter, 1919). They carried out the first descriptions of the developmental events on postmortem embryonic and fetal human brains. No detailed exhaustive anatomical study had been carried out with modern histological techniques before the work of Smart and colleagues (Smart et al., 2002). The author performed a detailed anatomical description of the macaque monkey germinal zones at several developmental stages all along the neurogenic period.

Figure 1.15 provides a comparative overview of the development of the primate and mouse germinal zones as described by Smart et al. (Smart et al., 2002). In the primate, the VZ is the only proliferative zone until E55 when the SVZ appears. An early emerging outer fibre layer (OFL) forms a major landmark from E55 onwards. Contrary to what is observed in the rodent, where the VZ is the major germinal compartment throughout corticogenesis, the primate VZ declines rapidly during the course of corticogenesis starting at E65 (Smart et al., 2002) (Fig 1.15). The SVZ by contrast, increases progressively in depth and by E65 is divided into an inner SVZ (ISVZ) and outer SVZ (OSVZ). At E78 an intruding inner fibre layer (IFL) separates the large OSVZ from the thin ISVZ. The increase in the OSVZ is particularly important between E65 and E72. After E72, the OSVZ starts to progressively decline, the IFL becomes larger and intrudes into the ISVZ and OSVZ. The VZ is characterized by dense elongated cells unlike the ISVZ with sparser round cells. The OSVZ however shares VZ properties with dense, radially oriented nuclei (Smart et al., 2002). An OSVZ with the same characteristics was then also found in developing human cortex (Zecevic et al., 2005).

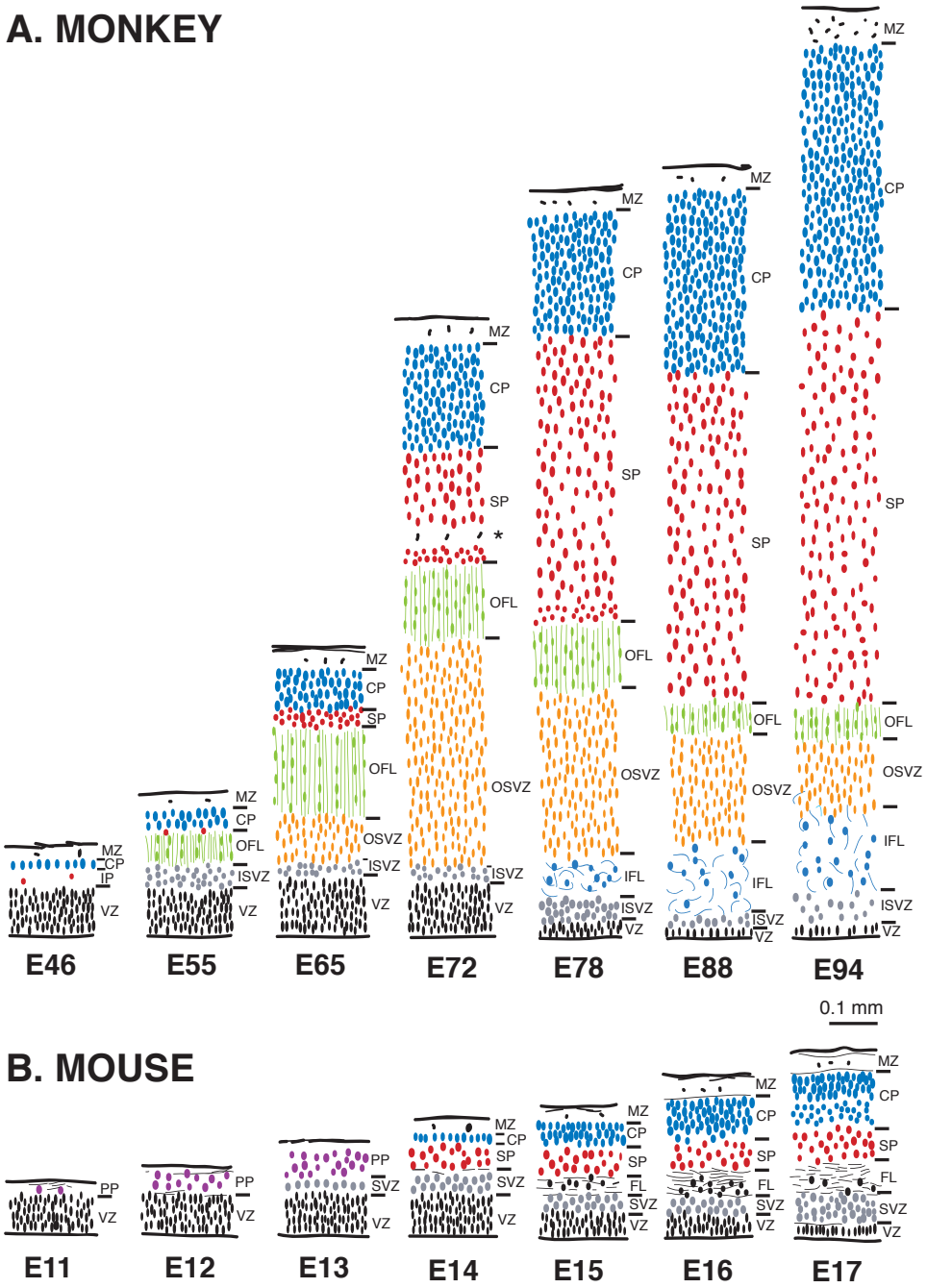

Figure 1.15. Comparison of primate **(A)** and mouse **(B)** germinal zones at equivalent developmental stages. The drawings represent transects through presumptive Area 17 in monkey and mouse dorsal cortex. The depth of each layer is drawn to a common scale. CP cortical plate; IFL inner fiber layer; IP intermediate plate; MZ marginal zone; OFL outer fiber layer; PP Preplate; SP subplate; VZ ventricular zone; SVZ sub ventricular zone; ISVZ inner SVZ; OSVZ outer SVZ. Figure from Smart et al., 2002.

Comparison of cortical germinal zones in different mammalian species

The VZ in both rodents and primates share the same characteristics. They contain densely packed cells with radially oriented nuclei that express the transcription factor Pax6 (Fish et al., 2008). The homologous structure of the rodent SVZ could be the primate ISVZ, which in these species display similar cellular properties with a lower cell density than the VZ, no particular cellular orientation and ISVZ cells express the transcription factor Tbr2 (Englund et al., 2005; Hansen et al., 2010; Fietz et al., 2010). The OSVZ does not have an equivalent in rodents where only few cells proliferate above the SVZ preferentially at the end of neurogenesis (Martinez-Cerdeno et al., 2012). Moreover, the OSVZ has a unique molecular signature. Virtually all OSVZ precursors express Pax6 (Fish et al., 2008; Hansen et al., 2010; Fietz et al., 2010). Tbr2 expression is also detected in the OSVZ but is mainly co-expressed with Pax6 (Hansen et al., 2010). The differences in molecular marker expression between the different primate proliferative zones provide an additional identification criteria, beside different cytoarchitectures. The VZ is identified by dense Pax6 positive nuclei, the OSVZ by sparse Tbr2 and Pax6 stainings above the dense Tbr2 staining band of the ISVZ. These molecular identification criteria have mainly been used in comparative studies on other mammalian animal models looking for equivalents of the VZ, ISVZ and OSVZ. (Fietz et al., 2010; Reillo et al., 2011; García-Moreno et al., 2011; Kelava et al., 2011; Martinez-Cerdeno et al., 2012).

The differences in the dimensions of developmental compartments in the rodent and the primate shown in Figure 1.15 reflect differences in mitotic activity. Hence, the distribution of mitoses in the developing primate cortical germinal zones is dramatically different from that observed in the rodent (Fietz et al., 2010; Hansen et al., 2010; Martinez-Cerdeno et al., 2012; Smart et al., 2002). In the rodent, the majority of mitotic figures are observed in the VZ during the whole period of corticogenesis (Martinez-Cerdeno et al., 2012; Smart, 1973). In primates, basally dividing precursors appear at very early stages. Once formed, the OSVZ remains the principal proliferative compartment throughout corticogenesis (Fietz et al., 2010; Hansen et al., 2010; Lukaszewicz et al., 2005; Martinez-Cerdeno et al., 2012; Smart et al., 2002). Basally located mitotic figures appear at comparatively later stages in the rodent. For instance it has been noted that during the production of infragranular layers at E65 in the primate, more than 43% of dividing precursors are located basally in the OSVZ (Lukaszewicz et al., 2005; Martinez-Cerdeno et al., 2012) whereas only 3% of mitotic precursors are reported in a basal SVZ at a comparable stage in the rodent

(Martinez-Cerdeno et al., 2012).

Recent studies report a compartmentalization of the germinal zones in ferret (Fietz et al., 2010; Reillo et al., 2011), agouti (García-Moreno et al., 2011), and marmoset (García-Moreno et al., 2011; Kelava et al., 2011) based on the density of Tbr2 expressing cells and the presence of Pax6+ cells in a basal location. These authors found a basal proliferative compartment above the SVZ with a low density of Tbr2+ cells, which they refer to as OSVZ. However, this proliferative zone appears radically different from the primate OSVZ: (1) It appears later during corticogenesis compared to the primate OSVZ, (2) the contribution of precursors from this zone is low compared to the VZ, (3) it lacks the distinctive cytoarchitecture of the primate OSVZ (absence of the tightly packed radial orientated cells), and (4) it is not bounded by fiber pathways. The dense, radially orientated precursors of an imposing OSVZ therefore constitute a unique primate feature.

Progeny of OSVZ precursors

The primate OSVZ contains a large pool of cortical precursors. The study of their contribution to cortical growth, neuronal diversity and glial cells demonstrated the fundamental role of the OSVZ during cortical development. *In vitro* and *ex vivo* studies pointed out the large diversity of cell types produced by the OSVZ (Mo et al., 2007; Mo and Zecevic, 2009; Letinic et al., 2002; Hansen et al., 2010).

In vitro studies on human germinal zones dissociated cultures showed the ability of precursors to differentiate into neurons, oligodendrocytes and astrocytes (Mo et al., 2007; Mo and Zecevic, 2009). Some precursors were restricted to either the neuronal or the glial lineage but some had the ability to generate both (Mo et al., 2007). In this study, cultures were expanded for 21 days in a medium containing growth factors before inducing differentiation by removing the growth factors. The artificial culture condition may have an impact on the precursors potentialities. Moreover, the authors did not study the OSVZ independently of the VZ. One cannot exclude that one cell type might be produced only by the VZ. But as the OSVZ contains a much greater number of precursors compared to the VZ at the studied developmental stage (GW20), this is very unlikely. More direct proof is needed to demonstrate the pluripotency of OSVZ precursors, although the expression of neuronal, astrocyte and oligodendrocyte markers by OSVZ precursors also suggests multiple potentialities (Mo et al., 2007; Mo and Zecevic, 2009; Rakic and Zecevic, 2003).

Some other groups tackled the issue of OSVZ precursor fate. Rakic's group demon-

strated that many interneurons are produced by the human OSVZ using fate mapping studies on organotypic slices (Letinic et al., 2002) (see section 1.3.3). Hansen et al. confirmed the neurogenic potential of OSVZ precursors (Hansen et al., 2010). They performed a BrdU pulse on dissociated OSVZ cells cultures and found that some cells that had incorporated BrdU were Beta3-tubulin positive hence neurons directly produced by OSVZ precursors. Precursors that incorporated BrdU were mostly Tbr2 so engaged in the glutamatergic neuronal differentiation. They confirmed this finding by clonal analysis in time lapse video microscopy on organotypic slice culture.

In the ferret on the other hand, specific retroviral injections of OSVZ precursors enabled an *in vivo* fate mapping of OSVZ precursors (Reillo et al., 2011). The authors showed that ferret OSVZ precursors generate many more astrocytes than neurons. More than anatomical differences and molecular differences, this data suggests also differences regarding the progeny of the OSVZ precursors between primates and non primate species.

Link between OSVZ and increased supra granular layer neurons in primates

The peak of OSVZ expansion coincides with the peak of granular and supra granular layer neuron production (Smart et al., 2002; Rakic, 1974) (Figure 1.13). The direct link has been established by Lukaszewicz and colleagues in the macaque monkey (Lukaszewicz et al., 2005). The authors performed tritiated thymidine pulses at E78 with either one hour or 87 day survival. After one-hour survival 80 to 90% labeled cells were located in the OSVZ. The 87 day survival indicated the fate of the cells labeled in S phase at E78. Labeled cells were located in layers 2 and 3. These results demonstrated that the OSVZ is the major source of supra granular neuron production.

1.3.5 Towards the identification of the primate cortical precursors heterogeneity and diversity

There is also a major difference in the cellular composition of the primate OSVZ with respect to the rodent SVZ. Whereas in the rodent all RG cell nuclei are restricted to the VZ, RG cell somata are morphologically identified in the OSVZ of the primate (Levitt et al., 1981; Lukaszewicz et al., 2005). There is evidence that precursors of the primate OSVZ express Pax6, which characterizes RG cell identity in the rodent (Fish et al., 2008).

The Pax6 positive precursors in the OSVZ have been further characterized in human

(Fietz et al., 2010; Hansen et al., 2010) and in ferret (Fietz et al., 2010; Reillo et al., 2011). A subset of Pax6 expressing cells divide basally and display features reminiscent of the RGCs located in the VZ and have thus been called basal radial glial-like cells (bRG) (Kelava et al., 2011). Other studies refer to them as OSVZ radial glial-like cells (Fietz et al., 2010; Hansen et al., 2010) or intermediate radial glial-like cells (Reillo et al., 2011). This precursor type accounts for around 40% of the OSVZ precursor pool in human (Hansen et al., 2010). bRGs express the RGCs makers Pax6 and Sox2 as well as GFAP, Nestin, and Glast but not the IP marker Tbr2. They possess a long basal process that reaches the pia, and they retain it during mitosis. They rarely exhibit an apical process, and if present, it does not contact the VZ surface. Despite those epithelial features, they fail to express apical domain proteins, and their centrosome is not located at the VZ border but instead close to the nucleus in the OSVZ (Fietz et al., 2010; Hansen et al., 2010). The bRGs show another major difference from the RGCs. The latter exhibit stereotypic migration of their nucleus in phase with the cell cycle, which ensures that the RGC division occurs at the ventricular border subsequent to an apical directed movement. In contrast, prior to division, bRG undergo a basally directed mitotic translocation (Hansen et al., 2010). This basal movement is thought to contribute to the radial expansion of the OSVZ. *Ex vivo* TLV analyses on human cortical organotypic slices demonstrated that RGCs produce bRGs following divisions with an oblique cleavage plane orientation (LaMonica et al., 2013).

Moreover, precursors expressing a variety of markers were described in the OSVZ. Some precursors express Tbr2 alone or together with Pax6 (Hansen et al., 2010). Interneuron markers such as Dlx1/2 and NKX2.1 or Ascl1 (often coexpressed with Tbr2 (Hansen et al., 2010)) were also detected in OSVZ precursors. All these findings suggest a high diversity of OSVZ precursors with potentially various lineages generating different neuronal types and probably oligodendrocytes and astrocytes.

1.3.6 Mechanisms of cortical gyrification

As brains get bigger, the gyrification index (the degree of folding) increases. This correlation between brain weight and gyrification index is found throughout the mammalian order with, however, some exceptions. The quantitative relationship is clade specific (Pillay and Manger, 2007). As previously mentioned in section 1.1.4, the primate brain folds more rapidly as the number of neurons increases compared to rodent brains. It means that the gyrification process might be different from one clade to another or might depend on a parameter that scales differently between clades (Mota and Herculano-Houzel, 2012).

The most intuitive explanation for the folding of the brain is essentially steric constraint. The skull size cannot increase isotropically to body size due to mechanical constraints on the vertebral column. To fit more cortical neurons, i.e. an expanded cortical tissue surface in the skull, a folding process is necessary. The first folds to appear are the primary convolutions (central and calcarine fissure) at mid-gestation and then the secondary convolutions (parieto-occipital sulcus and frontal and temporal gyri). These precocious folds are conserved in their location and configuration across individuals and even across species to some extent. Tertiary convolutions appear late in the third gestation trimester in humans and are fully developed only months after birth. These last convolutions are much more subjected to individual variations (Le Gros Clark and Medawar, 1945).

Except for the late convolutions, the folding pattern is extremely conserved across individuals and there are cytoarchitectonic features specific to gyri and sulci (Bok, 1960). These two facts are in favor of an active process of folding rather than mere mechanical constraints from the skull. There are two non mutually exclusive theories to explain the mechanical forces at the origin of the gyrification process. The so called "tension-based theory" states that folds are the results of tensions along axonal fibers in the white matter (Van Essen, 1997). The second theory postulates that the folding is due to differential growth rates in the gray matter (Richman et al., 1975).

The tension-based theory of gyrification

A recent study established the evolution of the gyrification index (GI) during macaque monkey corticogenesis by MRI (Sawada et al., 2010). The authors determined that the first convolutions appear in the macaque monkey at around E70. The gyrification index

(GI) remains low until E100 when it starts increasing rapidly and continues increasing linearly until E150 when the adult folding pattern is achieved. As at E100 all neurons have been produced by the macaque monkey germinal zones and the latest produced neurons are still radially migrating toward the cortical plate (Rakic, 1974), it is likely that the increase of GI observed after E100 is not due to differential growth but to other tension sources (Welker, 1990).

David Van Essen proposed a theory of cortical folding based on tension along axons (Van Essen, 1997). The theory postulates that tensions generated by the newly extended axonal fibers are at the origin of cortical folding 1.16. By E100 the first neurons have started to form connections in the cortex. Axons have been shown to produce tension *in vitro*. Neurite growth on an adhesive substrate produces tension (Lamoureux et al., 1989). Axons also have viscoelastic properties that enable them to maintain a steady tension during cortical growth (Dennerll et al., 1989). Neurons establish long-range connections early during development (Schwartz et al., 1991), such viscoelastic properties are needed for the axons to adjust their length within a growing and deforming structure. By generating tensions, axonal fibers create anisotropy in the developing cortex, a requirement for folding.

During cortical development forces are initially imposed by radial glial fibers, then tension is caused by connections between cortex (subplate) and subcortical nuclei. According to the tension-based hypothesis, the gyrification pattern is entirely linked to the brain connectivity. As cortico-cortical projections are established early during corticogenesis (Schwartz et al., 1991), and as there are topographically organized projections between for instance visual areas in macaque (Coogan and Van Essen, 1996; Dehay et al., 1996), cortico-cortical connections in neighboring areas (for example V1/V2) tend to produce forces facilitating folds at specific points related to cortical areas. As a consequence of the folding process, areas that are densely connected will be spatially closer and the travelled distance within the white matter will be reduced. This theory closely links the folding pattern with cortical connectivity.

Dehay et al. provide an experimental validation of the "tension based theory". After having performed a bilateral enucleation at midgestation, the authors found a change in the gyrification pattern of the macaque occipital cortex (Dehay et al., 1996). Enucleated animals display an extremely reduced Area 17. As in normal animals Area 17 and 18 are densely connected, the loss of Area17 in enucleated animals result in the loss of the

majority of these connections. The new tension distribution could be at the origin of the different gyrification pattern in enucleated animals.

Following this line, Mota and colleagues proposed a mathematical model of gyrification where folding is driven by tension along the axons in the white matter (Mota and Herculano-Houzel, 2012). Their model aims at explaining the increase of the GI with cortical neuron number. The hypothesis of the model is based on a previous study (Herculano-Houzel et al., 2010). Herculano-Houzel et al. demonstrated, using results in 11 primate species, that cortical folding can be universally predicted as a function of the fraction of neurons connected through the white matter, their average length and cross-sectional area (Herculano-Houzel et al., 2010). The model is based on this assumption and predicts that the gray matter does not drive the folding of the white matter but instead that the white matter drives the folding of the gray matter. The model explains the distinct scaling of gyrification among orders, by different connectivity, axonal cross-section and tension along fibers thus supporting the tension-based theory of gyrification (Mota and Herculano-Houzel, 2012).

Although some studies support the "tension based theory", this theory remains speculative. Much experimental data is lacking. The mechanical properties of CNS tissue are unknown. The physical forces (tension, pressure) should be examined in a wide range of species.

Differential growth theory

With the study of the cytoarchitecture of brains with abnormal gyrification (lissencephaly and polymicrogyria) Richman and colleagues found defects in cortical lamination in gyri and sulci (Richman et al., 1975). They proposed a model in which the infra granular and supra granular layers of the cortex have different growth rates leading to the folding of the cortical surface (Figure 1.16). This hypothesis is supported by Welker's observations of specific cortical cytoarchitectures in gyri and sulci (Welker, 1990). The differential growth hypothesis has been extended by Kriegstein et al., who noted that the OSVZ is thicker under presumptive gyri and thinner under presumptive sulci (Kriegstein et al., 2006). Hence the OSVZ would provide more supra granular neurons in presumptive gyri and the differential contribution of the OSVZ could be at the origin of a differential growth between infra and supra granular layer neurons. Reillo and colleagues noted a higher number of mitoses in the ferret OSVZ below presumptive gyri (Reillo et al., 2011)

supporting Kriegstein's hypothesis.

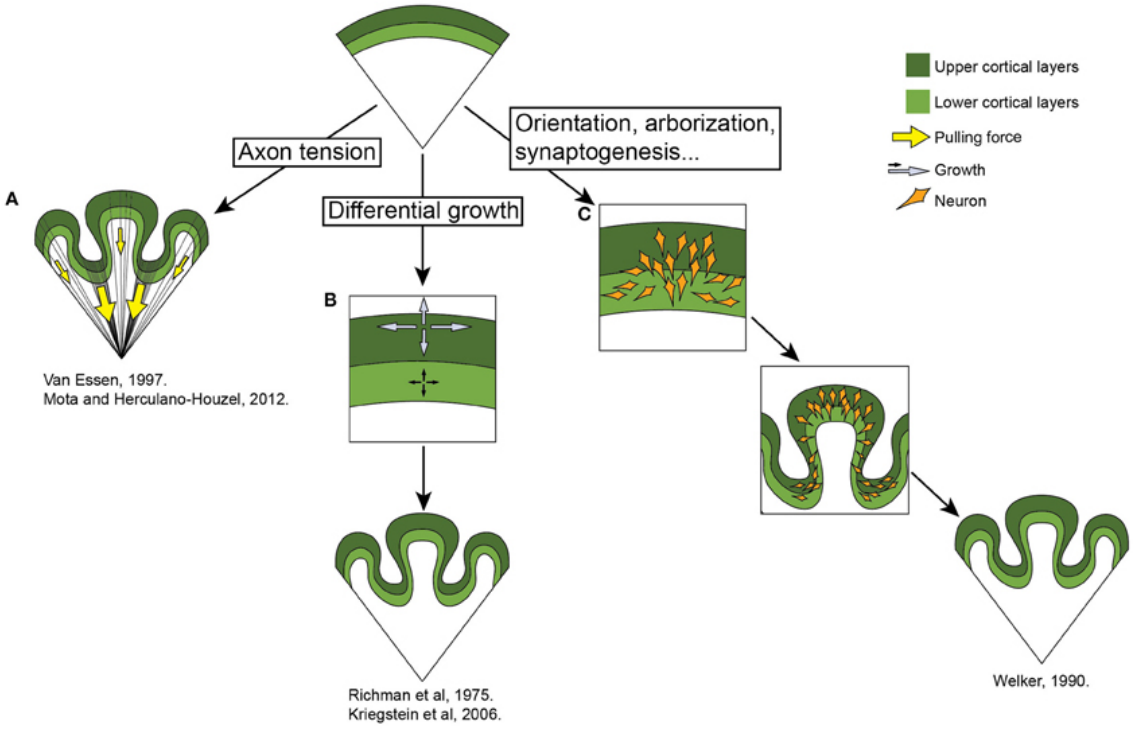

Figure 1.16. Illustration of the different gyrification theories. **A**. Van Essen and Mota and Herculano-houzel's theory postulates that axon tensions in the white matter are responsible for the folding of the brain (Van Essen, 1997; Mota and Herculano-Houzel, 2012). **B**. Richman et al. and Kriegstein et al. support the hypothesis according to which differential growth rates of the infra and supra granular layer neurons trigger the formation of convolutions (Richman et al., 1975; Kriegstein et al., 2006). **C**. Welker's theory postulates that the combined effect of fiber orientation, arborization, and synaptogenesis generate cortical folding (Welker, 1990). Figure from (Kelava et al., 2013).

Alternative theories

Welker proposed a theory in which cortical folding is induced by multiple factors that play a role in the gyrification process at specific timing during development. According to Welker, dendrogenesis, neuronal orientation, afferent arrival, arborization, synaptogenesis, among others, would be implicated (Welker, 1990) (Figure 1.16). On the other hand, Toro and Burnod built a morphogenetic model of cortical folding (Toro and Burnod,

2005). According to their model the folding is a consequence of cortical growth on a structure containing early geometric asymmetries. Mechanical properties as well as growth dynamics are supposed to induce and guide the formation of convolutions during cortical development.

There is an ongoing debate as to whether the newly discovered bRG are characteristic of gyrencephalic brains and required for cortical folding. First found in human and ferret, several studies have later described this precursor type in lissencephalic rodents (Martinez-Cerdeno et al., 2012; Shitamukai et al., 2011; Wang et al., 2011), in the agouti, a gyrencephalic rodent (García-Moreno et al., 2011), and in the marmoset, a lissencephalic primate (García-Moreno et al., 2011; Kelava et al., 2011). In contrast to small rodents where bRG are rare (5% of precursors), the relative proportions of bRG are claimed to be similar in human and ferret (40% of SVZ progenitors) (Kelava et al., 2011). bRG are thought to be required to provide more guiding fibers to the migrating neurons in a tangentially expanding structure (Borrell and Reillo, 2012; Reillo et al., 2011). As neuronal migration defects (Ross and Walsh, 2001) can lead to human brain malformations (lissencephaly, polymicrogyria for instance), bRG are supposed to be involved. Reillo and colleagues performed an experimental reduction of the number of bRG in ferret newborns and found a reduction of the cortical surface associated with a higher neuronal density suggesting a defect in neuronal tangential dispersion (Reillo et al., 2011). However, the gyrification index does not seem to be directly linked to the percentage of bRG because ferret and human have both around 40% of BP that are bRG but very different GI (2.5 for humans vs 1.8 in ferret). bRG are also present in lissencephalic or near-lissencephalic species. A unifying theory has been proposed, according to which gyrencephaly was present in the mammalian common ancestor and might have been secondary lost in some species (Kelava et al., 2013; Borrell and Reillo, 2012).

The different theories of gyrification remain still quite speculative. More experimental findings and computational modeling are required to elucidate this multifactorial process.

1.3.7 Hypotheses for primate cortical expansion

Theories for cortical expansion have evolved with the recent advances in understanding cortical development. The first hypothesis was the so-called "Radial Unit Hypothesis" formulated by Pasco Rakic (Rakic, 1988, 1995). The hypothesis is based on cellular results of cortical development and postulates that the control of the surface and thickness of the cortex is regulated by the proliferation kinetics of radial glial cells in the VZ. In the years 2000, the SVZ was discovered as a second proliferative pool generating neurons and thus also contributing to cortical expansion. This discovery led to the reevaluation and the extension of the Radial Unit Hypothesis. Pontious and colleagues formulated the "Radial Amplification Hypothesis" (Pontious et al., 2008), where intermediate progenitors in the SVZ amplify radial unit neuronal output that also contribute to the expansion of cortical surface without adding extra radial units.

The Radial Unit Hypothesis

The radial unit hypothesis takes its roots in the observations that during cortical evolution, there is a large expansion of surface (fold increase compared to mouse cortical surface of 100 for the macaque monkeys and 1000 for the humans) without a great increase of cortical thickness (maximum 2-fold increase). Why did the cortical expansion result in a surface expansion and not in a globe or a lump expansion like the striatum? Investigating cortical development helped provide a glimpse of the process. The second observation at the basis of the Radial Unit Hypothesis is the fact that neurons originating from the same radial glial cell tend to use their mother's glial fibers to migrate to the cortical plate and occupy the same column of cortex. In macaque monkeys, cells derived from a same clone remain in the same radial alignment (Kornack and Rakic, 1995). Actual radially oriented columns can be seen in the cortical plate during development, such columns have been called ontogenetic columns (Rakic, 1988). A "radial unit" is defined as an ontogenetic column, that is to say the ensemble of neurons generated at different time points during development but originating from the same spatial location and using the same radial fiber pathway to reach the cortical plate in a similar radial alignment (Figure 1.17). According to the Radial Unit Hypothesis, the cortex is formed by the addition of these ontogenetic columns. The number of radial units determines the surface of the cortex and the number of neurons generated by each column specifies cortical thickness. The number of radial

units and neurons that they produce depend on precursor proliferation kinetics.

During corticogenesis, two major phases can be identified. A phase of expansion of the VZ pool (until E40 in monkeys, E11 in mice) and a phase of neurogenesis (from E40 to E100 in monkeys, E11 to E18 in mice). During the expansion phase, RGCs divide symmetrically to generate new radial glial cells and hence generate more radial unit founders. During the neurogenic period, asymmetric divisions enable the self-renewal of RGCs and the generation of neurons that migrate along their mother's radial fiber. This second phase will determine how many neurons are produced by radial founder. The regulation of RGC mode of division is thus a fundamental aspect of cortical size control. The hypothesis explains the large primate cortical surface expansion by the lengthening of the expansion phase, so neurogenesis starts from a higher number of radial units. Small differences at this early point can lead to very different cortices, and to a particularly large expansion of surface that could explain primate cortical surface expansion (Rakic, 1995).

Experimental studies support the theoretical Radial Unit Hypothesis. Experimental amplification of radial glial founders resulted in a high cortical surface expansion (Haydar et al., 1999; Chenn and Walsh, 2002). Haydar and colleagues prevented cell death in the Caspase 9 KO mouse line, which resulted in the generation of more radial founders and an increased cortical surface. Chenn and Walsh artificially modified the mode of division of RGCs in a mouse mutant expressing a constitutively active Beta-catenin protein. They then observed a dramatic surface expansion of the cortex with even the formation of folds.

Hypotheses supporting the role of the basal progenitor pool in cortical expansion

The Radial Unit Hypothesis relies only on the proliferation kinetics of RGCs in the VZ, however neurons are also produced in the SVZ by intermediate progenitors (IPs) or more generally by basal progenitors (BPs). IPs are generated by RGCs and divide mostly symmetrically to give rise to two neurons and in rare cases can self-renew (Wu et al., 2005). IPs thus amplificy radial unit neuronal output.

Moreover, according to the Radial Unit Hypothesis, cortical and ventricular surfaces increase proportionally. But studies in different mammalian species have shown that there is a much larger expansion of the cortical surface compared to the ventricular surface in carnivores and primates (Martinez-Cerdeno et al., 2006). These authors also found a

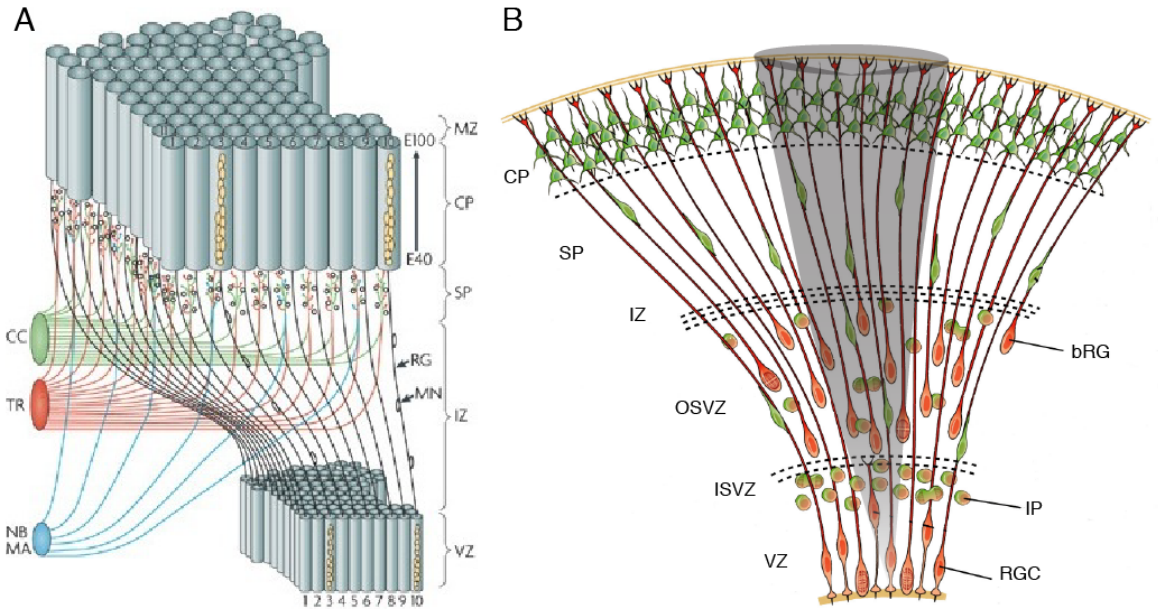

Figure 1.17. Illustration of the different hypotheses for primate cortical expansion. **A.** The Radial Unit Hypothesis postulates that the number of radial units determines the surface of the cortex and the amount of neurons generated by each unit gives the cortical thickness. The scheme illustrates the correspondence between proliferative units in the VZ and ontogenetic columns in the CP. The migrating path that the neuronal progeny of each VZ founder follows is determined by the radial glial fiber (RG) of their mother. Migrating neurons (MN) cross the intermediate zone (IZ) and the sub plate (SP) where axons from different source (thalamic radiations (TR), cortico-cortical connections (CC), nucleus basalis (NB), monoamine subcortical structures (MA)) reside before reaching the cortical plate in an inside out manner. The earlier generated neurons forming the deep layers and the later generating neurons migrating through the already generated layers to settle on top (from E40 to E100; modified from Rakic, 2009). **B.** The radial amplification hypothesis is an extension of the Radial Unit Hypothesis that takes into account the contribution of the basal proliferative compartment to cortical expansion. bRGs provide additional guiding fibers that allow a tangential dispersion of neurons and the formation of a "fanned out" radial unit indicated with the gray cone. Modified from Lui et al., 2011.

correlation between the size of the basal pool and the extent of cortical surface. These observations led to the reappraisal of the Radial Unit Hypothesis and to the theory of the role of BPs in cortical expansion (Martinez-Cerdeno et al., 2006; Kriegstein et al., 2006; Cheung et al., 2007; Pontious et al., 2008). The Radial Unit hypothesis holds true during the expansion phase of the RGCs where the radial units are formed. But during the neurogenenis period, BPs extend the neuronal output contributing potentially both to the increase of cortical thickness and surface. This extension of the Radial Unit Hypothesis has been called the Radial Amplification hypothesis (Pontious et al., 2008).

However, experimental findings and other observations suggest that the output of the radial amplification could have different effects in rodents and larger brained mammals. Experimental reduction of the BP pool in mice consistently led to a reduction of cortical thickness but cortical surface was only modestly decreased. (Schuurmans et al., 2004; Quinn et al., 2007; Roy et al., 2004; Bedford et al., 2005; Arnold et al., 2008; Sessa et al., 2008). Experiments of cell cycle reduction by means of Cyclin D1 over expression led to the increase of the BP pool (Lange et al., 2009; Pilaz et al., 2009).The two studies reported an increase mainly in cortical thickness. In humans, however, mutation of Pax6 (Glaser et al., 1994) or Tbr2 (Baala et al., 2007) leads to severe micrencephaly and cortical malformations where the cortical plate is extremely thin. The cortical surface is also reduced. It seems that in the case of primates, the BP pool could regulate both cortical thickness and surface.

These differences in BP pool contributions might be explained by different degrees of radial unit amplification between rodents and gyrencephalic species. In mice BPs barely self-renew whereas primate BPs are supposed to undergo several rounds of proliferative divisions although no direct evidence support this fact so far (Kriegstein et al., 2006; Lui et al., 2011). This led to the theory of the existence of transit-amplifying progenitors (TAPs) in the primate OSVZ that would serve to exponentially amplify the neuronal output of each radial unit (Lui et al., 2011; Fietz et al., 2010; Kriegstein et al., 2006; Martinez-Cerdeno et al., 2006; Pontious et al., 2008). The presence of bRGs with a basal process contacting the pia membrane would provide extra radial fibers oriented in a fanned manner to enable the tangential spread of the additional neurons (Borrell and Reillo, 2012; Reillo et al., 2011). These mechanisms could account for both the modest radial expansion, and the large tangential expansion of the cortex.

In conclusion, VZ precursor expansion will determine the number of radial founders but not directly the surface of the cortex. The radial units are probably not rectilinear in gyrencephalic species. The amplification of the neuronal output by the BP pool in the OSVZ and the additional curved radial fiber guides provided by bRG are supposed to enable the formation of a "fanned out" or "cone-shape" radial unit whereby increasing both cortical thickness and surface (Fietz and Huttner, 2011).

The role of the BP pool, and more specifically of OSVZ precursors, in primate cortical expansion has not been directly assessed yet. According to the Radial Amplification Hypothesis, the increased proliferative abilities of primate OSVZ precursors compared to mouse SVZ precursors allow cortical expansion. The crucial issues of primate OSVZ precursors identity, lineage and proliferative abilities are the main focus of this thesis.

.

Chapter 2

Results

The results chapter is composed of two parts. The first part is the manuscript of an article in press at Neuron, which provides evidence for high proliferative abilities of OSVZ precursors. Quantitative time-lapse video-microscopy (TLV) observations allowed the generation of a large database of OSVZ precursor properties and lineages. 5 types of OSVZ precursors were identified based on their morphology. Each precursor type is able to self-renew, to generate other precursor types or directly neurons. This first part illustrates the diversity of OSVZ precursors and the complexity of their lineages.

In the second part of the results, we analyzed the TLV lineage dataset with a different approach. We developed and used an automatic classification method based on the Hidden Markov Tree model to determine cell types taking in account all measured parameters equally in an unbiased manner. The two approaches converge toward 5 precursor types in the primate OSVZ characterized mainly by their morphological attributes.

2.1 Paper in press at Neuron: Precursor diversity and complexity of lineage relationships in the outer subventricular zone of the primate.

Marion Bétizeau[1,2], Véronique Cortay[1,2], Dorothée Patti[1,2], Sabina Pfister[3], Elodie Gautier[1,2], Angèle Bellemin-Ménard[1,2], Marielle Afanassieff[1,2], Cyril Huissoud[1,2,4], Rodney Douglas[3], Henry Kennedy[1,2], Colette Dehay[1,2]*

[1] - Stem cell and Brain Research Institute, INSERM U846, 18 Avenue Doyen Lepine, 69500 Bron, France.

[2] - Université de Lyon, Université Lyon I, 69003 Lyon, France

[3] - Institute of Neuroinformatics (INI), Winterthurerstrasse 190, University/ETH Zürich, CH-8057 Zürich Switzerland.

[4] - Service de gynécologie-obstétrique, hôpital de la Croix-rousse, Hospices Civils de Lyon, France

2.1.1 Abstract

Long-term ex vivo live imaging combined with unbiased sampling of cycling precursors shows that macaque OSVZ includes four distinct basal radial glial cell morphotypes (bRG), bearing apical and/or basal processes in addition to non-polar intermediate progenitors (IPs). Each of the five precursor types exhibits extensive self-renewal and proliferative capacities as well as the ability to directly generate neurons, albeit with different frequencies. Cell-cycle parameters exhibited an unusual stage-specific regulation with short cell-cycle duration and increased rates of proliferative divisions during supragranular layer production at late corticogenesis. State transition analysis of a large clonal database reveals bidirectional transitions between OSVZ precursor types as well as stage-specific differences in their progeny and topology of the lineage relationships. These results explore rodent-primate differences and show that primate cortical neurons are generated through complex lineage relationships by a mosaic of precursors, thereby providing a new framework for understanding unique features of primate corticogenesis.

2.1.2 Introduction

Besides its tangential expansion, one hallmark of human and nonhuman primate cortex is the selective enlargement of the supragranular layer compartment (Marin-Padilla, 1992), which is considered to underlie the highly developed computational abilities of the human brain (Kennedy et al., 2007). The enlarged supragranular primate layers originate from a specialized precursor pool, the OSVZ (Dehay et al., 1993; Lukaszewicz et al., 2005; Smart et al., 2002). Maximum dimensions of the OSVZ coincide with peak rates of supragranular neuron production (Fietz et al., 2010; Hansen et al., 2010; Smart et al., 2002).

The enlargement and complexification of the OSVZ is considered to be a key factor underlying evolutionary adaptive changes of primate corticogenesis, in turn leading to the structural characteristic and by consequence the functional dynamics of the primate neocortex (Dehay and Kennedy, 2007). A well-defined strategy to better understand the mechanisms leading to the evolutionary expansion of the primate cortex involves characterizing cortical progenitors (Fietz et al., 2010; Hansen et al., 2010; Lui et al., 2011). Two principal cortical precursor types have been reported in primates and non-primates: (i) apical progenitors (APs) undergoing mitosis at the ventricular surface in the ventricular zone (VZ); and (ii) basal progenitors (BPs) undergoing mitosis at abventricular locations, in the ISVZ and OSVZ. In rodents, APs comprise neuroepithelial cells, which transform into the apical radial glial cells (RG) of the VZ at the onset of neurogenesis (Gtz and Huttner, 2005), and short neural precursors (Stancik et al., 2010). Rodent BPs include intermediate progenitor (IP) cells and rare basal (or outer) radial glial (bRG) cells, the latter accounting for less than 5% of the BP population (Martinez-Cerdeno et al., 2012; Shitamukai et al., 2011; Wang et al., 2011). In contrast to IP cells, which undergo one terminal round of cell division, bRG cells are competent to undergo up to 2 rounds of division (Shitamukai et al., 2011; Wang et al., 2011).

Several studies (Bystron et al., 2008; Fietz et al., 2010; Garcia-Moreno et al., 2012; Hansen et al., 2010; Kelava et al., 2012; LaMonica et al., 2012; Levitt et al., 1981) have shown that the human and non human primate BPs of the OSVZ include a large fraction of bRG cells. An unexpected feature of primate BPs is that the maintenance of radial glial-like morphology is accompanied by the expression of the transcription factor Pax6 (Fietz et al., 2010; Fish et al., 2008), as well as various combinations of stem cell markers such as Sox2, and Hes1 (Lui et al., 2011), further reinforcing the similitude of the primate bRG cells to the APs (Englund et al., 2005; Gtz and Huttner, 2005). In addition, like

APs, primate bRG cells have a long basal process, connecting the basal membrane at the pia, but they supposedly differ from APs by being devoid of apical process, and undergo basally directed mitotic somal translocation (Fietz et al., 2010; Hansen et al., 2010).

The mechanisms responsible for the large increase of the BP pool in the primate are the subject of sustained speculations (Lui et al., 2011). During evolution there is an increase in the number of bRG cells (Fietz et al., 2010; Reillo et al., 2011), reported to undergo up to 2 rounds of division in human (Hansen et al., 2010; LaMonica et al., 2013). The prevailing theory is that the expansion of the BP pool is ensured by transit amplifying daughter progenitors (TAPs). It is further hypothesized that the TAPs undergo numerous symmetric divisions before differentiating into neurons. According to this theory the TAPs ensure the massive increase in neuronal production that characterizes the primate cortex and contribute to its increased size and complexification (Fietz et al., 2010; Kriegstein et al., 2006; Lui et al., 2011; Martinez-Cerdeno et al., 2006; Pontious et al., 2008).

Here, using a combination of real time imaging of individual precursors from long-term organotypic slice culture of embryonic macaque monkey and immunohistochemistry, we establish the first detailed description of the proliferative behavior, morphology and lineage relationships of OSVZ precursors. Using an unbiased sampling of cycling precursors, we have identified five distinct OSVZ precursor types, showing distinctive behavioral attributes. Besides the already described basal process-bearing bRG (bRG-*basal-P*) cells and IP cells (Fietz et al., 2010; Hansen et al., 2010), we have identified three distinct categories of bRG cells which include (i) apical process-bearing bRG (bRG-*apical-P*) cells, (ii) apical and basal process bearing bRG cells (bRG-*both-P*) (iii) bRG cells alternating between stages showing either an apical and/ or a basal process and stages with no process designed as transient bRG cells (tbRG). Each precursor type undergoes numerous successive rounds of proliferative divisions. This extensive proliferation of OSVZ precursors is accompanied by cell-cycle duration of the same order as that observed in the VZ, with a significant shortening during the production of supragranular layer neurons. This contrasts with the progressive increase in cell-cycle duration reported in rodent corticogenesis, (Caviness et al., 1995; Reznikov and Van Der Kooy, 1995).

The quantitative analysis of a large database of complex lineage trees generated by OSVZ precursors provided a powerful insight in rules governing precursor proliferative behavior and fate. State transition analyses of the lineage trees reveal frequent bidirectional transitions between precursor types. All five precursor types self-renew and directly

generate neurons. Comparison of early and late stages of corticogenesis indicates a change in the topology of the precursor state transition diagram.

These results indicate a higher level of complexity in both the identity and in the lineage relationships of OSVZ precursors than previously reported (Fietz et al., 2010; Hansen et al., 2010) and predicted (Lui et al., 2011; Martinez-Cerdeno et al., 2006; Pontious et al., 2008).

The present study points to rodent-primate differences in precursor diversity and proliferative abilities, combined with species-specific tempo of cell-cycle regulation, having a profound impact on the phenotype of the adult cortex in these two orders. We propose that these specific properties of primate OSVZ precursors account for the observed expansion of the cortex and the supragranular layer enlargement.

2.1.3 Results

OSVZ and Pax6/Tbr2 expression

We provide a comprehensive description of the VZ, ISVZ and OSVZ in presumptive area 17 covering the period of neurogenesis between E49 and E94, (Fig 1) (Rakic, 1974). Cortical neuron production starts at E45 and BPs are first observed at E49 when they form the SVZ which, compared to the VZ, exhibits a looser and sparser cell arrangement and includes a higher proportion of Tbr2+ precursors (Fig 1A). The OSVZ can be distinguished from the ISVZ at E58 and is characterized by compact and elongated precursors reminiscent of the VZ and distinct from the much looser disorganized appearance of the rodent SVZ (Lukaszewicz et al., 2005; Smart et al., 2002) (Fig 1B). In the occipital cortex the OSVZ is basally bordered by an outer fiber layer (OFL) and undergoes rapid expansion to become the predominant germinal zone (GZ) at E63 before proceeding to decline after E78, some 15 days after the decline of the VZ (Fig1 C-F). Quantification of the numbers of Ki67+ within the full thickness of the GZs shows that while the VZ is the major source of precursors prior to E58, as early as E63 the OSVZ becomes the prominent precursor pool (Fig 1G). From E70 there is a sharp drop in the proportions of cycling precursors in all compartments (Fig 1H).

Cycling precursors (Ki67+) express Pax6 and/or Tbr2 in a compartment specific pattern (Fig 1 A-F,I). In the VZ and up to E79, 60-80% of precursors express uniquely Pax6 (Pax6+only cells). After E79, 40% of VZ precursors co-express Pax6/Tbr2 and Tbr2+ only cells are rare. In the ISVZ, 60 to 80% of precursors co-express Pax6/Tbr2, 5-30% are Tbr2+ only and less than 15% are Pax6+only cells. In the OSVZ, 25-50% of precursors co-express Pax6/Tbr2, 20 to 35% are Pax6+only, 10-20% are Tbr2+only. Hierarchical clustering was used to explore the closeness/dissimilarity of the Pax6/Tbr2 expression patterns of the three GZs. On this basis, ISVZ and OSVZ appear more closely related with each other than with the VZ, and the early VZ is set apart as is the late OSVZ (Fig1I-J).

OSVZ precursors undergo multiple rounds of proliferative divisions and show unusual temporal regulation of cell-cycle parameters

Although the object of numerous speculations (Hansen et al., 2010; Kriegstein et al., 2006; Lui et al., 2011), the extent to which there is an expansion of OSVZ precursor pool has not been directly analyzed.

We have established optimal conditions for organotypic culture of monkey embryonic cortex (from E48 to E80) where tissue integrity is maintained for up to 15 days and where proliferation, migration to the cortical plate and neuronal differentiation are conserved (Lukaszewicz et al., 2005) (Fig S1A-E, Movie S1). Using 2-photon time-lapse videomicroscopy (TLV), we recorded 487 divisions in 1071 EGFP expressing cells labeled via EGFP retroviral infection on parasagittal E48, E65 and E78 organotypic slices, corresponding to infragranular and supragranular layer production respectively.

We reconstructed lineage trees containing three or more cells by playing back the video recordings frame by frame and mapping the birth order of the cells within each lineage. OSVZ precursors underwent up to 6 multiple rounds of proliferative divisions, allowing to reconstruct 91 lineage trees at E65 and 78 (Fig 2A, Movie S2). Compared to E65, E78 OSVZ precursors generated significantly more complex and extensive trees (Fig 2A). These stage-specific differences in proliferative behavior were consistently observed across four E65 and two E78 hemispheres. The smaller size of E65 OSVZ trees (not exceeding 3 ranks with no division observed beyond 160 hours of recording- Fig 2A) was not due to experimental conditions in the monitoring period since at E65, on the same slices used for the OSVZ, divisions in the VZ were observed over 5 ranks and 200 hours of recording (Fig S1F). Comparison of the depth of lineage trees (number of successive divisions) revealed that OSVZ precursors generate longer lineage trees at E78 compared to E65 (Fig 2B). No significant difference was observed between VZ and OSVZ at either E65 or E78 (Fig 2B, Fig S1F).

Based on daughter cell fate, we defined a proliferative division when a precursor gives rise to two daughter cells, both of which undergo further division. Differentiative divisions occur when a progenitor gives rise to at least one daughter that exits the cell-cycle. Compared to E65, E78 OSVZ and VZ precursors undergo significantly higher proportions of proliferative divisions (Fig 2C). From the TLV recordings we extracted cell-cycle durations (Tc) -defined as the time elapsed between two mitoses. VZ precursors show a mean Tc of 45h at E48 (n=14) increasing up to 63h at E65 (n=52) prior to shortening to 46h at E78 (n=84) (Fig 2D). Tc variation in OSVZ follows the same time course as in the VZ. The longer Tc at early stages and shorter Tc at late stages were confirmed by similar results obtained from different brains at E63, E64 and E65, as well as in two E78 brains. OSVZ precursors cycle slightly but significantly slower than VZ precursors (Fig 2D).

Interestingly, the shorter Tc values observed in VZ and OSVZ at E78 are associated

with increased proportions of proliferative divisions (Fig 2C) pointing to an upsurge in proliferative activity and coinciding with maximum tree size at this stage (Fig 2B). So as to quantify the dynamics of mode of division in vivo, we estimated the changes in rates of cell-cycle exit. NeuN immunoreactivity is selectively detected in postmitotic neurons of the subplate and cortical plate in the mouse and is a marker of neuronal differentiation (Wang et al., 2011). We observed low but significant levels of nuclear NeuN in a fraction of cycling precursors in the primate GZ (Fig S1G-H) (Lui et al., 2011). Hence, we used the percentage of Ki67+ NeuN+ double positive cells with respect to the total cycling population as an index of the rate of cell cycle exit (Fig 2E). In the VZ, the cell-cycle exit fraction increases slightly between E48 and E65 and decreases between E65 and E78. In the OSVZ/ISVZ, the cell-cycle exit fraction increases slightly between E48 and E70 before declining abruptly. At E78 in both the VZ and the OSVZ, compared to proliferative divisions, differentiative divisions showed significantly longer Tc values (52.3h vs 44.6, 17% increase, Fig 2F).

The above analysis at the single-cell level has been complemented by an in situ population analysis of the relative duration of cell-cycle phases, using a triple immunolabelling against PCNA, Ki67 and Geminin (Fig 2G). In the VZ, the proportion of G1 phase cells increases from E48 to E65 and is associated with a decrease in the proportion of S phase precursors (Fig 2H), suggesting a relative lengthening of the G1 phase (TG1) and a relative shortening of S phase (TS). In the OSVZ, G1 cells accounted for 65% of the total cycling precursor pool at both E65 and E78, which is inferior to the proportions observed in the VZ at similar stages (80%), suggesting that OSVZ precursors have a relatively shorter TG1 than their VZ counterparts.

Using Tc values obtained with TLV, we estimated the theoretical duration of cell-cycle phases in the different compartments (Fig 2I). This analysis reveals that the Tc decrease between E65 and E78 is largely due to a reduction in TG1 and to a lesser extent in TS in the VZ. In the OSVZ, the Tc decrease between E65 and E78 results from a reduction of both TG1 and TS. Interestingly, this shortening in TG1 at E78 in both VZ and OSVZ is associated with an increase in proliferative divisions (Fig 2C).

The OSVZ includes five precursor types, a fraction of which shows a dynamic morphology

The maintenance of Pax6 expression in OSVZ precursors (Fig 1) (Fietz et al., 2010; Fish et al., 2008; Hansen et al., 2010), combined with the present findings of their extensive proliferative abilities raise the question of the extent to which OSVZ precursors resemble VZ precursors.

Immunohistochemistry analysis performed a few days after EGFP retroviral infection showed that over 75% of OSVZ Ki67+ precursors correspond to radial oriented cells (Fig 3A- F; Fig S2A-J), that we broadly classify as bRG cells, 25% to non-polarized IP precursors (Fig 3G, Fig S2K-N) and less than 1% to tangentially oriented precursors (Fig S2O). Data in Figure 3H represent the pooled results of the two ages. (Note that when no significant difference was observed between the two stages, results are pooled and age is not specified).

We observed three different static bRG morphologies (i) 40% of bRG cells bear an extensive basal process (bRG-*basal-P*), sometimes reaching the pia (Fig 3A-B, Fig S2A-C) (ii) 10% of bRG cells bear a well developed apical process (bRG-*apical-P*), extending as far as the ISVZ and VZ, without however reaching the ventricular surface (Fig 3C-D, Fig S2D); (iii) 50% of bRG cells bear both an apical and a basal process (bRG-*both-P*) (Fig 3E-F, Fig S2E-J). Hence 60% of bRG cells exhibit an apical process (Fig 3I).

Immunohistochemistry combining EGFP, Ki67, Tbr2 and Pax6 showed that all three bRG types were predominantly Tbr2-Pax6+ and differed significantly from IP cells which were predominantly Tbr2+Pax6+ (Fig 3J). EGFP immunolabelling provides a high resolution allowing detailed morphometric analysis of the precursor processes. This showed that thick basal processes are more frequent than thick apical processes (Fig 3K). The apical process is more likely to be thick when belonging to a bRG-*apical-P* cell rather than to a bRG-*both-P* cell, whereas frequency of basal thick processes is equivalent in bRG-*basal-P* and bRG-*both-P* cells. Basal processes are significantly longer than apical processes (Fig 3L).

TLV recordings showed that, while OSVZ precursors do not undergo interkinetic nuclear migration observed in VZ precursors, 24% of bRG cells undergo a mitotic translocating movement prior to mitosis (MST, Fig 3M). MST was observed to be basally (upwards) as well as apically (downwards) directed (Fig 3N). Note that MST is exclusively downward in bRG-*apical-P* cells and upward in bRG-*basal-P* cells, while bRG-*both-P* cells and

tbRG cells undergo equal proportions of downward and upward MST. MST amplitude ranges from 10 to 50μm (Fig 3O) (the average diameter of precursors is 10 microns).

TLV observations confirmed the existence of IPs, bRG-*apical-P*, bRG-*basal-P* and bRG-*both-P* cells as four distinct categories of precursors that exhibit a constant morphology throughout their lifetime- defined as the interval between two successive mitoses (see upper cell in Fig 4A and Movie S3 for an example of a bRG-*basal-P* cell, Movie S4 and Fig 4B for an IP). Unexpectedly, TLV observations revealed the existence of a fifth precursor type corresponding to precursors alternating between stages showing either an apical and/ or a basal process and stages with no process (i.e. IP morphology) during at least 15% of their lifetime (Fig 4C, Fig S3A, lower daughter Movie S5). This fifth type was designated as transient bRG cells (tbRG).

In addition to morphology changes in tbRG cells, we also observed a certain degree of remodelling of the processes in bRG-*both-P* cells. Only 10% of bRG-*both-P* cells are born with the two processes and in most cases, the newborn bRG-*both-P* cell grows a second process shortly after birth and exhibit the two processes during the major part of its lifetime (Fig 4A lower cell, Fig S3B-C, upper daughter Movie S5). In a few cases bRG-*apical-P* cells (20%) and bRG-*basal-P* cells (14%), in addition to the continuous presence of their defining process, exhibit an additional short lived temporary process.

Because a fraction of bRG cells exhibit dynamic processes, it was necessary to establish a reliable identification criterion defining the overall morphology throughout the precursor lifetime. We observed that the morphology at mitosis correlates well with the morphology after birth and throughout the lifetime of the precursor (Fig 4D). Hence the morphology observed under TLV before division was used to define bRG cell identity.

Given that cells are rounding up during mitosis, TLV analysis of the morphology right before mitosis is likely to be more accurate than the classically used phosphovimentin (a RG cell specific mitotic marker) labeling to detect process-bearing precursors (Fig S3D). This is borne out by TLV observations, which, compared to phosphovimentin labeling, revealed lower proportions of dividing precursors devoid of process and higher proportions of mitotic bRG-*apical-P* cells and bRG-*both-P* cells (Fig 4E). This is in agreement with observations using phosphovimentin, that report that when RG cells round up to divide, the basal process becomes extremely thin and forms small varicosities (Weissman et al., 2003). Because the apical process is significantly thinner than the basal process (Fig 3K), it may fail to be detected by phosphovimentin immunolabelling. Alternatively, vimentin

may be expressed at low levels in the apical process.

Comparisons of the proportions of the five precursor types show that bRG-*both-P* cells and tbRG cells predominate at 25%, followed by bRG-*apical-P* cells (20%) and IP and bRG-*basal-P* cells correspond to the least numerous cell type at just under 15% each (Fig 4F).

Inheritance of processes in OSVZ precursors is determined by horizontal plane of division and affects precursor fate

Because morphology at mitosis is a good indicator of the morphology after birth and throughout the lifetime of a precursor (Fig 4D), we used morphology at mitosis to assess the inheritance of the basal or apical process as well as its influence on the fate of the progeny. Analysis of the paired daughter cells generated by the different bRG cell morphotypes takes into account: (i) bRG mother cell morphology prior to mitosis, (ii) morphology of the two daughter cells immediately following division i.e. at birth (iii) the relative position of each daughter cell after mitosis (upper basal or lower apical) (Fig 5A-B). This revealed that different bRG cell types differ in their paired daughter cells progeny and points to general rules of process inheritance.

In 80% of divisions of bRG-*both-P* cells, the basal process is inherited by the upper and the apical process by the lower daughter. In virtually all cases, the lower daughter of bRG-*apical-P* mother cells inherits the apical process and the upper daughter of bRG-*basal-P* the basal process. No upper daughter of a bRG-*basal-P* mother cell was found with an apical process confirming previous observations (Hansen et al., 2010; LaMonica et al., 2013).

These findings suggest a simple rule of process inheritance based on the position of the daughter cell. Further, TLV showed that the vast majority of bRG cells exhibit a horizontal cleavage plane (>80%, Fig 5C). Horizontal plane of division was also predominant in vivo at E78 (Fig 5D). The higher proportion of horizontal divisions at E65 observed on organotypic slices are likely due to the known influence of culture leading to increases in horizontal planes (Haydar et al., 2003; Konno et al., 2008).

We next examined how the inheritance of a given process at birth influences the identity of the precursor type (Fig5E). We observed that cells born either with an apical or a basal process are prone to become cycling bRG cells (with a predominance for maintaining the inherited process) and to a lesser extent tbRG cells, whereas cells born without a process acquire a tbRG or IP cell phenotype. This analysis reveals that bRG-*apical-P*

correspond mostly to lower daughters (79.3%) whereas bRG-*basal-P* correspond to upper daughters (94.7%). Interestingly, Tc of sister daughters that both divide again are correlated and show a certain degree of synchronization with that of the mother cell (Fig 5F-G). We failed to detect any effect of the relative upper or lower position of the two daughter cells on their neuron vs precursor fate (data not shown).

Stage-specific differences in progeny and lineage relationships of the five OSVZ precursor types

We have extracted quantitative information regarding the precursor fate by a clonal analysis of a database including 695 cells and 306 divisions at E65 and E78 (Fig S4A). This established distinctive stage-specific proliferative, self-renewing and neurogenic characteristics for the five precursor types.

The five precursor types exhibit marked statistical differences in their order of apparition in the lineage trees. At E78, bRG-*both-P* cells and bRG-*basal-P* cells are predominant in the early ranks of lineage trees, bRG-*apical-P* cells at intermediate ranks whereas tbRG and IP cells are observed at the later ranks of division (Fig 6A). A similar but less pronounced trend is observed at E65 (Fig S4B).

Quantitative analysis of the progeny of each precursor type showed important qualitative and quantitative differences. All five precursor types are able to generate neurons and to self-renew, i.e. to generate at least one daughter of the same type as the mother cell. At both E65 and E78, we observed a self-renewal gradient, which is maximum in bRG-*both-P*, bRG-*apical-P* and tbRG cells, intermediate in IP cells and low in bRG-*basal-P* cells (Fig 6B). This suggests that the presence of the apical process is an important factor in conferring self-renewal properties to bRG cells.

The five precursor types exhibit different trends in their neurogenic capacity. At E78 bRG-*both-P* cells show the highest and IP cells the lowest proportions of neuronal progeny (Fig 6C). Variations in the neurogenic capacity of the different precursor types influence the size of their progeny. For instance bRG-*both-P* and IP cells have comparable progeny (Fig 6D, S4C), despite the fact that they are respectively at the top and bottom ranks of the lineage trees. The similarity in progeny of these two precursor types is due to the fact that IP cells have considerably lower neurogenic potential compared to bRG-*both-P* cells (Fig 6C). The quantitative differences in the neurogenic potential and rates of self-renewal coupled with lineage rank suggest that different precursor types have distinct relationships. In order to investigate this, we developed a formal graphic description of

the full repertoire of precursor behavior. In these state transition diagrams (Harel, 1987), nodes (or states) represent precursor types and directed edges the transitions between precursors (ie precursor progeny). Note that in state transition diagrams, each transition is expressed as a percentage of all transitions observed in the database and therefore is influenced by the frequency of each precursor type.

The state transition diagram formalizes statistically the hierarchical lineage relationships between the 5 precursor subtypes (Fig 6E). Of note, state transition analysis shows that precursors can transit bidirectionally between different types. At both stages and with only 2 exceptions, the downward transitions rates, going from low to high lineage ranks (ie down directed in the diagram), are stronger than upward transition rates.

At E65, average precursor ranks and precursor progeny variations are comparable to that observed at E78 (Fig 6A,D, Fig S4B-C). Interestingly, state transition diagrams are denser at E78 than at E65, with 28 out 30 possible transitions occurring vs 22 out of 30 respectively. The topology of the state transition graphs differs between the two stages in several salient ways. In particular, tbRG cells-which occur on average at rank 4 (Fig 6A) and represent the predominant precursor type generated at both stages by all precursors-are highly clustered with bRG-*apical-P* and IP cells via bidirectional transitions at E78. Interestingly, although tbRG cells have a much higher input at E78 than at E65, the frequency of tbRG cell transition to neurons does not change between the two stages. Instead, the increased tbRG cells output at E78 is characterized by new transitions to bRG-*apical-P* and bRG-*basal-P* cells as well as by an important strengthening of its transition to IP cells to which it becomes the strongest contributor. Because tbRG cells are characterized by both stronger inputs and outputs at E78 than at E65, they are endowed with a hub status at E78. IP cell production, self-renewal and output are increased at E78 compared to E65.

All precursor types generate neurons with distinct frequencies. Neuron production is significantly higher for all precursor types at E65 than at E78. State diagrams reveal that bRG-*both-P* cells are the largest provider of neuronal progeny, followed by bRG-*apical-P*, tbRG, bRG-*basal-P* and finally IP cells. These data show the existence of stage-specific differences in lineage relationships that result in precursor-specific differences in self-renewal, precursor pool amplification and neuron production.

2.1.4 Discussion

Technical considerations

Compared to previous studies, our approach includes two major technical improvements. First, we have used an unbiased procedure to label cycling precursors, via retroviral infection. This reveals a higher diversity of BPs types (Fig 7A) than previously reported in human (Fietz et al., 2010; Hansen et al., 2010; LaMonica et al., 2013). We have identified five precursor categories and found that the previously reported bRG-*basal-P* cells and IPs account each only for 15% of the total precursor population. bRG-*both-P*, tbRG represent each 25% and bRG-*apical-P* 20% of the total population. The fact that previous human studies reported occasional OSVZ precursor cells bearing an apical processes but failed to identify bRG-*apical-P* cells and bRG-*both-P* cells as major precursor types (Fietz et al., 2010; Hansen et al., 2010; LaMonica et al., 2013) is in most part due to the labeling technique used. Whereas the retroviral infection technique used here provides an unbiased sampling of cycling precursors, the retrograde labeling of bRG cells via placement of dye or adenovirus on the pial membrane (Fietz et al., 2010; Hansen et al., 2010; LaMonica et al., 2013) will uniquely label bRG-*basal-P* cells. Of note, we have been able to implement dual labeling of Pax6 and Tbr2 on single morphologically distinct precursor types, which has not been done in other studies. Contrary to previous claims these transcription factors fail to qualitatively distinguish IPs vs bRG cells.

Second, we have been able to implement long-term live imaging of precursor behavior in the preserved environment of a cortical slice, as opposed to short-term observations reported in human tissue of reduced viability (LaMonica et al., 2013). This reveals for the first time that primate OSVZ precursors exhibit extensive proliferative abilities, undergoing up to six successive rounds of proliferative division. This long term ex vivo assay provided an extensive and unique database of clonal observations of OSVZ precursors lineages, including key attributes of single precursor behavior (Tc, mode of division, direction of MST, upper or lower position at birth, size of progeny, self-renewal, transitions). Quantitative analysis of this database makes it possible to extract precursor type-specific behavioral signature as well as to unravel the complex lineage relationships.

Specific properties of OSVZ precursors

The present study shows that macaque OSVZ progenitors exhibit several key morphological and behavioral characteristics of VZ RG cells. These include a radial glial morphology with basal and apical processes as well as extensive proliferative abilities. Like VZ RG cells, each of the five precursor types of the OSVZ are able to undergo symmetric proliferative divisions and to self-renew (Fig 6C-D).

Of note, a fraction of bRG cells show precursor type-specific complex nuclear dynamics, reminiscent of interkinetic migration in RG cells in the VZ. In agreement with previous studies we observe basally directed MSTs in bRG-*basal-P* cells (Hansen et al., 2010; LaMonica et al., 2012; Nelson et al., 2013). In addition we observed apically directed MST and showed that bRG-*apical-P* exclusively undergo downwards apical MST while bRG-*basal-P* undergo exclusively upwards basal MST. Proper nuclear positioning is thought to be critical to ensure sufficient transcriptional capacity as well as to minimize transport distances between the nuclei and the cytoplasm in elongated cells (Gundersen and Worman, 2013).

Our findings suggest that the inheritance of the apical process plays a significant role in conferring self-renewal properties to macaque bRG daughter cells. This contrasts with the mechanism reported in mouse cortical precursors where the daughter cell is required to inherit the basal process in order to retain proliferative abilities (Shitamukai et al., 2011). Of note, OSVZ IPs which are devoid of basal process undergo numerous proliferative divisions and/or self-renew (Fig S4A, Movie S4), as opposed to mouse IPs which almost undergo uniquely symmetric neuronal terminal divisions (Huttner and Kosodo, 2005). Our results suggest that bipolar epithelial-like morphology may be an important feature for self-renewal since bRG-*both-P* show the highest self-renewal rates.

The detailed analysis of precursors divisions showed that bRG-*apical-P* and bRG-*basal-P* differ by their upper or lower position immediately following mitosis: bRG-*apical-P* correspond mostly to lower daughters and bRG-*basal-P* to upper daughters. Further, the analysis of the fate of paired daughter cells generated by bRGs revealed that the rule that has been described for asymmetric divisions in the mouse and zebrafish VZ (Alexandre et al., 2010) - whereby the lower cell becomes the neuron and the upper cell remains a progenitor- does not operate in macaque OSVZ, in accordance with the non prominent role of the basal process in maintaining self-renewal abilities. Among the five precursor types, bRG-*both-P* cells stand at the early rank of the lineages and generate

large progenies. This is in agreement with the recently reported bipolar RG cell in the embryonic mouse ventral telencephalon shown to exhibit extensive capacity to generate progeny (Pilz et al., 2013).

A striking property of a fraction of OSVZ precursors revealed by our TLV observations is the structural re-patterning of their cytoskeleton during their lifetime, which underlines the need to perform high-resolution exhaustive observations in order to detect the full repertoire of morphotypes. In particular, we uncovered the occurrence of tbRG cells, which alternate between stages showing one or two processes and stages with none during their lifetime.

Morphological diversity of bRG cells provides the basis for dynamic cell interactions

The above observations point to the OSVZ being a zone enriched in dynamic basal and apical processes (Fig 7A) that may serve to sample the micro-environment stretching from the pia to the VZ, and thereby integrating signals from pre and postmitotic cells as well as from fiber layers. Apical processes could be seen extending as far as the VZ without however reaching the ventricular surface, providing the substrate for novel transient cellular interactions between bRG cells and precursor cells from the ISVZ and the VZ (Nelson et al., 2013; Yoon et al., 2008). Basal processes can underlie interactions between cycling precursors and postmitotic neurons from the subplate and the cortical plate, which may subserve a feed-back signal (Polleux et al., 2001). Filopodia were also occasionally observed, providing the basis for lateral interactions with cycling or differentiating neighbor cells via Notch-Delta signaling (Nelson et al., 2013; Shitamukai et al., 2011; Yoon et al., 2008).

Extensive proliferative abilities of OSVZ precursors

The present study provides the first evidence that OSVZ precursors undergo numerous successive rounds of proliferative divisions, generating complex precursor lineage trees.

The balance between proliferative and differentiative divisions is key for OSVZ evolutionary expansion and therefore must be tightly controlled by both intrinsic and extrinsic mechanisms. Notch signaling (Hansen et al., 2010) as well as Beta integrin signaling relayed via the basal process (Fietz et al., 2010) have been shown to contribute to the control of OSVZ precursor proliferation. The present data show that OSVZ precursors exhibit sustained proliferative abilities, with cell-cycle parameters comparable to the RG

cells of the VZ. By contrast with earlier studies predicting that OSVZ progenitors predominantly divide in an asymmetric, neurogenic manner (Fish et al., 2008), we observed that, although not anchored at the apical junctional belt and/or basal lamina, BP cells are nevertheless able to undergo numerous rounds of symmetric proliferative divisions- that are ultimately finely controlled. This appears as a remarkable feature since loss of polarity or epithelial integrity as well as delamination from the epithelium have been shown to lead to uncontrolled proliferation in numerous tissues (Gomez-Lopez et al., 2013; Lee and Vasioukhin, 2008). The OSVZ has been suggested to correspond to an extra-cellular matrix (ECM) component enriched micro-environment (Fietz et al., 2012). There is evidence that ECM molecules bind to specific growth factors and morphogens and regulate their bioavailability, thereby providing a dynamic microenvironment for local integration of adhesive and growth factor signaling (Brizzi et al., 2012). The OSVZ therefore provides a niche, harboring signals controlling stemness, proliferation and differentiation (Fietz et al., 2012; Marthiens et al., 2010), which are complemented by signaling from other precursors and/or progeny outside the OSVZ, presumably via the basal and apical processes.

Spatiotemporal regulation of cell-cycle parameters in OSVZ: a regulatory framework underlying the enlarged supragranular layer compartment in the macaque and human cortex.

Examination of the timing of the macaque GZ suggested that high proliferative rates are required to maintain and amplify the OSVZ progenitor pool over the protracted period of supragranular neuron production in the macaque (Dehay and Kennedy, 2007; Lukaszewicz et al., 2005). Here, we have been able to extract cell-cycle durations and proliferative behavior of precursors, which show a developmental regulation that departs from what has been described in the rodent (Arai et al., 2011; Caviness et al., 1995; Reznikov and Van Der Kooy, 1995) in several respects. First, we observed a smaller difference (15 - 7% at E65 and E78 respectively) in Tc between APs and BPs than has been reported in the mouse (30%) (Arai et al., 2011). Second, while rodent precursor global Tc has been shown to steadily increase during corticogenesis, we observed a shortening of Tc both in the VZ - in agreement with P. Rakic's findings (Kornack and Rakic, 1998) - and in the OSVZ.

This reduction in Tc, by means of a reduction in TG1 and to a lesser extent in TS (Fig 2I) is associated with an increase in proliferative divisions (Fig 2C) and a reduction of cell-cycle exit (Fig 2E), in agreement with the relationship between TG1 and the mode

of division in cortical precursors (Pilaz et al., 2009). Combined, these two processes contribute to the expansion of the OSVZ precursor pool observed at midcorticogenesis (Fig 7C). Tc shortening and decrease in cell-cycle exit rates are observed simultaneously in OSVZ and VZ. However, whereas the OSVZ continues to expand, the VZ declines, which suggests that the OSVZ expansion may benefit from a sustained or increased seeding by VZ precursors (LaMonica et al., 2013). The VZ starts to expand at early stages, before the generation of the OSVZ (Rakic, 2009). The observed coordination between Tc regulation in VZ and OSVZ at late stages underlies the important role of the VZ in cortical expansion throughout corticogenesis.

Supragranular layer neurons are generated by the OSVZ (Lukaszewicz et al., 2005). Therefore, this expansion of the OSVZ pool via Tc shortening and decrease in cell-cycle exit accounts for the sustained production of supragranular neurons during the second half of corticogenesis. This leads to postulate that these specific properties of macaque OSVZ precursors account for the expansion of the cortex and the supragranular layer enlargement that characterize this species as well as the human.

One can hypothesize that the fine regulation of the cell-cycle, beyond its impact on the size of the progenitor pools, will also influence distinct transcriptional sequences in precursors that will in turn determine postmitotic transcriptional programs generating neuronal diversity (Molyneaux et al., 2007), as suggested by a recent study showing that the combinatorial temporal patterning of precursors is responsible for increasing diversity in drosophila CNS (Bayraktar and Doe, 2013).

Cortical neurons of the primate are generated by a mosaic of precursor subtypes via stage-specific lineages

In addition to their capacity to undergo symmetric proliferative divisions, as well as to self-renew, each of the five precursor types is able to generate neurons at E65 and E78. This indicates that OSVZ precursors generate neurons destined for infragranular and supragranular layers (Dehay et al., 1993; Rakic, 1974).

The lineage relationships between the different OSVZ precursor types revealed by the state transition diagrams provide a new model of cortical development, which departs from the prevailing view where bRGs produce TAPS- identified as IPs- which symmetrically amplify before producing neurons (Fig 7B) (Fietz and Huttner, 2011; Fietz et al., 2010; Kriegstein et al., 2006; Lui et al., 2011). We report frequencies of transitions at the total precursor population level (Fig 6E) as well as neurogenic transitions for individual

precursor types (Fig 6C). Our study shows that, at the two stages examined, IPs are in fact the smallest provider of neuronal progeny, the largest provider being bRG-*both-P*, followed in order of importance by bRG-*apical-P*, tbRG and bRG-*basal-P* cells.

State transition analysis of lineages provides an explicit graphic description of data obtained from numerous lineage trees and reveals complex relationships between OSVZ precursors. One salient characteristic of OSVZ precursor lineage is the occurrence of bidirectional transitions that depart from the classical unidirectional lineage genealogy including that reported in rodent corticogenesis (Noctor et al., 2004; Qian et al., 1998; Tyler and Haydar, 2013). One can hypothesize that precursor diversity and their complex lineages relationships changing over time reflects a process that allows for the self-organization of the cortex (Kennedy and Dehay, 2012).

Although the basic module of five precursor types is present at E65 and E78, the state transition analysis shows that lineage relationships between precursors show stage-specific differences. Specifically, the present results reveal differences in the topology of lineage state transitions during the generation of infra- and supragranular layer neurons. This provides a novel conceptual framework for understanding the mechanisms ensuring the ordered production of phenotypically distinct neuronal populations.

While it is generally agreed that the Old World macaque monkey is a valid model for understanding many features of the human brain, future comparative studies of a range of different members of the primate order and non-primates will be necessary in order to better define primate specific features.

Temporal changes in competence have been shown to contribute to the generation of distinct neuronal types in distinct numbers during corticogenesis by a common pool of precursors (Jacob et al., 2008; Qian et al., 1998). The present results show that, superimposed on these changes in temporal competence, there are modifications in lineage relationships that are consistent with the observed changes in cell cycle parameters (Fig 7C). This would imply that the interplay of temporal competence and lineage state transition topology is a widespread developmental mechanism in the CNS (Ulvklo et al., 2012).

2.1.5 Material and methods

Animals

Fetuses from timed-pregnant cynomolgus monkeys (Macaca fascicularis, gestation period 165 days) were delivered by caesarian section as previously described (Lukaszewicz et al., 2005). All experiments were in compliance with national and European laws as well as with institutional guidelines concerning animal experimentation. Surgical procedures were in accordance with European requirements 2010/63/UE. The protocol C2EA42-12-11-0402-003 has been reviewed and approved by the Animal Care and Use Committee CELYNE (C2EA #42).

Organotypic slice culture and retroviral infection

Occipital poles of embryonic hemispheres were isolated and embedded in 3% low melting agarose in supplemented HBSS at 37°C. 300μm-thick parasagittal slices were cut in 4°CC supplemented HBSS using a vibrating blade microtome (Leica VT1000 S). Slices were incubated in GMEM medium containing pCMV-EGFP retrovirus (1 to 5.105 pi/mL), for 2 to 3h at 37°C. Slices were then mounted on on laminin/poly-lysine coated 0.4μm Millicell culture inserts in a drop of type I collagen and cultured at 37°C, 7.5% CO2, in 6-well plates in GMEM supplemented with 1% sodium pyruvate, 7.2μM beta-mercaptoethanol, 1% nonessential amino acids, 2mM glutamine, 1% penicillin/streptomycin, and 10% FCS.

Antibodies

Primary antibodies used were rabbit anti-Ki67 (Neomarker, 1:400), rabbit anti-Ki67 FITC conjugated (Neomarker, 1:100), mouse anti NeuN (Milipore 1/100), mouse anti-Pax6 (DSHB, 1/1000), rabbit anti-Tbr2 (Abcam 1/4000), sheep anti-EOMES (R&D 1:800), chicken anti-GFP (Invitrogen, 1:1000), rabbit anti-Geminin (Santa-Cruz, 1:400), mouse anti-PCNA (Dako, 1/100). Secondary antibodies were Alexa Fluor 488 goat anti-chicken IgG (Invitrogen, 1/800), Alexa Fluor 555 goat anti-mouse IgG (Invitrogen, 1/800), Alexa 647 goat anti rabbit (Invitrogen, 1:400), Alexa 488 goat anti FITC (Invitrogen, 1:1000), Alexa 555 donkey anti mouse (Invitrogen, 1:400), Alexa 555 donkey anti rabbit (Invitrogen, 1:200), Alexa 647 donkey anti mouse (Invitrogen, 1:400) Alexa 647 donkey anti sheep (Invitrogen, 1:200), Dylight 405 donkey anti rabbit (Jackson, 1:200), Dylight 488 donkey anti chicken (Jackson, 1:400).

Lineage tree reconstruction

6003.3 hours (ie $\sim$ 250 days) of recording have been performed in this study. Images were taken every 1 to 1.5 hour up to 15 days. A cell was considered proliferative if it underwent division during the recording period. It was designated as a neuron if it started radial migration with typical migrating neuron morphology or when it was observed non dividing for a duration exceeding 1.5 time the average cell-cycle length of the zone and age under consideration (E48>67 hours, E65> 101h and 108h, at E78> 69h and 74h in the VZ and OSVZ respectively). 1071 cells were examined (56 cells at E48; 50 at E67; 71 at E75, 2 hemisphere; 335 at E65; 559 at E78, 4 hemispheres). 487 divisions were analyzed (22 at E48; 142 at E65; 31 at E67; 45 at E75; 247 at E78).

Statistical analysis

Quantitative data are presented as the mean +/- SEM from representative experiments. Statistical analyses were performed using the R software. The tests and the corresponding p-values are indicated in the figure legends. For data involving proportions of small number of data points the Fisher exact test was used. Non-parametric statistical tests were preferred because the data did not follow a normal distribution. Wilcoxon test was performed for mean comparison, Kruskal-Wallis test for one-way anaysis of variance. $p < 0.05$ was considered statistically significant. The hierarchical clustering (Fig 1J) was performed using the factoMineR package of R (Lê et al., 2008).

2.1.6 Acknowledgements

We thank K. Knoblauch for invaluable and expert guidance in R statistics. We are grateful to M. Valdebenito, M. Seon, F. Piollat, and B. Beneyton for excellent animal care. We are indebted to N. Doerflinger , S. Zouaoui , P. Misery and C. Lamy for technical assistance and to P. Giroud and J.P. Laigneau for help with the iconography. Administrative and logistic support from C. Nay, N. Kolomitre, and J. Beneyton is acknowledged. Financial support was from FP7 SECO grant (FP7-2007 ICT-216593), LABEX CORTEX (ANR-11-LABX-0042), and LABEX DEVweCAN (ANR-10-LABX- 061) of Universit de Lyon, within the program "Investissements d'Avenir" (ANR-11-IDEX-0007) operated by the French National Research Agency (ANR).

2.1.7 References

Alexandre, P., Reugels, A.M., Barker, D., Blanc, E., and Clarke, J.D. (2010). Neurons derive from the more apical daughter in asymmetric divisions in the zebrafish neural tube. Nat Neurosci 13, 673-679.

Arai, Y., Pulvers, J.N., Haffner, C., Schilling, B., Nusslein, I., Calegari, F., and Huttner, W.B. (2011). Neural stem and progenitor cells shorten S-phase on commitment to neuron production. Nat Commun 2, 154.

Bayraktar, O.A., and Doe, C.Q. (2013). Combinatorial temporal patterning in progenitors expands neural diversity. Nature 498, 449-455.

Brizzi, M.F., Tarone, G., and Defilippi, P. (2012). Extracellular matrix, integrins, and growth factors as tailors of the stem cell niche. Curr Opin Cell Biol 24, 645-651.

Bystron, I., Blakemore, C., and Rakic, P. (2008). Development of the human cerebral cortex: Boulder Committee revisited. Nat Rev Neurosci 9, 110-122.

Caviness, V.S., Takahashi, T., and Nowakowski, R.S. (1995). Numbers, time and neocortical neuronogenesis: a general developmental and evolutionary model. Trends Neurosci 18, 379-383.

Dehay, C., Giroud, P., Berland, M., Smart, I., and Kennedy, H. (1993). Modulation of the cell cycle contributes to the parcellation of the primate visual cortex. Nature 366, 464-466.

Dehay, C., and Kennedy, H. (2007). Cell-cycle control and cortical development. Nat Rev Neurosci 8, 438-450.

Englund, C., Fink, A., Lau, C., Pham, D., Daza, R.A., Bulfone, A., Kowalczyk, T., and Hevner, R.F. (2005). Pax6, Tbr2, and Tbr1 are expressed sequentially by radial glia, intermediate progenitor cells, and postmitotic neurons in developing neocortex. J Neurosci 25, 247-251.

Fietz, S.A., and Huttner, W.B. (2011). Cortical progenitor expansion, self-renewal and neurogenesis-a polarized perspective. Curr Opin Neurobiol 21, 23-35.

Fietz, S.A., Kelava, I., Vogt, J., Wilsch-Brauninger, M., Stenzel, D., Fish, J.L., Corbeil, D., Riehn, A., Distler, W., Nitsch, R., and Huttner, W.B. (2010). OSVZ progenitors of human and ferret neocortex are epithelial-like and expand by integrin signaling. Nat Neurosci 13, 690-699.

Fietz, S.A., Lachmann, R., Brandl, H., Kircher, M., Samusik, N., Schroder, R., Lakshmanaperumal, N., Henry, I., Vogt, J., Riehn, A., et al. (2012). Transcriptomes of

germinal zones of human and mouse fetal neocortex suggest a role of extracellular matrix in progenitor self-renewal. Proc Natl Acad Sci U S A 109, 11836-11841.

Fish, J.L., Dehay, C., Kennedy, H., and Huttner, W.B. (2008). Making bigger brains-the evolution of neural-progenitor-cell division. J Cell Sci 121, 2783-2793.

Garcia-Moreno, F., Vasistha, N.A., Trevia, N., Bourne, J.A., and Molnar, Z. (2012). Compartmentalization of Cerebral Cortical Germinal Zones in a Lissencephalic Primate and Gyrencephalic Rodent. Cereb Cortex 22, 482-492.

Gomez-Lopez, S., Lerner, R.G., and Petritsch, C. (2013). Asymmetric cell division of stem and progenitor cells during homeostasis and cancer. Cell Mol Life Sci [2013/06/19 Epub ahead of print] 10.1007/s00018-013-1386-1.

Götz, M., and Huttner, W.B. (2005). The cell biology of neurogenesis. Nat Rev Mol Cell Biol 6, 777-788.

Gundersen, G.G., and Worman, H.J. (2013). Nuclear positioning. Cell 152, 1376-1389.

Hansen, D.V., Lui, J.H., Parker, P.R., and Kriegstein, A.R. (2010). Neurogenic radial glia in the outer subventricular zone of human neocortex. Nature 464, 554-561.

Harel, D. (1987). Statecharts: A Visual Formalism for Complex Systems. Sci Comput Programming 8, 231-274.

Haydar, T.F., Ang, E., Jr., and Rakic, P. (2003). Mitotic spindle rotation and mode of cell division in the developing telencephalon. Proc Natl Acad Sci U S A 100, 2890-2895.

Huttner, W.B., and Kosodo, Y. (2005). Symmetric versus asymmetric cell division during neurogenesis in the developing vertebrate central nervous system. Curr Opin Cell Biol 17, 648-657.

Jacob, J., Maurange, C., and Gould, A.P. (2008). Temporal control of neuronal diversity: common regulatory principles in insects and vertebrates? Development 135, 3481-3489.

Kelava, I., Reillo, I., Murayama, A.Y., Kalinka, A.T., Stenzel, D., Tomancak, P., Matsuzaki, F., Lebrand, C., Sasaki, E., Schwamborn, J.C., et al. (2012). Abundant Occurrence of Basal Radial Glia in the Subventricular Zone of Embryonic Neocortex of a Lissencephalic Primate, the Common Marmoset Callithrix jacchus. Cereb Cortex 22, 469-481.

Kennedy, H., and Dehay, C. (2012). Self-organization and interareal networks in the primate cortex. Prog Brain Res 195, 341-360.

Kennedy, H., Douglas, R., Knoblauch, K., and Dehay, C. (2007). Self-organization

and pattern formation in primate cortical networks. Novartis Found Symp 288, 178-194 discussion 195-178, 276-181.

Konno, D., Shioi, G., Shitamukai, A., Mori, A., Kiyonari, H., Miyata, T., and Matsuzaki, F. (2008). Neuroepithelial progenitors undergo LGN-dependent planar divisions to maintain self-renewability during mammalian neurogenesis. Nat Cell Biol 10, 93-101.

Kornack, D.R., and Rakic, P. (1998). Changes in cell-cycle kinetics during the development and evolution of primate neocortex. PNAS 95, 1242-1246.

Kriegstein, A., Noctor, S., and Martinez-Cerdeno, V. (2006). Patterns of neural stem and progenitor cell division may underlie evolutionary cortical expansion. Nat Rev Neurosci 7, 883-890.

LaMonica, B.E., Lui, J.H., Hansen, D.V., and Kriegstein, A.R. (2013). Mitotic spindle orientation predicts outer radial glial cell generation in human neocortex. Nat Commun 4, 1665.

LaMonica, B.E., Lui, J.H., Wang, X., and Kriegstein, A.R. (2012). OSVZ progenitors in the human cortex: an updated perspective on neurodevelopmental disease. Curr Opin Neurobiol 22, 747-753.

Lê, S., Josse, J., and Husson, F. (2008). FactoMineR: An R package for multivariate analysis. J Stat Soft 25, 1-18.

Lee, M., and Vasioukhin, V. (2008). Cell polarity and cancer–cell and tissue polarity as a non-canonical tumor suppressor. J Cell Sci 121, 1141-1150.

Levitt, P., Cooper, M.L., and Rakic, P. (1981). Coexistence of neuronal and glial precursor cells in the cerebral ventricular zone of the fetal monkey: an ultrastructural immunoperoxidase analysis. J Neurosci 1, 27-39.

Lui, J.H., Hansen, D.V., and Kriegstein, A.R. (2011). Development and evolution of the human neocortex. Cell 146, 18-36.

Lukaszewicz, A., Savatier, P., Cortay, V., Giroud, P., Huissoud, C., Berland, M., Kennedy, H., and Dehay, C. (2005). G1 phase regulation, area-specific cell cycle control, and cytoarchitectonics in the primate cortex. Neuron 47, 353-364.

Marin-Padilla, M. (1992). Ontogenesis of the pyramidal cell of the mammalian neocortex and developmental cytoarchitectonics: a unifying theory. J Comp Neurol 321, 223-240.

Marthiens, V., Kazanis, I., Moss, L., Long, K., and Ffrench-Constant, C. (2010). Adhesion molecules in the stem cell niche - more than just staying in shape? J Cell Sci

123, 1613-1622.

Martinez-Cerdeno, V., Cunningham, C.L., Camacho, J., Antczak, J.L., Prakash, A.N., Cziep, M.E., Walker, A.I., and Noctor, S.C. (2012). Comparative analysis of the subventricular zone in rat, ferret and macaque: evidence for an outer subventricular zone in rodents. PLoS One 7, e30178.

Martinez-Cerdeno, V., Noctor, S.C., and Kriegstein, A.R. (2006). The role of intermediate progenitor cells in the evolutionary expansion of the cerebral cortex. Cereb Cortex 16 Suppl 1, i152-161.

Molyneaux, B.J., Arlotta, P., Menezes, J.R., and Macklis, J.D. (2007). Neuronal subtype specification in the cerebral cortex. Nat Rev Neurosci 8, 427-437.

Nelson, B.R., Hodge, R.D., Bedogni, F., and Hevner, R.F. (2013). Dynamic Interactions between Intermediate Neurogenic Progenitors and Radial Glia in Embryonic Mouse Neocortex: Potential Role in Dll1-Notch Signaling. J Neurosci 33, 9122-9139.

Noctor, S.C., Martinez-Cerdeno, V., Ivic, L., and Kriegstein, A.R. (2004). Cortical neurons arise in symmetric and asymmetric division zones and migrate through specific phases. Nat Neurosci 7, 136-144.

Pilaz, L.J., Patti, D., Marcy, G., Ollier, E., Pfister, S., Douglas, R.J., Betizeau, M., Gautier, E., Cortay, V., Doerflinger, N., et al. (2009). Forced G1-phase reduction alters mode of division, neuron number, and laminar phenotype in the cerebral cortex. Proc Natl Acad Sci U S A 106, 21924-21929.

Pilz, G.A., Shitamukai, A., Reillo, I., Pacary, E., Schwausch, J., Stahl, R., Ninkovic, J., Snippert, H.J., Clevers, H., Godinho, L., et al. (2013). Amplification of progenitors in the mammalian telencephalon includes a new radial glial cell type. Nat Commun 4, 2125.

Polleux, F., Dehay, C., Goffinet, A., and Kennedy, H. (2001). Pre- and post-mitotic events contribute to the progressive acquisition of area-specific connectional fate in the neocortex. Cereb Cortex 11, 1027-1039.

Pontious, A., Kowalczyk, T., Englund, C., and Hevner, R.F. (2008). Role of intermediate progenitor cells in cerebral cortex development. Dev Neurosci 30, 24-32.

Qian, X., Goderie, S.K., Shen, Q., Stern, J.H., and Temple, S. (1998). Intrinsic programs of patterned cell lineages in isolated vertebrate CNS ventricular zone cells. Development 125, 3143-3152.

Rakic, P. (1974). Neurons in rhesus monkey visual cortex: systematic relation between time of origin and eventual disposition. Science 183, 425-427.

Rakic, P. (2009). Evolution of the neocortex: a perspective from developmental biology. Nat Rev Neurosci 10, 724-735.

Reillo, I., de Juan Romero, C., Garcia-Cabezas, M.A., and Borrell, V. (2011). A role for intermediate radial glia in the tangential expansion of the mammalian cerebral cortex. Cereb Cortex 21, 1674-1694.

Reznikov, K., and Van Der Kooy, D. (1995). Variability and partial synchrony of the cell cycle in the germinal zone of the early embryonic cerebral cortex. J Comp Neurol 360, 536-554.

Shitamukai, A., Konno, D., and Matsuzaki, F. (2011). Oblique radial glial divisions in the developing mouse neocortex induce self-renewing progenitors outside the germinal zone that resemble primate outer subventricular zone progenitors. J Neurosci 31, 3683-3695.

Smart, I.H., Dehay, C., Giroud, P., Berland, M., and Kennedy, H. (2002). Unique morphological features of the proliferative zones and postmitotic compartments of the neural epithelium giving rise to striate and extrastriate cortex in the monkey. Cereb Cortex 12, 37-53.

Stancik, E.K., Navarro-Quiroga, I., Sellke, R., and Haydar, T.F. (2010). Heterogeneity in ventricular zone neural precursors contributes to neuronal fate diversity in the postnatal neocortex. J Neurosci 30, 7028-7036.

Tyler, W.A., and Haydar, T.F. (2013). Multiplex Genetic Fate Mapping Reveals a Novel Route of Neocortical Neurogenesis, Which Is Altered in the Ts65Dn Mouse Model of Down Syndrome. J Neurosci 33, 5106-5119.

Ulvklo, C., MacDonald, R., Bivik, C., Baumgardt, M., Karlsson, D., and Thor, S. (2012). Control of neuronal cell fate and number by integration of distinct daughter cell proliferation modes with temporal progression. Development 139, 678-689.

Wang, X., Tsai, J.W., LaMonica, B., and Kriegstein, A.R. (2011). A new subtype of progenitor cell in the mouse embryonic neocortex. Nat Neurosci 14, 555-561.

Weissman, T., Noctor, S.C., Clinton, B.K., Honig, L.S., and Kriegstein, A.R. (2003). Neurogenic radial glial cells in reptiles, rodent, and human: from mitosis to migration. Cerbral Cortex 13, 550-559.

Yoon, K.J., Koo, B.K., Im, S.K., Jeong, H.W., Ghim, J., Kwon, M.C., Moon, J.S., Miyata, T., and Kong, Y.Y. (2008). Mind bomb 1-expressing intermediate progenitors generate notch signaling to maintain radial glial cells. Neuron 58, 519-531.

2.1.8 Figures

Figure 1: Germinal zones specific patterns of Pax6/Tbr2 expression. A-F. Microphotographs of parasagittal transects of Pax6/Tbr2/Ki67 immunostained visual cortex GZ from E49 to E94. Scale bar 20μm. VZ: ventricular zone; SVZ: subventricular zone, IFL: inner fiber layer, ISVZ: inner SVZ, OFL: outer fiber layer, OSVZ: outer SVZ, CP: cortical plate. **G.** Distribution of cycling precursors in each GZ during cortical neurogenesis. **H.** Proportion of Ki67+ precursors in VZ, ISVZ and OSVZ at different stages. (Mean +/- SEM; n=3-4 representative transects per age, >500 cells counted per group). **I.** Proportions of Ki67+ progenitors expressing Pax6 and/or Tbr2 in VZ, ISVZ and OSVZ (Mean +/- SEM; n=3-4 representative images per stage, >500 cells counted per zone for each age). **J.** Hierarchical clustering of the GZ compartments. The proportions of each type of precursor presented in I were transformed into a Euclidian distances matrix and subjected to a hierarchical clustering using Wards minimum variance method.

Figure 1

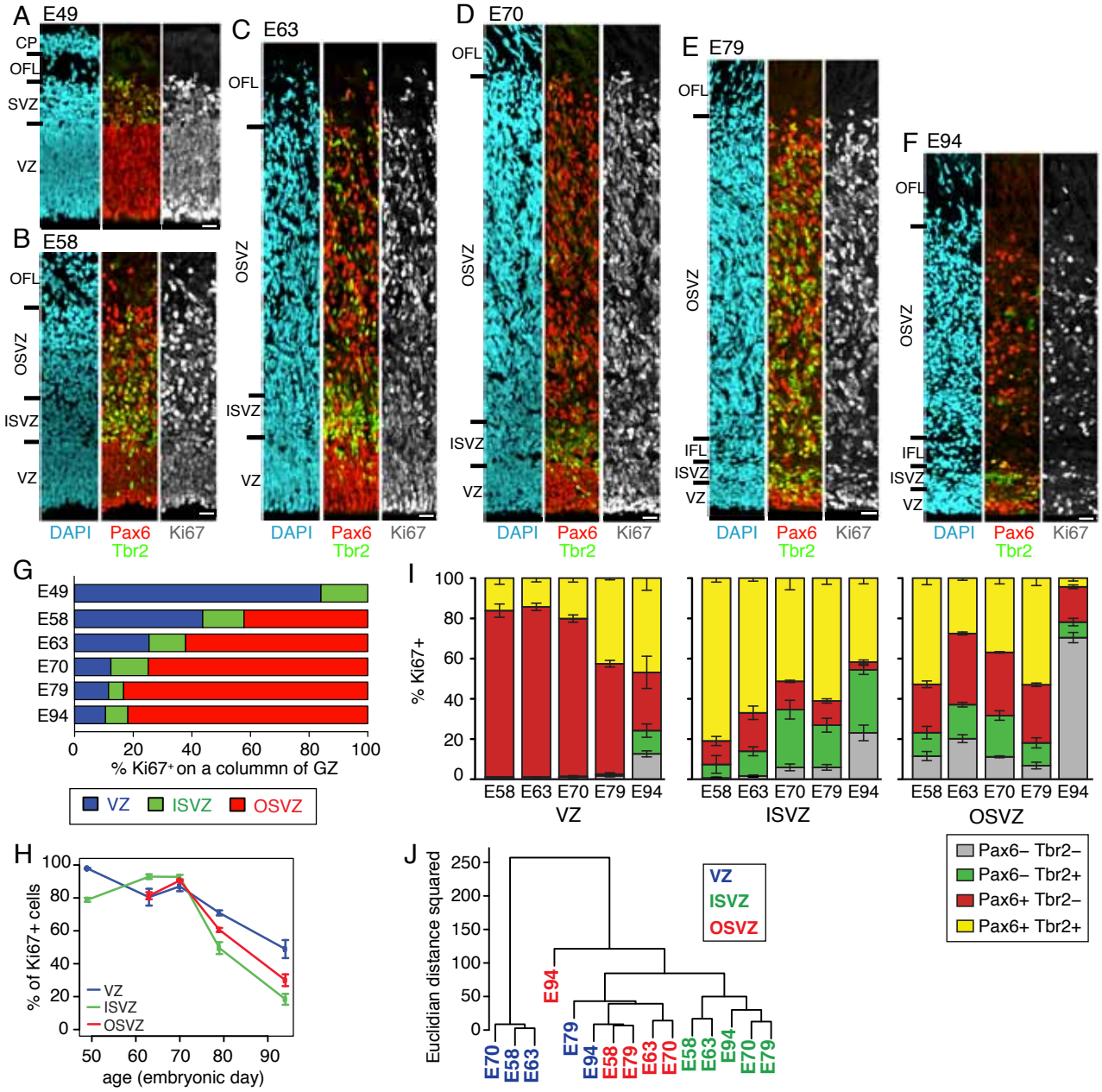
A E49
CP
OFL
SVZ
VZ
B E58
OFL
OSVZ
ISVZ
VZ
C E63
OFL
OSVZ
ISVZ
VZ
D E70
OFL
OSVZ
ISVZ
VZ
E E79
OFL
OSVZ
IFL
ISVZ
VZ
F E94
OFL
OSVZ
IFL
ISVZ
VZ
DAPI Pax6 Tbr2 Ki67
G
E49
E58
E63
E70
E79
E94
0 20 40 60 80 100
% Ki67+ on a columnn of GZ
VZ ISVZ OSVZ
I
% Ki67+
0 20 40 60 80 100
E58 E63 E70 E79 E94
VZ
ISVZ
OSVZ
Pax6– Tbr2–
Pax6– Tbr2+
Pax6+ Tbr2–
Pax6+ Tbr2+
H
% of Ki67+ cells
0 20 40 60 80 100
VZ
ISVZ
OSVZ
50 60 70 80 90
age (embryonic day)
J
Euclidian distance squared
0 50 100 150 200 250
VZ
ISVZ
OSVZ
E70 E58 E63
E94
E79 E94 E58 E79 E63 E70
E58 E63 E94 E70 E79

Figure 2: OSVZ precursors extensive proliferative abilities and temporal regulation of cell cycle parameters. **A.** Ex vivo reconstruction of lineage trees. Summary of 44 representative lineage trees reconstructed from TLV in the OSVZ (E65: 4 hemispheres, 10 slices; E78: 2 hemispheres, 3 slices). **B.** Distribution of the depth (number of successive divisions) of the OSVZ and VZ lineages shown in Fig1A and Fig S1F. Fisher exact test. **C.** Frequency of proliferative and differentiative divisions in OSVZ and VZ at E65 and E78 (E65: 4 hemispheres, 10 slices; E78: 4 hemispheres, 10 slices). * $p < 0.05$, ** $p < 0.01$ Fisher exact test. **D.** Comparison of Tc between VZ and OSVZ (Mean +/- SEM, E48: n=14 VZ; E65: n=52 VZ, n=40 OSVZ; E78: n=84 VZ, n=133 OSVZ, 4 hemispheres, 10 slices per stage, except E48 (2 hemispheres, 4 slices)). Dots represent sparse data at intermediate stages (E67, 1 hemisphere, 1 slice and E75, 1 hemisphere, 2 slices). * $p<0.05$, *** $p<0.001$ Wilcoxon test. **E.** Cell-cycle exit rate estimated by the percentage of Ki67+/NeuN+ precursors. (Mean +/- SEM; n=3-4 representative images per age, >500 cells counted per group). **F.** Tc of proliferative versus differentiative divisions at E78. Mean +/- SEM, * $p<0.05$ Wilcoxon test. **G-I.** Cell-cycle kinetics vary between the different GZ. **G.** Identification of the different phases of the cell-cycle using PCNA, Geminin and Ki67 immolabelling. Scale bar 5μm. G1 phase cells are Ki67+ Geminin-. Other phases are labelled by Geminin. S phase cells display punctuate PCNA staining. G2 cells are round, slightly bigger with homogeneous PCNA staining. M phase cells correspond to mitotic figures. **H.** Proportions of precursors in the different cell-cycle phases in VZ and OSVZ. (Mean +/- SEM; 3 to 6 representative GZ transects per age, >500 cells counted per group). * $p<0.05$ Kruskal-Wallis test. **I.** Length of the individual cell-cycle phases estimated from the proportions of precursors in each phase with respect to Tc measured with TLV in each zone. See also Figure S1.

Figure 2

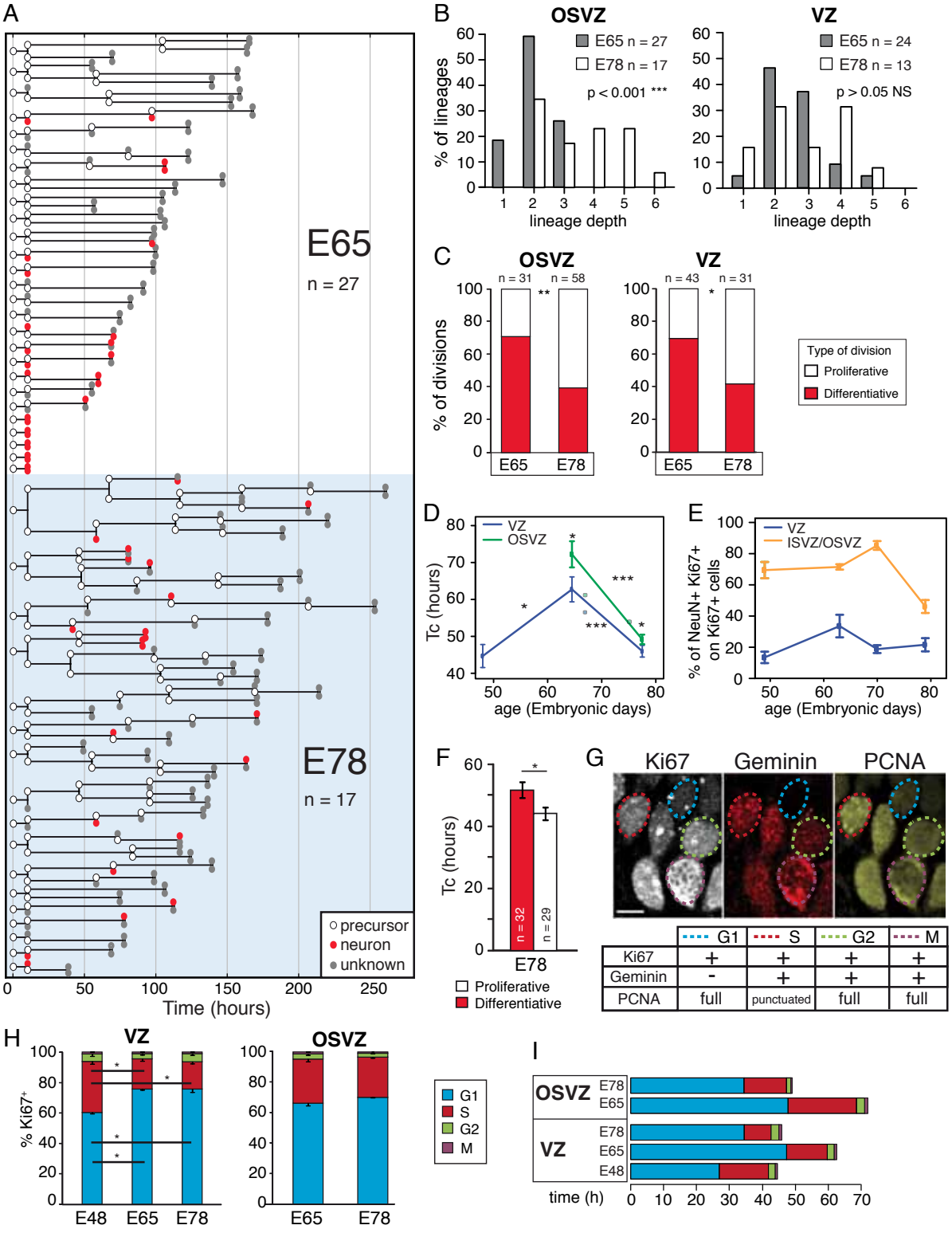
A
E65
n = 27
E78
n = 17
precursor
neuron
unknown
Time (hours)
B
OSVZ
VZ
E65 n = 27
E78 n = 17
p < 0.001 ***
E65 n = 24
E78 n = 13
p > 0.05 NS
% of lineages
lineage depth
C
OSVZ
VZ
% of divisions
Type of division
Proliferative
Differentiative
D
VZ
OSVZ
Tc (hours)
age (Embryonic days)
E
VZ
ISVZ/OSVZ
% of NeuN+ Ki67+ on Ki67+ cells
age (Embryonic days)
F
Tc (hours)
n = 32
n = 29
E78
Proliferative
Differentiative
G
Ki67
Geminin
PCNA
G1 S G2 M
Ki67 + + + +
Geminin - + + +
PCNA full punctuated full full
H
VZ
OSVZ
% Ki67+
E48 E65 E78
E65 E78
G1
S
G2
M
I
OSVZ E78 E65
VZ E78 E65 E48
time (h)

Figure 3: OSVZ precursors show an unexpected degree of morphological and molecular diversity. A-G. Examples of the different morphotypes of OSVZ EGFP+ precursors on organotypic slices immunostained for EGFP/Ki67/Pax6/Tbr2 after 3 to 6 days in vitro following EGFP retroviral infection at E78. Scale bar 5μm. **A-B**. bRG with only a basal process are referred to as bRG-*basal-P* (basal process length > 100μm in A, dark blue arrowheads). Note that the bRG-*basal-P* in A expresses Pax6 but not Tbr2 whereas the bRG-*basal-P* in B expresses both markers. textbfC-D. bRG cells bearing a well-developed apical process referred to as bRG-*apical-P* (length >100μm in C, cyan arrowheads). Both cells express Pax6 but only the bRG in C expresses Tbr2. **E-F.** bRG bearing both an apical and a basal process referred to as bRG-*both-P*. The two processes have different thicknesses (see Fig 3K). The apical process of F extends as far as the ISVZ and basal VZ. **G.** Multipolar cell with 5 processes (orange arrowheads) expressing both Pax6 and Tbr2. **H.** Proportions of IP and bRG static morphology types in the OSVZ (4 hemispheres, 2 slices per hemisphere, 3 GZ transects per slice). **I.** Quantification of the different static bRG morphotypes in the OSVZ (4 hemispheres, 2 slices per hemisphere, 3 GZ transects per slice). **J.** Proportions of Pax6+ and/or Tbr2+ precursors in IP and bRG cells static morphology types in the OSVZ. *** $p<0.001$ Fischer exact test. **K.** Proportions of thick basal or apical processes in bRG-*both-P*, bRG-*basal-P* or bRG-*apical-P*. 4 hemispheres per stage, 2 to 3 slices per hemisphere, 3 GZ transects per slice. Mean +/- SEM. * $p<0.05$ Kruskal-Wallis test. **L.** Box-and-whisker plot of the length of basal and apical processes (basal process n=396, apical process n=339, 4 hemispheres, 2 to 3 slices per hemisphere, 3 GZ transects per slice). *** $p<0.005$ Wilcoxon test. **M.** Percentages of bRG cells undergoing mitotic somal translocation (MST) towards the ventricle (downward) or towards the pia (upward) in the OSVZ. **N.** Example of a bRG undergoing a MST of 35μm amplitude (cyan line) towards the ventricular surface in the ISVZ. Scale bar 10μm. **O.** Box-and-whisker plot of downward or upward MST amplitude. Not significant (NS) Wilcoxon test (downward n=16, upward n=16). See also Figure S2.

Figure 3

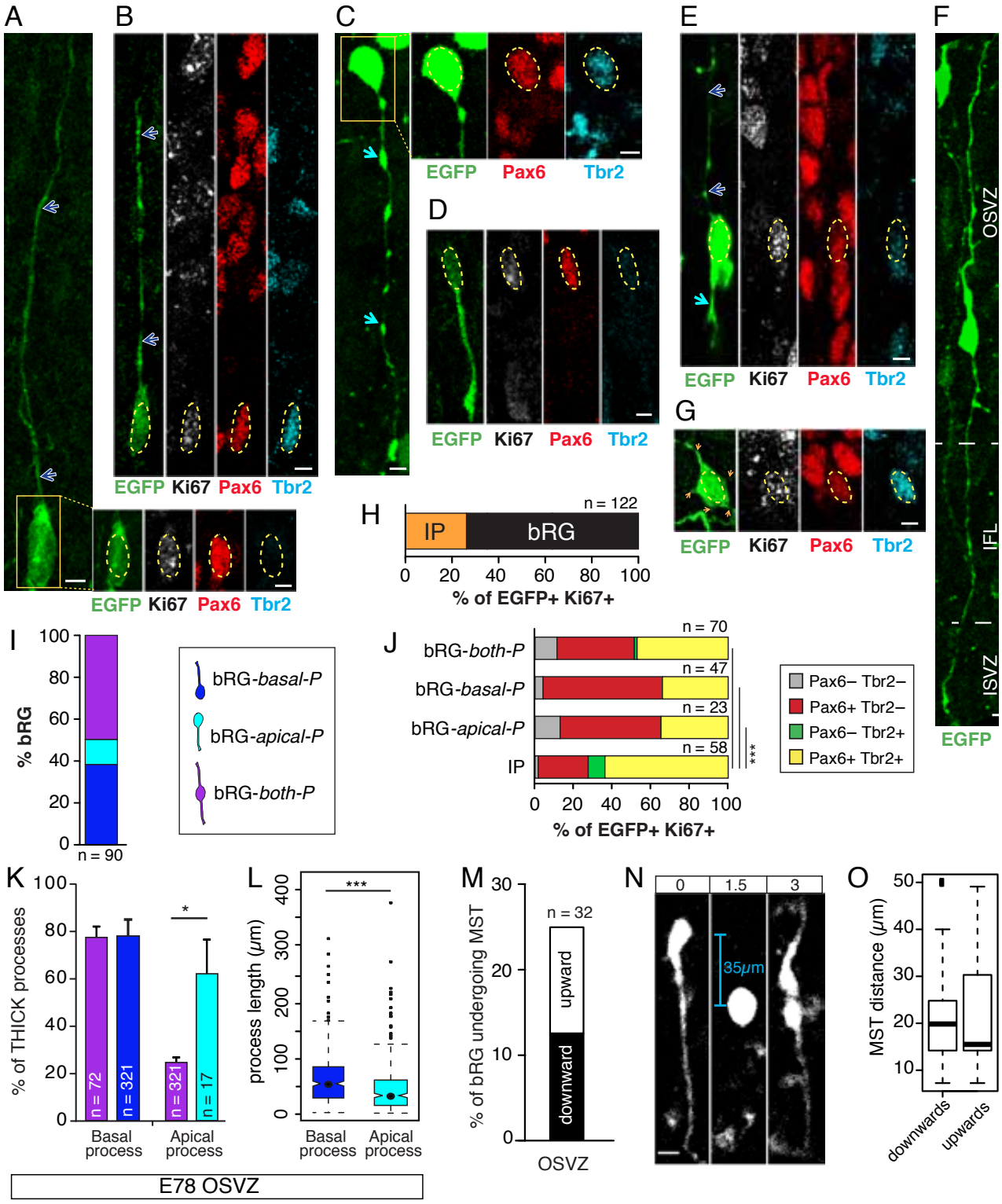
A
B
C
D
E
F
G
H
I
J
K
L
M
N
O
EGFP Ki67 Pax6 Tbr2
EGFP Pax6 Tbr2
EGFP Ki67 Pax6 Tbr2
OSVZ
IFL
ISVZ
EGFP
n = 122
IP
bRG
% of EGFP+ Ki67+
% bRG
n = 90
bRG-basal-P
bRG-apical-P
bRG-both-P
n = 70
n = 47
n = 23
n = 58
Pax6– Tbr2–
Pax6+ Tbr2–
Pax6– Tbr2+
Pax6+ Tbr2+
***
% of THICK processes
n = 72
n = 321
n = 321
n = 17
*
Basal process
Apical process
process length (μm)
***
E78 OSVZ
% of bRG undergoing MST
n = 32
upward
downward
OSVZ
0
1.5
3
35μm
MST distance (μm)
downwards
upwards

Figure 4: OSVZ includes five precursor types, with stable and dynamic morphologies. A-C. Selected images from TLV ex vivo recordings of GFP-retrovirus labelled precursors illustrating stable or changing morphologies at E78 in the OSVZ. The images span the whole cell cycle (the life-time) of the progenitor. The time at which the image was taken is indicated in hours at the top of each picture. Progenitor morphology is schematized below each picture. Red dots indicate the cell under consideration, red stars divisions, dark blue arrowheads basal processes and cyan arrowheads apical processes. Scale bars 10μm. **A.** Example of bRG cells with a stable apical process (lower daughter) or a stable basal process (upper daughter). Note the MST of the upper daughter at t=46.5h. **B.** Example of an IP which never displays a process during its life-time. **C.** Example of a precursor born with no process which acquires a basal process 14 hours later. It is non polar for 20% of its life-time and otherwise shows a bRG morphology and therefore corresponds to a transient tbRG. **D.** Correlation between the morphology observed in TLV at birth and at mitosis. The proportions of the morphologies at birth are represented according to the morphology at mitosis. **E.** Quantification of the morphology types at mitosis in the OSVZ as revealed by Ph-Vimentin staining or as observed in TLV observations of GFP+ precursors right before mitosis (8 hemispheres, 20 slices). **F.** Proportions of the 5 types of precursors identified in TLV (8 hemispheres, 20 slices). See also Figure S3.

Figure 4

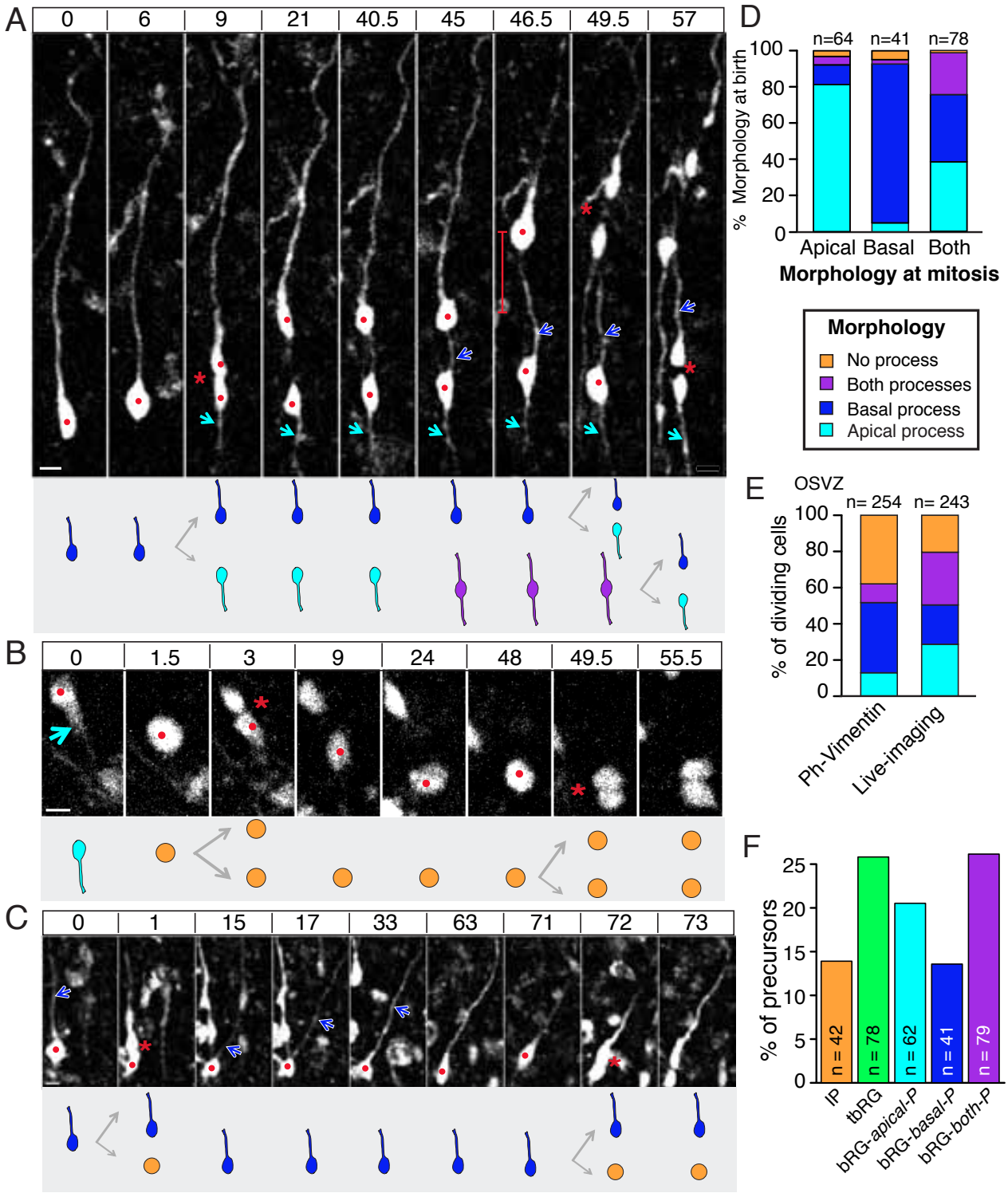
A
0
6
9
21
40.5
45
46.5
49.5
57
B
0
1.5
3
9
24
48
49.5
55.5
C
0
1
15
17
33
63
71
72
73
D
n=64
n=41
n=78
% Morphology at birth
100
80
60
40
20
0
Apical
Basal
Both
Morphology at mitosis
Morphology
No process
Both processes
Basal process
Apical process
E
OSVZ
n= 254
n= 243
% of dividing cells
Ph-Vimentin
Live-imaging
F
% of precursors
25
20
15
10
5
0
n = 42
n = 78
n = 62
n = 41
n = 79
IP
tbRG
bRG-apical-P
bRG-basal-P
bRG-both-P

Figure 5: Rules of process inheritance and link with cell fate. A-B. bRGs lower and upper daughter progeny varies with respect to the mother cell morphology before mitosis both at E65 (A) and E78 (B). Each table represents morphology frequencies of the paired daughter cells after mitosis with respect to bRG mother cell morphology before division. Row entry: upper daughter cell morphology; column entry: lower daughter cell morphology. Numbers correspond to percentages of occurrence of daughter cells morphology combination. Only values $> 10\%$ are indicated. 2p = both processes (apical and basal), Ap = apical process, B = basal process, No = no process. 4 hemispheres, 10 slices per stage. **C-D.** bRG cleavage plane orientation of OSVZ divisions quantified in TLV (C) and in situ (D). Horizontal cleavage plane: 0 to 45° angle relative to the ventricular surface; vertical cleavage plane: 45 to 90° angle. C: 4 hemispheres, 10 slices at each stage. NS Fisher exact test, D: 5 sections at each stage. * $p<0.05$ Fisher exact test. **E.** Influence of the inheritance of a process at birth on the daughter proliferative fate at E78. Morphology at birth refers to the morphology of the daughter cells right after the division of the mother cell. The daughter cell can inherit either an apical, a basal or no process from the mother cell. 4 hemispheres, 10 slices. *** $p<0.001$ Fisher exact test. **F.** Cell-cycle durations (Tc) of pairs of daughter cells are correlated (n=55 pairs from 4 hemispheres, 10 slices, Sperman rank correlation). **G.** Tc of lower and upper daughter cells show a certain degree of synchronisation with Tc of the mother cell at E78. For each triad (mother cells and its upper and lower daughters) the relative contribution of the Tc of each cell to the sum of the 3 Tc was computed and displayed in the triangle plot. For instance the relative contribution of mother cell Tc corresponds to mother Tc / (Mother Tc + Upper daughter Tc + Lower daughter Tc). Black lines indicate the mean values for each triad cell type. 27 triads from 4 hemispheres, 10 slices.

Figure 5

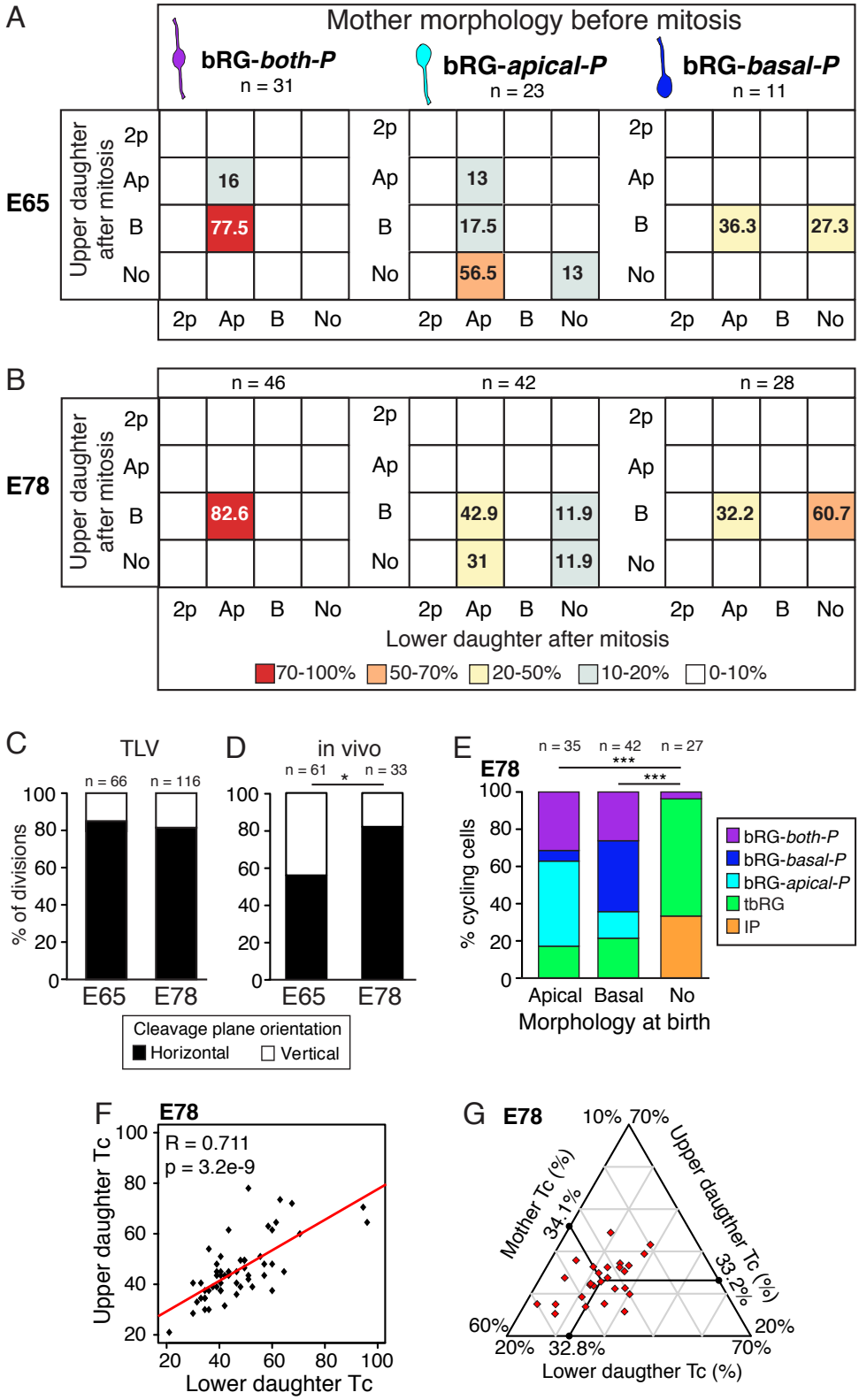
A
Mother morphology before mitosis
bRG-both-P
n = 31
bRG-apical-P
n = 23
bRG-basal-P
n = 11
E65
Upper daughter after mitosis
2p
Ap
B
No
16
77.5
13
17.5
56.5
13
36.3
27.3
B
E78
n = 46
n = 42
n = 28
82.6
42.9
11.9
31
11.9
32.2
60.7
Lower daughter after mitosis
70-100%
50-70%
20-50%
10-20%
0-10%
C
TLV
n = 66
n = 116
% of divisions
E65
E78
D
in vivo
n = 61
n = 33
*
Cleavage plane orientation
Horizontal
Vertical
E
E78
n = 35
n = 42
n = 27
***
% cycling cells
bRG-both-P
bRG-basal-P
bRG-apical-P
tbRG
IP
Apical
Basal
No
Morphology at birth
F
E78
R = 0.711
p = 3.2e-9
Upper daughter Tc
Lower daughter Tc
G
E78
10%
70%
Mother Tc (%)
34.1%
Upper daughter Tc (%)
33.2%
60%
20%
20%
32.8%
70%
Lower daugther Tc (%)

Figure 6: Progeny and lineage relationships between the five precursor types. A. Rank of each precursor type in the lineage trees at E78 (Mean +/- SEM, 4 hemispheres). ** $p<0.01$, *** $p<0.005$ Wilcoxon test. **B.** Self-renewal of each precursor type (8 hemispheres). * $p<0.05$ Fisher exact test. **C.** Quantification of the neuronal vs proliferative progeny of the different precursor types at 65 and E78. 4 hemispheres per developmental stage. * $p<0.05$ Fisher exact test. **D.** Histogramms of the number of cells in the progeny of each precursor type (Mean +/- SEM, 2 hemispheres, 3 slices). NS Wilcoxon test. **E.** State transition diagrams illustrating the lineage relationships in OSVZ at E65 and E78. The diagrams consist of two components: nodes represent precursor types (states) and directed edges represent the transitions between precursors. There are a total of 30 possible transitions; from each of the five precursor types to the five precursor types (25 transitions) and to neurons (5). The size of the nodes is proportional to the frequency of each precursor type with respect to the total number of precursors and the thickness of the arrows to the frequency of each transition with respect to the total number of transitions. Numbers located near nodes indicate the transition frequency towards the node. The position of the nodes with respect to the vertical axis is determined by the mean rank of occurrence of each precursor type in the lineage trees (Fig 6D). Rank scale is indicated by light gray horizontal lines. The neurons have been extracted from the graph to ease the viewing of precursors relationships. The size of the neuron nodes have been normalized with respect to the size of the samples at the two ages. E65: 34 lineage trees; 216 cells; 95 transitions. E78: 57 lineages trees; 479 cells; 192 transitions. (A- C, E) Data collected from 4 hemispheres, 10 slices at each stage. See also Figure S4

Figure 6

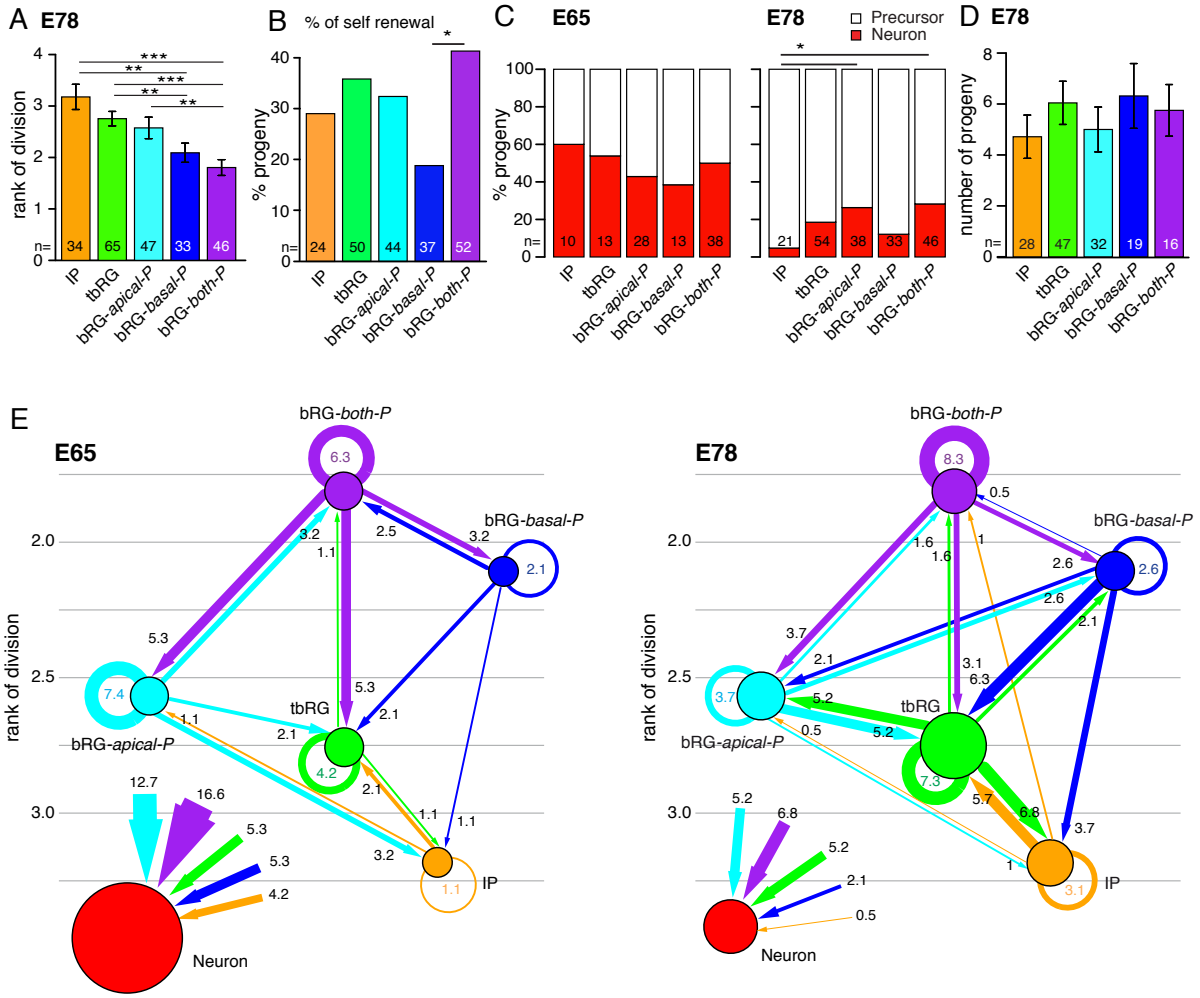
A E78
rank of division
n=
34
65
47
33
46
IP
tbRG
bRG-apical-P
bRG-basal-P
bRG-both-P
B % of self renewal
% progeny
24
50
44
37
52
C E65
E78
Precursor
Neuron
10
13
28
13
38
21
54
38
33
46
D E78
number of progeny
28
47
32
19
16
E
E65
E78
bRG-both-P
bRG-basal-P
bRG-apical-P
tbRG
IP
Neuron
rank of division

Figure 7: Model of primate corticogenesis. A. Cartoon of the cell composition of the mouse and the macaque GZ. Note the scarcity of non-polarized IP in the primate and the prevalence of radially oriented precursors bearing extensive apical and/or basal processes. **B.** Mode of OSVZ amplification. The prevailing hypothesis postulates that bRG-*basal-P* divide asymmetrically to generate a new bRG-*basal-P* and a transit amplifying cell (TAP), presumed to correspond to IP- that undergoes several proliferative symmetric divisions before generating neurons (Lui et al., 2011). Here, we show that every precursor type, self-renew and directly generates neurons, with however a varying contribution (proportional to the thickness of the red arrow). **C.** Stage-specific differences in cell-cycle parameters and lineage relationships of OSVZ precursors. Tc, cell-cycle exit and lineage relationship between OSVZ precursors vary between early and late stages of corticogenesis, corresponding to the generation of infra and supragranular neurons respectively. The shortening of Tc as well as the reduction of cell-cycle exit at later stages results in the amplification of the OSVZ precursor pool via multiple transitions between precursors. LF: leaving fraction which corresponds to cell-cycle exit.

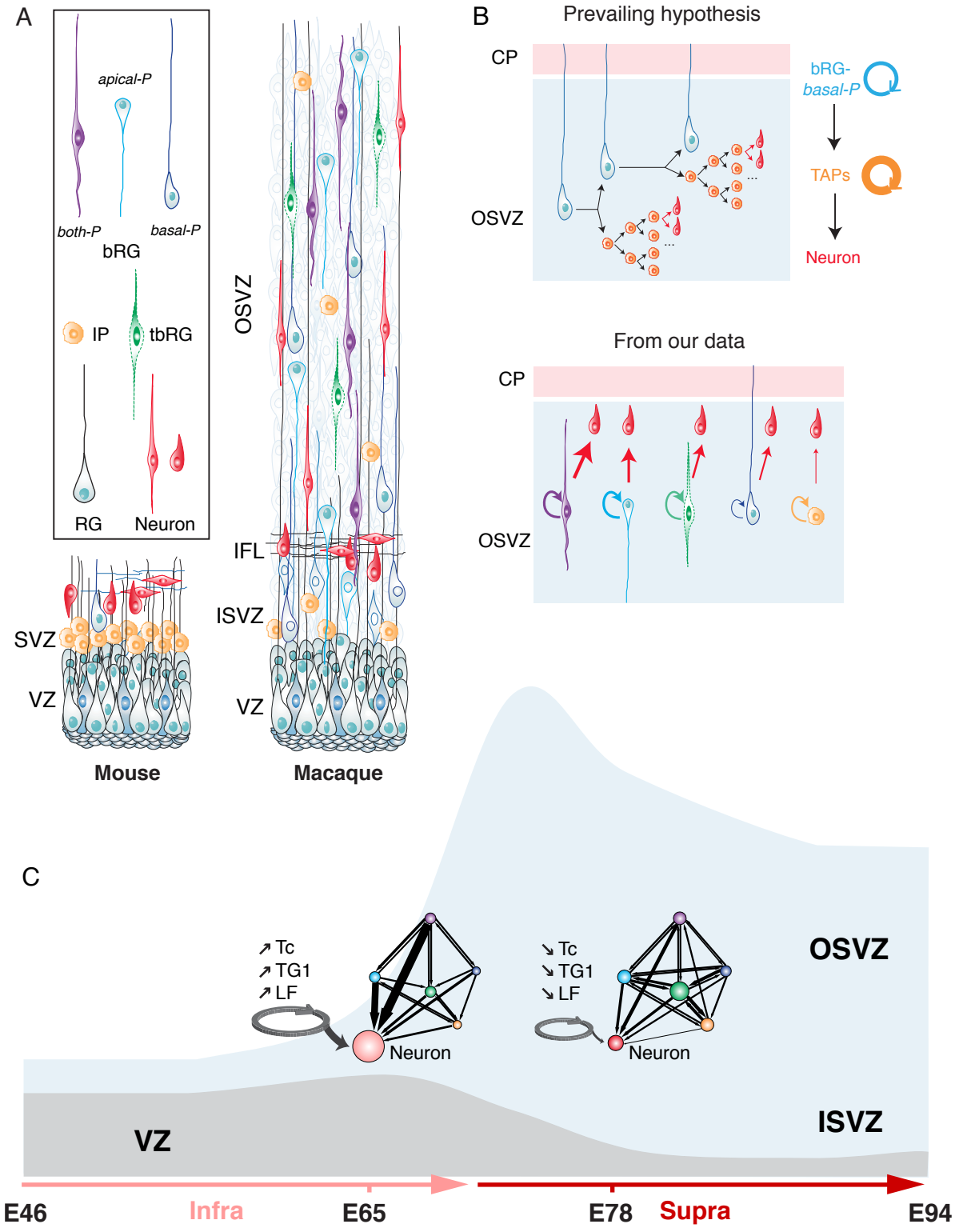
A
apical-P
both-P
basal-P
bRG
IP
tbRG
RG
Neuron
SVZ
VZ
Mouse
OSVZ
IFL
ISVZ
VZ
Macaque
B
Prevailing hypothesis
CP
OSVZ
bRG-
basal-P
TAPs
Neuron
From our data
CP
OSVZ
C
↗ Tc
↗ TG1
↗ LF
Neuron
↘ Tc
↘ TG1
↘ LF
Neuron
OSVZ
ISVZ
VZ
E46
Infra
E65
E78
Supra
E94

2.1.9 Supplemental information

Supplemental data

Figure S1, related to Figure 2: Optimal long-term culture allows complex lineage tree reconstruction. A. Microphotograph of a column of E78 cortex from a 6 DIV (days in vitro) organotypic slice infected with an EGFP-retrovirus immunolabelled with GFP (green), Ki67 (gray) and Pax6 (red). Note the predominance of EGFP+ cells in the GZ in agreement with a high proliferation at this stage (see Fig 2). Few cells have migrated radially outside of the GZ. **B.** Microphotograph of a column of E78 cortex from a 10 DIV organotypic slice infected with an EGFP-retrovirus immunolabelled with GFP (green), Ki67 (gray) and NeuN (red). Note the cohort of EGFP+ migrating postmitotic neurons at the top of the subplate (SP). Some EGFP+ cells have already entered the CP. Few EGFP+ cells remain in the GZ. **C.** Example of an EGFP mature neuron in the CP after 10 DIV (E78). **D.** Postmitotic EGFP cells (Ki67-) express NeuN (red) in the OSVZ after 15 DIV (E78). **E.** EGFP precursors (Ki67+) express Pax6 in the OSVZ after 6 DIV (E78). **F.** Representative lineage trees reconstructed from TLV recordings in the VZ/ISVZ (E65: 4 hemispheres; E78: 2 hemispheres). **G.** Microphotograph of E63 cortex stained with NeuN and Ki67. Note the presence of numerous NeuN+ cells in the ISVZ and OSVZ as opposed to the VZ. **H.** High magnification of the OSVZ showing NeuN +only (green arrowheads), Ki67+ only (red arrowheads), NeuN+ Ki67+ cells (yellow arrowheads) immunolabelled cells. Scale bars: A and B: 100μm, C and D: 20μm; E and G: 50μm; H: 10μm.

Figure S1

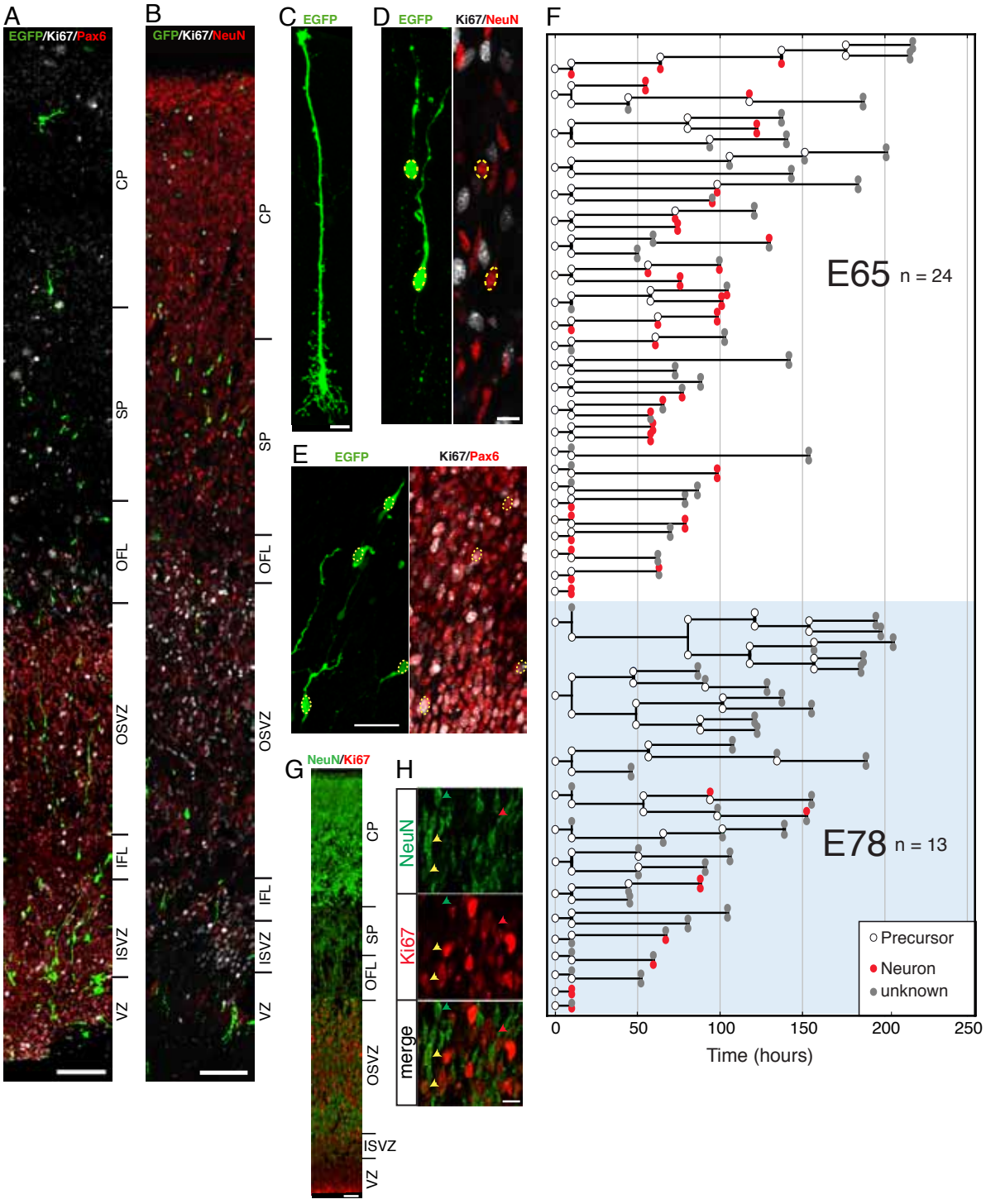
A
EGFP/Ki67/Pax6
CP
SP
OFL
OSVZ
IFL
ISVZ
VZ
B
GFP/Ki67/NeuN
CP
SP
OFL
OSVZ
IFL
ISVZ
VZ
C EGFP
D EGFP Ki67/NeuN
E EGFP Ki67/Pax6
G NeuN/Ki67
CP
SP
OFL
OSVZ
ISVZ
VZ
H
NeuN
Ki67
merge
F
E65 n = 24
E78 n = 13
Precursor
Neuron
unknown
0
50
100
150
200
250
Time (hours)

Figure S2, related to Figure 3: OSVZ precursor morphology in fixed tissue. **A.** DiO diffusing from the pia membrane along radial processes on fixed tissue (parietal cortex E63) labels RG cell bodies in VZ and bRG cell bodies in OSVZ (red and dark blue arrowheads respectively). Scale bar 50μm. **B-O** Examples of retrovirus-GFP morphologies on organotypic slices maintained for 3-6 DIV. Scale bar 5μm. **B-C.** bRGs with only a basal process (bRG-*basal-P*, dark blue arrowheads). **D.** bRG bearing only an apical process (bRG-*apical-P*). **E-J.** bRGs showing both an apical and a basal process (bRG-*both-P*, cyan and dark blue arrowheads respectively). **K-N.** Non polarized (IP) cells. Note that the IP in M expressed Tbr2 and Pax6 whereas the IP in N expressed Pax6 but not Tbr2. **O.** Tangential cell (red dotted circle and red arrowheads).

Figure S2

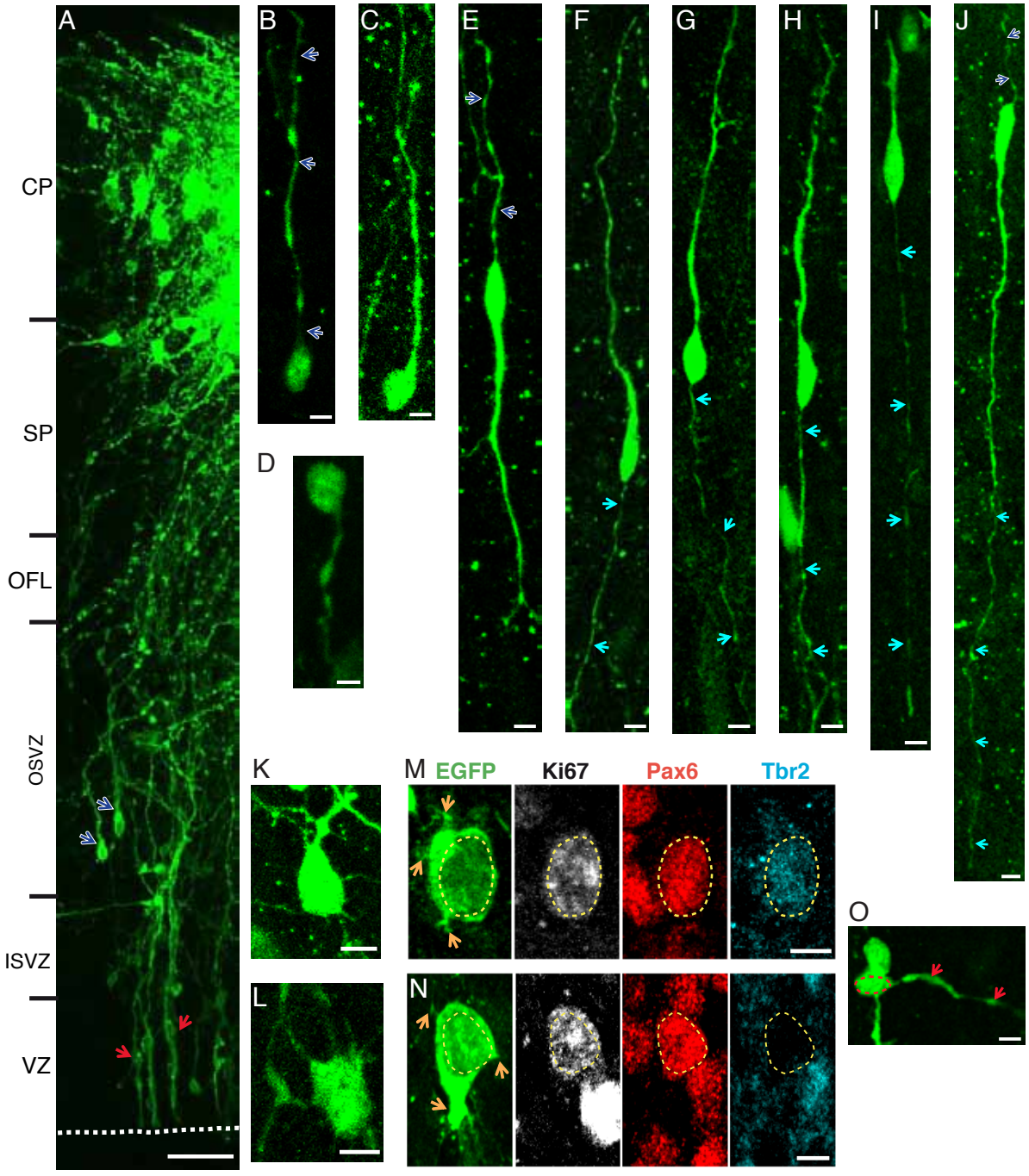

Figure S3, related to Figure 4: Diversity of OSVZ precursor morphologies in TLV. A-C Selected images from TLV ex vivo recordings of GFP-retrovirus labelled precursors illustrating stable or changing morphologies at E78 in the OSVZ. The images span the whole cell cycle (the life-time) of the progenitor. The time at which the image was taken is indicated in hours at the top of each picture. Progenitor morphology is schematized below each picture. Red dots indicate the cell under consideration, red stars divisions, dark blue arrowheads basal processes and cyan arrowheads apical processes. Scale bars 10μm. **A.** Example of a precursor that looses its only apical process 9 hours after its birth and therefore categorized as a transient bRG (tbRG) cell. **B.** Example of a bRG with a stable basal process that acquires an apical process and keeps both processes until mitosis (bRG-*both-P*). Note the upward mitotic somal translocation of 25μm between time 0 and 1h. **C.** Example of a bRG bearing alternatively an apical and a basal process. **D.** Examples of OSVZ precursor morphologies at mitosis revealed by phospho-vimentin (Ph-Vimentin) staining. Scale bar 5μm.

Figure S3

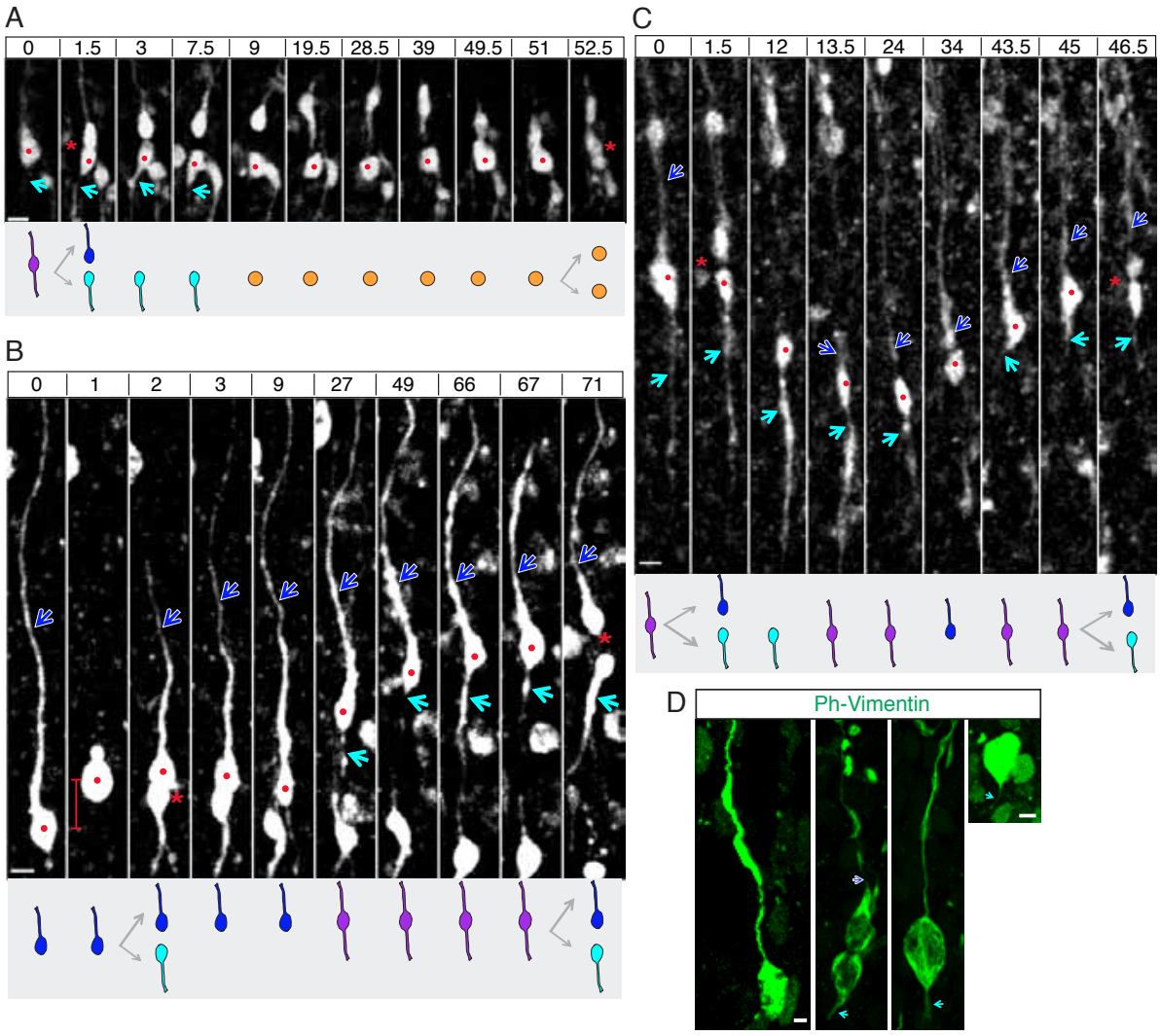
A
0
1.5
3
7.5
9
19.5
28.5
39
49.5
51
52.5
B
0
1
2
3
9
27
49
66
67
71
C
0
1.5
12
13.5
24
34
43.5
45
46.5
D
Ph-Vimentin

Figure S4 related to figure 6: Lineage relationship between the five precursor types. A. Representative lineage trees illustrated in Fig 2A, showing precursor identity. The color code indicates the precursor types and the neurons (E65: 4 hemispheres, 10 slices; E78: 2 hemispheres, 3 slices). **B.** Rank of each precursor type in the lineage trees at E65 (Mean +/- SEM, 4 hemispheres, 10 slices). ** p<0.01, *** p < 0.005 Wilcoxon test. **C.** Histograms of the number of cells in the progeny of each precursor type (E65, Mean +/- SEM, 4 hemispheres, 10 slices). * p< 0.05 Wilcoxon test.

Figure S4

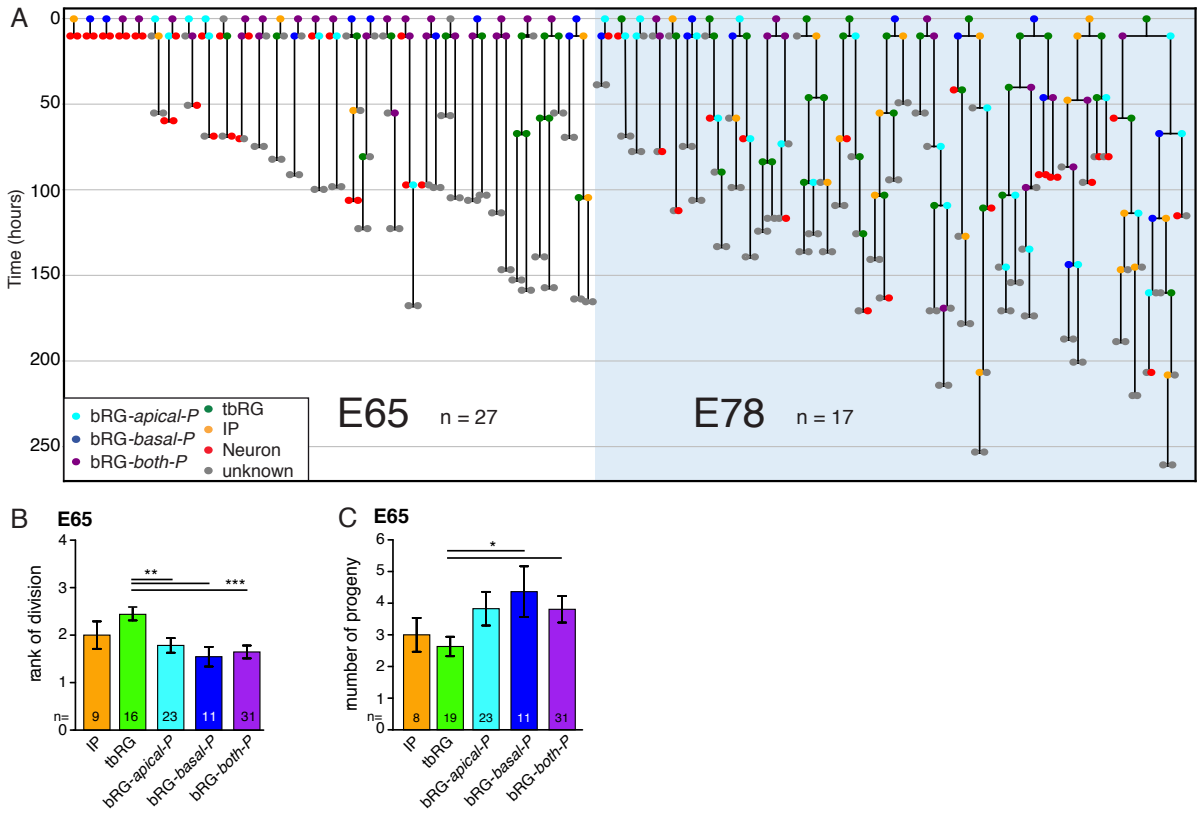

Supplemental movies

Movie S1 related to Figure 2: Interkinetic nuclear migration (INM), delamination and radial migration at E65 in the VZ.

Movie S2, related to Figure2: Successive divisions in the OSVZ at E78.

Recorded lineage tree in the OSVZ. Each cell is highlighted by a small dot. The color code corresponds to the generation in the lineage (red: 1st generation, green: 2nd, blue: 3rd, magenta: 4th, cyan: 5th). Note the synchrony of the divisions. Images taken every 1.5h.

Movie S3, related to Figure 4: Illustration of stable apical and basal processes.

The mother bRG-*basal-P* cell divides and gives rise to an upper cell which inherits the basal process and to a lower daughter which inherits the apical process. Both daughters exhibit a process during their whole lifetime (between 2 divisions) and are thus bRG cells. Of note, the lower daughter displays a stable apical process and the upper daughter a stable basal process. Note that the lower daughter regrows a basal process before dividing.

Movie S4 related to Figure 4: Self-renewing division of an IP in the OSVZ at E78.

Movie S5, related to Figure 4: Illustration of a dynamic apical process.

Note the retraction of the processes at division. The lower cell inherits an apical process which undergoes dynamic changes. The inherited apical process retracts, which is later followed by the growth of a substantially longer apical process bearing a growth cone.

Supplemental methods

Animals

Lethally anesthetized fetuses (via intraperitoneal injection of Sodium Pentobarbital 60mg/kg) were perfused through the heart with cold supplemented HBSS (HBSS with glucose 18%, MgSO4 and CaCl2) before culture experiments and with buffered 4% paraformaldehyde (PFA) during 30min before *in situ* immunofluorescence experiments. *Ex vivo* experiments were performed on one brain at E48, two at E65, one at E67, one

at E75 and two at E78. *In situ* observations were carried out on one brain at each developmental stage (E49, E58, E63, E70, E78, E94).

Brain cryosections

After cryoprotection in 10% and 20% sucrose (in phosphate buffer), brains were embedded in Tissue-Tek. 20μm-thick parasagittal cryosections were cut, mounted on superfrost glass slides and stored at -20°C.

Organotypic slices cryosections

Fetal brain slices were fixed by immersion in cold-buffered 2% PFA in 120 mM phosphate buffer overnight. After cryoprotection in 10% and 20% sucrose (in phosphate buffer), slices were embedded in Tissue-Tek and 20μm-thick cryosections were performed. Sections were mounted on superfrost glass slides and stored at -20°C. For morphology analysis 80μm-thick sections were performed on a freezing microtome after cryoprotection and stored at 4°C in phosphate buffer.

Immunofluorescence and antibodies

Cryosections were air-dried for 30 min and hydrated in Tris-buffered saline (TBS) for 30min. Slices were permeabilized with TBS + TritonX (0.5%). Aspecific binding was blocked by incubating in TBS + BSA 1% + normal goat serum (10%) or normal donkey serum (10%) (when using a sheep or goat primary antibody) in TBS for 30 min. Primary antibodies were co-incubated overnight in TBS + 1% BSA at 4°C as follows: rabbit anti-Ki67 (Neomarker, 1:400), rabbit anti-Ki67 FITC conjugated (Neomarker, 1:100), mouse anti NeuN (Milipore 1/100), mouse anti-Pax6 (DSHB, 1/1000), rabbit anti-Tbr2 (Abcam 1/4000), sheep anti-EOMES (R&D 1:800), chicken anti-GFP (Invitrogen, 1:1000), rabbit anti-Geminin (Santa-Cruz, 1:400), mouse anti-PCNA (Dako, 1/100). Secondary antibodies were co-incubated in Dako Diluent (Dako) 1h at RT (2h for floating organotypic slices), at the following concentrations: Alexa Fluor 488 goat anti-chicken IgG (Invitrogen, 1/800), Alexa Fluor 555 goat anti-mouse IgG (Invitrogen, 1/800), Alexa 647 goat anti rabbit (Invitrogen 1:400), Alexa 488 goat anti FITC (Invitrogen, 1:1000), Alexa 555 donkey anti mouse (Invitrogen, 1:400), Alexa 555 donkey anti rabbit (Invitrogen, 1:200), Alexa 647 donkey anti mouse (Invitrogen 1:400), Alexa 647 donkey anti sheep (Invitrogen, 1:200), Dylight 405 donkey anti rabbit (Jackson, 1:200), Dylight 488 donkey anti chicken (Jackson, 1:400). Nuclear staining was performed using Dapi (Invitrogen,

D1306, 2μg/mL in TBS) 10min at RT. Sections were mounted in Fluoromount G. For the Pax6/Tbr2/Ki67 staining, mouse Pax6 and rabbit Tbr2 antibodies were incubated overnight followed by mouse and rabbit secondary antibodies incubation. Blocking with rabbit normal serum was performed before incubating 2 hours at RT with rabbit anti-Ki67 FITC-conjugated followed by 1h incubation with Alexa 488 goat anti FITC. For some stainings heat-mediated antigen retrieval was performed at 95°C for 15 min (Geminin and PCNA staining) or 5 min (Tbr2 staining with R&D antibody) in Dako antigen retrieval reagent.

Confocal imaging

Images were collected by confocal microscopy using a LEICA DM 6000 CS SP5. Acquisitions were performed using a Leica HCX PL AP immersion oil 40x/1.25 0.75 with a digital zoom of 2 (zoom 3 for the PCNA/Gemini/Ki67 staining). Tiled scans were automatically acquired using the LAS AF software (Leica). For cryosections, stacks of 5 optical sections spaced 2μm apart were taken. For the morphology analysis on 80μm thick sections, stacks throughout the entire section thickness were acquired spaced 1μm apart.

Image analysis and cell counting

All image analyses were performed in the ImageJ software (Schneider et al., 2012). For the Pax6/Tbr2/Ki67/Dapi and NeuN/Ki67/Dapi analyses at various developmental stages on cryosections, single plane confocal pictures were analyzed. The contours of the nuclei were determined using a custom semi automatic segmentation algorithm performing a succession of filters followed by a watershed transformation. The median intensity in every channel is measured for each segmented nucleus. Cells were counted positive for each marker if their median intensity was above a threshold determined in a zone free of any staining. The analysis of the proportions of the single and double positive cells in the different conditions was performed using a custom R script. For the other stainings, cells were counted manually using the Cell Counter Plugin in ImageJ after having adjusted the brightness and contrast. EGFP positive precursors morphologies were examined on whole stacks, the number of processes was reported for each cell as well as their marker expression. Cells were considered radial if they exhibited one or two processes oriented perpendicularly to the ventricular border. Cells with no or more than 2 processes were considered IP cells. The length of the processes was measured using the segment tool of

ImageJ.

Zones identification

The borders between the different compartments of the germinal zones (VZ, ISVZ, OSVZ) were drawn manually according to cytological cues (cell density and shape of the cells). The ISVZ was identified by the band of Tbr2 dense staining.

Dye-O labeling

Dye-O crystals were placed at the pial suface on organotypic brain slices at 1 day in culture. Slices were fixed the following day in 2% PFA and the dye was allowed to diffuse at 37°C for 2 months.

Two-photon video microscopy (TLV) recordings

Two-photon time-lapse video recordings were performed using an inverted Axio-Observer Z1 (Zeiss) two-photon microscope, equipped with Zeiss optics and a Chameleon system Ultra (I) Titane Sapphire 80 Mhz laser. Temperature was maintained at 37°C and CO2 at 7.5%. Milicell inserts were imaged in a 6-well glass bottom plate (Iwaki), where the medium was changed twice a day thanks to a tubing system. Laser was tuned to 880nm for EGFP imaging, with a power between 12 and 20%. Observations were performed using a plan apochromatic dry objective 10x/0.45. Time lapse analysis was usually started 24 hrs after retroviral EGFP labelling. By using the Multi Time Series macro of Zeiss Zen software, 4D 95μm-thick stacks were acquired (20 optical sections spaced 3 to 5μm apart). Recording was performed using a single scanning run at 1024x1024 pixels resolution with a scanning speed of 6 μsec/pix. Images were taken every 1 to 1.5 hours during up to 15 days.

Data base assembly

The long-term organotypic slice culture system enabled to image precursors over up to 15 days (Gautier et al., 2010). 12 parameters were determined for each cell. Localization parameters were determined keeping track of the age (1) and proliferative zone (2) of the cell. The morphology was documented at every time point enabling to assess the stability of the processes (3). The morphologies at birth (4) and at the end (5) of the cells life were measured as well as a possible retraction (6) of the process before mitosis. Parameters related to division were measured: the cell cycle duration (7), the cleavage plane orientation (8), the relative position of the two daughter cells (9), the type of division

(10), the rank of division (11) and a possible somal translocation (12). For E50 cells only the cell cycle length was documented.

Supplemental reference

Gautier, E., Pfister, S., Cortay, V., Btizeau, M., Doerflinger, N., Patti, D., Douglas, R.J., Kennedy, H., and Dehay, C. (2010). Area-specific dynamics of proliferation and migration during primate corticogenesis: Role of the modular protein p27kip1. In Society for Neuroscience (San Diego, CA, Neuroscience Meeting Planner.).

Schneider, C.A., Rasband, W.S., and Eliceiri, K.W. (2012). NIH Image to ImageJ: 25 years of image analysis. Nat Methods 9, 671-675.

2.2 Cell lineage analysis in the primate germinal zones based on a Hidden Markov Tree model

Manuscript in preparation. These results were presented in front of the SECO review panel.
This work was carried out in collaboration with Michael Pfeiffer, Sabina Pfister and Rodney Douglas from the Institute of Neuroinformatics (ETH / University Zurich).

The TLV observations described in the first section of the results enabled the identification of 5 OSVZ precursor types, defined on the basis of the stability of their morphology and their morphology at mitosis (see section 2.1). This classification is supported by the fact that morphological features are also at the basis of rodent cortical precursor type definition, and are correlated with specific molecular signatures (Tyler and Haydar, 2013). Based on this a priori classification, analyses of the lineage relationships between the 5 defined primate precursor types were carried out and revealed bidirectional transitions in complex lineages.

However, the database of primate precursor lineages generated in section 2.1 contains substantial information about non morphological parameters such as cell cycle duration, mitotic somal translocation, cleavage plane orientation or relative position after division. To test the validity of our first categorization, our objective was to to implement an unsupervised classification of precursor types, taking into account all parameters equally. In order to to test hypotheses about lineage relationships between precursors and especially the relevance of bidirectional transitions between precursor types, we wanted the classification tool to allow us to apply constraints on lineage transitions. In this section, we describe a clustering tool based on the Hidden Markov Tree model that allows the determination of a statistical categorization of precursor types and the assessment of the influence of constraints in the lineage transitions.

2.2.1 Introduction

Here, we introduce a new advanced clustering method to automatically characterize different types of cells in lineages observed in the macaque germinal zones (GZ). The data provides information about the morphology of the observed cells (e.g. the existence of basal and apical processes), the behavior of the cell (e.g. length of the cell cycle), and

information about the daughter cells after division at developmental stage E78. The working hypothesis for this study was that the characteristic features of the cell itself, as well as the features of the cells that result from division, are influenced by an internal, unobservable cell state, which represents the expression level of proteins within the cell and in its local environment. In other words, we want to infer the cell type using their morphological, proliferative parameters as well as the lineage information between the different cells.

Clustering is an unsupervised machine learning method, which finds statistical regularities in the data, and can be used to automatically extract information from a large, unordered dataset. Clustering algorithms try to find groups of data points that have a similar distribution of features.

In the model cell states are determined by the measured features (morphology, cell cycle length, plane of divisions...) but they also depend on the state of the mother cell. The clustering algorithm is based on learning a so called *Hidden Markov Tree* (HMT) model (Durand et al., 2004), which is an extension of the well-known Hidden Markov Model, used frequently for modeling time series (e.g. in speech recognition) (Moon and Hwang, 1997). In a Hidden Markov Tree model, every cell has a discrete hidden state, which we want to infer from a vector of observations (the measured morphological features), and the hidden state of the mother cell. On the other hand this means that from the state of the mother cell and some observed features we can make a prediction about the state of the daughter cells.

Learning such a model means that the definitions of hidden states and transition probabilities between hidden states are automatically extracted from the data, such that the likelihood of observing the dataset under this probabilistic model is maximized. A hidden state in this task corresponds to a particular cell state, which is characterized by a model that tells which morphological features should be expected from a cell that is assigned to this state. We also use the term "cluster of cells" to talk about groups of cells that are assigned to the same hidden state.

In order to learn such a model, one has to specify how many possible hidden states there are, and potential constraints on the allowed transitions between cell states. One can for example define constraints such that cells only go from less differentiated to more differentiated states, or one can define hidden states that have no further daughter cells, which would correspond to neurons. We found that imposing some constraints

typically improves the results in the sense that cells from the same cluster become more homogeneous in the expressed morphological features, and / or in the states of their daughter cells. However, even if we did not impose any constraints, the algorithm would in most cases learn a model where the allowed transitions are sparse, i.e. not all transitions are possible. Here we compare several models with more or less constraints, but we will not give a definitive answer to the question which model is the best.

We tried to keep the number of possible cell states as low as possible, usually between 5 and 6. A higher number of states will always fit the dataset better, but at the same time increases the risk of overfitting the data, which means that small groups of cells are extracted, which share some features by chance or because of measurement errors, but have no significance as an own type of cells. One indicator for this is when the algorithm finds clusters of cells with only very few datapoints in them.

One problem with clustering methods is that there is no clear, objective measure to quantify the quality of the learned result. Although statistical indicators exist, like e.g. the log-likelihood of the observed data, or the similarity of points within clusters compared to the similarity between clusters, they do not always indicate whether the clustering has any biological meaning, or is just a statistical artifact. Thus, clustering of cell states is a very useful tool to improve our understanding of the data, and can make the formulation of new hypotheses easier, but can never replace the interpretation of the results by an expert. In this report we compare the cell states found by automatic clustering with types of cells reported in the literature (Hansen et al., 2010; Betizeau et al, section 2.1).

This report is structured as follows: In *Methods* we give a brief description of the data, and give a short introduction to learning algorithms for Hidden Markov Tree models, and different constraints that were used. In *Results* we show the clustering results for different types of constraints. Finally we analyze whether it is possible to predict the state of cells after division from the type of the mother cell, as well as some morphological features known at the cell birth. In *Discussion* we formulate some of our observations and hypotheses.

2.2.2 Methods

Dataset

We used the dataset of cell lineages in the developing macaque cortex at E78 (presented in section 2.1). In this dataset, every cell is described by an ensemble of observed features. Briefly, 10 features were determined for each cell. The morphology was documented at every time point enabling to assess the stability of the processes (1). The morphologies at birth (2) and at the end (3) of the cells life were measured as well as a possible retraction (4) of the process before mitosis. Parameters related to division were recorded: the cell cycle duration (5), the cleavage plane orientation (6), the relative position of the two daughter cells (7), the type of division (8), the rank of division (9) and a possible somal translocation (10). A summary and the meaning of the abbreviations are presented in Table 2.1. The dataset consists of 487 cells from 43 lineage trees.

The size of the lineage trees ranges from 3 to 31 cells. Figure 2.1 shows the distribution of lineage tree sizes (i.e. numbers of cells), and maximum depths of the trees (i.e. the number of successors of the original mother cell). More than 50% of the trees have less than 10 cells, and there are only very few trees with 20 or more cells. The average depth of the lineage trees is around 3.

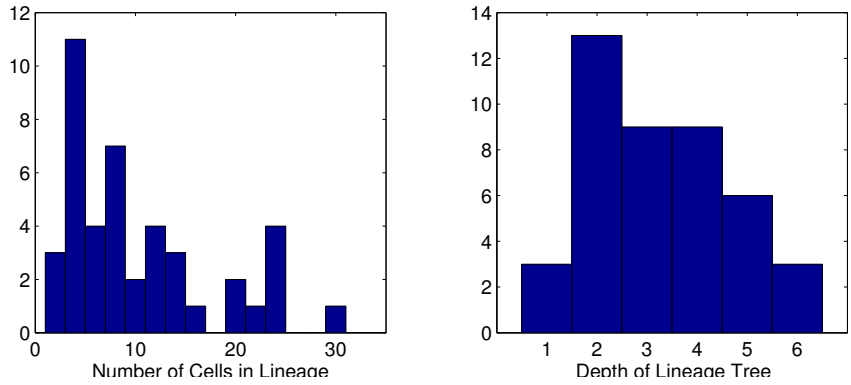

Figure 2.1. Statistics of the lineage trees: (left) Distribution of the number of cells within each lineage tree. (right) Distribution of the maximum depths of the lineage trees.

Feature	Description	Possible Values
END_MORPH_B	Existence of basal process at the end of the cell's life	0 ... no process 1 ... has basal process
END_MORPH_AP	Existence of apical process at the end of the cell's life	0 ... no process 1 ... has apical process
BIRTH_MORPH_B	Existence of basal process at the birth of the cell	0 ... no process 1 ... has basal process
BIRTH_MORPH_AP	Existence of apical process at the birth of the cell	0 ... no process 1 ... has apical process
TYPE	Type of the cell (cycling or post-mitotic)	0 ... post-mitotic 1 ... cycling
PROCESS	Whether a cell loses or gains a process during lifetime	0 ... does not have a process 1 ... transient 2 ... permanent
RETRACT	Whether a process retracts at the moment of division	0 ... Cell does not divide 1 ... no retraction 2 ... at least one process retracts
TC	Cell cycle length (in hours)	0 ... Cell is not cycling 1 ... 20-40 hours 2 ... 40-60 hours 3 ... 60-80 hours 4 ... 80-100 hours
PLANE	Orientation of division plane	0 ... Cell does not divide 1 ... 0° - 30° 2 ... 30° - 60° 3 ... 60° - 90°
TRANSLOC	Translocation movement before division	0 ... Cell does not divide 1 ... downward translocation 2 ... no translocation 3 ... upward translocation
DIV_POS	Position of the cell after division	0 ... lower daughter cell 1 ... upper daughter cell
DIV	Proliferative versus differentiative divisions	1 ... Cell does not divide 2 ... D = 1D + ? (1 post-mitotic) 3 ... DP = 1D + 1P (1 post-mitotic, 1 proliferative) 4 ... P1 = 1P + ? (1 post-mitotic) 5 ... P2 = 2P (2 proliferative) 6 ... unknown

Table 2.1. Cell parameters measured by TLV.

Hidden Markov Trees

A Hidden Markov Tree (HMT) model is an extension of Hidden Markov Models (HMMs). HMMs are frequently used in machine learning to model time series. The idea behind both models is that there are two types of random variables: observations and hidden states. In HMMs the input is assumed to be a time series, and the hidden state at one time step is only dependent on the hidden state at the previous time step. The observations at one time step, on the other hand, are only dependent on the current hidden state, but not on previous hidden states or observations. In the HMT model, the observations are again dependent only on the hidden state, but in contrast to HMMs one state has always more than one successor states, which complicates the statistical model. Figure 2.2 illustrates the model. Starting from an initial hidden state s_0, the subsequent states are arranged in a tree, such that the two direct successor states s_1 and s_2 are only dependent on s_0, but are conditionally independent from any entry in the observation vector for s_0. s_1 and s_2 can have successors (and observations) as well, and so a whole tree is generated. Each cell is in one out of K possible states, i.e. $s_i \in \{1, \ldots, K\}$.

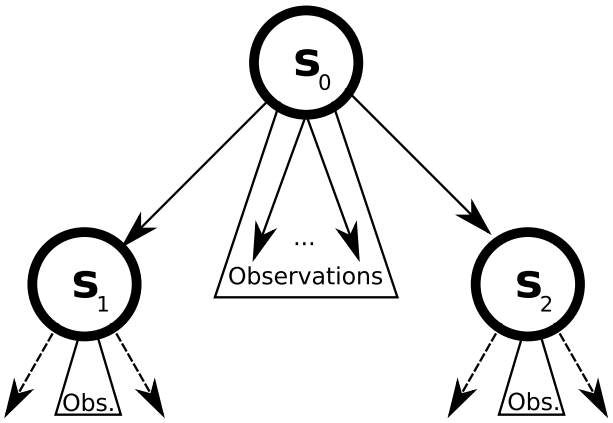

Figure 2.2. Hidden Markov Tree (HMT) Model. Each cell is characterized by a hidden state s_i, and a vector of observations. In the HMT model the assumption is that the distribution of the observed features depends only on the hidden state, and the hidden state of the daughter cells (s_1, s_2) depends only on the hidden state of the mother cell (s_0).

A Hidden Markov Tree model is characterized by three sets of parameters:

1. $\pi = (\pi_1, \ldots, \pi_K)$: Prior distribution for the state of the first cell in a lineage.

$\pi_k = p(s_0 = k)$ is the probability that the first cell of a lineage is in state k.

2. $\mathbf{A} = (a_{ij})_{i,j=1,\ldots,K}$: Transition probabilities between states. $a_{ij} = p(s_{child} = j | s_{mother} = i)$ is the probability that the next hidden state of the daughter cell (s_{child}) is j, given that the state of the mother cell (s_{mother}) is i.

3. $\mathbf{\Theta} = (\theta_1, \ldots, \theta_K)$: Parameter vector that describes the observation model for each hidden state. Depending on the nature of the observation model (discrete or continuous values, Gaussian or uniform, ...) and the number of features $\mathbf{\Theta}$ is a vector that consists of a variable number of parameters. For an observation vector $\vec{x}$ we write $p_{\theta_k}(\vec{x}) = p(\vec{x}|s_i = k, \theta_k)$ as the probability that observation $\vec{x}$ resulted from the hidden state $s_i = k$.

For $\mathbf{\Theta}$ we have to decide on a probabilistic model that provides a distribution over feature values given the hidden state. Since we used only discrete (or discretized) values for all measured features, we used a mixture-of-multinomials model, in which we assume that the individual features become conditionally independent from each other when the hidden state is known. In other words, the hidden state contains all the information about the distribution of values for each feature, and knowing the value of one feature does not provide more information about the value for another feature than what can be inferred from the hidden state alone. This does not mean that features need to be uncorrelated, because they are linked via the hidden state, and for example the distributions of two features for a given hidden state may be very similar. Although this model (also known as a "Naive Bayesian" model) is clearly a simplification, it is known in the statistical literature to produce very good results for most tasks, even though it neglects many potential statistical dependencies between features (Zhang, 2004). More complex models are not only more difficult to implement, but also tend to overfit the data. For an observation vector $\vec{x} = (x_1, \ldots, x_P)$ and hidden state $s_i = k$ the likelihood of the observation is then given by $p_{\theta_k}(\vec{x}) = \prod_{j=1}^{P} p(x_j | s_i = k, \theta_k)$. Since our observations are discrete, the parameter θ_k that describes the observation model for the k-th state contains for every feature variable x_j a vector of numbers $\theta_{k,j}(l) = p(x_j = l | s = k)$, i.e. the probability that x_j takes on the value l if the cell is in hidden state k.

If π, $\mathbf{A}$, and $\mathbf{\Theta}$ were known, one can use a variant of the well-known Viterbi algorithm to infer for a set of observations $\vec{x}_0, \ldots, \vec{x}_N$ and known lineage relationships the most

likely hidden state $s_0, \ldots, s_N$ for each node in the HMT (see (Durand et al., 2004) for a description of that algorithm).

However, for this clustering task we first have to infer the parameters $(\pi, \mathbf{A}, \mathbf{\Theta})$ that best describe the data. This is done with a variant of the Expectation-Maximization (EM) algorithm adapted for HMT models. This algorithm is called the Upward-Downward algorithm, and a particularly efficient and robust method described by Durand et al. (Durand et al., 2004) was implemented for this task. The algorithm iteratively learns a probabilistic model described by the three parameter vectors that should maximize the likelihood of the observations (i.e. the measured morphological features), given the lineage information.

The algorithm is quite complex, so we refer to (Durand et al., 2004) for a thorough description. We implemented the algorithm in Matlab, and it runs quite efficiently and reliably. One potential problem, which is common to most clustering algorithms, is that the parameters initially need to be initialized randomly, and every random initialization will lead to slightly different results. However, we found that for many models, even though there are slight changes in the learned models, the results are qualitatively not very different. We typically tried between 3 and 10 random initializations for each model we tested, and decided on the best model based on the homogeneity of the clusters.

Model Constraints

One advantage of learning probabilistic models with EM, or specifically with the Upward-Downward algorithm is that constraints on the model that should be learned can easily be imposed. As described earlier, before the start of the Upward-Downward algorithm all parameters need to be initialized randomly. However, one of these values is set to zero, it will stay at zero throughout the learning process, and only the other parameters will be optimized to match the data.

For our scenario it is specifically interesting to set the entries in the transition probability matrix $\mathbf{A}$ to zero, as this would prevent specific transitions between states. The entries a_{ij} of $\mathbf{A}$ are the probabilities that a mother cell in state i creates a daughter cell in state j. So setting a_{ij} to zero means that a cell of state i can never have a daughter cell of state j. One can e.g. use this to enforce that cells when they divide can only stay in the same state or become more differentiated, but can never go back to a less differentiated state. This is done by setting the entries in $\mathbf{A}$ below the diagonal to zero, which results

in a upper-triangular matrix:

$$\mathbf{A} = \begin{pmatrix} a_{11} & a_{12} & a_{13} & \cdots & a_{1K} \\ 0 & a_{22} & a_{23} & \cdots & a_{2K} \\ 0 & 0 & a_{33} & \cdots & a_{3K} \\ \vdots & & \ddots & \dots & \vdots \\ 0 & 0 & 0 & \dots & a_{KK} \end{pmatrix}$$

Starting with this structure for $\mathbf{A}$, and random initial values for a_{ij}, one will learn a model in which cells of hidden state $s = 1$ can give rise to daughter cells of all other states (including another state 1 cell), but a cell in state 2 cell can never have a state 1 cell as progeny. By setting a complete row in $\mathbf{A}$ to zero, one can enforce that cells belonging to this type never have progeny and thus never divide, which forces this state to specialize on cells at the end of the lineage (such as neurons). We call this type of constraints **one-way constraints**, because the state of daughter cells can only change in one direction (from lower to higher numbered states).

We also looked at another type of model, in which $\mathbf{A}$ consists of multiple blocks in which transitions between all states in the block are possible, but transitions to another block are only possible in one direction. With such a model one allows that cells can perform one or more rounds of division before changing to a more differentiated state. This gives cells a "window of plasticity", in which they can freely go back and forth between different less differentiated states, before dividing into a more differentiated state. An example for such a block-matrix with two blocks of three states each is given below in (2.1): Cells of state 1, 2, and 3 can after division go to any possible state from 1 to 6. State 4, 5, or 6 cells can never go back to state 1, 2, or 3, but can only go to states 4, 5, or 6. We call this type of constraints **block-structure constraints**.

$$\mathbf{A} = \begin{pmatrix} a_{11} & a_{12} & a_{13} & a_{14} & a_{15} & a_{16} \\ a_{21} & a_{22} & a_{23} & a_{24} & a_{25} & a_{26} \\ a_{31} & a_{32} & a_{33} & a_{34} & a_{35} & a_{36} \\ 0 & 0 & 0 & a_{44} & a_{45} & a_{46} \\ 0 & 0 & 0 & a_{54} & a_{55} & a_{56} \\ 0 & 0 & 0 & a_{64} & a_{65} & a_{66} \end{pmatrix} \tag{2.1}$$

It is important to note that by imposing this type of constraints one only restricts

the structure of the possible transitions between hidden states. The actual transition probabilities are automatically learned by the algorithm, and are not specified by the modeler.

In our experiments we typically experimented with full, triangular, and block-structured **A** matrices. However, it is still an open debate which type of constraints is most plausible for the data at hand. In biology it has been observed that cells may go back to a less differentiated state but only following a traumatic event. Dedifferentiation has been observed in amphibians after limb amputation (Stocum, 2004). This process is also observed in cancer formation (Schwitalla et al., 2013), but has not been reported in normal development (Wang et al., 2010). We will use different types of constraints and analyze the obtained models.

2.2.3 Results

In this main subsection we show the results obtained for different clustering models with different constraints and numbers of clusters. We also analyze the capability of the models to predict the state of daughter cells after a division, and try to characterize the types of cells that are extracted by the clustering algorithm. We show the results for the whole dataset, but the same cell types were also found in the different GZ taken separately (data not shown).

Learned Probabilistic Models

We display the clusters of cells by plotting the probabilistic models θ_k that define a cluster. Since our model assumes conditionally independent, discrete features, every model is defined by a distribution over the possible discrete values that every feature can take on. Figure 2.3 illustrates an example for the feature TC (cell-cycle length). For the i-th feature, the height of the j-th bar in the k-th model defines the probability $p(x_i = j|s = k, \theta_k)$.

In addition we plot the distribution of direct successor states (state of the daughter cells) for every cluster. These plots illustrate the effect of the learned state transition matrix **A**, and give insight into which transitions between states are likely or unlikely. To have a better overview of the possible transitions between clusters, we also generated state transition diagrams for each model.

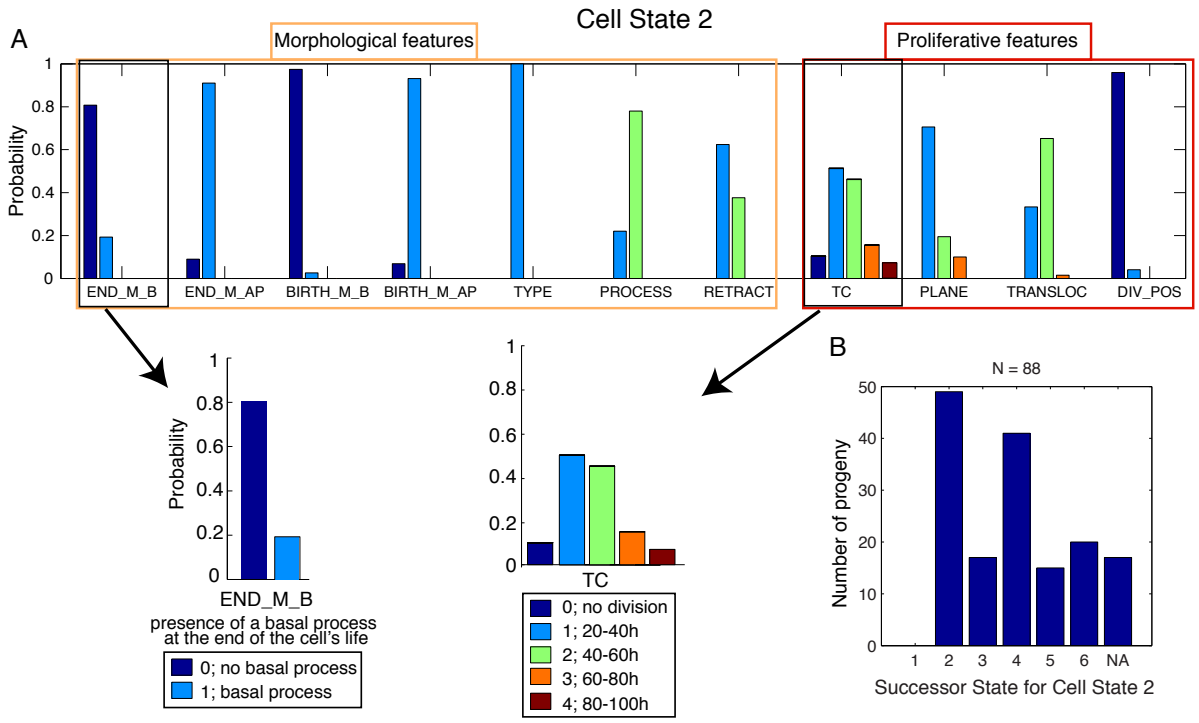

Figure 2.3. Example of a learned probabilistic model. **A.** Illustration of the learned distribution of values for every feature for a given cell state. Each subplot corresponding to a feature indicates which characteristic we can expect from a cell belonging to this cell state. We extracted two of these subplots: for the END_M_B (presence or not of a basal process at the end of the cell's life) and the cell cycle length TC. Each bar represents the probability under the model that a feature takes on a specific value. In this case e.g. END_M_B indicates that the cell does not bear a basal process (value 0) with probability 0.8 and bears a basal process with probability 0.2. TC takes on the value 0 (meaning the cell does not divide) with probability 0.1, the value 2 (cell cycle length between 40-60 hours, see Table 2.1) with probability 0.5, etc. The color code is the same for each feature and corresponds to the code defined in Table 2.1. Some features have fewer possible values than others (END_M_B e.g. has only two possible values), and therefore not all colors are used. **B.** Illustration of the successor model. The plot shows the empirical frequency of successor states in the lineages for cells belonging to this cluster. *NA* means that the cell has no daughter cells (either because the cells were neurons, or because the fate was not identified due to technical limitations).

Daughter Cell State Prediction

One interesting quantification of the quality of the clustering is whether the states of the daughter cells can be predicted by knowing the state of the mother cell, and the morphological features of the daughter cells known at birth. From the full set of features described in Table 2.1 we chose only the features BIRTH_MORPH_B, BIRTH_MORPH_AP, and DIV_POS to predict the likelihood for each daughter cell to be in any of the potential states. We chose these features because they can be known soon after the cell is born, whereas other features (like TC, TRANSLOC, etc.) are only known at the end of the cell's life. The likelihood from the reduced set of features was combined with the likelihood of every cell state to result from the mother cell, of which the state is known, and we predicted the most likely state for every daughter cell.

The statistical model does not allow to directly take into account features of the mother cell (like cell-cycle length or translocation direction) for the inference of the daughter cell state, because these are assumed to be conditionally independent, given the mother cell state. We then computed the number of errors between this assignment and the actual state of the cell.

We found that most cell states can be very accurately predicted (80-100 % accuracy), with the exception of the neuron cell state (accuracies around 10%). The reason for this lower accuracy seems to be that the clusters for neuron-type cells have a very high morphological diversity, compared to the other cell states. In addition, although some cell states are more likely to differentiate into neurons, there is always at least one other very likely successor state, which contributes to a high error rate.

Tree Depth

To further characterize the cell type properties we took into consideration features that can be inferred from the lineage trees. For example, we computed the average depth (average rank of division) within the lineage tree, and the average spatial position for cells of the same cluster.

The tree depth is an indicator whether a cell appears early in a lineage tree (low depth), or only after several divisions (high depth). Since the recorded lineage trees do not have the same maximum depth (some lineages have up to 6 divisions, others end after only one division), we also computed the relative depth, where the depth of each cell is divided by the maximum depth of their lineage tree (i.e. the deepest cell has relative depth 1).

Division Patterns

For each cluster we also measured whether divisions of cells of each state were symmetric (i.e. both daughter cells have the same state), or asymmetric (the daughter cells have different states). We also observed the most common division patterns for the recorded lineages and the learned models.

Unconstrained Model

We trained a model with 6 potential cell states, and allowed all possible transitions between cell states Figure 2.4 shows the learned probability models for the 6 different states.

Observations:

One can clearly see that there are quite distinct feature combinations that characterize all six clusters of cells, and the cells within a cluster are usually very homogeneous at least in a subset of features. Even though we did not impose any constraints on possible transitions between cell states, there are some transitions between states that occur very rarely or not at all (e.g. from state 2 to states 1, 4, 5, or from state 3 to 4). Some cells are also more likely to be at the end of a lineage than others, indicated by the high transition probability to "NA" (e.g. state 1 and 2 cells are often at the end of a lineage, whereas state 4 cells are not). The only cluster of completely non-proliferative cells is number 1, which consists exclusively of neurons. From the model one can see that cells of states 4, 5 and 6 are particularly likely to become neurons after division, whereas this rarely happens for state 2 or 3 cells.

State 1 cells are non-proliferative cells, most likely neurons, which is why the values for RETRACT, TC, PLANE, and TRANSLOC remained undefined (indicated by the 100% dark-blue bars). Their morphology is quite heterogeneous, and they frequently have transient processes. They equally originate from upper or lower cells.

State 2 cells never display a process, neither at birth nor at the end and thus correspond to IP cells described in the mouse model (Haubensak et al., 2004; Noctor et al., 2004). Their fate is often unknown because they appear rather at the end the lineages. Interestingly, they produce neurons in only rare cases. They have a rather short cell cycle, and rarely undergo translocations. Type 2 mother cells generate mostly type 2 or 3 cells.

State 3 cells rarely have any processes at birth or end, and processes are always transient. We called this state transient bRG type (tbRG, see Section 2.1). They have

Figure 2.4. Models learned for K=6 cell states for all cells without constraints on the transition matrix. (left) Learned probability model for each of the features. (right) Distribution of direct successor states, and number of cells that fall into that cluster (N = ...). NA means that no daughter cells were recorded.

rather short cell cycle length (although there is a small group with very long TC), and rarely undergo translocations. Except for the transient PROCESS feature, this cell state is very similar to state 2. State 3 cells also rarely become neurons, and if they divide the daughter cells are mostly of state 2.

State 4 cells always have an apical process at mitosis and also a basal process in almost 60% of the cases. They often have a basal but rarely an apical process at birth. Processes are mostly permanent, and rarely retracted before division. These cells and are often found at the beginning of a lineage. This state is more heterogeneous than state 2 and 3 and we called it the bRG-*both-P* type (see Section 2.1). Their cell cycle length is longer than for states 2 and 3, and they have mostly horizontal division planes. Downwards translocations are quite common for this cell type, and almost all cells of this type are the upper cells after division. Cells of this type frequently give rise to state 6 cells after division, but daughter cells can take on any cell state, except for state 2, which is very unlikely. State 4 cells are more common in the apical VZ than in any other zone.

State 5 cells have basal processes at birth and mitosis, and (almost) never have apical processes. Processes are permanent, but they may sometimes retract before division. Upward translocations are quite common for cells of this state. Cells of this type are mostly found as the upper cells after division (seen by DIV_POS). Daughter cells of state 5 cells can take on any type, although type 4 is very rare, and types 3 and 5 are most common. State 5 cells may also differentiate into neurons. State 5 cells are in many respects similar to the so-called *bRG* cells described in previous reports (Hansen et al., 2010; Fietz et al., 2010). To avoid confusion with other bRG types we called this type bRG-*basal-P* (see Section 2.1).

State 6 cells are characterized by the presence of a permanent apical process (at birth and mitosis), which sometimes retracts before division. By analogy with bRG-*basal-P* we refer to this type as bRG-*apical-P* (see Section 2.1). They have slightly longer cell cycles, mostly horizontal division planes, and frequently perform downwards translocations. Many of these cells are either at the end of a lineage, or generate new state 6 cells, although transitions to all other cell types (including neurons) are possible and almost equally likely. Cells of this type always are the lower cells after division (see DIV_POS).

In Figure 2.5 we look at the distribution of the feature DIV in every class. The histograms for DIV show a tendency for proliferative division for state 4 and 5, whereas

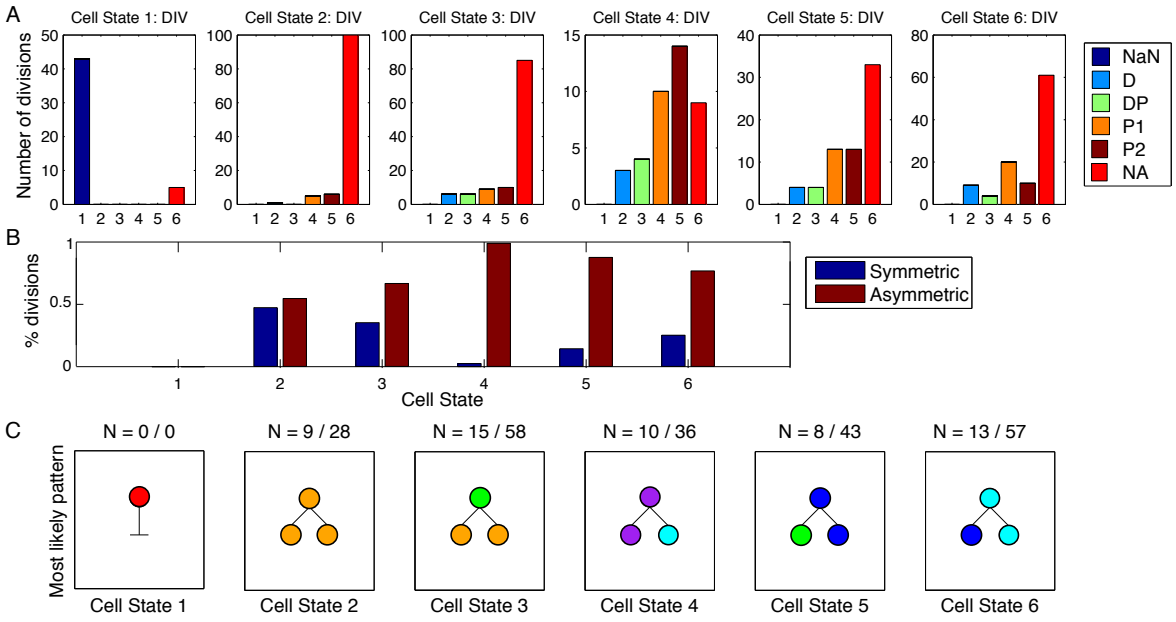

Figure 2.5. Types of division for each cell state, learned without constraints. **A.** Histogram of DIV for cells from all 6 cell states. **B-C.** Observed division patterns for all 6 cell states. **B.** Frequency of symmetric vs. asymmetric divisions for each cell state. **C.** Most common division pattern for every cell state. Colors correspond to different cell states. The numbers above the illustration show the absolute number of such division patterns, in relation to the absolute number of divisions observed for cells of this state.

state 4 has more symmetric proliferative divisions. We also show in Figure 2.5 B-C the common patterns of divisions for each cell state. We found that symmetric divisions are only common for state 2 and 3 cells, whereas state 4, 5, and 6 cells divide mostly asymmetrically, and state 1 cells do not divided at all. The most common division pattern for state 2 and 3 cells is to become a pair of state 2 cells. The other three cell types frequently have at least one cell of the same type as successor.

We also looked whether any characteristics of the cell types can be observed by looking at the average depth within the lineage tree (Figure 2.6). We find that state 4 cells have the lowest depth, meaning that they are most commonly found at the beginning of a lineage. On the other hand, state 1, 2, and 3 cells are mostly found after several rounds of cell divisions. State 5 and 6 cells occupy an intermediate position in lineage trees.

The state of the next daughter cell can be predicted with an accuracy of only 58.27%, using only the BIRTH_MORPH_AP, BIRTH_MORPH_B, and DIV_POS features of the

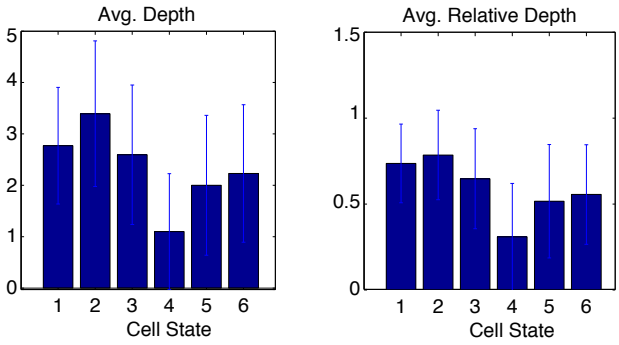

Figure 2.6. Lineage-tree dependent features computed for all 6 cell states, learned without constraints. (Left) Average absolute depth within the lineage tree. (Right) Average relative depth within the lineage tree.

daughter cell. State 1 is the hardest to predict, and is only predicted correctly with an accuracy of 4.17%. Classes 3 and 4 are also hard to predict, as they are often confused with clusters 2 or 5 respectively. The chance level for $K = 6$ is 16.67%.

In summary, even though we did not impose any constraints, the model finds apparently meaningful types of cells, and a sparse transition model. Nevertheless, the lack of constraints makes it difficult to predict the next cell state from the state of the mother cell and the features known at birth. A potential problem is that cycles between cell states (e.g. state 2 $\rightarrow$ state 3 $\rightarrow$ state 2 $\rightarrow$ ...) are possible and even very likely. This means that the states alone give no clear indication whether a cell is more or less differentiated.

One-way Constraints

We trained a model with 6 potential cell states, and only allowed transitions between cell states in one direction (i.e. a state 1 cell can become any type of cell after division, but a state 4 cell can only become another state 4, 5 or 6 cell). Figure 2.7 shows the learned probability models for the 6 different states.

Observations:
There are quite distinct feature combinations that characterize all six clusters of cells, and the cells within a cluster are generally homogeneous at least in a subset of features. Some transitions between states occur very rarely or not at all (e.g. between state 1 and 5, or state 5 and 6). The only cluster of non-proliferative cells is number 6, which was expected

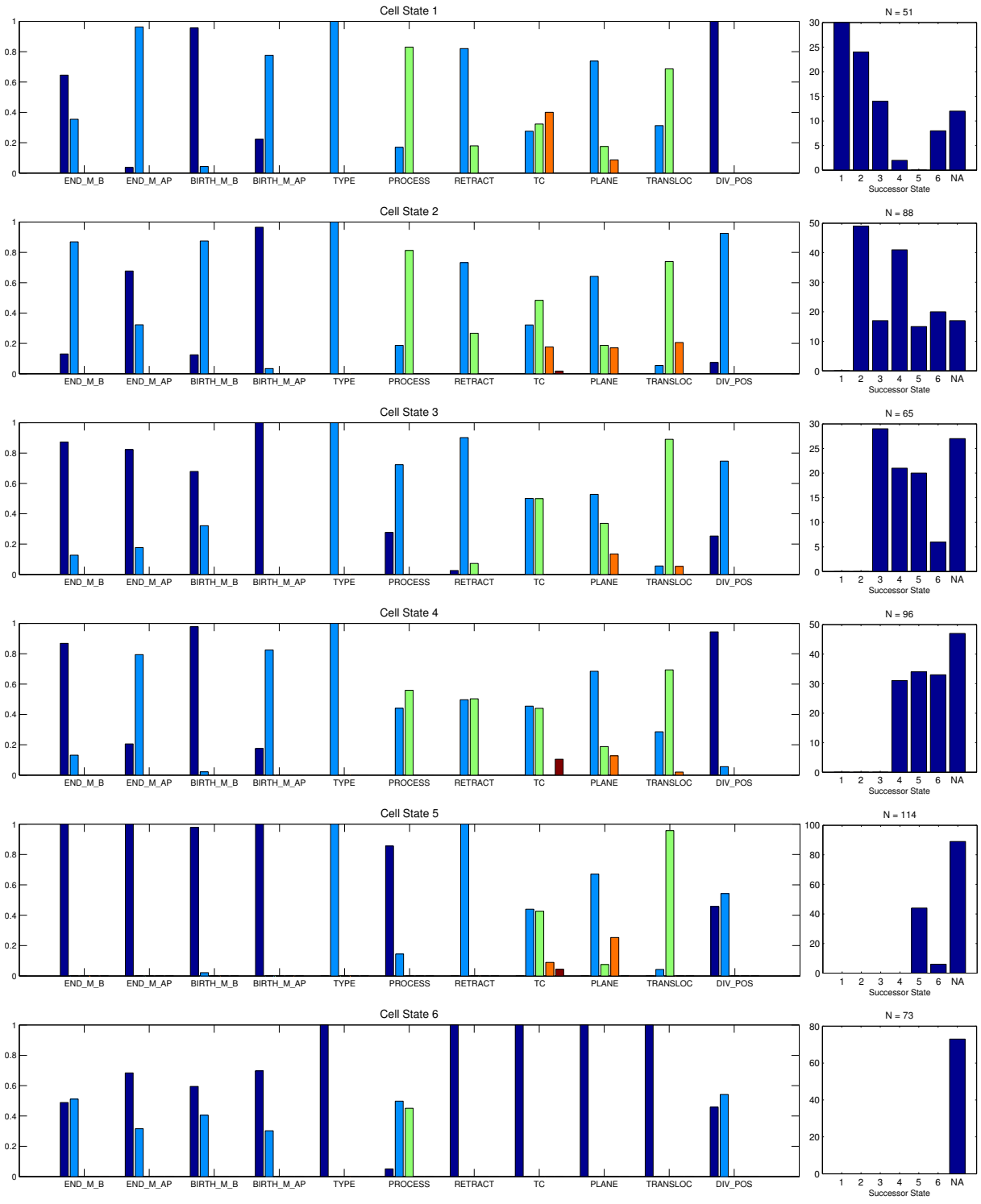

Figure 2.7. Models learned for K=6 cell states for all cells with one-way constraints. (left) Learned probability model for each of the features. (right) Distribution of direct successor states, and number of cells that fall into that cluster (N = ...). NA means that no daughter cells were recorded.

from the definition of the one-way constraints, since neurons do not divide anymore. Cells of states 1 and 5 have a low likelihood to become neurons, whereas many neurons result from division of state 2 and especially 4 cells.

State 1 cells are proliferative cells that have no basal process at birth, and are either the first cells of a lineage, or the lower cells after division (indicated by the DIV_POS distribution: dark blue = lower, light blue = higher). They almost always have a stable apical process and have sometimes also a basal process at mitosis. They often perform downwards mitotic somal translocation. They rarely retract their processes before division, and have a rather long cell cycle. State 1 cells become preferentially state 1, 2, and 3 cells after division, but never produce state 5 cells and very rarely state 4. This type is similar to type 6 (bRG-*apical-P*) in the unconstrained model (Figure 2.4).

State 2 cells have a stable basal process present both at birth and at mitosis. They often also display an apical process at mitosis. They are usually the upper cells after division, and sometimes perform upwards mitotic somal translocation. Their daughter cells take on any cell states (except state 1), and they might also become neurons. This type resemble type 5 (bRG-*basal-P*) of the unconstrained model.

State 3 cells frequently have transient processes. They rarely have apical processes. They are mostly the upper cells after divisions, and have a short cell cycle. Their cleavage plane orientation is more often oblique or vertical than other cell states. These cells share many properties with state 3 (tbRG) from the unconstrained model. Cells of this type mainly self-renew and frequently become state 4, 5 cells and rarely neurons.

State 4 cells almost always bear an apical process at birth and mitosis but it can be transient or permanent with similar probabilities. They often retract their process at mitosis, perform downward mitotic somal translocation and are mostly the lower cell after division. They have mostly a short Tc although a minor subpopulation has a long Tc. State 4 cells are the main contributors to neuron production. State 4 (mixed bRG-*apical-P*) cells share properties with types 3 and 6 from the unconstrained model.

State 5 cells have no processes. They mostly self-renew and rarely differentiate into neurons. Their fate is very often unknown because they arise mostly at the end of lineage trees (Figure 2.9). If they divide they have a rather short cell cycle duration. This type is identified as cell state 2 (IP) in the previous model.

State 6 cells are neurons, which do not divide anymore, that is why the values for RETRACT, TC, PLANE, and TRANSLOC remained unknown (indicated by the 100%

dark-blue bars). Their process morphology is almost uniformly distributed.

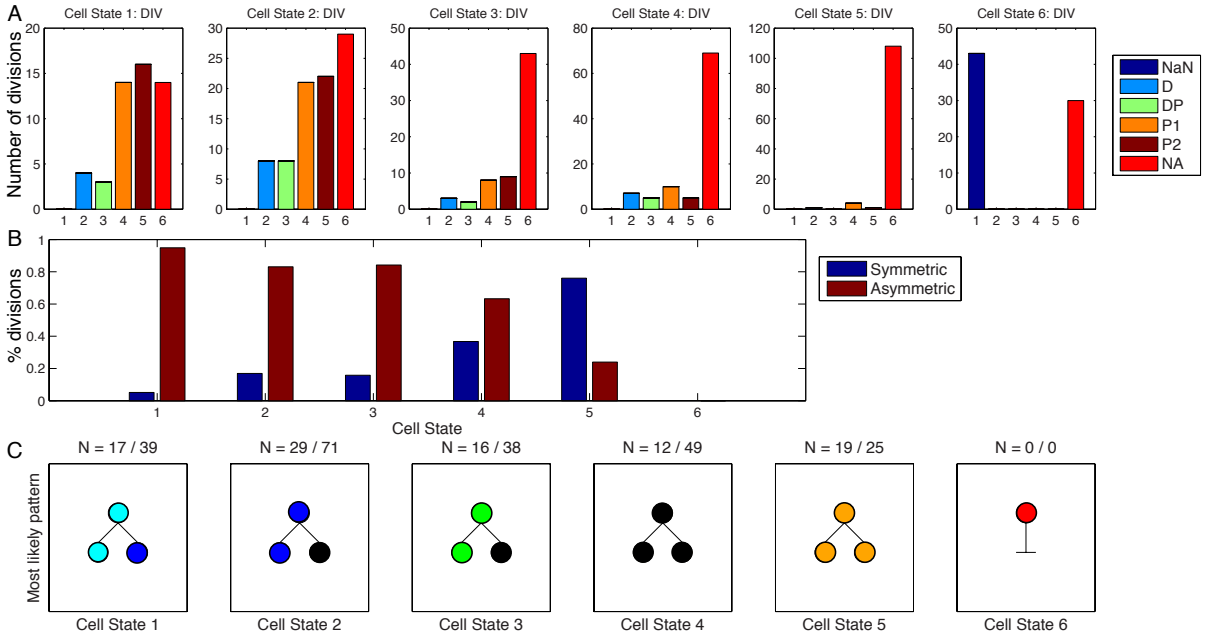

Figure 2.8. Types of division for each cell state, learned with one-way constraints. **A.** Histogram of DIV for cells from all 6 cell states. **B-C.** Observed division patterns for all 6 cell states. **B.** Frequency of symmetric vs. asymmetric divisions for each cell state. **C.** Most common division pattern for every cell state. Colors correspond to different cell states. The numbers above the illustration show the absolute number of such division patterns, in relation to the absolute number of divisions observed for cells of this state.

In Figure 2.8 we look at the distribution of the feature DIV in every class. The histograms for DIV show a strong tendency for proliferative division for state 1. We found that symmetric divisions are common for state 5 cells (IP), and also occur for state 4 cells (tbRG), whereas state 1 and 2 cells divide mostly asymmetrically, and state 6 cells do not divided at all. For states 1, 2, and 3 the most common division pattern results in another cell of the same state, and a cell of a more differentiated state. In contrast, state 4 and 5 cells often divide symmetrically into a pair of state 4 or 5 cells respectively.

The state of the next daughter cell can be predicted with an accuracy of 72.18%, using only the BIRTH_MORPH_AP, BIRTH_MORPH_B, and DIV_POS features of the daughter cell. State 6 is the hardest to predict, and is only predicted correctly with an accuracy of 29.9% (which is rather high for the models we tested).

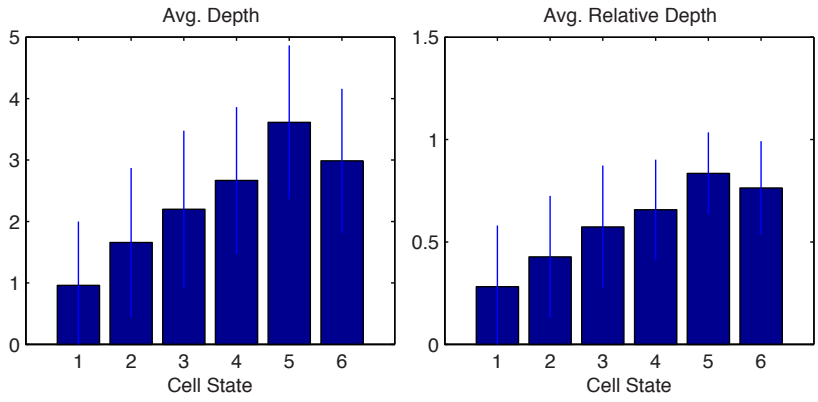

Figure 2.9. Lineage-tree dependent features computed for all 6 cell states, learned with one-way constraints. Average absolute depth within the lineage tree (left), Average relative depth within the lineage tree (right).

We also looked whether any characteristics of the cell types can be observed by looking at the average depth within the lineage tree, and the average spatial position computed for cells of the same cluster (see Figure 2.9). Not surprisingly we find that cells with higher states (less differentiated) have a higher absolute and relative depth within the tree. This is actually a consequence of the imposed constraints.

We think that this type of constraints is a useful model, since it finds very characteristic groups of cells with clear transition pathways. The constraints also make it easier to predict the state of the daughter cell, compared to the unconstrained model.

Block-Structure Constraints

We trained a model with block-structure constraints, using two blocks of three states each, and allowing only transitions within the blocks, or from the first block (states 1,2,3) to the second (states 4,5,6), but not back from the second block to the first.

Observations:

In Figure 2.10 one can see the two blocks of cells. Whereas the first block (states 1,2,3) consists mostly of proliferative cells, the second block (states 4,5,6) consists mostly of cells at the end of a lineage, or differentiated neurons. The cluster models themselves are again quite distinct from each other, and we find similar classes of cells as in the experiments without constraints or with one-way constraints.

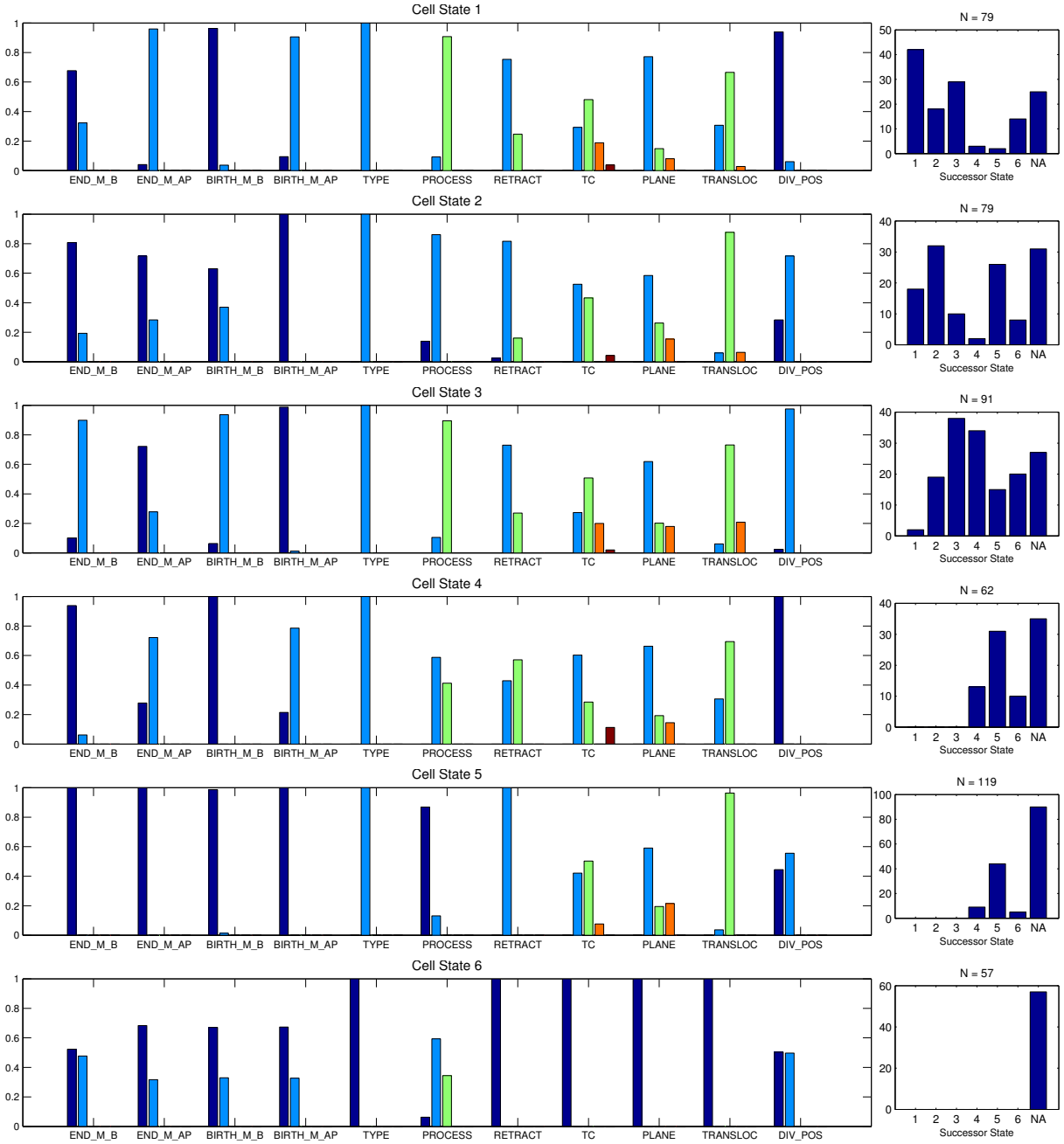

Figure 2.10. Models learned for K=6 cell states for all cells with block-structure constraints, using 2 blocks of 3 states each, and allowing only one-way transitions from block 1 (states 1, 2, 3) to block 2 (states 4, 5, 6). (left) Learned probability model for each of the features. (right) Distribution of direct successor states, and number of cells that fall into that cluster (N = ...). NA means that no daughter cells were recorded.

Due to the block-structure, different pathways of differentiations are found for cell states in the first block. When state 1 cells e.g. differentiate into a state in the second block, they mostly become state 6 cells (= neurons). State 2 cells on the other hand can go to state 5, and state 3 cells are most likely to become state 4 cells. Each of the states in the first block has a high probability of self-renewal, i.e. cells staying in the same state after division. In the second block, state 4 states mostly become state 5 cells, and state 5 cells mostly stay in the same state after division. State 6 cells are neurons. The cells from different zones are evenly distributed among all clusters.

State 1 cells are proliferative cells with permanent apical process at birth and mitosis, and frequently undergo downward translocations. They are typically the lower cells after division, and have longer cell cycles. After division the daughter cells can either stay in the first block (most likely state 1 again), or become neurons. This state is similar to state 2 in Fig. 2.7 and state 6 in Fig. 2.4: bRG-*apical-P* type.

State 2 cells display rarely processes, and never have an apical process at birth. If they have processes, they are transient and rarely retracted before division. This state is similar to state 3 in Fig. 2.4 and to state 2 in Fig. 2.7 and corresponds to the tbRG type. The cell cycle time is short, and translocations are rare. This type of cell consists mostly of upper cells after division. State 2 cells frequently self-renew or generate 5 cells after division.

State 3 is similar to state 2 in Fig. 2.7, and therefore similar to bRG-*basal-P* cells.

State 4 is similar to state 1, although the processes are more often transient, and retract before division. The cell cycle length length is also relatively short. They remind state 4 (mixed bRG-*apical-P*) of the one-way constraints model (Figure 2.7)

State 5 is similar to the IP type (state 5 in Fig. 2.7,) and typically stays within the same state after division, or is at the end of the lineage. State 5 cells mainly self-renew or often result from divisions of state 2 or 4 cells.

State 6 cells are neurons.

In Figure 2.11 we look at the distribution of the feature DIV in every class. The histograms for DIV show a tendency for proliferative division for state 1 and 3. In both cases symmetric proliferative divisions occur more often. Figure 2.11B-C shows that most cell states perform asymmetric divisions, with the exception of state 5 cells (IP) for which it is more common to divide symmetrically. Again we found that the most common asymmetric pattern of division is to produce another cell of the same type (self-renewal)

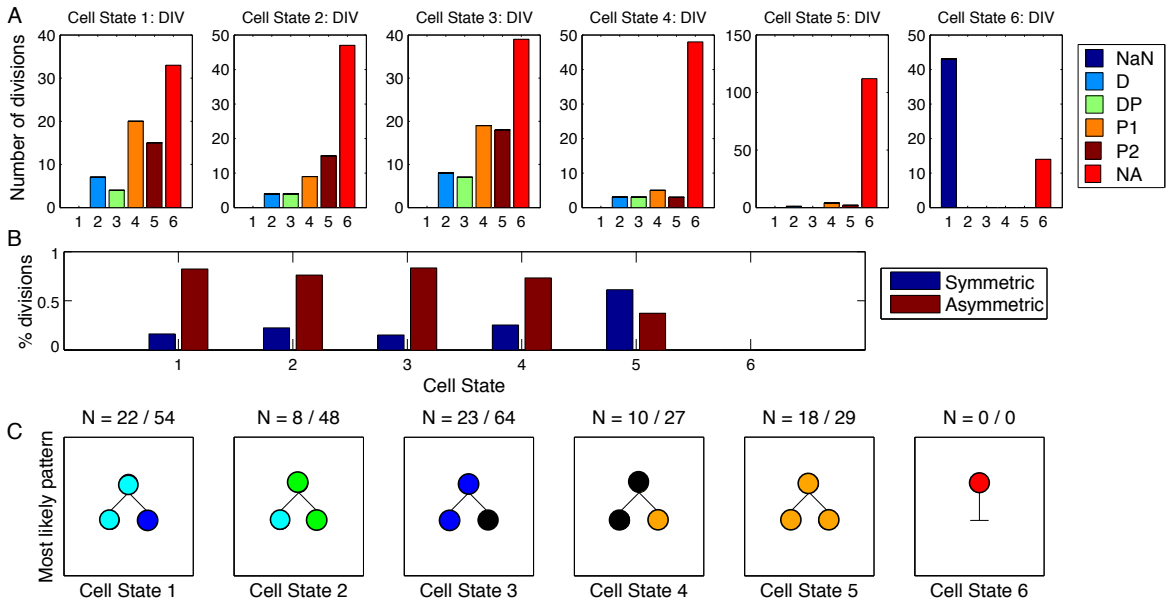

Figure 2.11. Type and pattern of divisions of the 6 cell states learned with block-structure constraints (2 blocs of 3 states each). A. Histogram of DIV for cells from all 6 cell states. B-C. Observed division patterns for all 6 cell states. B. Frequency of symmetric vs. asymmetric divisions for each cell state. C. Most common division pattern for every cell state. Colors correspond to different cell states (violet = 1, blue = 2, green = 3, yellow = 4, orange = 5, red = 6). The numbers above the illustration show the absolute number of such division patterns, in relation to the absolute number of divisions observed for cells of this state.

and a more differentiated cell. State 5 cells mostly divide symmetrically into a pair of state 5 cells.

We also looked whether any characteristics of the cell types can be observed by looking at the average depth within the lineage trees for cells of the same cluster (see Figure 2.12). Not surprisingly, we find that cells from the first block are typically earlier in the lineage than cells from the second block. State 5 cells appear particularly late in the lineage.

The state of the next daughter cell can be predicted with an accuracy of 66.33%, using only the BIRTH_MORPH_AP, BIRTH_MORPH_B, and DIV_POS features of the daughter cell. States 2 and 4 are the most difficult to predict, and are only predicted correctly with an accuracy of 16.46% or 24.56% respectively.

The model is a compromise, which allows some constraints on the transitions between

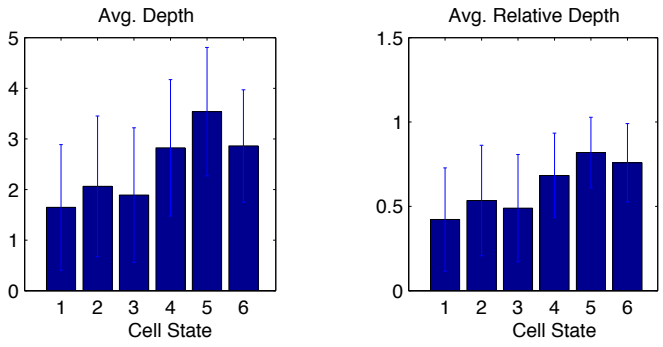

Figure 2.12. Lineage-tree dependent features computed for all 6 cell states, learned with block-structure constraints (2 blocks with 3 states each). (Left) Average absolute depth within the lineage tree. (Right) Average relative depth within the lineage tree.

cell states, but also allows going back and forth between states within a block. The prediction performance is better than for the unconstrained case, but not as good as for the one-way constraints.

Analysis of the Prediction Error for Daughter Cell States

In addition to the prediction of daughter cell states for the individual clusterings presented above, we also analyzed how the prediction performance changes with the number of clusters, and the type of constraints imposed. We computed 10 different clusterings (i.e. different random model initializations) for each combination of constraints and number of states, and plotted the average prediction error for each combination. There is a trade-off between the number of clusters used and the prediction accuracy: using fewer clusters makes it easier to predict the correct state of the daughter cell by chance. On the other hand, if more clusters are used, the clusters become more specialized, and it might be easier to predict the correct daughter cell state.

Figure 2.13 shows the results of this comparison for unconstrained or one-way constrained models, and different values of K (= number of hidden states) between 2 and 12 (always trained on the whole dataset). One can see that the best results are obtained for intermediate values of K (between 5 and 7) and one-way constraints. For low K, the models without constraints typically perform slightly better. The reason for this might be that the learned models are not very meaningful, because there are more than K significantly different cell types, and so allowing more transitions is a good idea, as cells of

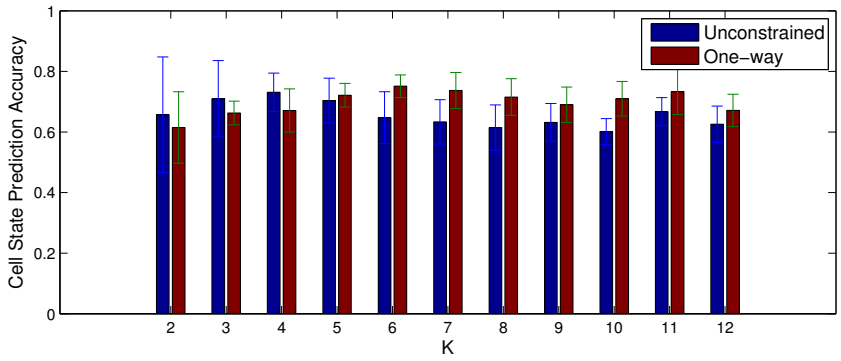

Figure 2.13. Prediction accuracy for daughter cell states, based on the state of the mother cell and the features available at birth of the cell (BIRTH_MORPH_AP, BIRTH_MORPH_B, DIV_POS), shown for different numbers of clusters, and different constraints (unconstrained vs. one-way constraints).

different types necessarily are merged into the same cluster.

For higher K, the performance of the unconstrained models goes down, whereas the performance with one-way constraints stays approximately at the same level. Taking into account that the chance level of predicting the right class goes down with higher K, this is a good sign that models with more states can still be meaningful, as long as one employs the right type of constraints.

For the experiments we manually tried out several values for K and observed the prediction performance, the stability of the results to random initializations, and the homogeneity of the resulting clusters of cells. This comforted us in our choice of $K = 6$.

2.2.4 Discussion

The main contribution of this work is a new algorithmic method for the analysis of cell lineages and relationships between measured features of cells in such lineages. The obtained results and our observations show a good congruence with the biological interpretation (see Section 2.1). We will describe the identified cell types and also address the issue of the relationship between type of lineage constraints and homogeneity of the cell types.

Identified Cell Types

The clustering with different types of constraints or number of classes always find biologically relevant clusters. In virtually all cases some classes containing uniquely neurons are found, irrespective of how many clusters we used. The cell types we find can usually be characterized by a very homogeneous morphology. Other cell types are morphologically more diverse, and seem to be characterized more by: their position within the lineage, or by other parameters: their position after division, or their mitotic somal translocation behavior. The cell cycle duration is quite heterogeneous in all clusters and does not seem to be a characteristic of cell states.

Among the cell types we identified using the clustering algorithm, the bRG-*basal-P* and IP types had already been reported in various species (Hansen et al., 2010; Fietz et al., 2010; García-Moreno et al., 2011; Kelava et al., 2011; Shitamukai et al., 2011; Wang et al., 2011; Noctor et al., 2004; Haubensak et al., 2004). 3 other types were first described during this thesis work in the same dataset using the morphology-only based classification presented in Section 2.1: bRG-*apical-P*, tbRG and bRG-*both-P*. One last type, the mixed bRG-*apical-P* was only detected by the clustering when applying constraints on the lineage transitions. We now list the characteristic types of cells that we could identify in the three generated models and that were present in the morphological classification (see Section 2.1):

1. **bRG-*basal-P* cells**: this type was first discovered in the human OSVZ by Hansen et al. (Hansen et al., 2010). They are described as having long basal, but no apical processes. They have a horizontal cleavage plane and undergo upward mitotic translocation. We find this type of cell in all our 3 models. For the whole database we identify the bRG-*basal-P* cells with state 5 in the unconstrained, state 2 in the one-way constraints, and state 3 in the block-structure constraints models (Figure 2.14). All these cells are proliferative, and participate substantially to neuronal production. They mainly undergo asymmetric divisions generating preferentially a new bRG-*basal-P* (self-renewal) and a tbRG or a precursor bearing an apical process. This type is almost exclusively the upper cell after a division. bRG-*basal-P* cells are typically found at all depths of the lineage trees and except self-renewal, are generated by bRG-*apical-P* and bRG-*both-P* in the unconstrained model (Figure 2.14).

2. **bRG-*apical-P* cells:** We identify cells with a stable apical, but no basal process, that perform downward mitotic translocations. bRG-*apical-P* cells are usually the lower of the two daughter cells, and the cell cycle length is variable, including long durations. bRG-*apical-P* cells mainly self-renew and generate bRG-*basal-P* and tbRG cells, but also have a high probability to differentiate into neurons. bRG-*apical-P* cells are very common, although less than IP cells. They are typically at the same depth of the lineage trees as bRG-*basal-P* cells. For the whole database we identify bRG-*apical-P* cells with state 6 in the unconstrained, state 1 in the one-way constrained, and state 1 in the block-structure constrained models (Figure 2.14). bRG-*apical-P* are generated by tbRG, bRG-*both-P* and to a lesser extent bRG-*basal-P* cells.

3. **tbRG:** tbRG cells are characterized by the presence of transient processes. tbRG are found with state 3 in the unconstrained and in the one-way constraints and state 2 in the block-structure constraints (Figure 2.14). They have rather a short cell cycle length and can arise from both the upper and the lower cells at mitosis. They are generated by the other bRG types and give rise mainly to IP cells.

4. **IP cells**: In every model we have at least one large class of cells that do not bear any processes. Cells of this type are also characterized by short to medium cell cycle lengths. For the whole database we identify IP cells with state 2 in the unconstrained, state 5 in the one-way constraints and in the block-structure constraints (Figure 2.14). IP cells arise from tbRG and mixed bRG-*apical-P* cells. We also noticed that IP cells frequently divide symmetrically into a pair of new IP cells, which distinguishes them from all other cell types. IP cells are often found towards the end of the lineage, and if they divide, they almost never differentiate into neurons. This means that lineage trees below an IP cell consist mostly of other IP cells amplifying their pool. The IP type is typically the largest class of cells.

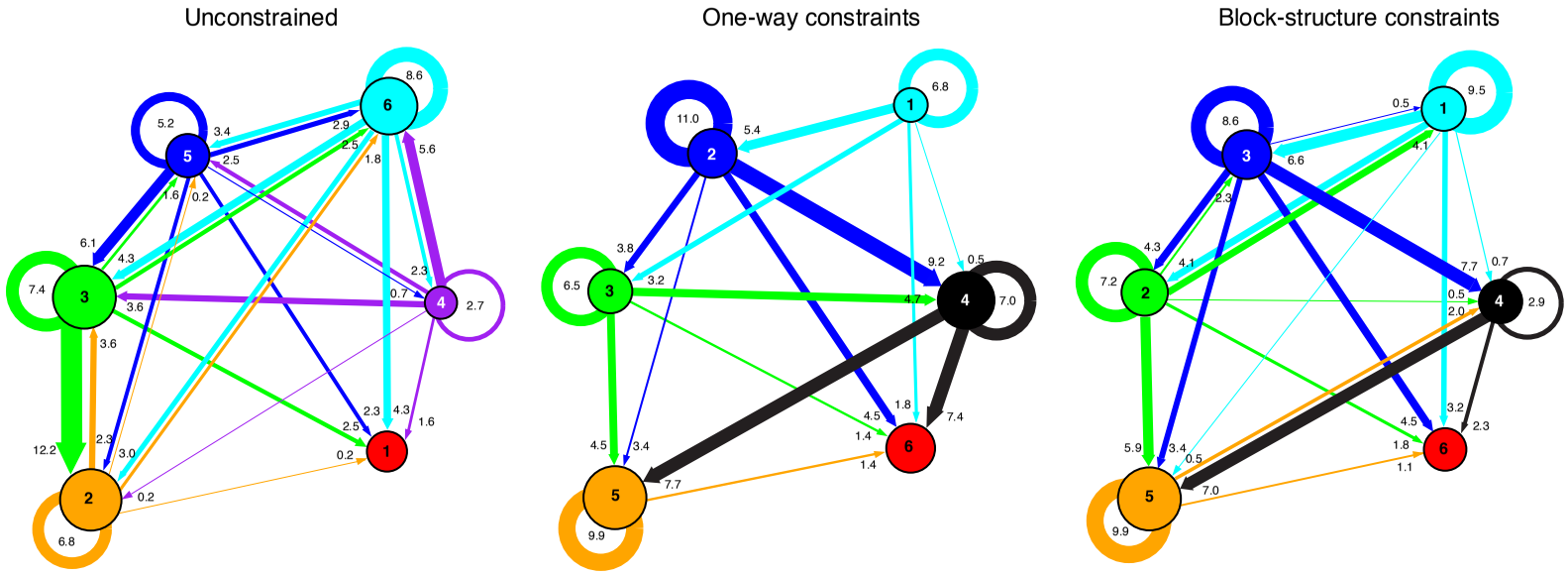

Figure 2.14. Comparison of the transitions between cell states learned without constraints (left), with one-way constrained (middle) and with block-structure constraints (right). Graphs represent state transition diagrams. The diagrams consist of two components: nodes represent cell states (clusters, numbers in the nodes refer to the cell state number in the corresponding model) and directed edges represent the transitions between states. The size of the nodes is proportional to the number of cells that belong to the cluster with respect to the total number of cells. The thickness of the arrows is proportional to the frequency of each transition with respect to the total number of transitions. Numbers close to arrows indicate the frequency of each transition. Transitions to an undefined state have not been considered. Same colors are used for cell states with similar properties in the different models. Cyan: bRG-*apical-P*, blue: bRG-*basal-P*, green: tbRG, red: neurons, purple: bRG-*both-P*, black: mixed bRG-*apical-P*.

We identified 2 other types of cells that are more heterogeneous. Moreover, they only appeared in some of the models either when no constrained are imposed on the lineage transitions (bRG-*both-P*) or on the contrary when constraints are imposed (mixed bRG-*apical-P*). These two other cell types seem thus less robust than the above mentioned types.

1. **bRG-*both-P* cells:** this cell type is present only in the unconstrained model and was first described in (Lukaszewicz et al., 2005). bRG-*both-P* cells always display at least one process but their morphology can vary. They are usually born with a basal process and always grow an apical process before dividing. This cell type contains the smallest number of cells from the different models. They arise from upper cells after divisions, undergo mostly proliferative divisions and generate mainly bRG-*apical-P* and tbRG cells. They also divide almost exclusively with a horizontal cleavage plane orientation. As cells belonging to this cluster share some morphological features with the bRG-*apical-P* and bRG-*basal-P* categories, additional constraints on the lineage transitions might push them towards these clusters. This is indeed the case. 65% of these cells fall in the bRG-*basal-P* and 28% in the bRG-*apical-P* categories under the one-way and block-structure constraints models.

2. **mixed bRG-*apical-P*:** this cell type is found when applying constraints on the lineage transitions. This more heterogeneous cluster is made of precursors arising from the lower cells after division and bearing a transient or permanent apical process. In the two models where they are identified, the bRG-*apical-P*, and tbRG cells are less frequent than under the unconstrained model. Mixed bRG-*apical-P* cells are indeed made of 65% of bRG-*apical-P*, and 30% of tbRG cells identified in the unconstrained model. This type is the main neuron producer in the one-way constrained model and generate many IP cells in the two models where they appear. The existence of this cluster suggests that cells that have slightly different morphological features can be clustered together on the basis of a similar progeny.

Constraints on lineage transitions and cluster homogeneity

There is a trade-off between the homogeneity of the cell types found by the model and the simplicity of their lineage relationships. When constraints are applied on the transitions between cell types, clusters become more heterogeneous. Cell types defined by

the unconstrained model are sharper and subtle morphological differences can lead to the formation of an independent cluster (e.g bRG-*both-P* type). When constraints are applied on the lineage transitions, cell types can still be identified (bRG-*apical-P*, bRG-*basal-P*, tbRG and IP) but some cells with slightly different features are added due to their lineage relationships. This relative loss of cluster definition is compensated by a higher cell state prediction accuracy for the biologically relevant number of clusters (around $K = 6$, Figure 2.13).

If no constraints are applied on lineage relationships, bidirectional transitions spontaneously arise between cell types, indicating that cells can come back to a less differentiated state. When one-way constraints are applied, bidirectional transitions are prevented. This results in subsets of cell types involved in reverse transitions to be moved to another cluster. Some tbRGs and bRG-*apical-P* are involved in bidirectional transitions (Figure 2.14 unconstrained and block-structure models). Those cells are moved into the mixed bRG-*apical-P* type, which eliminates bidirectional transitions. These cells seem to preferentially produce neurons because mixed bRG-*apical-P* a high proportion of neurons unlike bRG-*apical-P* and tbRG whose contribution to neuron production is smaller than without constraints.

Conclusion

This approach does not provide a definitive answer of what the different precursor types in the macaque developing cortex are. 4 clusters appear consistently with a sufficient homogeneity to be considered as independent precursor types: bRG-*basal-P*, bRG-*apical-P*, tbRG and IP. Among them two types had already been described by several previous studies (Hansen et al., 2010; Fietz et al., 2010; Section 2.1 of this thesis) reenforcing the validity of our approach. Two other more heterogeneous types are detected depending on the applied constraints on the lineage relationships. From a biological point of view, it is not known whether the homogeneity of the features is more important than the similarity of lineage relationships to define a cell type. So far, every lineage reported was clearly defined and no bidirectional transitions had been reported in normal development. This means that there is not only one solution to the clustering of the primate precursors, but exploring the different possibilities gives us more insights into potential relevant subtypes within the above mentioned precursor types. However, we expect cells that belong to the same type to be homogeneous in term of their molecular signature and thus in their

morphology. The bRG-*both-P* type is therefore more likely than the mixed bRG-*apical-P*, even though gene expression studies at a single cell resolution would be needed to confirm this assumption.

Chapter 3

General discussion

Our exhaustive live-imaging analysis of OSVZ precursors in the macaque monkey model uncovered two major characteristics of primate corticogenesis. First, OSVZ precursors exhibit extensive proliferative abilities that contribute to primate brain expansion. Contrary to the mouse model where there is a progressive increase of cell cycle exit paralleled by an increase of cell cycle length (especially of the G1 phase, (Takahashi et al., 1993)), our study points out stage-specific variations of these two parameters in the primate GZ. Higher proliferation rates resume at the time of the supragranular layer neuron production, correlated with a decrease in cell cycle length. This enables to increase the supragranular layer precursor pool and as a consequence, the number of neurons produced.

Second, our work revealed a high variety of precursors in the OSVZ. We identified 5 different precursor types: an intermediate progenitors (IP) type and 4 types of bRG cells, as opposed to the single previously reported bRG type (reviewed in (Lui et al., 2011)). The quantitative long term TLV analysis and the generation of an unique, extensive database of precursor properties and behavior made it possible to describe for the first time the lineage relationships in the primate developing cortex. We show that the lineages are complex and stage-specific. Unexpectedly, and to the best of our knowledge, we report the first evidence of bidirectional lineage transitions in normal development. Of note, both the diversity of precursors and the bidirectional transitions were confirmed by an unsupervised classification method.

In the following chapter, we shall discuss potential molecular mechanisms underlying primate cortical expansion and a time-dependent regulation of mode of division and cell cycle duration. We shall also speculate about the origin and causes of the apparition of

a higher precursor diversity during evolution. We shall finish by putting all these new findings in the context of the "epigenetic landscape" framework defined by Conrad Hal Waddington (Waddington, 1957), in an attempt to grasp the essence of the difference of neuronal lineages between rodents and primates.

3.1 Mechanisms for neuronal output amplification in primate cortical development

Our TLV analyses revealed that the primate GZ generate neurons in a stage specific manner. The rate of neuronal production is high at E65 and decreases at E78. It is interesting to note that the balance between proliferation and differentiation is virtually identical between the VZ and the OSVZ (see section 2.1, Figure 2C). This means that both GZ contribute neurons to infra- and supragranular layer neurons in agreement with the previous birthdating studies of the team where at E64 30% of precursors in S-phase were located in the OSVZ, and 20% in the VZ at E78 (Lukaszewicz et al., 2005). It seems that proliferation is controlled in a concerted manner in both VZ and OSVZ of the primate. There is thus a direct link between the amount of neurons generated by each zone and the proportion of precursors it contains. The infragranular layers are predominantly generated by the VZ (around 70%) and the supragranular layers by the OSVZ (about 80%) (Lukaszewicz et al., 2005). These findings support the idea that Basal Precursors (BPs) contribute neurons to all cortical layers (Kowalczyk et al., 2009) and are not only restricted to supragranular layer neurons production.

Our results point to an increased proliferation in the BP pool as the main driver of cortical expansion in primates. We observed several rounds of divisions in the OSVZ both at E65 (up to 3 successive divisions) and E78 (up to 6 successive divisions). This is in striking contrast with the mouse situation where BPs have been shown to mainly generate a pair of neurons and self-renew in only 5% of divisions (Haubensak et al., 2004; Noctor et al., 2004; Miyata et al., 2004; Wu et al., 2005). Hereafter, we will provide some insights into possible molecular mechanisms responsible for the BP pool expansion based on studies in the mouse model. We will then evaluate the impact of a time-dependent regulation of Tc and cell-cycle exit on neuronal production and examine the potential causal factors.

3.1.1 Candidate proteins for primate cortical expansion : proteins involved in rodent BP pool amplification

Recent studies in the mouse model pointed out several genes involved in cortical expansion that might have a similar role in primate cortical development.

Magdalena Götz's group identified Trnp1, a DNA-associated protein, as involved in cortical size regulation (Stahl et al., 2013). They showed that Trnp1 regulates both apical and basal progenitor pools. Trnp1 over expression results in an expansion of the AP pool and in a tangential expansion, confirming the Radial Unit Hypothesis (see section 1.3.7). On the other hand, Trnp1 knock down leads to an increase of the BP pool, including bRGs by RGCs delamination, at the expense of the AP pool, and results into an impressive increase in cortical thickness. Indeed, low levels of Trnp1 expression prevent the expression of BP maturating factors enabling an increased expansion. Trnp1 levels control thus AP mode of division and regulates both the expansion in surface and thickness. Stahl et al., provided also evidence supporting a proliferative zone and area specific regulation of this gene in humans. They found it expressed at high levels in the VZ and at lower levels in the OSVZ. This suggests that Trnp1 is a good candidate for primate cortical expansion, where a fine regulation of its level of expression can have a major impact on cortical size, via the AP pool amplification in the VZ combined with the amplification of the BP pool in the OSVZ. In mice, Trnp1 is expressed in RGCs, we can hypothesize that this gene might be expressed in the different types of primate bRGs thereby controlling their expansion. It remains however necessary to confirm the different levels of Trnp1 expression at the protein level in RGCs and bRGs. It would also be interesting to examine whether the Trnp1 expression levels change in the different proliferative zones at E65 and E78 where we showed different proliferative behaviors (see section 2.1).

A subunit of the chromatin remodeling complex mSWI/SNF, BAF170, was also recently showed to play a crucial role in cortical size regulation in the mouse (Tuoc et al., 2013). BAF170 conditional KO (cKO) results in an important expansion of the cortex both in surface and thickness via the increase of indirect neurogenesis and expansion of the BP pool. In the cKO mutant, BPs are more numerous but do not proliferate more than the control. On the contrary, BAF170 over-expression displays the opposite phenotype with a marked microencephaly. After having noticed that the cKO and the Pax6 KO displayed opposite cortical growth and lamination defects (Warren et al., 1999; Mi

et al., 2013), the authors found out that most of the genes upregulated by Pax6 are repressed by BAF170. They showed that BAP170 binds to the Pax6/Rest complex, recruits a co-repressor complex and prevents the expression of IP and late precursor genes. This process limits IP generation, indirect neurogenesis and cortical expansion. BAF170 cKO has the opposite effect.

A recent study identified Axin, a scaffold protein known to be involved in different signaling pathways such as the Wnt pathway, as a key molecule involved in the generation, amplification and differentiation of BPs (Fang et al., 2013). When localized in the cytoplasm Axin interacts with GSK3β and promotes indirect neurogenesis; that is to say self-renewal of RGC and generation of BPs. Phosphorylation by CDK5 in BPs induces Axin translocation into the nucleus where it interacts with β-catenin and results into neuronal differentiation. Post-tranlational regulation of Axin through adaptive evolution could provide a way of altering the balance proliferation/differentiation of the BP pool during evolution.

The regulation of these three molecules, through the control of the BP pool size, leads to the repression of cortical expansion during normal mouse development. This suggests that a brake effect is exerted on mouse BP proliferation, as if extra proliferation could not be regulated in BPs, which have lost their epithelial properties as observed in tumorigenesis (Gomez-Lopez et al., 2013; Lee and Vasioukhin, 2008). In primates, other mechanisms such as the enrichment of extracellular matrix proteins in the OSVZ (Fietz et al., 2012) are likely to allow a controlled proliferation of non epithelial cells in this zone.

3.1.2 A time-dependent cell cycle duration / mode of division regulation allowing an upsurge of proliferation

Our TLV observations revealed a lengthening of Tc and an increase in the proportion of differentiative divisions at E65 compared to E48, as opposed to a Tc shortening and an increase in the proportion of proliferative divisions at E78 compared to E65 (section 2.1). This mechanism enables an upsurge of proliferation at the time of the supra granular layer neurons generation and contributes in turn to an extra production of upper layer neurons in primates. The upsurge of proliferation at E78 is in agreement with the high levels of Cyclin E expression in a substantial proportion of precursors at this stage (Lukaszewicz et al., 2005), indicating high rates of G1/S transitions. In addition, we have evidence for

the existence of a primate specific miRNA, specifically expressed in the OSVZ, regulating Mll2 expression, a protein involved in the regulation of the G1/S transition (Arcila, Betizeau et al, in preparation). Moreover, an experimental Tc shortening in mice, by mean of Cyclin D1 and Cyclin E over-expression, resulted in the amplification of the BP pool and ultimately in an increased production of supra granular layer neurons, via the control of AP and BP mode of division (Pilaz et al., 2009). This experiment provides the functional proof that a shortening of Tc - which induces higher rates of divisions- at the time of supragranular layer neuron generation can result in an extra production in these neuron types.

The lengthening of the Tc and increase in cell-cycle exit observed from E48 to E65 fits with what has been shown in the mouse model. In this model, there is a progressive increase in Tc and cell-cycle exit as neurogenesis proceeds. A reduction of Tc has been measured in the ferret (Reillo and Borrell, 2011). However, Tc shortening along with a reduction in cell-cycle exit -as observed between E65 and E78- has never been observed outside the primate order. Hence, a primate-specific event taking place between E65 and E78 is probably responsible for this phenomenon. Moreover, this Tc shortening is observed in both the VZ, as previously described by P. Rakic's group (Kornack and Rakic, 1998), and in the OSVZ. All precursor types are equally affected. This suggests that a global signal is exerted on APs and BPs. Alternatively, this phenomenon could be explained by the existence of feedback regulatory loops between the 2 precursor pools (Nelson et al., 2013; Yoon et al., 2008).

Several sources could be responsible for this dynamic change in proliferation. Thalamic axons are able to secrete proliferative signals that can change cell cycle dynamics in the mouse model (Dehay et al., 2001). Thalamic axons invade the primate cortex in the OFL at mitcorticogenesis and are likely to contribute to the control of proliferation (reviewed in (Dehay and Kennedy, 2007)). On the other hand, other fibers reach the occipital cortex between E65 and E78 in the IFL. The exact origin and nature of these fibers remain uncertain (García-Moreno et al., 2011), but an influence on proliferation cannot be excluded. The vascular system has already been shown to provide a niche for adult neural stem cells (Bovetti et al., 2007; Riquelme et al., 2008) and also for BPs during development (Javaherian and Kriegstein, 2009; Stubbs et al., 2009). In mice the appearance of Tbr2 expressing cells is paralleled by the vascularization of the SVZ. The OSVZ at E65 and E78 is thus likely to be vascularized to a similar degree, but a proliferative signal such as

the vascular endothelial growth factor (VEGF) could be delivered at E78 by capillaries or endothelial cells (Javaherian and Kriegstein, 2009; Shen et al., 2004). Signals from the meninges, via retinoid acid for example (Siegenthaler et al., 2009), could also be involved in regulating proliferation via the extensive basal processes of bRG-*basal-P* and bRG-*both-P* that reach the basal lamina. bRG-*both-P* could, in turn, relay this signal and/or feedback to other precursors via their apical process.

Although the mechanisms causing Tc shortening and proliferation upsurge at E78 remain elusive, these phenomena are likely to account for the expansion of the supragranular layer neurons in primates.

3.2 Diversity of precursor types and complex lineage relationships in the primate developing cortex

Beside an increased proliferative potential of the BP pool, our TLV analyses revealed an increased diversity of cell types in the primate OSVZ (see section 2.1). In line with the rodent precursor classification and the recently described precursor type in humans (Hansen et al., 2010; Fietz et al., 2010), we identified OSVZ precursors based on morphological parameters. The analysis of our extensive database of precursor characteristics allowed us to validate this classification using an unbiased clustering approach, considering every parameter equally. In the next paragraphs, we will compare the results of the two approaches at E78. We will then comment on the possible consequences of an increased complexity in primate neuronal lineages.

3.2.1 5 types of precursors in the primate OSVZ

Although some studies have unraveled a certain degree of diversity in mouse cortical precursors (Tyler and Haydar, 2013), our TLV observations showed an unexpected morphological diversity of OSVZ precursors. In mouse cortical precursors types, morphological characteristics are tightly linked with gene expression (Tyler and Haydar, 2013; Englund et al., 2005). Of note, morphologies of glioblastoma cells have been correlated with their molecular signature (Cooper et al., 2011). We categorized OSVZ precursors with respect to their morphological characteristics as observed under TLV (see section 2.1).

In a second step, we used an unbiased clustering approach to classify the precursors

based on all parameters (Tc, plane of division, relative position of the daughter cells..) with an equal weight (see section 2.2). The clustering of the primate lineage data, without applying constraints on the lineage relationships, returned the same precursor types as those determined uniquely on the basis of morphology (Figure 3.1). This validates our first categorization criteria and confirmed that cells with a similar morphology are also homogeneous for other parameters.

There are however some small differences when we compare in details the cell types and their lineage relationships found with the two methods (Figure 3.1). First, one needs to be aware that the clustering method used is a predictive model. That is to say, cells at the end of the lineage trees, whose fate has not been determined, will be assigned to a cluster depending on their subset of measured parameters. This is why there are more identified transitions in the clustering state diagram and in proportion less transitions toward neurons. The main difference regarding cell types concerns the bRG-*both-P* type. The bRG-*both-P* type found by the clustering is less prominent than the one returned by the morphological classification. A closer look at the cluster parameters reveals that only upper daughters after division, with a basal process, are present. Lower cells that inherit an apical process and grow a basal process before dividing fall in the bRG-*apical-P* category. The main transitions between cell types are the same in the two classifications. There are only a few minor transitions that differ (transitions from IP to bRG-*both-P* (1%) and from tbRG to bRG-*both-P* (1.6%) are present only in the morphological categorization (Figure 3.1A), transitions from IP to bRG-*basal-P* (0.2%) and from bRG-*both-P* to IP (0.2%) are found only in the automatic classification (Figure 3.1B)).

The cell types identified by the morphological and the automatic classifications are the same. Some cells with more heterogeneous characteristics can however be assigned to a different category in the two classifications.

Although precursor morphology is assumed to be correlated to their molecular signature, a next step in the characterization of OSVZ precursor types has to be undertaken, aiming at determining their transcriptome. Using the Pax6 and Tbr2 markers, we did not detect any significant difference between the bRG types, we only found that IP cells express more often Tbr2 (see section 2.1 Figure 3J). The different bRG types could probably be differentiated based on their whole transcriptome or their miRNA signature. New techniques are currently available to allow single cell resolution in transcriptomic studies (Plessy et al., 2013). Along this line, a study in the hematopoietic system using

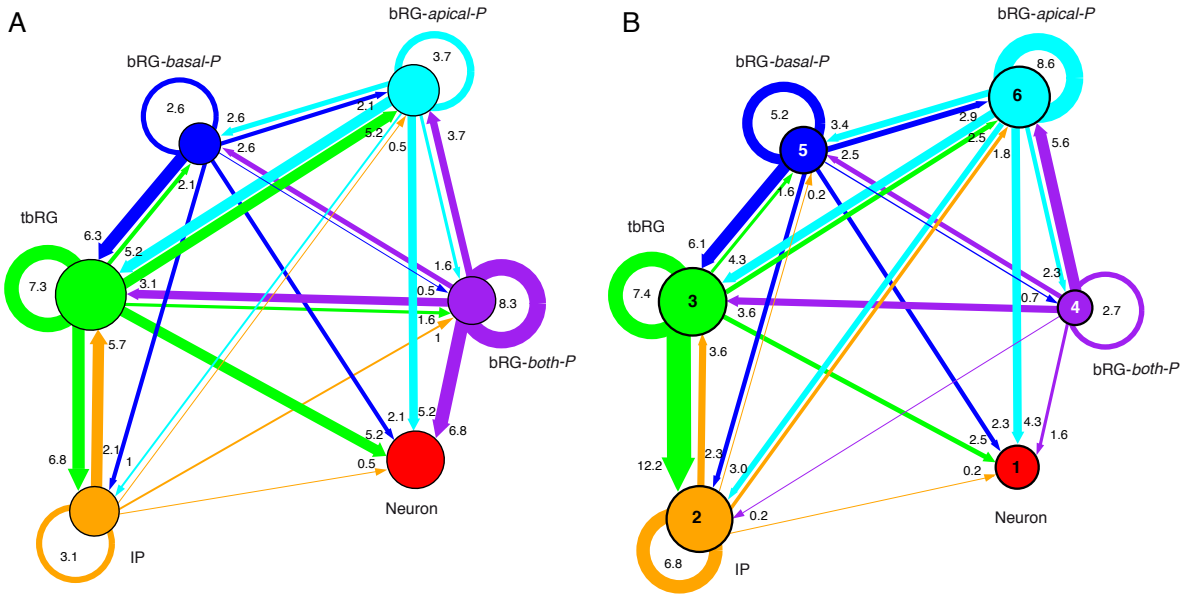

Figure 3.1. Comparison of precursor types and lineage relationships between the categorization based on morphological parameters **(A)** and the results of the clustering algorithm without constraints **(B)** at E78. In each case a state diagram is represented. The diagrams consist of two components: nodes represent cell states and directed edges represent the transitions between states. The size of the nodes is proportional to the number of cells that belong to the cluster with respect to the total number of cells. The thickness of the arrows is proportional to the frequency of each transition with respect to the total number of transitions. Numbers close to arrows indicate the frequency of each transition. Transitions to an undefined state have not been considered.

miRNA high throughput microfluidic RT-qPCR enabled a better delineation of the multiple stem/progenitor cells of this system (Petriv et al., 2010). A similar method based on miRNA or mRNA signature would improve the definition of the 5 OSVZ precursor types that we identified.

3.2.2 An emerging neuronal lineage complexity during evolution?

A cell lineage is defined as the pattern of cell division in the development of an organism. In C. *elegans* the complete cell lineage has been identified (Sulston, 1988). The lineage from the egg cell to the different cell types is highly reproducible between individuals in

this species. There is almost no stochasticity involved except few examples of stochastic fate choices at the end of lineage (reviewed in (Chisholm, 2001)). Chilsholm suggests that invariant lineage trees reflect both cell-autonomous mechanisms of fate determination and highly reproducible cell/cell interactions. Regularities in the genetic regulation, in the intrinsic factor inheritance and in the environment seem to be needed to produce similar lineages.

In insects, cell lineages have been shown to be variable between individuals although the nervous system development contains stereotyped sublineages that correspond to functional units (Spindler and Hartenstein, 2010). In vertebrates, lineages contain many more cells, and one cell can generate a variety of progeny under the control of intrinsic regulation and environmental cues (Shen et al., 2006). These findings suggest that the more cells the organism contain, the more likely it is that the cell's local environment will change from one individual to another and thus, the more likely it is that lineages will be variable.

Recent studies have assessed the variability and complexity of retinal and cortical neuronal lineages. Using quantitative TLV reconstruction of retinal lineage trees, two studies point to an important role of stochasticity in cell fate decision in highly variable retinal lineages (He et al., 2012; Gomes et al., 2010). It is important to remind here that a stochastic process is not a random process. But as opposed to a deterministic process in which the outcome is 100% sure, completely reproducible, a stochastic process has different potential outcomes reached with particular probabilities (Zernicka-Goetz and Huang, 2010). In the case of retinal precursors, instead of observing a sequential generation of the different cell types similar in all lineages as previously reported (Cepko et al., 1996), He et al in the zebrafish *in vivo*, and Gomes et al in the rat *in vitro* found that, at each cell cycle, retinal precursors generate the different retinal cellular types with a probability that corresponds to the proportion of the cell type in the adult retina. They proposed a stochastic model in which biasing factors influence the probability of generating the different cell types. An example of such a biasing factor (Ikaros) was described both in mouse retinal and cortical developments (Alsio et al., 2013; Elliott et al., 2008). Despite a preserved order of cell type apparition, the lineages of cortical precursors recorded *in vitro* (Shen et al., 2006) display a high variability in size and are compatible with a stochastic model in which the probability of division is weighted according to the number of divisions the precursor already underwent (Slater et al., 2009).

Our lineage data in the developing primate cortex do not allow the direct assessment of the stochasticity of fate decision because we do not know the final type of neuron produced. We can however speculate about the potential stochasticity of transitions among precursor types and toward neurons. In contrast to the prevalent hypothesis (Lui et al., 2011), we do not report deterministic lineages starting from a given precursor type, passing through different intermediate types before generating neurons. We instead identified precursor types that generate other precursor types and neurons with particular probabilities, in accordance with stochastic lineage relationships. In addition, we reported differences in lineage topology during the generation of infra- and supragranular layer neurons. This indicates that in primate stochastic neuronal lineages, the probabilities of each progeny outcome are stage-specific. This suggests that different biasing factors are involved at different stages and in potentially different precursor types. According to this process, neurons are produced in parallel streams by the different precursor types. It would be interesting to know whether precursor types are biased to the generation of specific neuron types.

The study of neuronal lineages in different species suggests that lineage variability increases with organism complexity and with neuronal diversification. Neurons in primates are produced by a mosaic of precursors displaying stage-specific and stochastic lineage relationships leading to the generation of complex lineage trees and resulting potentially into the generation of more diverse neuronal types. It would be interesting to assess the complexity of neuronal lineages in other primates, and non primate species (ferret for instance) to define whether neuronal lineage complexification is primate specific or increases progressively in mammals.

3.3 Hypothesis for the origin of precursor type diversification and lineage relationships complexification during evolution

In this last part of the general discussion, we will build on the metaphor of the "epigenetic landscape" enunciated by Conrad Hal Waddington (Waddington, 1957) to make hypotheses about the mechanisms at the origin of neuronal lineage differences between mouse and primate cortical development.

3.3.1 The metaphor of Waddington epigenetic landscape

Conrad Hal Waddington was one of the first biologists to propose a theoretical model of embryonic development based on genetic regulation. He defined a so called "epigenetic landscape" at the basis of cell differentiation and diversification during development (Waddington, 1957). The interactions between the different genes and proteins within a cell generate a multidimensional space represented in a metaphor as a landscape of valleys and ridges that constraint the potential cell types and cell differentiation trajectories, or chreodes, during development (Figure 3.2D). Cells are represented as balls that roll down a mountain starting from an undifferentiated pluripotent state. They then follow a particular trajectory through valleys defined by the landscape to end up at the bottom of a given valley in an attractor state that corresponds to a differentiated cell type.

Each point of the landscape corresponds to a particular combination of the gene expression (expression pattern) in the cell undergoing differentiation (Figure 3.2D). All expression patterns are not equally stable because of the gene interactions governed by the Gene Regulatory Network (GRN). For example, if a gene A inhibits the genes B and C, an expression pattern where all 3 genes are highly expressed will not be stable and will evolved towards a decrease of B and C expression. In the epigenetic landscape, stable expression patterns correspond to valleys and unstable to ridges. We will use this formulation of the epigenetic landscape based on the GRN (Kauffman, 1993), which allows a graphical representation of abstract concepts, to postulate differences of neuronal lineages in rodents and primates.

3.3.2 Different landscapes in mouse and primate cortical developments?

Our data on primate precursor types and neuronal lineages revealed new and primate specific precursor types and a complexification of the neuronal lineages. This implies that some expression patterns very unstable in mice are stabilized in primates. Pax6 and Tbr2 expression is for example barely detected in mice whereas the co-expression is stable is primates. There are two non mutually-exclusive possible explanations. Either the epigenetic landscapes are similar in mice and primates and some ontogenic differences allow the stabilization of new precursor types. Or the GRNs are different in mice and primates and result in different epigenetic landscapes with new valleys enabling different

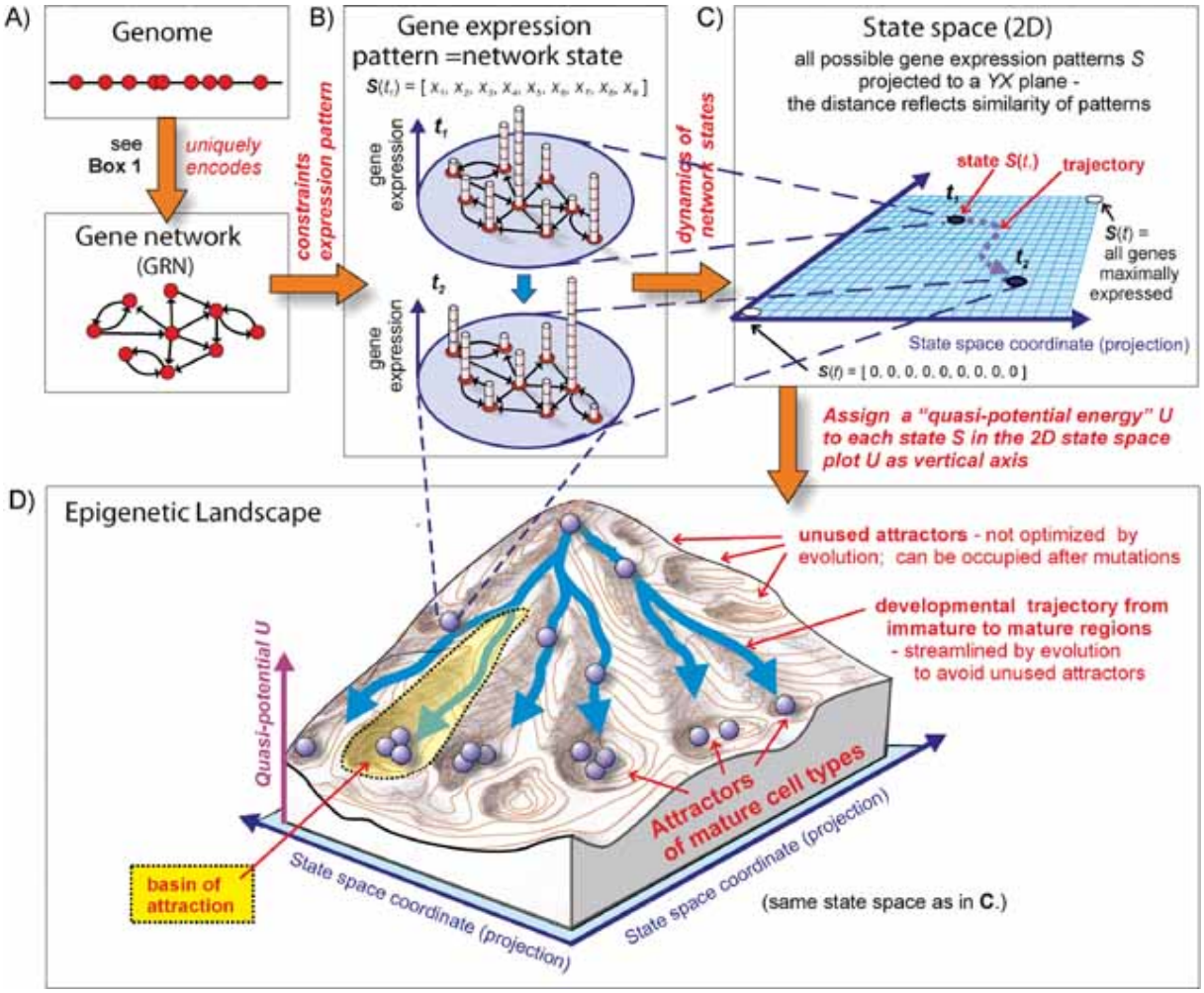

Figure 3.2. Towards a quantitative description of Waddington epigenetic landscape. Example of an epigenetic landscape for 9 genes **(A)**. These 9 genes interact, activating/inhibiting each other expression in a Gene Regulatory Network (GRN). This GRN constraints the potential expression level of each gene resulting in the epigenetic landscape **(D)**. Mountains represent unstable gene expression patterns and valleys stable expression patterns defined by the topology of the GRN. The gene expression pattern (or cell state) of a cell is defined by the expression level of the 9 genes **(B)**. Here are represented the expression patterns of a cell at two different time points t_1, t_2. The gene expression pattern can be represented in a 2 dimension state space **(C)** as a function of time which will give the trajectory. To each state corresponds a quasi-potential energy associated to the stability of the state, determined by the GRN. A low quasi-potential energy corresponds to a stable state, a high to an unstable state. This represented as the third dimension in the epigenetic landscape **(D)**. Figure from (Huang, 2012).

developmental trajectories. We will hereafter discuss the relevance of the two different theories.

Firstly, a parsimonious hypothesis would be that the epigenetic landscapes involved in mouse and primate neuronal differentiation are similar. Many genes (85%) are indeed conserved between mice and humans (Makalowski et al., 1996). The stabilization of cells in some valleys allowing the identification of new precursor types in primates could happen by "decreasing the steepness" of the landscape. This would result in the stabilization of previously very unstable expression patterns. In primates, cortical development occurs in a protracted period of time (8 days in mice, 60 days in macaque monkeys), with a much longer cell cycle duration. If we take the metaphor of the ball rolling down the mountain into the landscape, a protracted period of corticogenesis might decrease the slope of the valleys and allow the ball to take more minor valleys allowing the stabilization of new precursor types and thus a diversification. The epigenetic landscape would be travelled with a higher resolution in primates.

An alternative hypothesis would be that the GRNs are different to some extent in mice and primates resulting in different epigenetic landscapes. Recent genomic studies have pointed out the higher frequency and diversity of alternative splicing in human cortical development (Johnson et al., 2009). In addition, not much is known about differences in regulatory regions that are crucial to determine the GRN. There is the example of the GFAP promoter. The mouse version does not allow GFAP expression in RGCs whereas the human version allows the expression in human and also in mouse RGCs (Malatesta et al., 2000; Levitt and Rakic, 1980). These findings are in favor of partially different GRNs in mice and primates. The differences in the GRN could stabilize previously unstable expression patterns and allow the emergence of a refined epigenetic landscape with new valleys, allowing the existence of new precursor types and new routes for neuronal differentiation.

In both cases the higher complexity of neuronal lineages can be explained by the existence and stabilization of new valleys of the epigenetic landscape allowing parallel streams of neuronal differentiation which potentially contribute to the increased diversity of neuronal types. Some of these new valleys might get closer to each other as development proceeds with the existence of lower ridges that noise in gene expression could enable to cross. This is a potential mechanism for the observed bidirectional transitions between precursor types.

The use of the epigenetic landscape metaphor reveals that some expression patterns are stabilized in primates compared to rodents allowing the detection of new precursor types either very transient or inexistent in rodents. The epigenetic landscape is probably more detailed in primates with a higher number of routes leading to neuronal differentiation.

3.4 General conclusion

The results of this PhD thesis provide novel insights into the mechanisms of cortical expansion during evolution. In agreement with the different scaling rules of rodent and primate cortices (Section 1.1.4), we reported qualitative differences between mouse and macaque cortical development which result into a higher supra granular layer neuron production in primates. Our data supports the idea that this increased neuronal production is achieved by an expansion of the BP pool in the OSVZ. Probably linked to this BP pool expansion, we pointed out a high diversity of precursor types generating complex lineages in the OSVZ. Each of the five identified types is able to self-renew and to directly generate neurons. The diversification of primates BPs, especially the maintenance of a radial morphology in a supposedly extra-cellular matrix enriched environment, might be the key event in evolution that enabled a controlled proliferation of non epithelial cells in the OSVZ and in turn an amplified neuronal production.

In light of the precursor diversity that we reported in macaque, a reexamination of the precursor types is needed in other species to determine its apparition and role during evolution. It is likely that this BP diversity and higher proliferative abilities is also present in human cortical development, where a longer neurogenesis period could account for the increased neuronal production compared to macaques. The question of a diversity of BPs in relation to their proliferative abilities in other primates, other orders, gyrencephalic or lissencephalic species remains to be addressed. This would help understanding whether a higher diversity of precursors is primate specific or represents a more widespread feature in mammalian cortical development.

Bibliography

Aboitiz, F. (1999). Feature article: Evolution of isocortical organization. a tentative scenario including roles of reelin, p35/cdk5 and the subplate zone. *Cerebral Cortex*, 9(7):655–661.

Allman, J. and Hakeem, A. (2002). Two phylogenetic specializations in the human brain. *The Neuroscientist*, 8(4):335–46.

Alsio, J. M., Tarchini, B., Cayouette, M., and Livesey, F. J. (2013). Ikaros promotes early-born neuronal fates in the cerebral cortex. *Proceedings of the National Academy of Sciences*, 110(8):E716–E725.

Altman, J. and Bayer, S. A. (1990). Horizontal compartmentation in the germinal matrices and intermediate zone of the embryonic rat cerebral cortex. *Experimental Neurology*, 107(1):36–47.

Anderson, S. A., Eisenstat, D. D., Shi, L., and Rubenstein, J. L. (1997). Interneuron migration from basal forebrain to neocortex: dependence on dlx genes. *Science*, 278(5337):474–476.

Anderson, S. A., Kaznowski, C. E., Horn, C., Rubenstein, J. L. R., and McConnell, S. K. (2002). Distinct origins of neocortical projection neurons and interneurons in vivo. *Cerebral Cortex*, 12(7):702–709.

Anderson, S. A., Marín, O., Horn, C., Jennings, K., and Rubenstein, J. L. (2001). Distinct cortical migrations from the medial and lateral ganglionic eminences. *Development*, 128(3):353–363.

Angevine, J. B. and Sidman, R. L. (1961). Autoradiographic study of cell migration during histogenesis of cerebral cortex in the mouse. *Nature*, 192(4804):766–768.

Anthony, T. E., Klein, C., Fishell, G., and Heintz, N. (2004). Radial glia serve as neuronal progenitors in all regions of the central nervous system. *Neuron*, 41(6):881–890.

Arlotta, P., Molyneaux, B. J., Chen, J., Inoue, J., Kominami, R., and Macklis, J. D. (2005). Neuronal subtype-specific genes that control corticospinal motor neuron development in vivo. *Neuron*, 45(2):207–221.

Arnold, S. J., Huang, G.-J., Cheung, A. F. P., Era, T., Nishikawa, S.-I., Bikoff, E. K., Molnár, Z., Robertson, E. J., and Groszer, M. (2008). The t-box transcription factor Eomes/Tbr2 regulates neurogenesis in the cortical subventricular zone. *Genes & Development*, 22(18):2479–2484.

Aschoff, J. (1971). *Energiehaushalt und Temperaturregulation, von Jürgen Aschoff, Bruno Günther [und] Kurt Kramer.* Urban & Schwarzenberg, München.

Ascoli, G. A., Alonso-Nanclares, L., Anderson, S. A., Barrionuevo, G., Benavides-Piccione, R., Burkhalter, A., Buzsáki, G., Cauli, B., DeFelipe, J., Fairén, A., Feldmeyer, D., Fishell, G., Fregnac, Y., Freund, T. F., Gardner, D., Gardner, E. P., Goldberg, J. H., Helmstaedter, M., Hestrin, S., Karube, F., Kisvárday, Z. F., Lambolez, B., Lewis, D. A., Marin, O., Markram, H., Muñoz, A., Packer, A., Petersen, C. C. H., Rockland, K. S., Rossier, J., Rudy, B., Somogyi, P., Staiger, J. F., Tamas, G., Thomson, A. M., Toledo-Rodriguez, M., Wang, Y., West, D. C., and Yuste, R. (2008). Petilla terminology: nomenclature of features of GABAergic interneurons of the cerebral cortex. *Nature Reviews Neuroscience*, 9(7):557–568.

Azevedo, F. A. C., Carvalho, L. R. B., Grinberg, L. T., Farfel, J. M., Ferretti, R. E. L., Leite, R. E. P., Jacob Filho, W., Lent, R., and Herculano-Houzel, S. (2009). Equal numbers of neuronal and nonneuronal cells make the human brain an isometrically scaled-up primate brain. *The Journal of comparative neurology*, 513(5):532–541.

Baala, L., Briault, S., Etchevers, H. C., Laumonnier, F., Natiq, A., Amiel, J., Boddaert, N., Picard, C., Sbiti, A., Asermouh, A., Attié-Bitach, T., Encha-Razavi, F., Munnich, A., Sefiani, A., and Lyonnet, S. (2007). Homozygous silencing of t-box transcription factor EOMES leads to microcephaly with polymicrogyria and corpus callosum agenesis. *Nature Genetics*, 39(4):454–456.

Balsters, J., Cussans, E., Diedrichsen, J., Phillips, K., Preuss, T., Rilling, J., and Ramnani, N. (2010). Evolution of the cerebellar cortex: The selective expansion of prefrontal-projecting cerebellar lobules. *NeuroImage*, 49(3):2045–2052.

Bartos, M., Vida, I., and Jonas, P. (2007). Synaptic mechanisms of synchronized gamma oscillations in inhibitory interneuron networks. *Nature Reviews Neuroscience*, 8(1):45–56.

Beaulieu, C. (1993). Numerical data on neocortical neurons in adult rat, with special reference to the GABA population. *Brain Research*, 609(1–2):284–292.

Beaulieu, C. and Colonnier, M. (1989). Number and size of neurons and synapses in the motor cortex of cats raised in different environmental complexities. *The Journal of Comparative Neurology*, 289(1):178–187.

Bedford, L., Walker, R., Kondo, T., van Crüchten, I., King, E. R., and Sablitzky, F. (2005). Id4 is required for the correct timing of neural differentiation. *Developmental Biology*, 280(2):386–395.

Bernard, A., Lubbers, L. S., Tanis, K. Q., Luo, R., Podtelezhnikov, A. A., Finney, E. M., McWhorter, M. M., Serikawa, K., Lemon, T., Morgan, R., Copeland, C., Smith, K., Cullen, V., Davis-Turak, J., Lee, C.-K., Sunkin, S. M., Loboda, A. P., Levine, D. M., Stone, D. J., Hawrylycz, M. J., Roberts, C. J., Jones, A. R., Geschwind, D. H., and Lein, E. S. (2012). Transcriptional architecture of the primate neocortex. *Neuron*, 73(6):1083–1099.

Bok, S. (1960). Histonomy of the cerebral cortex. *British Journal of Surgery*, 47(204):454–454.

Borello, U. and Pierani, A. (2010). Patterning the cerebral cortex: traveling with morphogens. *Current Opinion in Genetics & Development*, 20(4):408–415.

Borrell, V. and Reillo, I. (2012). Emerging roles of neural stem cells in cerebral cortex development and evolution. *Developmental Neurobiology*, 72(7):955–971.

Bovetti, S., Hsieh, Y.-C., Bovolin, P., Perroteau, I., Kazunori, T., and Puche, A. C. (2007). Blood vessels form a scaffold for neuroblast migration in the adult olfactory bulb. *The Journal of Neuroscience*, 27(22):5976–5980.

Braitenberg, V. and Schuz, A. (1991). *Anatomy of the cortex: statistics and geometry*. Springer-Verlag.

Britanova, O., Akopov, S., Lukyanov, S., Gruss, P., and Tarabykin, V. (2005). Novel transcription factor satb2 interacts with matrix attachment region DNA elements in a tissue-specific manner and demonstrates cell-type-dependent expression in the developing mouse CNS. *European Journal of Neuroscience*, 21(3):658–668.

Broca, P. (1861). Remarques sur le siège de la faculté du langage articulé, suivies d'une observation d'aphémie (perte de la parole). *Bulletin de la Société Anatomique*, 6:330–357.

Brodmann, K. (1909). *Vergleichende Lokalisationslehre der Grosshirnrinde: in ihren Prinzipien dargest. auf Grund d. Zellenbaues*. Barth, Leipzig.

Bulfone, A., Smiga, S. M., Shimamura, K., Peterson, A., Puelles, L., and Rubenstein, J. L. (1995). T-brain-1: A homolog of brachyury whose expression defines molecularly distinct domains within the cerebral cortex. *Neuron*, 15(1):63–78.

Butti, C., Sherwood, C. C., Hakeem, A. Y., Allman, J. M., and Hof, P. R. (2009). Total number and volume of von economo neurons in the cerebral cortex of cetaceans. *The Journal of Comparative Neurology*, 515(2):243–259.

Bystron, I., Rakic, P., Molnar, Z., and Blakemore, C. (2006). The first neurons of the human cerebral cortex. *Nat Neurosci*, 9(7):880–886.

Carlo, C. N. and Stevens, C. F. (2013). Structural uniformity of neocortex, revisited. *Proceedings of the National Academy of Sciences*, 110(4):1488–1493.

Caviness, V S, J. and Sidman, R. L. (1973). Time of origin or corresponding cell classes in the cerebral cortex of normal and reeler mutant mice: an autoradiographic analysis. *The Journal of comparative neurology*, 148(2):141–151.

Cepko, C. L., Austin, C. P., Yang, X., Alexiades, M., and Ezzeddine, D. (1996). Cell fate determination in the vertebrate retina. *Proceedings of the National Academy of Sciences*, 93(2):589–595.

Chapouton, P., Skupien, P., Hesl, B., Coolen, M., Moore, J. C., Madelaine, R., Kremmer, E., Faus-Kessler, T., Blader, P., Lawson, N. D., and Bally-Cuif, L. (2010). Notch

activity levels control the balance between quiescence and recruitment of adult neural stem cells. *The Journal of Neuroscience*, 30(23):7961–7974.

Charvet, C. J., Cahalane, D. J., and Finlay, B. L. (2013). Systematic, cross-cortex variation in neuron numbers in rodents and primates. *Cerebral Cortex*.

Chen, B., Schaevitz, L. R., and McConnell, S. K. (2005). Fezl regulates the differentiation and axon targeting of layer 5 subcortical projection neurons in cerebral cortex. *Proceedings of the National Academy of Sciences of the United States of America*, 102(47):17184–17189.

Chenn, A. and Walsh, C. A. (2002). Regulation of cerebral cortical size by control of cell cycle exit in neural precursors. *Science*, 297(5580):365–369.

Cheung, A. F. P., Pollen, A. A., Tavare, A., DeProto, J., and Molnár, Z. (2007). Comparative aspects of cortical neurogenesis in vertebrates. *Journal of Anatomy*, 211(2):164–176.

Chisholm, A. (2001). Cell lineage. In *The Encyclopedia of Genetics*. Academic press edition.

Coogan, T. A. and Van Essen, D. C. (1996). Development of connections within and between areas v1 and v2 of macaque monkeys. *The Journal of comparative neurology*, 372(3):327–342.

Cooper, L. A., Kong, J., Wang, F., Kurc, T., Moreno, C. S., Brat, D. J., and Saltz, J. H. (2011). Morphological signatures and genomic correlates in glioblastoma. pages 1624–1627. IEEE.

Count, E. W. (1947). Brain and body weight in man: their antecedents in growth and evolution: a study in dynamic somatometry. *Annals of the New York Academy of Sciences*, 46(10):993–1122.

Cubelos, B., Sebastián-Serrano, A., Kim, S., Moreno-Ortiz, C., Redondo, J. M., Walsh, C. A., and Nieto, M. (2008). Cux-2 controls the proliferation of neuronal intermediate precursors of the cortical subventricular zone. *Cerebral Cortex*, 18(8):1758–1770.

D'Arcangelo, G. and Curran, T. (1998). Reeler: new tales on an old mutant mouse. *BioEssays*, 20(3):235–244.

Deacon, T. W. (1997). What makes the human brain different? *Annual Review of Anthropology*, 26(1):337–357.

Deaner, R. O., Isler, K., Burkart, J., and van Schaik, C. (2007). Overall brain size, and not encephalization quotient, best predicts cognitive ability across non-human primates. *Brain, Behavior and Evolution*, 70(2):115–124.

DeFelipe, J. (2002). Chapter 17 cortical interneurons: from cajal to 2001. In Efrain C. Azmitia, J. D., editor, *Progress in Brain Research*, volume Volume 136 of *Changing Views of Cajal's Neuron*, pages 215–238. Elsevier.

DeFelipe, J. (2011). The evolution of the brain, the human nature of cortical circuits, and intellectual creativity. *Frontiers in Neuroanatomy*, 5.

DeFelipe, J., Alonso-Nanclares, L., and Arellano, J. I. (2002). Microstructure of the neocortex: Comparative aspects. *Journal of Neurocytology*, 31(3-5):299–316.

Defelipe, J., González-Albo, M. C., Del Río, M. R., and Elston, G. N. (1999). Distribution and patterns of connectivity of interneurons containing calbindin, calretinin, and parvalbumin in visual areas of the occipital and temporal lobes of the macaque monkey. *The Journal of Comparative Neurology*, 412(3):515–526.

Dehay, C., Giroud, P., Berland, M., Killackey, H., and Kennedy, H. (1996). Contribution of thalamic input to the specification of cytoarchitectonic cortical fields in the primate: effects of bilateral enucleation in the fetal monkey on the boundaries, dimensions, and gyrification of striate and extrastriate cortex. *The Journal of comparative neurology*, 367(1):70–89.

Dehay, C., Giroud, P., Berland, M., Smart, I., and Kennedy, H. (1993). Modulation of the cell cycle contributes to the parcellation of the primate visual cortex. *Nature*, 366(6454):464–466.

Dehay, C. and Kennedy, H. (2007). Cell-cycle control and cortical development. *Nature Reviews. Neuroscience*, 8(6):438–450.

Dehay, C., Savatier, P., Cortay, V., and Kennedy, H. (2001). Cell-cycle kinetics of neocortical precursors are influenced by embryonic thalamic axons. *The Journal of Neuroscience*, 21(1):201–214.

Dennerll, T. J., Lamoureux, P., Buxbaum, R. E., and Heidemann, S. R. (1989). The cytomechanics of axonal elongation and retraction. *The Journal of cell biology*, 109(6 Pt 1):3073–3083.

Douglas, R. J. and Martin, K. A. (2004). Neuronal circuits of the neocortex. *Annual Review of Neuroscience*, 27(1):419–451.

Durand, J.-B., Goncalves, P., and Guedon, Y. (2004). Computational methods for hidden markov tree Model;An application to wavelet trees. *IEEE Transactions on Signal Processing*, 52(9):2551–2560.

Elliott, J., Jolicoeur, C., Ramamurthy, V., and Cayouette, M. (2008). Ikaros confers early temporal competence to mouse retinal progenitor cells. *Neuron*, 60(1):26–39.

Englund, C., Fink, A., Lau, C., Pham, D., Daza, R. A. M., Bulfone, A., Kowalczyk, T., and Hevner, R. F. (2005). Pax6, tbr2, and tbr1 are expressed sequentially by radial glia, intermediate progenitor cells, and postmitotic neurons in developing neocortex. *The Journal of Neuroscience*, 25(1):247–251.

Falconer, D. S. (1951). Two new mutants, 'trembler' and 'reeler', with neurological actions in the house mouse (mus musculus l.). *Journal of Genetics*, 50(2):192–205.

Fang, W.-Q., Chen, W.-W., Fu, A. K., and Ip, N. Y. (2013). Axin directs the amplification and differentiation of intermediate progenitors in the developing cerebral cortex. *Neuron*, 79(4):665–679.

Fietz, S. A. and Huttner, W. B. (2011). Cortical progenitor expansion, self-renewal and neurogenesis—a polarized perspective. *Current Opinion in Neurobiology*, 21(1):23–35.

Fietz, S. A., Kelava, I., Vogt, J., Wilsch-Bräuninger, M., Stenzel, D., Fish, J. L., Corbeil, D., Riehn, A., Distler, W., Nitsch, R., and Huttner, W. B. (2010). OSVZ progenitors of human and ferret neocortex are epithelial-like and expand by integrin signaling. *Nature Neuroscience*, 13(6):690–699.

Fietz, S. A., Lachmann, R., Brandl, H., Kircher, M., Samusik, N., Schröder, R., Lakshmanaperumal, N., Henry, I., Vogt, J., Riehn, A., Distler, W., Nitsch, R., Enard, W., Pääbo, S., and Huttner, W. B. (2012). Transcriptomes of germinal zones of human and mouse fetal neocortex suggest a role of extracellular matrix in progenitor self-renewal. *Proceedings of the National Academy of Sciences*, page 201209647.

Fish, J. L., Dehay, C., Kennedy, H., and Huttner, W. B. (2008). Making bigger brains-the evolution of neural-progenitor-cell division. *Journal of Cell Science*, 121(Pt 17):2783–2793.

Fishell, G. and Rudy, B. (2011). Mechanisms of inhibition within the telencephalon: "Where the wild things are". *Annual Review of Neuroscience*, 34(1):535–567.

Fonseca-Azevedo, K. and Herculano-Houzel, S. (2012). Metabolic constraint imposes tradeoff between body size and number of brain neurons in human evolution. *Proceedings of the National Academy of Sciences*, 109(45):18571–18576.

Franco, S. J., Gil-Sanz, C., Martinez-Garay, I., Espinosa, A., Harkins-Perry, S. R., Ramos, C., and Müller, U. (2012). Fate-restricted neural progenitors in the mammalian cerebral cortex. *Science*, 337(6095):746–749.

Franco, S. J., Martinez-Garay, I., Gil-Sanz, C., Harkins-Perry, S. R., and Müller, U. (2011). Reelin regulates cadherin function via Dab1/Rap1 to control neuronal migration and lamination in the neocortex. *Neuron*, 69(3):482–497.

Franco, S. J. and Müller, U. (2013). Shaping our minds: Stem and progenitor cell diversity in the mammalian neocortex. *Neuron*, 77(1):19–34.

Frantz, G. D., Weimann, J. M., Levin, M. E., and McConnell, S. K. (1994). Otx1 and otx2 define layers and regions in developing cerebral cortex and cerebellum. *The Journal of neuroscience: the official journal of the Society for Neuroscience*, 14(10):5725–5740.

Gabbott, P. L. and Bacon, S. J. (1996). Local circuit neurons in the medial prefrontal cortex (areas 24a,b,c, 25 and 32) in the monkey: I. cell morphology and morphometrics. *The Journal of Comparative Neurology*, 364(4):567–608.

Gabi, M., Collins, C. E., Wong, P., Torres, L. B., Kaas, J. H., and Herculano-Houzel, S. (2010). Cellular scaling rules for the brains of an extended number of primate species. *Brain, Behavior and Evolution*, 76(1):32–44.

Gal, J. S., Morozov, Y. M., Ayoub, A. E., Chatterjee, M., Rakic, P., and Haydar, T. F. (2006). Molecular and morphological heterogeneity of neural precursors in the mouse neocortical proliferative zones. *Journal of Neuroscience*, 26(3):1045.

García-Moreno, F., Vasistha, N. A., Trevia, N., Bourne, J. A., and Molnár, Z. (2011). Compartmentalization of cerebral cortical germinal zones in a lissencephalic primate and gyrencephalic rodent. *Cerebral Cortex*, page bhr312.

Georgala, P. A., Manuel, M., and Price, D. J. (2011). The generation of superficial cortical layers is regulated by levels of the transcription factor pax6. *Cerebral Cortex*, 21(1):81–94.

Glaser, T., Jepeal, L., Edwards, J. G., Young, S. R., Favor, J., and Maas, R. L. (1994). PAX6 gene dosage effect in a family with congenital cataracts, aniridia, anophthalmia and central nervous system defects. *Nature Genetics*, 7(4):463–471.

Goffinet, A. M., Daumerie, C., Langerwerf, B., and Pieau, C. (1986). Neurogenesis in reptilian cortical structures: 3H-thymidine autoradiographic analysis. *The Journal of Comparative Neurology*, 243(1):106–116.

Gomes, F. L. A. F., Zhang, G., Carbonell, F., Correa, J. A., Harris, W. A., Simons, B. D., and Cayouette, M. (2010). Reconstruction of rat retinal progenitor cell lineages in vitro reveals a surprising degree of stochasticity in cell fate decisions. *Development*, 138(2):227–235.

Gomez-Lopez, S., Lerner, R. G., and Petritsch, C. (2013). Asymmetric cell division of stem and progenitor cells during homeostasis and cancer. *Cellular and Molecular Life Sciences*, pages 1–23.

Götz, M. and Huttner, W. B. (2005). The cell biology of neurogenesis. *Nature Reviews. Molecular Cell Biology*, 6(10):777–788.

Götz, M., Stoykova, A., and Gruss, P. (1998). Pax6 controls radial glia differentiation in the cerebral cortex. *Neuron*, 21(5):1031–1044.

Hakeem, A. Y., Sherwood, C. C., Bonar, C. J., Butti, C., Hof, P. R., and Allman, J. M. (2009). Von economo neurons in the elephant brain. *The Anatomical Record: Advances in Integrative Anatomy and Evolutionary Biology*, 292(2):242–248.

Hansen, D. V., Lui, J. H., Parker, P. R. L., and Kriegstein, A. R. (2010). Neurogenic radial glia in the outer subventricular zone of human neocortex. *Nature*, 464(7288):554–561.

Hartfuss, E., Galli, R., Heins, N., and Götz, M. (2001). Characterization of CNS precursor subtypes and radial glia. *Developmental Biology*, 229(1):15–30.

Haubensak, W., Attardo, A., Denk, W., and Huttner, W. B. (2004). Neurons arise in the basal neuroepithelium of the early mammalian telencephalon: A major site of neurogenesis. *Proceedings of the National Academy of Sciences of the United States of America*, 101(9):3196–3201.

Haug, H. (1987). Brain sizes, surfaces, and neuronal sizes of the cortex cerebri: A stereological investigation of man and his variability and a comparison with some mammals (primates, whales, marsupials, insectivores, and one elephant). *American Journal of Anatomy*, 180(2):126–142.

Haydar, T. F., Kuan, C.-Y., Flavell, R. A., and Rakic, P. (1999). The role of cell death in regulating the size and shape of the mammalian forebrain. *Cerebral Cortex*, 9(6):621–626.

He, J., Zhang, G., Almeida, A. D., Cayouette, M., Simons, B. D., and Harris, W. A. (2012). How variable clones build an invariant retina. *Neuron*, 75(5):786–798.

Hendry, S. H., Schwark, H. D., Jones, E. G., and Yan, J. (1987). Numbers and proportions of GABA-Immunoreactive neurons in different areas of monkey cerebral cortex. *The Journal of Neuroscience*, 7(5):1503–1519.

Herculano-Houzel, S. (2009). The human brain in numbers: a linearly scaled-up primate brain. *Frontiers in Human Neuroscience*, 3:31.

Herculano-Houzel, S. (2011). Not all brains are made the same: New views on brain scaling in evolution. *Brain, Behavior and Evolution*, 78(1):22–36.

Herculano-Houzel, S., Collins, C. E., Wong, P., and Kaas, J. H. (2007). Cellular scaling rules for primate brains. *Proceedings of the National Academy of Sciences*, 104(9):3562–3567.

Herculano-Houzel, S., Collins, C. E., Wong, P., Kaas, J. H., and Lent, R. (2008). The basic nonuniformity of the cerebral cortex. *Proceedings of the National Academy of Sciences*, 105(34):12593–12598.

Herculano-Houzel, S. and Kaas, J. H. (2011). Gorilla and orangutan brains conform to the primate cellular scaling rules: Implications for human evolution. *Brain, Behavior and Evolution*, 77(1):33–44.

Herculano-Houzel, S. and Lent, R. (2005). Isotropic fractionator: A simple, rapid method for the quantification of total cell and neuron numbers in the brain. *The Journal of Neuroscience*, 25(10):2518–2521.

Herculano-Houzel, S., Mota, B., and Lent, R. (2006). Cellular scaling rules for rodent brains. *Proceedings of the National Academy of Sciences*, 103(32):12138–12143.

Herculano-Houzel, S., Mota, B., Wong, P., and Kaas, J. H. (2010). Connectivity-driven white matter scaling and folding in primate cerebral cortex. *Proceedings of the National Academy of Sciences*.

Hevner, R. F., Shi, L., Justice, N., Hsueh, Y.-P., Sheng, M., Smiga, S., Bulfone, A., Goffinet, A. M., Campagnoni, A. T., and Rubenstein, J. L. (2001). Tbr1 regulates differentiation of the preplate and layer 6. *Neuron*, 29(2):353–366.

Hill, R. S. and Walsh, C. A. (2005). Molecular insights into human brain evolution. *Nature*, 437(7055):64–67.

His, W. (1904). *Die Entwicklung des menschlichen Gehirns während der ersten Monate*. S. Hirzel, Leipzig.

Hochstetter, F. (1919). *Beitraege zur Entwicklungsgeschichte des menschlichen Gehirns*. Wien F. Deuticke.

Horton, J. C. and Adams, D. L. (2005). The cortical column: a structure without a function. *Philosophical Transactions of the Royal Society B: Biological Sciences*, 360(1456):837–862.

Huang, S. (2012). The molecular and mathematical basis of waddington's epigenetic landscape: A framework for post-darwinian biology? *BioEssays*, 34(2):149–157.

Hubel, D. H. and Wiesel, T. N. (1962). Receptive fields, binocular interaction and functional architecture in the cat's visual cortex. *The Journal of physiology*, 160:106–154.

Iacopetti, P., Michelini, M., Stuckmann, I., Oback, B., Aaku-Saraste, E., and Huttner, W. B. (1999). Expression of the antiproliferative gene TIS21 at the onset of neurogenesis identifies single neuroepithelial cells that switch from proliferative to neuron-generating division. *Proceedings of the National Academy of Sciences of the United States of America*, 96(8):4639–4644.

Inta, D., Alfonso, J., von Engelhardt, J., Kreuzberg, M. M., Meyer, A. H., van Hooft, J. A., and Monyer, H. (2008). Neurogenesis and widespread forebrain migration of distinct GABAergic neurons from the postnatal subventricular zone. *Proceedings of the National Academy of Sciences*, 105(52):20994–20999.

Jakovcevski, I., Mayer, N., and Zecevic, N. (2011). Multiple origins of human neocortical interneurons are supported by distinct expression of transcription factors. *Cerebral Cortex*, 21(8):1771–1782.

Javaherian, A. and Kriegstein, A. (2009). A stem cell niche for intermediate progenitor cells of the embryonic cortex. *Cerebral Cortex*, 19(suppl 1):i70.

Johnson, M. B., Kawasawa, Y. I., Mason, C. E., Krsnik, Z., Coppola, G., Bogdanovic, D., Geschwind, D. H., Mane, S. M., State, M. W., and Sestan, N. (2009). Functional and evolutionary insights into human brain development through global transcriptome analysis. *Neuron*, 62(4):494–509.

Jones, E. G. (2000). Microcolumns in the cerebral cortex. *Proceedings of the National Academy of Sciences*, 97(10):5019–5021.

Jones, E. G., DeFelipe, J., Hendry, S. H., and Maggio, J. E. (1988). A study of tachykinin-immunoreactive neurons in monkey cerebral cortex. *The Journal of Neuroscience: The Official Journal of the Society for Neuroscience*, 8(4):1206–1224.

Jones, E. G. and Rakic, P. (2010). Radial columns in cortical architecture: It is the composition that counts. *Cerebral Cortex*, 20(10):2261–2264.

Kandel, E. R., Schwartz, J. H., and Jessell, T. M. (2000). *Principles of neural science*. McGraw-Hill, Health Professions Division.

Kauffman, S. A. (1993). *The origins of order: self-organization and selection in evolution*. Oxford University Press, New York.

Kelava, I., Lewitus, E., and Huttner, W. B. (2013). The secondary loss of gyrencephaly as an example of evolutionary phenotypical reversal. *Frontiers in Neuroanatomy*, 7:16.

Kelava, I., Reillo, I., Murayama, A. Y., Kalinka, A. T., Stenzel, D., Tomancak, P., Matsuzaki, F., Lebrand, C., Sasaki, E., Schwamborn, J. C., Okano, H., Huttner, W. B., and Borrell, V. (2011). Abundant occurrence of basal radial glia in the subventricular zone of embryonic neocortex of a lissencephalic primate, the common marmoset callithrix jacchus. *Cerebral Cortex*, page bhr301.

Kennedy, H. and Dehay, C. (1993). Cortical specification of mice and men. *Cerebral cortex (New York, N.Y.: 1991)*, 3(3):171–186.

Kohwi, M., Petryniak, M. A., Long, J. E., Ekker, M., Obata, K., Yanagawa, Y., Rubenstein, J. L. R., and Alvarez-Buylla, A. (2007). A subpopulation of olfactory bulb GABAergic interneurons is derived from emx1- and dlx5/6-expressing progenitors. *The Journal of Neuroscience*, 27(26):6878–6891.

Kornack, D. R. and Rakic, P. (1995). Radial and horizontal deployment of clonally related cells in the primate neocortex: Relationship to distinct mitotic lineages. *Neuron*, 15(2):311–321.

Kornack, D. R. and Rakic, P. (1998). Changes in cell-cycle kinetics during the development and evolution of primate neocortex. *Proceedings of the National Academy of Sciences of the United States of America*, 95(3):1242.

Kowalczyk, T., Pontious, A., Englund, C., Daza, R. A. M., Bedogni, F., Hodge, R., Attardo, A., Bell, C., Huttner, W. B., and Hevner, R. F. (2009). Intermediate neuronal progenitors (basal progenitors) produce Pyramidal–Projection neurons for all layers of cerebral cortex. *Cerebral Cortex*, 19(10):2439 –2450.

Kriegstein, A., Noctor, S., and Martínez-Cerdeño, V. (2006). Patterns of neural stem and progenitor cell division may underlie evolutionary cortical expansion. *Nature Reviews Neuroscience*, 7(11):883–890.

Krubitzer, L. (2007). The magnificent compromise: Cortical field evolution in mammals. *Neuron*, 56(2):201–208.

Krubitzer, L., Huffman, K., and Molnar, Z. (1998). Constructing the neocortex: influences on the pattern of organization in mammals. In *Brain and mind: evolutionary perspectives*, pages 19–34. Human Frontier Science Program, Strasbourg, gazzaniga MS, altman j edition.

Kwan, K. Y., Šestan, N., and Anton, E. S. (2012). Transcriptional co-regulation of neuronal migration and laminar identity in the neocortex. *Development*, 139(9):1535–1546.

LaMonica, B. E., Lui, J. H., Hansen, D. V., and Kriegstein, A. R. (2013). Mitotic spindle orientation predicts outer radial glial cell generation in human neocortex. *Nature Communications*, 4:1665.

Lamoureux, P., Buxbaum, R. E., and Heidemann, S. R. (1989). Direct evidence that growth cones pull. *Nature*, 340(6229):159–162.

Lange, C., Huttner, W. B., and Calegari, F. (2009). Cdk4/CyclinD1 overexpression in neural stem cells shortens g1, delays neurogenesis, and promotes the generation and expansion of basal progenitors. *Cell Stem Cell*, 5(3):320–331.

Le Gros Clark, W. E. L. G. and Medawar, P. B. (1945). *Essays on growth and form*. Clarendon Press.

Lee, M. and Vasioukhin, V. (2008). Cell polarity and cancer – cell and tissue polarity as a non-canonical tumor suppressor. *Journal of Cell Science*, 121(8):1141–1150.

Letinic, K., Zoncu, R., and Rakic, P. (2002). Origin of GABAergic neurons in the human neocortex. *Nature*, 417(6889):645–649.

Levitt, P., Cooper, M. L., and Rakic, P. (1981). Coexistence of neuronal and glial precursor cells in the cerebral ventricular zone of the fetal monkey: an ultrastructural

immunoperoxidase analysis. *The Journal of neuroscience: the official journal of the Society for Neuroscience*, 1(1):27–39.

Levitt, P. and Rakic, P. (1980). Immunoperoxidase localization of glial fibrillary acidic protein in radial glial cells and astrocytes of the developing rhesus monkey brain. *The Journal of comparative neurology*, 193(3):815–840.

Lorente de Nó, R. (1938). The cerebral cortex: architecture, intracortical connections and motor projections. In Fulton, J., editor, *Physiology of the nervous system*, pages 291–301. Oxford University Press.

Lui, J. H., Hansen, D. V., and Kriegstein, A. R. (2011). Development and evolution of the human neocortex. *Cell*, 146(1):18–36.

Lukaszewicz, A., Savatier, P., Cortay, V., Giroud, P., Huissoud, C., Berland, M., Kennedy, H., and Dehay, C. (2005). G1 phase regulation, area-specific cell cycle control, and cytoarchitectonics in the primate cortex. *Neuron*, 47(3):353–364.

Makalowski, W., Zhang, J., and Boguski, M. S. (1996). Comparative analysis of 1196 orthologous mouse and human full-length mRNA and protein sequences. *Genome Research*, 6(9):846–857.

Malatesta, P., Hack, M. A., Hartfuss, E., Kettenmann, H., Klinkert, W., Kirchhoff, F., and Götz, M. (2003). Neuronal or glial progeny: Regional differences in radial glia fate. *Neuron*, 37(5):751–764.

Malatesta, P., Hartfuss, E., and Götz, M. (2000). Isolation of radial glial cells by fluorescent-activated cell sorting reveals a neuronal lineage. *Development*, 127(24):5253–5263.

Marin, O. and Rubenstein, J. L. R. (2001). A long, remarkable journey: Tangential migration in the telencephalon. *Nature Reviews Neuroscience*, 2(11):780–790.

Marin-Padilla, M. (1992). Ontogenesis of the pyramidal cell of the mammalian neocortex and developmental cytoarchitectonics: a unifying theory. *The Journal of comparative neurology*, 321(2):223–240.

Martinez-Cerdeno, V., Cunningham, C. L., Camacho, J., Antczak, J. L., Prakash, A. N., Cziep, M. E., Walker, A. I., and Noctor, S. C. (2012). Comparative analysis of the subventricular zone in rat, ferret and macaque: Evidence for an outer subventricular zone in rodents. *PLoS ONE*, 7(1):e30178.

Martinez-Cerdeno, V., Noctor, S. C., and Kriegstein, A. R. (2006). The role of intermediate progenitor cells in the evolutionary expansion of the cerebral cortex. *Cerebral Cortex*, 16(Supplement 1):i152.

McCarthy, M., Turnbull, D. H., Walsh, C. A., and Fishell, G. (2001). Telencephalic neural progenitors appear to be restricted to regional and glial fates before the onset of neurogenesis. *The Journal of Neuroscience*, 21(17):6772–6781.

McConnell, S. K. and Kaznowski, C. E. (1991). Cell cycle dependence of laminar determination in developing neocortex. *Science*, 254(5029):282.

Métin, C., Baudoin, J.-P., Rakić, S., and Parnavelas, J. G. (2006). Cell and molecular mechanisms involved in the migration of cortical interneurons. *European Journal of Neuroscience*, 23(4):894–900.

Meyer, G. (2010). Building a human cortex: the evolutionary differentiation of cajal-retzius cells and the cortical hem. *Journal of Anatomy*, 217(4):334–343.

Meyer, G., Schaaps, J., Moreau, L., and Goffinet, A. (2000). Embryonic and early fetal development of the human neocortex. *The Journal of Neuroscience*, 20(5):1858–1868.

Meyer, H. S., Wimmer, V. C., Oberlaender, M., Kock, C. P. J. d., Sakmann, B., and Helmstaedter, M. (2010). Number and laminar distribution of neurons in a thalamocortical projection column of rat vibrissal cortex. *Cerebral Cortex*, 20(10):2277–2286.

Mi, D., Carr, C. B., Georgala, P. A., Huang, Y.-T., Manuel, M. N., Jeanes, E., Niisato, E., Sansom, S. N., Livesey, F. J., Theil, T., Hasenpusch-Theil, K., Simpson, T. I., Mason, J. O., and Price, D. J. (2013). Pax6 exerts regional control of cortical progenitor proliferation via direct repression of cdk6 and hypophosphorylation of pRb. *Neuron*, 78(2):269–284.

Miyata, T., Kawaguchi, A., Okano, H., and Ogawa, M. (2001). Asymmetric inheritance of radial glial fibers by cortical neurons. *Neuron*, 31(5):727–741.

Miyata, T., Kawaguchi, A., Saito, K., Kawano, M., Muto, T., and Ogawa, M. (2004). Asymmetric production of surface-dividing and non-surface-dividing cortical progenitor cells. *Development*, 131(13):3133–3145.

Mo, Z., Moore, A. R., Filipovic, R., Ogawa, Y., Kazuhiro, I., Antic, S. D., and Zecevic, N. (2007). Human cortical neurons originate from radial glia and neuron-restricted progenitors. *The Journal of Neuroscience: The Official Journal of the Society for Neuroscience*, 27(15):4132–4145.

Mo, Z. and Zecevic, N. (2009). Human fetal radial glia cells generate oligodendrocytes in vitro. *Glia*, 57(5):490–498.

Molyneaux, B. J., Arlotta, P., Hirata, T., Hibi, M., and Macklis, J. D. (2005). Fezl is required for the birth and specification of corticospinal motor neurons. *Neuron*, 47(6):817–831.

Molyneaux, B. J., Arlotta, P., Menezes, J. R., and Macklis, J. D. (2007). Neuronal subtype specification in the cerebral cortex. *Nature Reviews Neuroscience*, 8(6):427–437.

Moon, S. and Hwang, J.-N. (1997). Robust speech recognition based on joint model and feature space optimization of hidden markov models. *IEEE Transactions on Neural Networks*, 8(2):194–204.

Mota, B. and Herculano-Houzel, S. (2012). How the cortex gets its folds: an inside-out, connectivity-driven model for the scaling of mammalian cortical folding. *Frontiers in Neuroanatomy*, 6:3.

Mountcastle, V. B. (1957). Modality and topographic properties of single neurons of cat's somatic sensory cortex. *Journal of neurophysiology*, 20(4):408–434.

Nadarajah, B., Brunstrom, J. E., Grutzendler, J., Wong, R. O. L., and Pearlman, A. L. (2001). Two modes of radial migration in early development of the cerebral cortex. *Nature Neuroscience*, 4(2):143–150.

Nelson, B. R., Hodge, R. D., Bedogni, F., and Hevner, R. F. (2013). Dynamic interactions between intermediate neurogenic progenitors and radial glia in embryonic mouse neocortex: Potential role in dll1-notch signaling. *The Journal of Neuroscience*, 33(21):9122–9139.

Nelson, S. B. (2002). Cortical microcircuits: Diverse or canonical? *Neuron*, 36(1):19–27.

Nieto, M., Monuki, E. S., Tang, H., Imitola, J., Haubst, N., Khoury, S. J., Cunningham, J., Gotz, M., and Walsh, C. A. (2004). Expression of cux-1 and cux-2 in the subventricular zone and upper layers II–IV of the cerebral cortex. *The Journal of Comparative Neurology*, 479(2):168–180.

Noctor, S. C., Flint, A. C., Weissman, T. A., Dammerman, R. S., and Kriegstein, A. R. (2001). Neurons derived from radial glial cells establish radial units in neocortex. *Nature*, 409(6821):714–720.

Noctor, S. C., Martinez-Cerdeno, V., Ivic, L., and Kriegstein, A. R. (2004). Cortical neurons arise in symmetric and asymmetric division zones and migrate through specific phases. *Nat Neurosci*, 7(2):136–144.

O'Leary, D. D. (1989). Do cortical areas emerge from a protocortex? *Trends in Neurosciences*, 12(10):400–406.

O'Leary, D. D. and Nakagawa, Y. (2002). Patterning centers, regulatory genes and extrinsic mechanisms controlling arealization of the neocortex. *Current Opinion in Neurobiology*, 12(1):14–25.

Panatier, A., Vallée, J., Haber, M., Murai, K. K., Lacaille, J.-C., and Robitaille, R. (2011). Astrocytes are endogenous regulators of basal transmission at central synapses. *Cell*, 146(5):785–798.

Petanjek, Z., Berger, B., and Esclapez, M. (2008). Origins of cortical GABAergic neurons in the cynomolgus monkey. *Cerebral Cortex*, 19(2):249–262.

Petriv, O. I., Kuchenbauer, F., Delaney, A. D., Lecault, V., White, A., Kent, D., Marmolejo, L., Heuser, M., Berg, T., Copley, M., Ruschmann, J., Sekulovic, S., Benz, C., Kuroda, E., Ho, V., Antignano, F., Halim, T., Giambra, V., Krystal, G., Takei, C. J. F., Weng, A. P., Piret, J., Eaves, C., Marra, M. A., Humphries, R. K., and Hansen, C. L. (2010). Comprehensive microRNA expression profiling of the hematopoietic hierarchy. *Proceedings of the National Academy of Sciences*, 107(35):15443–15448.

Pilaz, L.-J., Patti, D., Marcy, G., Ollier, E., Pfister, S., Douglas, R. J., Betizeau, M., Gautier, E., Cortay, V., Doerflinger, N., Kennedy, H., and Dehay, C. (2009). Forced

g1-phase reduction alters mode of division, neuron number, and laminar phenotype in the cerebral cortex. *Proceedings of the National Academy of Sciences of the United States of America*, 106(51):21924–21929.

Pillay, P. and Manger, P. R. (2007). Order-specific quantitative patterns of cortical gyrification. *European Journal of Neuroscience*, 25(9):2705–2712.

Pilz, G.-A., Shitamukai, A., Reillo, I., Pacary, E., Schwausch, J., Stahl, R., Ninkovic, J., Snippert, H. J., Clevers, H., Godinho, L., Guillemot, F., Borrell, V., Matsuzaki, F., and Götz, M. (2013). Amplification of progenitors in the mammalian telencephalon includes a new radial glial cell type. *Nature Communications*, 4.

Pinto, L., Mader, M. T., Irmler, M., Gentilini, M., Santoni, F., Drechsel, D., Blum, R., Stahl, R., Bulfone, A., Malatesta, P., Beckers, J., and Götz, M. (2008). Prospective isolation of functionally distinct radial glial subtypes—Lineage and transcriptome analysis. *Molecular and Cellular Neuroscience*, 38(1):15–42.

Plessy, C., Desbois, L., Fujii, T., and Carninci, P. (2013). Population transcriptomics with single-cell resolution: A new field made possible by microfluidics. *BioEssays*, 35(2):131–140.

Polleux, F., Dehay, C., and Kennedy, H. (1997). The timetable of laminar neurogenesis contributes to the specification of cortical areas in mouse isocortex. *The Journal of Comparative Neurology*, 385(1):95–116.

Pontious, A., Kowalczyk, T., Englund, C., and Hevner, R. F. (2008). Role of intermediate progenitor cells in cerebral cortex development. *Developmental Neuroscience*, 30(1-3):24–32.

Price, D. J. and Willshaw, D. J. (2000). *Mechanisms of Cortical Development*. Oxford University Press.

Puzzolo, E. and Mallamaci, A. (2010). Cortico-cerebral histogenesis in the opossum monodelphis domestica: generation of a hexalaminar neocortex in the absence of a basal proliferative compartment. *Neural Development*, 5(1):8.

Quinn, J. C., Molinek, M., Martynoga, B. S., Zaki, P. A., Faedo, A., Bulfone, A., Hevner, R. F., West, J. D., and Price, D. J. (2007). Pax6 controls cerebral cortical cell number by

regulating exit from the cell cycle and specifies cortical cell identity by a cell autonomous mechanism. *Developmental Biology*, 302(1):50–65.

Rakic, P. (1974). Neurons in rhesus monkey visual cortex: Systematic relation between time of origin and eventual disposition. *Science*, 183(4123):425 –427.

Rakic, P. (1988). Specification of cerebral cortical areas. *Science (New York, N.Y.)*, 241(4862):170–176.

Rakic, P. (1995). A small step for the cell, a giant leap for mankind: a hypothesis of neocortical expansion during evolution. *Trends in Neurosciences*, 18(9):383–388.

Rakic, P. (2008). Confusing cortical columns. *Proceedings of the National Academy of Sciences*, 105(34):12099–12100.

Rakic, P. (2009). Evolution of the neocortex: a perspective from developmental biology. *Nature Reviews Neuroscience*, 10(10):724–735.

Rakic, S. and Zecevic, N. (2003). Early oligodendrocyte progenitor cells in the human fetal telencephalon. *Glia*, 41(2):117–127.

Reillo, I. and Borrell, V. (2011). Germinal zones in the developing cerebral cortex of ferret: Ontogeny, cell cycle kinetics, and diversity of progenitors. *Cerebral Cortex*.

Reillo, I., Romero, C. d. J., García-Cabezas, M. Á., and Borrell, V. (2011). A role for intermediate radial glia in the tangential expansion of the mammalian cerebral cortex. *Cerebral Cortex*, 21(7):1674–1694.

Richman, D. P., Stewart, R. M., Hutchinson, J. W., and Caviness, V S, J. (1975). Mechanical model of brain convolutional development. *Science (New York, N.Y.)*, 189(4196):18–21.

Riquelme, P. A., Drapeau, E., and Doetsch, F. (2008). Brain micro-ecologies: neural stem cell niches in the adult mammalian brain. *Philosophical Transactions of the Royal Society B: Biological Sciences*, 363(1489):123–137.

Rockel, A. J., Hiorns, R. W., and Powell, T. P. (1980). The basic uniformity in structure of the neocortex. *Brain: a journal of neurology*, 103(2):221–244.

Ross, M. E. and Walsh, C. A. (2001). Human brain malformations and their lessons for neuronal migration. *Annual Review of Neuroscience*, 24(1):1041–1070.

Roth, G. and Dicke, U. (2005). Evolution of the brain and intelligence. *Trends in Cognitive Sciences*, 9(5):250–257.

Roy, K., Kuznicki, K., Wu, Q., Sun, Z., Bock, D., Schutz, G., Vranich, N., and Monaghan, A. P. (2004). The tlx gene regulates the timing of neurogenesis in the cortex. *The Journal of Neuroscience*, 24(38):8333–8345.

Russ, A. P., Wattler, S., Colledge, W. H., Aparicio, S. A. J. R., Carlton, M. B. L., Pearce, J. J., Barton, S. C., Surani, M. A., Ryan, K., Nehls, M. C., Wilson, V., and Evans, M. J. (2000). Eomesodermin is required for mouse trophoblast development and mesoderm formation. *Nature*, 404(6773):95–99.

Sahara, S. and O'Leary, D. D. (2009). Fgf10 regulates transition period of cortical stem cell differentiation to radial glia controlling generation of neurons and basal progenitors. *Neuron*, 63(1):48–62.

Sarko, D. (2009). Cellular scaling rules of insectivore brains. *Frontiers in Neuroanatomy*, 3.

Sauer, F. C. (1935). Mitosis in the neural tube. *The Journal of Comparative Neurology*, 62(2):377–405.

Sawada, K., Sun, X.-Z., Fukunishi, K., Kashima, M., Saito, S., Sakata-Haga, H., Sukamoto, T., Aoki, I., and Fukui, Y. (2010). Ontogenetic pattern of gyrification in fetuses of cynomolgus monkeys. *Neuroscience*, 167(3):735–740.

Schuurmans, C., Armant, O., Nieto, M., Stenman, J. M., Britz, O., Klenin, N., Brown, C., Langevin, L.-M., Seibt, J., Tang, H., Cunningham, J. M., Dyck, R., Walsh, C., Campbell, K., Polleux, F., and Guillemot, F. (2004). Sequential phases of cortical specification involve neurogenin-dependent and -independent pathways. *The EMBO Journal*, 23(14):2892–2902.

Schüz, A. and Palm, G. (1989). Density of neurons and synapses in the cerebral cortex of the mouse. *The Journal of Comparative Neurology*, 286(4):442–455.

Schwartz, M. L., Rakic, P., and Goldman-Rakic, P. S. (1991). Early phenotype expression of cortical neurons: evidence that a subclass of migrating neurons have callosal axons. *Proceedings of the National Academy of Sciences of the United States of America*, 88(4):1354.

Schwitalla, S., Fingerle, A. A., Cammareri, P., Nebelsiek, T., Göktuna, S. I., Ziegler, P. K., Canli, O., Heijmans, J., Huels, D. J., Moreaux, G., Rupec, R. A., Gerhard, M., Schmid, R., Barker, N., Clevers, H., Lang, R., Neumann, J., Kirchner, T., Taketo, M. M., van den Brink, G. R., Sansom, O. J., Arkan, M. C., and Greten, F. R. (2013). Intestinal tumorigenesis initiated by dedifferentiation and acquisition of stem-cell-like properties. *Cell*, 152(1-2):25–38.

Semendeferi, K., Lu, A., Schenker, N., and Damasio, H. (2002). Humans and great apes share a large frontal cortex. *Nature Neuroscience*, 5(3):272–276.

Sessa, A., Mao, C.-a., Hadjantonakis, A.-K., Klein, W. H., and Broccoli, V. (2008). Tbr2 directs conversion of radial glia into basal precursors and guides neuronal amplification by indirect neurogenesis in the developing neocortex. *Neuron*, 60(1):56–69.

Shen, Q., Goderie, S. K., Jin, L., Karanth, N., Sun, Y., Abramova, N., Vincent, P., Pumiglia, K., and Temple, S. (2004). Endothelial cells stimulate self-renewal and expand neurogenesis of neural stem cells. *Science*, 304(5675):1338–1340.

Shen, Q., Wang, Y., Dimos, J. T., Fasano, C. A., Phoenix, T. N., Lemischka, I. R., Ivanova, N. B., Stifani, S., Morrisey, E. E., and Temple, S. (2006). The timing of cortical neurogenesis is encoded within lineages of individual progenitor cells. *Nat Neurosci*, 9(6):743–751.

Sherwood, C. C., Stimpson, C. D., Raghanti, M. A., Wildman, D. E., Uddin, M., Grossman, L. I., Goodman, M., Redmond, J. C., Bonar, C. J., Erwin, J. M., and Hof, P. R. (2006). Evolution of increased glia–neuron ratios in the human frontal cortex. *Proceedings of the National Academy of Sciences*, 103(37):13606–13611.

Shimojo, H., Ohtsuka, T., and Kageyama, R. (2008). Oscillations in notch signaling regulate maintenance of neural progenitors. *Neuron*, 58(1):52–64.

Shitamukai, A., Konno, D., and Matsuzaki, F. (2011). Oblique radial glial divisions in the developing mouse neocortex induce self-renewing progenitors outside the germinal zone that resemble primate outer subventricular zone progenitors. *The Journal of Neuroscience*, 31(10):3683 –3695.

Siegenthaler, J. A., Ashique, A. M., Zarbalis, K., Patterson, K. P., Hecht, J. H., Kane, M. A., Folias, A. E., Choe, Y., May, S. R., Kume, T., Napoli, J. L., Peterson, A. S., and Pleasure, S. J. (2009). Retinoic acid from the meninges regulates cortical neuron generation. *Cell*, 139(3):597–609.

Skoglund, T., Pascher, R., and Berthold, C.-H. (1996). Heterogeneity in the columnar number of neurons in different neocortical areas in the rat. *Neuroscience Letters*, 208(2):97–100.

Slater, J., Landman, K., Hughes, B., Shen, Q., and Temple, S. (2009). Cell lineage tree models of neurogenesis. *Journal of Theoretical Biology*, 256(2):164–179.

Smart, I. H. (1973). Proliferative characteristics of the ependymal layer during the early development of the mouse neocortex: a pilot study based on recording the number, location and plane of cleavage of mitotic figures. *Journal of Anatomy*, 116(Pt 1):67.

Smart, I. H. M., Dehay, C., Giroud, P., Berland, M., and Kennedy, H. (2002). Unique morphological features of the proliferative zones and postmitotic compartments of the neural epithelium giving rise to striate and extrastriate cortex in the monkey. *Cerebral Cortex (New York, N.Y.: 1991)*, 12(1):37–53.

Spindler, S. R. and Hartenstein, V. (2010). The drosophila neural lineages: a model system to study brain development and circuitry. *Development Genes and Evolution*, 220(1-2):1–10.

Stahl, R., Walcher, T., De Juan Romero, C., Pilz, G. A., Cappello, S., Irmler, M., Sanz-Aquela, J. M., Beckers, J., Blum, R., Borrell, V., and Götz, M. (2013). Trnp1 regulates expansion and folding of the mammalian cerebral cortex by control of radial glial fate. *Cell*, 153(3):535–549.

Stancik, E. K., Navarro-Quiroga, I., Sellke, R., and Haydar, T. F. (2010). Heterogeneity in

ventricular zone neural precursors contributes to neuronal fate diversity in the postnatal neocortex. *The Journal of Neuroscience*, 30(20):7028–7036.

Stevens, C. F. (2001). An evolutionary scaling law for the primate visual system and its basis in cortical function. *Nature*, 411(6834):193–195.

Stocum, D. L. (2004). Amphibian regeneration and stem cells. In Heber-Katz, E., editor, *Regeneration: Stem Cells and Beyond*, number 280 in Current Topics in Microbiology and Immunology, pages 1–70. Springer Berlin Heidelberg.

Stubbs, D., DeProto, J., Nie, K., Englund, C., Mahmud, I., Hevner, R., and Molnár, Z. (2009). Neurovascular congruence during cerebral cortical development. *Cerebral Cortex*, 19(suppl 1):i32–i41.

Sulston, J. (1988). Cell lineage. In *The Nematode Caenorhabditis elegans*. Wood W.B, cold spring harbor press edition.

Sur, M. and Rubenstein, J. L. R. (2005). Patterning and plasticity of the cerebral cortex. *Science*, 310(5749):805–810.

Tabata, H., Kanatani, S., and Nakajima, K. (2009). Differences of migratory behavior between direct progeny of apical progenitors and basal progenitors in the developing cerebral cortex. *Cerebral Cortex*, 19(9):2092.

Takahashi, T., Nowakowski, R. S., and Caviness Jr, V. S. (1993). Cell cycle parameters and patterns of nuclear movement in the neocortical proliferative zone of the fetal mouse. *Journal of Neuroscience*, 13(2):820.

Tamamaki, N., Fujimori, K. E., and Takauji, R. (1997). Origin and route of tangentially migrating neurons in the developing neocortical intermediate zone. *The Journal of Neuroscience*, 17(21):8313–8323.

Teissier, A., Waclaw, R. R., Griveau, A., Campbell, K., and Pierani, A. (2011). Tangentially migrating transient glutamatergic neurons control neurogenesis and maintenance of cerebral cortical progenitor pools. *Cerebral Cortex*, page bhr122.

Toro, R. and Burnod, Y. (2005). A morphogenetic model for the development of cortical convolutions. *Cerebral Cortex*, 15(12):1900 –1913.

Tuoc, T. C., Boretius, S., Sansom, S. N., Pitulescu, M.-E., Frahm, J., Livesey, F. J., and Stoykova, A. (2013). Chromatin regulation by BAF170 controls cerebral cortical size and thickness. *Developmental Cell*, 25(3):256–269.

Tyler, W. A. and Haydar, T. F. (2013). Multiplex genetic fate mapping reveals a novel route of neocortical neurogenesis, which is altered in the Ts65Dn mouse model of down syndrome. *The Journal of Neuroscience*, 33(12):5106–5119.

Valverde, F., De Carlos, J. A., and López-Mascaraque, L. (1995). Time of origin and early fate of preplate cells in the cerebral cortex of the rat. *Cerebral cortex (New York, N.Y.: 1991)*, 5(6):483–493.

Van der Loos, H. and Woolsey, T. A. (1973). Somatosensory cortex: structural alterations following early injury to sense organs. *Science (New York, N.Y.)*, 179(4071):395–398.

Van Essen, D. C. (1997). A tension-based theory of morphogenesis and compact wiring in the central nervous system. *Nature*, 385(6614):313–318.

Ventura-Antunes, L., Mota, B., and Herculano-Houzel, S. (2013). Different scaling of white matter volume, cortical connectivity, and gyrification across rodent and primate brains. *Frontiers in Neuroanatomy*, 7:3.

von Economo, C. and Koskinas, G. (1929). *The cytoarchitectonics of the human cerebral cortex*. London, oxford university press edition.

Waddington, C. H. (1957). *The Strategy of the Genes*. George Allen & Unwin, first edition.

Wang, J., Xu, L., Wang, E., and Huang, S. (2010). The potential landscape of genetic circuits imposes the arrow of time in stem cell differentiation. *Biophysical Journal*, 99(1):29–39.

Wang, X., Tsai, J.-W., LaMonica, B., and Kriegstein, A. R. (2011). A new subtype of progenitor cell in the mouse embryonic neocortex. *Nat Neurosci*, 14(5):555–561.

Warren, N., Caric, D., Pratt, T., Clausen, J. A., Asavaritikrai, P., Mason, J. O., Hill, R. E., and Price, D. J. (1999). The transcription factor, pax6, is required for cell

proliferation and differentiation in the developing cerebral cortex. *Cerebral Cortex*, 9(6):627–635.

Welker, W. (1990). Why does cerebral cortex fissure and fold? In Jones, E. G., Peters, A., Jones, E. G., and Peters, A., editors, *Cerebral Cortex*, volume 8B, pages 3–136. Springer US, Boston, MA.

Williams, B. P. and Price, J. (1995). Evidence for multiple precursor cell types in the embryonic rat cerebral cortex. *Neuron*, 14(6):1181–1188.

Wimmer, V. C., Bruno, R. M., Kock, C. P. J. d., Kuner, T., and Sakmann, B. (2010). Dimensions of a projection column and architecture of VPM and POm axons in rat vibrissal cortex. *Cerebral Cortex*, 20(10):2265–2276.

Wonders, C. P. and Anderson, S. A. (2006). The origin and specification of cortical interneurons. *Nature Reviews Neuroscience*, 7(9):687–696.

Woolsey, T. A. and Wann, J. R. (1976). Areal changes in mouse cortical barrels following vibrissal damage at different postnatal ages. *The Journal of comparative neurology*, 170(1):53–66.

Workman, A. D., Charvet, C. J., Clancy, B., Darlington, R. B., and Finlay, B. L. (2013). Modeling transformations of neurodevelopmental sequences across mammalian species. *The Journal of Neuroscience*, 33(17):7368–7383.

Wu, S., Esumi, S., Watanabe, K., Chen, J., Nakamura, K. C., Nakamura, K., Kometani, K., Minato, N., Yanagawa, Y., Akashi, K., Sakimura, K., Kaneko, T., and Tamamaki, N. (2011). Tangential migration and proliferation of intermediate progenitors of GABAergic neurons in the mouse telencephalon. *Development*, page dev.063032.

Wu, S.-X., Goebbels, S., Nakamura, K., Nakamura, K., Kometani, K., Minato, N., Kaneko, T., Nave, K.-A., and Tamamaki, N. (2005). Pyramidal neurons of upper cortical layers generated by NEX-positive progenitor cells in the subventricular zone. *Proceedings of the National Academy of Sciences of the United States of America*, 102(47):17172 –17177.

Yanez, I. B., Muñoz, A., Contreras, J., Gonzalez, J., Rodriguez-Veiga, E., and DeFelipe, J. (2005). Double bouquet cell in the human cerebral cortex and a comparison with other mammals. *The Journal of Comparative Neurology*, 486(4):344–360.

Yoon, K.-J., Koo, B.-K., Im, S.-K., Jeong, H.-W., Ghim, J., Kwon, M.-c., Moon, J.-S., Miyata, T., and Kong, Y.-Y. (2008). Mind bomb 1-expressing intermediate progenitors generate notch signaling to maintain radial glial cells. *Neuron*, 58(4):519–531.

Yu, X. and Zecevic, N. (2011). Dorsal radial glial cells have the potential to generate cortical interneurons in human but not in mouse brain. *J. Neurosci.*, 31(7):2413–2420.

Zecevic, N., Chen, Y., and Filipovic, R. (2005). Contributions of cortical subventricular zone to the development of the human cerebral cortex. *The Journal of comparative neurology*, 491(2):109–122.

Zecevic, N., Hu, F., and Jakovcevski, I. (2011). Interneurons in the developing human neocortex. *Developmental Neurobiology*, 71(1):18–33.

Zernicka-Goetz, M. and Huang, S. (2010). Stochasticity versus determinism in development: a false dichotomy? *Nat Rev Genet*, 11(11):743–744.

Zhang, H. (2004). The optimality of naive bayes. AAAI Press.

Zhang, H. and Miller, R. H. (1996). Density-dependent feedback inhibition of oligodendrocyte precursor expansion. *The Journal of neuroscience: the official journal of the Society for Neuroscience*, 16(21):6886–6895.

Zhang, K. and Sejnowski, T. J. (2000). A universal scaling law between gray matter and white matter of cerebral cortex. *Proceedings of the National Academy of Sciences*, 97(10):5621–5626.

Zimmer, C., Tiveron, M.-C., Bodmer, R., and Cremer, H. (2004). Dynamics of cux2 expression suggests that an early pool of SVZ precursors is fated to become upper cortical layer neurons. *Cerebral Cortex*, 14(12):1408–1420.

Appendix A

Abbreviation list

AP: apical progenitor
BP : basal progenitor
BrdU: bromodeoxyuridine
bRG: basal radial glial-like cell
bRG-*apical-P*: bRG apical process cell
bRG-*basal-P*: bRG basal process cell
bRG-*both-P*: bRG both process cell
CNS: central nervous system
CP: cortical plate
DNA: deoxyribonucleic acid
E: embryonic day
EGFP: enhanced green fluorescent protein
EM: expectation maximization
GE: ganglionic eminence
GFAP: glial fibrillary acidic protein
GRN: gene regulatory network
GW: gestational week
GZ: germinal zones
IFL: inner fiber layer
IP: intermediate progenitor
ISVZ: inner subventricular zone
IZ: intermediate zone
KO: knock out
LL: lower layers
MZ: marginal zone
OFL: outer fiber layer
OSVZ: outer subventricular zone
PP: preplate
RGC: radial glial cell
SAP: subapical progenitor
SNP: short neural precursor
SP: subplate
SVZ: subventrcular zone
Tc: cell cycle duration
Ts: S phase duration
UL: upper layers
VZ: ventricular zone

Appendix B

Correspondence of developmental stages in mice, macaque monkeys and humans

Neuronal layer	Mouse	Macaque monkey	Human
SP	9.8	41	5.7
layer 6	11 / 13 / 16	45 / 56 / 74	6.9 / 9.4 / 14.4
layer 5	13 / 14 / 15	56 / 65 / 71	9.4 / 12 / 13.7
layer 4	14 / 16 / 17	65 / 74 / 82	11.9 / 14.4 / 17
layer 2/3	16 / 18 / 22	78 / 89 / 112	15.7 / 19.1 / 27.3

Table B.1. Correspondence of the timing of cortical neuronal layer formation in mice, macaque monkeys and humans. Stages are expressed in embryonic days for mice and monkeys and gestational weeks for humans (start / peak / end of layer production). Stages estimated for the developing cortex using (Workman et al., 2013).

Appendix C

Notch model in neural stem cells

Student project developed at the Computational Cell Biology summer school, Cold Spring Harbor laboratory, summer 2012.

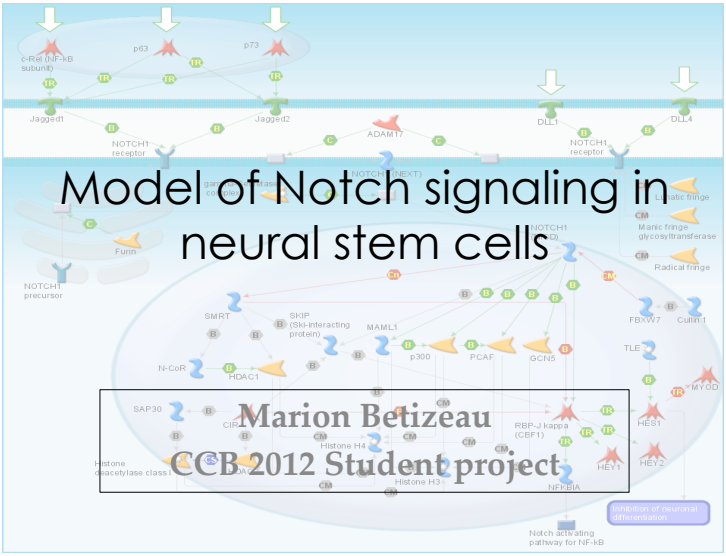

An important part of the course was dedicated to the work on a personal project. I chose to model the Notch signaling pathway in neural stem cells. Notch signaling is a well-known signaling pathway involved in lateral inhibition between neighboring cells in various contexts from flies to mammals (Chapouton et al., 2010). In the particular case of neural stem cells during embryonic development it was known for a long time that newborn neurons generated by neural stem cells express the Notch ligand Delta that activates the Notch receptor expressed at the surface of the neural stem cells (Figure C.1).

The activation of the Notch pathway in the stem cell prevents it from differentiating and maintains its properties of stem cells.

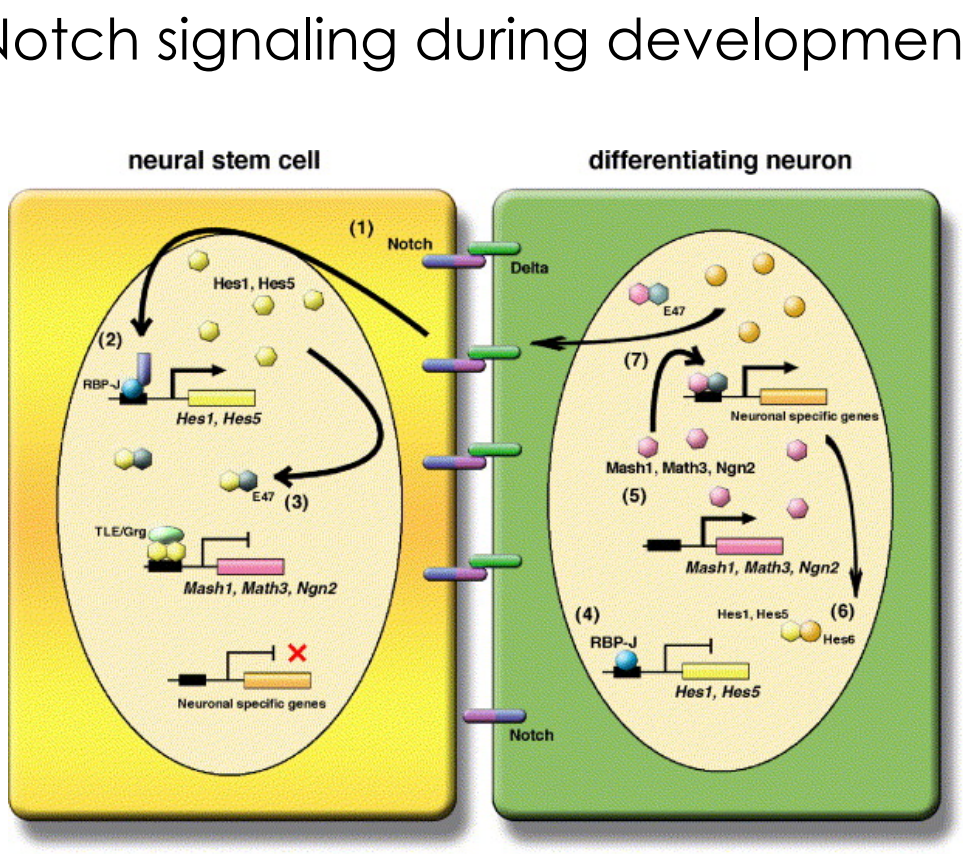

Figure C.1. Schematic representation of Notch signaling in neighboring cells.

It has recently been discovered by precise video-microscopy analyses that this old view needed to be revised because some proteins involved in the pathway are actually oscillating between neighboring neural stem cells at a time in development when neurogenesis has not yet started. Cells alternatively turn the pathway on and off. The old view holds only true when neurons are born and express proneural genes and Notch ligand in a sustained manner (Shimojo et al., 2008).

My goal was to build a simple model of the signaling pathway that would allow these two states of the pathway, oscillations and stable steady state. I implemented the model

and explored the behavior of the systems for different parameters using the bifurcation theory.

Figure C.1 represents the common static view of the signaling pathway. The green cell is becoming a neuron and express proneural genes (pink hexagones), they activate among other genes the expression of Delta, which is a transmembrane protein. The extracellular domain of Delta can bind to the Notch receptor (1) expressed at the membrane of neural stem cells (yellow cell). Upon activation of Notch by Delta the intracellular domain of Notch is cleaved and goes into the nucleus where it activates genes enabling the maintenance of neural stem cells (2) and inhibits proneural genes (3).

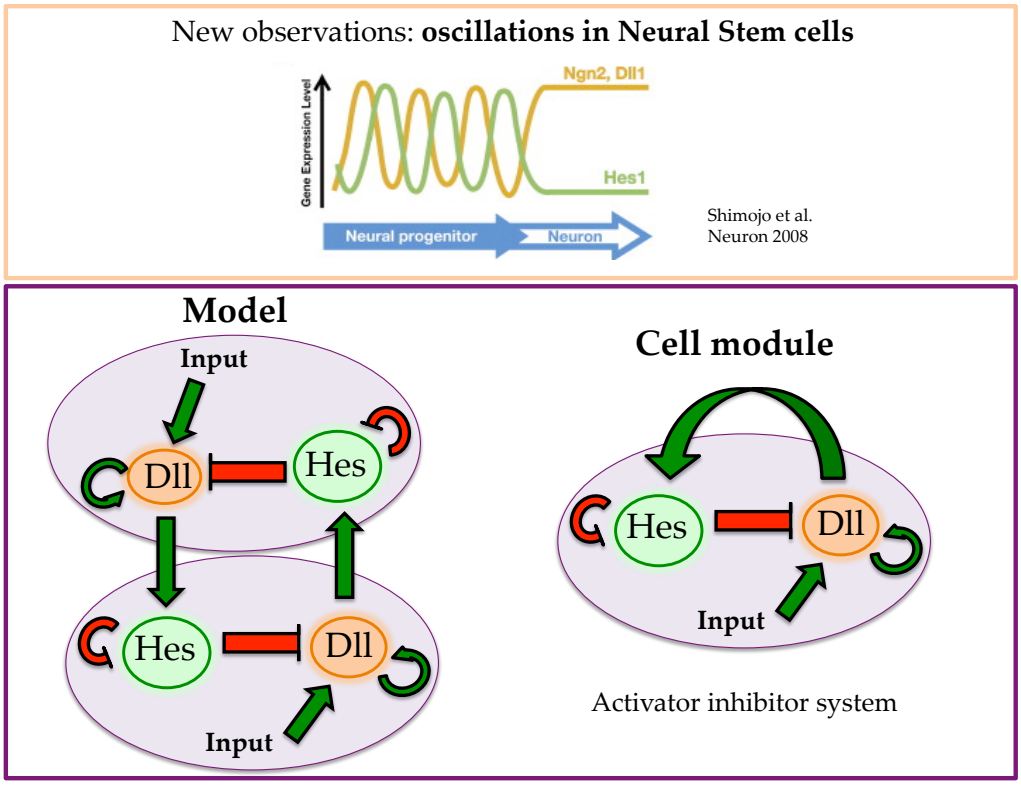

Figure C.2. Rationale of the model

Precise video-microscopy analyses have shown that the traditional view of Notch signaling needed to be revised because some proteins involved in the pathway are actually oscillating between neighboring neural stem cells at a time in development when neurogenesis has not yet started. Cells alternatively turn the pathway on and off (Figure C.2

top panel). The old view holds only true when neurons are born and express proneural genes and Notch ligand in a sustained manner (Shimojo et al., 2008).

The model uses the known interactions between 2 actors of the signaling pathway: Hes1 (Hes, later simply referred to as H) and Delta (Dll, later referred to as D). Taking only 2 interactors into account is a drastic simplification but makes the study of the dynamics of the system much easier. My initial idea was to simulate two neighboring cells but it turns out that what happens in the two cells is perfectly symmetric. I thus further simplified the model studying only a cell module (Figure C.2).

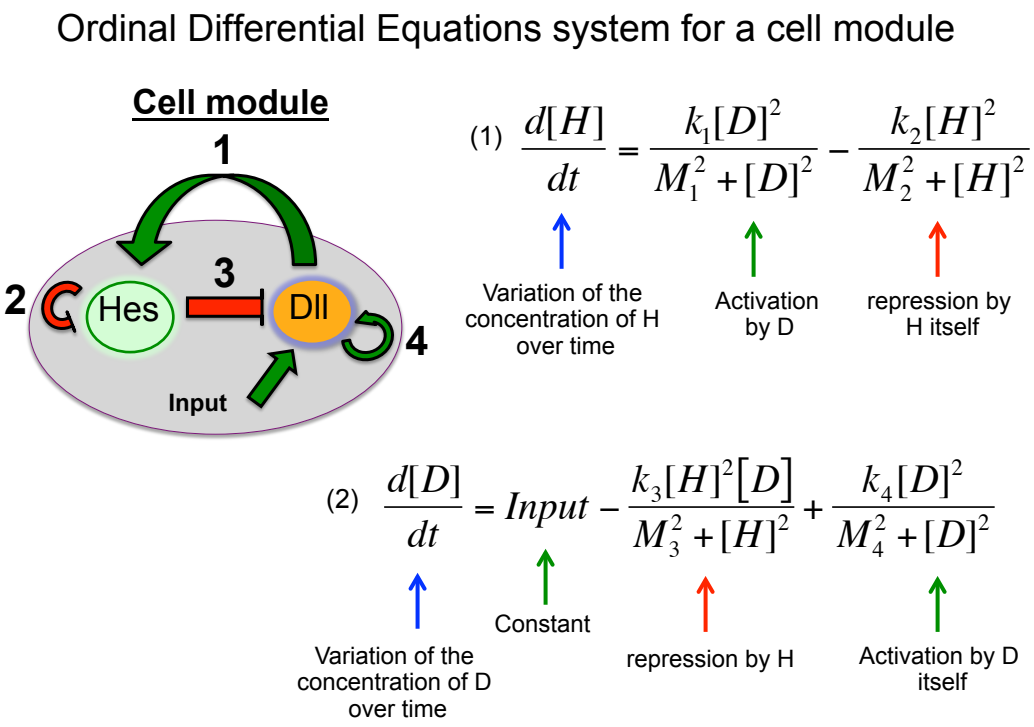

Figure C.3. Mathematical description of the model

The evolution of the concentration of H and D is modeled by Ordinary Differential Equations using Hill functions as mathematical formulation (Figure C.3). The k_i parameters represent the speeds of the reaction and the M_i the affinities of the molecules. Those values are not known in my model, so I just tried out different sets of parameters. But this is a limitation to make the model biologically relevant.

Each ODE enables me via a software to calculate the concentrations of the 2 proteins at each simulation time point knowing the concentrations at the previous time point. The more D is present in the cell, the more the concentration of H will be activated (reaction 1 in the scheme) represented by the first term in equation (1). But as H concentration increases its auto-inhibition will also be stronger (reaction 2) leading to the reduction of the concentration of H (second term in equation (1)). When H concentration is high it represses more the expression of D (reaction 3) and D concentration decreases (second term in equation (2)). At the beginning I intuitively thought and also had evidence from the literature for a constant input (see equation (2)) that would activate D so that it is not completely repressed by H. But it turned out it was not sufficient to produce sustained oscillations and I had to introduce a self-activation loop on D (reaction 4 and third term of equation (2)). Having set the relationships between the two proteins I started to randomly try to run simulations with different sets of parameters to get a better idea of what will be the concentrations of D and H over time in each case.

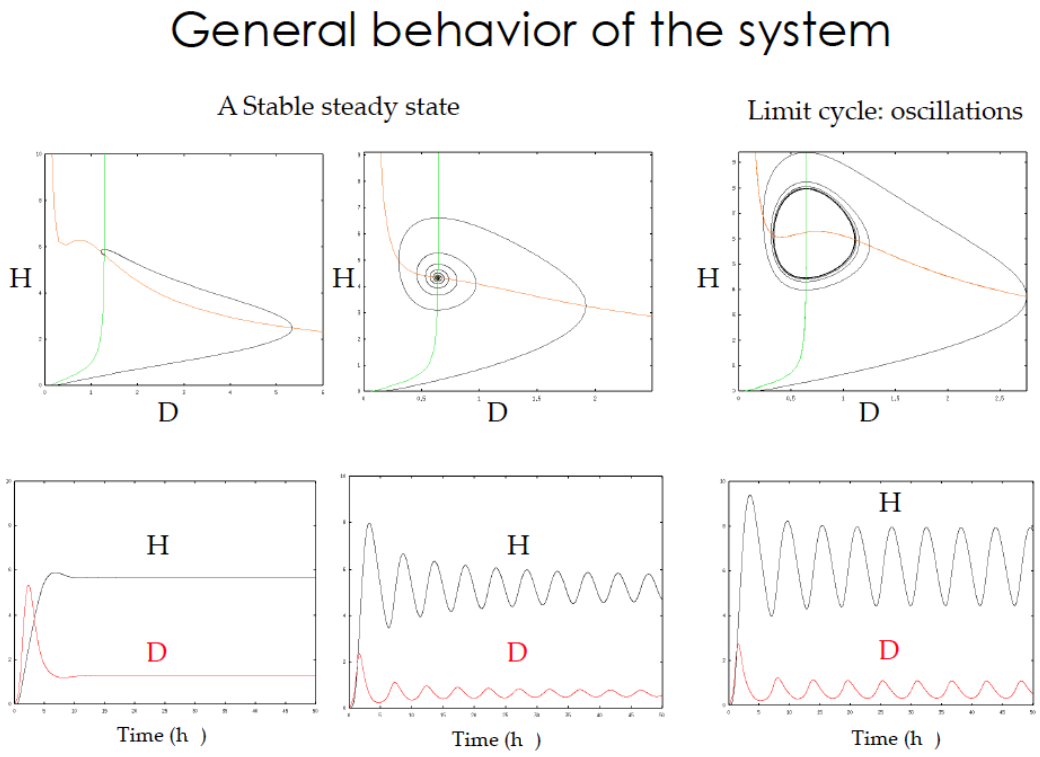

Figure C.4. Different regimes of the model

Simulations have been carried out in the XPP/Auto software. The first line of the Figure C.4 displays phase plane analysis graphs. The green and orange lines represent the nullclines that is to say the points in the phase plane where only one concentration of the molecule will change. The intersection of the 2 nullclines is the steady state: the concentration of the molecules at equilibrium reached after a very long time. The second line of Figure C.4 represents the corresponding evolution of the concentration of H and D over time. For the first column the set of parameters used enables the system to quickly reach a steady state. For a second set of parameters in the second column oscillations start to appear but they dampen to finally reach a stable steady state. In the third case the set of parameters enables stables oscillations of the concentrations of H and D.

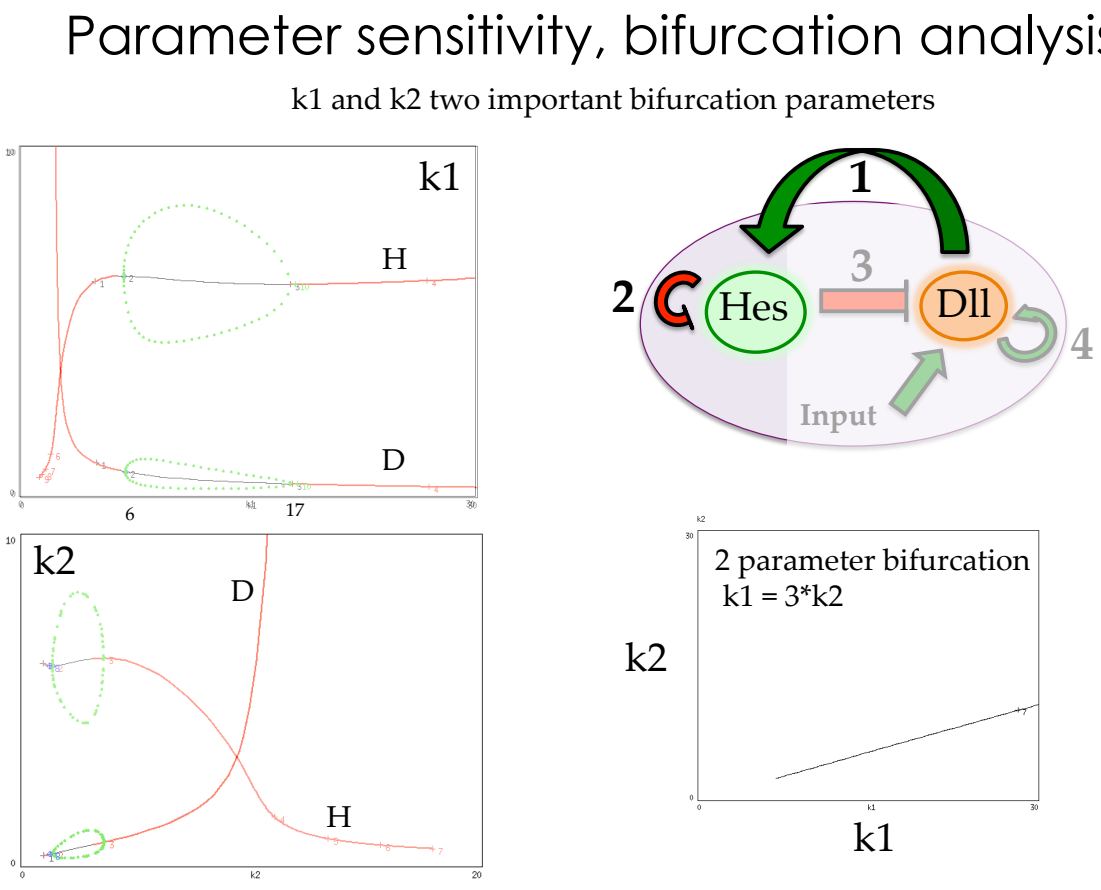

Figure C.5. Exploration of the model

The next question to address is: for which range of parameters can the model allow stable oscillations? This is what is called bifurcation analysis. I tested the sensitivity of the system to certain parameters. Figure C.5 shows the result of the bifurcation analysis for k_1 the strength of activation of H, and k_2 the H auto-inhibition strength. The plots display the concentrations of H and D at steady state for each value of k_1 or k_2. In the case of k_1 for values between 0 and 6, the concentrations of H and D reach a stable steady state. For k1= 6 stable oscillations start to appear symbolized by the dots (highest and lowest concentrations during oscillations). There are stable oscillations until $k_1 = 17$ and then the system reaches again a steady state. The range of k_1 values that allow oscillation is quite broad whereas the range of k_2 values is much narrower and the auto-inhibition needs to be quite low.

To conclude, my model although very simple recapitulates the qualitative behavior of the biological system with the possibility of reaching stable steady states or enabling stable oscillations. I also found that a self-activation loop on D is necessary to produce stable oscillations. Moreover my model predicts a state of the system with a high concentration of H and a low concentration of D that has not been observed in the biological system but that could be found in a different environment. But my model remains quite crude. Taking only two proteins of the pathway is a big approximation. The lack of biologically measured parameters does not allow me to make quantitative predictions, and knowing at least some of those values would help me constraining the other parameters. It will be very interesting to extent the model to several cells and perform simulations on a whole tissue.